Department of Electrical and Computer Engineering

High-Resolution Multipath Channel Parameter Estimation Using Wavelet Analysis

Olusegun Abiola Aboaba

This thesis is presented for the Degree of
Doctor of Philosophy
of
Curtin University

February 2014

Declaration

To the best of my knowledge and belief this thesis contains no material previously published by any other person except where due acknowledgment has been made.

This thesis contains no material which has been accepted for the award of any other degree or diploma in any university.

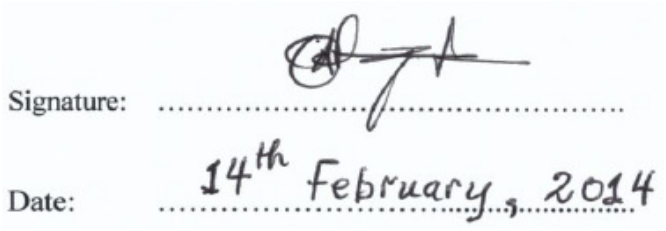

ABSTRACT

The ever increasing requirement for high transmission capacity in digital radio systems necessitates the need for large bandwidth. As a result, discerning the effect of a radio channel on wideband signals is of paramount importance. Multipath propagation is a prominent attribute of wideband radio channels. Multipath produces delayed versions of a signal. Multipath effects can cause severe problems and, especially in urban areas, is generally the most destructive influence on wireless communication systems. In order to characterise a mobile radio communication channel, for the mitigation of these multipath effects, knowledge of the multipath geometries involved is required. A method that is used in practice to characterise the mobile radio channel is known as channel sounding. Resolving two or more very closely spaced multipath signals, with a channel sounder, calls for channel measurements of extremely large bandwidth. Moreover, the requirements for costly hardware systems with a very high resolution, as well as legal transmission bandwidth restriction, inhibit the use of such large bandwidths. Consequently, the intrinsic time resolution capability of channel sounding equipments is more easily enhanced by using high-resolution digital signal processing algorithms. However, it has been shown that the model order selection is usually a difficult problem in these conventional high-resolution algorithms.

This thesis explores the novel use of wavelet analysis as a high-resolution digital signal processing algorithm for estimating the multipath channel parameters. Wavelet analysis is a technique for converting a signal into some other form, which then enables certain features of the original signal to be more tractable to study. It uses small wave-like functions known as wavelets, which have been found to be useful in analysing transient signals. There is a plethora of wavelets that can be chosen from for use in signal analysis. The best wavelet for a given application hinges upon both the nature of the signal to be analysed as well as what is needed from the analysis. Generally, the best one to use will be that which matches the shape of the signal to be analysed at a given location and scale.

The results obtained from this research indicate that this wavelet-based digital signal processing algorithm overcomes the resolution limitation in traditional high-resolution algorithms such as the multiple signal classification (MUSIC) algorithm. It is shown, from computer simulations, that this wavelet-based algorithm can be successfully applied to improve the intrinsic resolution of a channel sounder by more than a factor of ten.

The original contributions of this thesis are in three major parts; first, the central contribution of the thesis is in the development of a wavelet-based digital signal post-processing algorithm for estimating the number of impinging waves and time-delays in mobile radio environments. This procedure uses a novel wavelet family named "Pathlet," designed for this study. This technique may result in a more cost-effective means of implementing channel sounding equipments for very high-resolution measurements. Second, this thesis presents a new noise reduction scheme that exploits the stationary wavelet transform multiscale dependencies. This scheme has been named the "stationary wavelet transform multilevel products (SWTMP)." Third, a novel amplitude estimation algorithm, used to determine the amplitudes of the individual paths in synthetic mobile radio environments, has been derived.

ACKNOWLEDGEMENTS

First and foremost, I thank the Almighty God for the successful completion of this thesis. I would like to thank my supervisors, Dr Yee-Hong Leung and Professor Kah-Seng Chung, for their assistance and suggestions.

I would like to express my gratitude to Curtin University for the scholarship award to cover my tuition fees. I would also like to thank the Abdus Salam International Centre for Theoretical Physics (ICTP) Trieste, Italy, for the award to visit the centre. Thanks also to Professor Jo Ward, from the School of Science, for the discussions about wavelet theory and general questions. Thanks are also due to all my colleagues and friends in the Communication Technology and Signal Processing Research Groups.

I would also like to acknowledge the administrative staff in the Department of Electrical & Computer Engineering, as well as the faculty of Science & Engineering Graduate Studies Officers, for their help over the years; especially during the difficult times when I had to take a Leave of Absence.

Finally, I dedicate this thesis to my parents' memory; my father - late Alfred Oladokun Aboaba (who passed away in 1991) and my mother - late Prophetess M.A.I Balogun Aboaba (who passed away in 2006).

TABLE OF CONTENTS

LIST OF FIGURES

LIST OF TABLES

ABBREVIATIONS

AIC	Akaike information criterion
APCC2006	Asia-pacific conference on communications 2006
AR	Autoregressive
ARMA	Autoregressive moving average
AWGN	Additive white Gaussian noise
BPSK	Binary phase shift keyed
BW	Bandwidth
CDF	Cumulative distribution function
CIR	Channel impulse response
CW	Continuous wave
CWT	Continuous wavelet transform
DFT	Discrete Fourier transform
DWT	Discrete wavelet transform
ECG	Electrocardiogram
EEG	Electroencephalogram
EM	Expectation-maximization
ESPRIT	Estimation of signal parameters by rotational invariance techniques
FBI	Federal bureau of investigation
FFT	Fast Fourier transform
FIR	Finite impulse response
IF	Intermediate frequency
IIR	Infinite impulse response
ISI	Intersymbol interference
ISM	Industrial, scientific, and medical bands
I & Q	In-phase and the quadrature
LOS	Line-of-sight
MA	Moving average

MAD	Median absolute deviation
MDL	Minimum description length
MIMO	Multiple-input multiple-output
MRA	Multiresolution analysis
MUSIC	Multiple signal classification
NLOS	Non-line-of-sight
PDF	Probability density function
PHD	Pisarenko harmonic decomposition
PN	Pseudo-noise
PRBS	Pseudo-random binary sequence
RF	Radio frequency
RMS	Root mean square
SAGE	Space-alternating generalized expectation-maximization
SCCS	Sliding correlator channel sounder
SNR	Signal-to-noise ratio
STDCC	Swept time-delay cross-correlator
STFT	Short time Fourier transform
SVDP	Singular value decomposition prony
SWT	Stationary wavelet transform
SWTMP	Stationary wavelet transform multilevel products
TF	Time-frequency
TFR	Time-frequency representation
TLS-ESPRIT	Total least squares - ESPRIT
VNA	Vector network analyser
WPT	Wavelet packet transform

LIST OF PRINCIPAL SYMBOLS AND NOTATIONS

ν	Time sliding factor in the SCCS
τ_{PN}	PN sequence period in the SCCS
α_i	Amplitude of the i^{th} multipath component
τ_i	Relative time-delay of the i^{th} multipath component
$\eta(t)$	AWGN
σ_η	RMS value of $\eta(t)$
$\hat{\sigma}_\eta$	An estimate of σ_η
τ_m	Mean excess delay
τ_{rms}	RMS delay spread
ΔT	Time interval, between maximal correlations, in the SCCS
$\delta(\cdot)$	Dirac delta function
ω	Angular frequency
ω_n	Discrete values of ω
$\Delta\omega$	Spacing of the angular frequencies
ω_0	Lowest angular frequency
$\downarrow 2$	Downsampling (i.e. decimation) operation
$\|g_k\|_{\max}$	Maximum norm of g_k
β_i	Complex amplitudes in the Prony algorithm
$\{\lambda_m\}$	Autoregressive coefficients
$\{\boldsymbol{v}_k\}$	Eigenvectors in the noise subspace
$\psi(t)$	Mother wavelet (i.e. the analysing wavelet)
$\{\psi_{j,k}(t)\}$	Wavelet basis functions
$\langle \cdot\ ,\ \cdot \rangle$	Inner product operator

$\chi(n)$	Impulse response of a low-pass IIR filter
$\varphi(t)$	Scaling function
$\varphi_{j,k}(t)$	Translated and dilated scaling function
ρ	Peak amplitude of a single triangular waveform
υ	Noise level
$\Phi_E(\omega)$	Characteristic function of random variable E
ξ_E	Mean of random variable E
σ_E^2	Variance of random variable E
Υ	Noise threshold level
$\hat{\sigma}_{(mad)}$	MAD standard deviation estimate of noise
$\lvert h_k \rvert$	Absolute value of h_k
$\mathbb{Z}$	Set of all integer numbers
$\mathbb{R}$	Set of all real numbers
$\Leftrightarrow$	Two way implications
$\oplus$	Orthogonal direct sum of two subspaces
$\boldsymbol{a}$	A data vector
$\mathbf{A}$	A data matrix
$\mathbf{A}^{\mathrm{T}}$	Transpose of matrix $\mathbf{A}$
$\mathbf{A}^{\mathrm{H}}$	Hermitian transpose of matrix $\mathbf{A}$
$d_{j,k}$	Noisy detail coefficients of the SWT
$\tilde{d}_{j,k}$	Band-limited replica of $d_{j,k}$
$\vec{d}_{j,k}$	Non-negative replica of $d_{j,k}$
$e_{j,k}$	AWGN in wavelet transform domain
$erf(\cdot)$	Error function
$f_E(e)$	Probability density function of random variable E
f_c	Carrier frequency in the SCCS

f_{TX}	Transmitter chip clock rate in the SCCS
f_{RX}	Receiver chip clock rate in the SCCS
$F_E(e)$	Cumulative distribution function of random variable E
$g_{j,k}$	SWT decomposition high-pass filter coefficients
g_k^o	DWT and WPT decomposition high-pass filter coefficients
$g(n)$	Impulse response of a high-pass FIR filter
$h_{j,k}$	SWT decomposition low-pass filter coefficients
$h(n)$	Impulse response of a low-pass FIR filter
h_k^o	DWT and WPT decomposition low-pass filter coefficients
$H(\omega)$	Multipath channel transfer function
H_n	Discrete values of $H(\omega)$
H_n^*	Complex conjugate of H_n
$H(z)$	The z-transform of $h(n)$
j	Wavelet transform level
J	Coarsest resolution level in a MRA
k	Translation (i.e. shifting) parameter
K	Number of multipath components
$L^2(\cdot)$	Hilbert space of square integrable functions
M	Size of the eigenvectors in the noise subspace
$O_{j,k}$	Denoised SWT detail coefficients by thresholding
$\vec{\vec{O}}_{(r1\times r2),\,k}$	Denoised SWT detail coefficients by SWTMP
p	Size of the signal subspace in the MUSIC algorithm
$P(f)$	Weighted spectral estimate with weights $\{w_k\}$
$P_K(z)$	Predictor polynomial, with roots z_i, in the Prony algorithm
$\boldsymbol{s}(f)$	Vector of complex sinusoids

$std\{d_{j,k}\}$	Standard deviation of $d_{j,k}$
S_n	Weighted sums, with weights $\{\lambda_m\}$, in the Prony algorithm
t_{actual}	Actual propagation time scale in the SCCS
$t_{observed}$	Observed time scale on the oscilloscope in the SCCS
t_{TX}	Transmitter chip duration in the SCCS
T_{bb}	Pulse width for the direct RF pulse channel sounder
$v_{j,k}$	Noiseless approximation coefficients of the SWT
$v_{j,k}^{o}$	DWT and WPT noiseless approximation coefficients
V_j	Approximation subspace
$w_{j,k}$	Noiseless detail coefficients of the SWT
$w_{j,k}^{o}$	DWT and WPT noiseless detail coefficients
W_j	Detail subspace, or wavelet space
x_n	An n^{th} element of a discrete data sequence
$x(t)$	Noiseless output waveform in the SCCS
$y(t)$	Noisy output waveform in the SCCS
$\tilde{y}_N(n)$	Band-limited replica of $y_N(n)$
z	The z-transform variable

CHAPTER 1

INTRODUCTION

1.1 Aim and Scope of the Thesis

The aim of the research described in this thesis is identification and development of a novel high-resolution digital signal processing algorithm, based on wavelet analysis, for multipath channel parameter estimation.

The ever increasing requirement for high transmission capacity in digital radio systems necessitates the need for large bandwidth. Therefore, an understanding of the effect of a radio channel on wideband signals is of paramount importance. In a mobile radio environment, due to scattering of radiowaves, the transmitted signal reaches the receiver by more than one path, causing a phenomenon known as multipath fading. The closely spaced paths add vectorially, according to their relative phases and amplitudes, and the resultant waveform of their sum is observed. Furthermore, when adjacent multipath components have very large differential amplitudes then a strong ray may completely mask the weaker ones.

Multipath propagation is a prominent feature of wideband radio channels. Multipath produces delayed replicas of an original signal. When the multipath delay spread becomes a substantial fraction of the symbol period, then intersymbol interference (ISI) results and this may limit the data rates achievable with digital radio systems. In order to

characterise the mobile radio communication channel for the mitigation of multipath effects, knowledge of the multipath geometries involved is needed.

Wideband channel measurements are often used to provide the propagation data required to characterise the mobile radio communication channels. A method which is utilised in practice for these wideband channel measurements is that of channel sounding (Parsons 1992); in which a transmission is made over the radio channel to be characterised and the received signal is subsequently analysed (Saleh and Valenzuela 1987; Bultitude, Mahmoud et al. 1989). In order to carry out high-resolution measurements with a channel sounder, large bandwidth must be used. However, the requirements for costly hardware systems to be implemented with a very high-resolution, and legal transmission bandwidth restriction, inhibit the usage of such huge measurement bandwidths. As a consequence, the intrinsic time resolution of channel sounding equipments is usually enhanced through the use of high-resolution digital signal processing algorithms.

Various high-resolution techniques have been proposed in the literature for estimating some of the parameters of the impinging waves in mobile radio environments; such as their complex amplitudes and relative arrival times (Kay and Marple 1981; Schmidt 1986; Marple 1987; Kay 1988; Roy and Kailath 1989; Stoica and Moses 1997). The review of a number of these signal parameter estimation techniques is presented in Section 2.3.

This study explores the novel use of wavelet analysis as a high-resolution digital signal processing algorithm for multipath channel parameter estimation. Wavelet analysis is a technique of converting a signal into some other form which then makes certain features of the original signal more amenable to analyse. Wavelet transforms do not have a unique set of basis functions, unlike Fourier-based techniques, which is one of the reasons why wavelets are used in diversified fields.

Wavelet transforms can be continuous or discrete types, depending on the application. The discrete wavelet transform (DWT) minimises the redundancies that are inherent in

the continuous wavelet transform (CWT). Three basic manipulations can be performed on a wavelet to make it more flexible; a wavelet can be dilated, contracted, and translated (i.e. moved). If the dilation and contraction parameter is denoted by $a > 0$ while the shifting of the wavelet along the time axis is denoted by parameter b, then the shifted and dilated or contracted versions of the mother wavelet $\psi(t)$ is represented by

$$\psi(at - b). \tag{1.1}$$

The wavelet transform decomposes a discrete or continuous-time signal to produce the wavelet transform coefficients. These coefficients are then examined or operated on instead of the original signal. The coefficients containing the low-frequency components of the signal are known as the approximation coefficients while those containing the high-frequency components are known as the detail coefficients. The approximation coefficients capture the global feature content of the signal, whereas the detail coefficients extract the irregular and transient events such as the signal peaks. A review of wavelet analysis, and applications, is discussed further in Section 2.4.

In this research, the wavelet transform coefficients are used to provide information about the time-delays and number of propagation paths in a multipath delay profile by observing the locations of the positive peaks in the detail coefficients.

1.2 Thesis Overview

The thesis has been organised into seven chapters as follows:

Chapter 1 presents the aim, scope and original contributions of the thesis. In Chapter 2, a review of wideband channel sounding and a number of conventional signal parameter estimation techniques are presented. A survey of various channel sounding experiments is first given. Then a review of the conventional signal parameter estimation algorithms is carried out, to examine their advantages, limitations, and time resolution capabilities. This is followed by a description of wavelet analysis and applications.

Chapter 3 presents the development of the proposed algorithm for multipath channel parameter estimation. This chapter starts with the design of customised mother wavelets for the current study. This newly derived family of wavelets is named "Pathlet." Each member of this wavelet family is distinguished by the number of coefficients. For example, Pathlet with five wavelet coefficients is referred to as Pathlet 5. Next, the formulation of noise reduction strategies to be used in extracting the multipath components that are immersed in noise is presented. The chapter concludes with the derivation of a novel amplitude estimation algorithm, to be used in estimating the amplitudes of the individual multipath components in synthetic mobile radio environments.

Chapter 4 presents the implementation of the algorithm proposed in Chapter 3, by means of computer simulations. Two noise reduction schemes are investigated in this chapter. The first noise reduction scheme is based on using hard thresholding and the median absolute deviation (MAD) standard deviation estimate (Donoho and Johnstone 1994; Donoho 1995; Donoho and Johnstone 1995; Percival and Walden 2000). While the second denoising procedure is based on exploiting the stationary wavelet transform multiscale dependencies.

Since the measured signals from channel sounding systems are bandwidth limited in order to minimise noise, Chapter 5 therefore presents another series of computer

simulations which were carried out to examine the effect on time resolution, caused by bandwidth limitations.

In Chapter 6, the algorithm developed in this research is applied to resolve the multipath components in measured delay profiles. These delay profiles were obtained by connecting the transmitter and receiver units of an experimental sliding correlator channel sounder back-to-back. Chapter 7 gives a summary of the main results and recommendations for future research.

1.3 Summary of Original Contributions

The original contributions made in this thesis are presented as follows:

- The main contribution of this thesis is in the development of a novel high-resolution digital signal processing algorithm, based on wavelet analysis, for resolving the impinging waves that made up the received signal in mobile radio environments. The results obtained indicate that this wavelet-based digital signal processing algorithm overcomes the resolution limitation in traditional high-resolution algorithm such as the MUSIC algorithm. This may provide a more cost-effective means of implementing channel sounding equipments for very high-resolution measurements.

- The design of a novel set of finite filter coefficients having symmetric impulse response, resulting in the development of a wavelet family named “Pathlet,” is presented in Section 3.2. It is then shown that certain members of this new wavelet family named “Pathlet 7” and “Pathlet 9” are more robust to noise when compared with conventional Daubechies Symlet 2 wavelet (Daubechies 1992; Mallat 1999).

- A new means of estimating the number of paths and time-delays in mobile radio environments, using the detail coefficients of the wavelet transform, is proposed in Sections 3.3.2 and 3.3.3. In practice, the number of impinging waves in mobile radio environments is often set through the use of classical information theoretic methods for model order selection, such as the Akaike's information criterion (AIC) (Marple 1987) and Rissanen's minimum description length (MDL) (Rissanen 1978; Wax and Kailath 1985). However, it has been shown that the AIC gives an inconsistent estimate that gravitates to, asymptotically, overestimate the number of multipath signals (Kashyap 1980; Wax and Kailath 1985).

- A new amplitude estimation algorithm has been derived in Section 3.4 and used to determine the amplitudes of the individual paths in synthetic mobile radio environments.

- A new denoising technique that exploits the stationary wavelet transform multiscale dependencies is proposed in Section 3.3.3. This scheme has been named the "stationary wavelet transform multilevel products (SWTMP)."

CHAPTER 2

REVIEW OF WIDEBAND CHANNEL SOUNDING AND SIGNAL PARAMETER ESTIMATION TECHNIQUES

2.1 Introduction

The astounding success of wireless communication systems in rendering ubiquitous communications at any time, anywhere in the world, has paved the way toward breaking the location hindrance in telecommunications. However, the performance of wireless communication systems is restricted by the mobile radio channel.

In a typical radio system, the mobile portables communicate with a fixed base-station antenna that is installed in an elevated position. Due to the scattering of radiowaves by buildings, obstacles, and even people moving around, the transmitted signal is degraded. The transmit signal usually reaches a receiver after following more than one path. The resulting paths arrive with different delays, attenuations, and phase values due to different path lengths. These multipath components then add in accordance to their relative amplitudes, arrival times, and phases, and their random envelope sum is that observed by the receiver. A typical multipath fading environment is shown in Fig. 2.1.

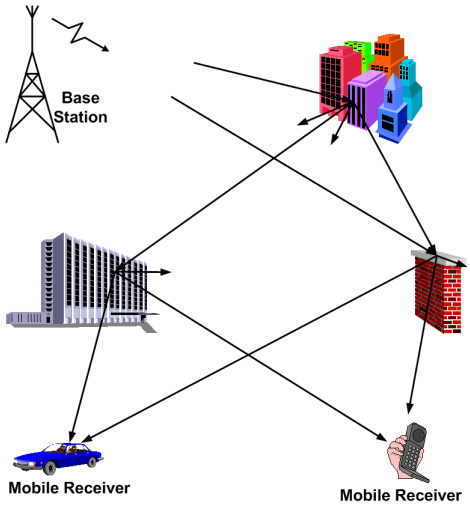

Figure 2.1 An example of multipath propagation in an outdoor environment.

The presence of multiple propagation paths, or multipaths, with different time-delays, attenuations, and phases, gives rise to a highly complex radio propagation channel. Multipath effects can cause severe problems and, especially in urban areas, is often the single most destructive influence on wireless communication systems. The trend in wireless communication system design is therefore directed towards the mitigation of such multipath effects. The techniques used to mitigate these impairments may take the form of channel equalisation, diversity or selective reception. Moreover, these may well demand accurate estimation of channel impulse response of high resolution which could only be achieved through the use of a large measurement bandwidth. Hence, the multiple ray paths that are otherwise not individually identifiable in the presence of noise are often separated by using digital signal post-processing algorithms.

This chapter reviews the various signal parameter estimation techniques that are published in the literature. It begins with a survey of wideband channel sounding techniques in Section 2.2. Next, a review of signal parameter estimation techniques is carried out to examine their advantages and limitations. Finally, a description of wavelet analysis and a number of applications are presented in Section 2.4.

2.2 Wideband Channel Sounding Techniques

2.2.1 Overview

Channel parameters such as the rms delay spread and mean excess delay, provide a description of mobile radio channels that are useful for system designers. Such information is essential for establishing channel models, the equalisation techniques, as well as types of diversity. Measuring equipments that can be used to obtain the experimental data, from which these parameters can be derived, are known as channel sounders. The choice of channel sounding techniques depends upon the intended application; whether a narrowband or wideband radio system is desired and whether a time or frequency domain characterisation is needed. In narrowband channels, the frequency-dependent feature of each individual ray becomes negligible because all the frequency components are affected by the channel in the same way. Once the range of frequencies over which a channel is considered to have flat frequency response, i.e. the coherence bandwidth, is exceeded the channel is then termed wideband and becomes frequency selective. In frequency selective fading, some frequency components undergo different degrees of fading from others.

The mean excess delay τ_m and rms delay spread τ_{rms}, are defined as (Rappaport 2002)

$$\tau_m = \frac{\sum_{i=1}^{K} \alpha_i^2 \tau_i}{\sum_{i=1}^{K} \alpha_i^2}, \tag{2.1}$$

$$\tau_{rms} = \sqrt{\left\{ \tau_m^2 - (\tau_m)^2 \right\}}, \tag{2.2}$$

where

$$\tau_m^2 = \frac{\sum_{i=1}^{K} \alpha_i^2 \tau_i^2}{\sum_{i=1}^{K} \alpha_i^2}, \tag{2.3}$$

while α_i and τ_i are the amplitude and delay, respectively, of the i^{th} path. The rms delay spread is a good measure of multipath spread, and provides an indication of the potential for intersymbol interference.

In general, wideband channel sounding techniques may be classified as direct radio frequency (RF) pulse channel sounding, spread spectrum sliding correlation channel sounding (SCCS), and frequency domain measurements. This classification of channel sounding techniques is shown in Fig. 2.2. In the literature, spread spectrum sliding correlator channel sounding is also referred to as swept time-delay cross-correlation (STDCC) channel sounding (Parsons, Demery et al. 1991; Parsons 1992).

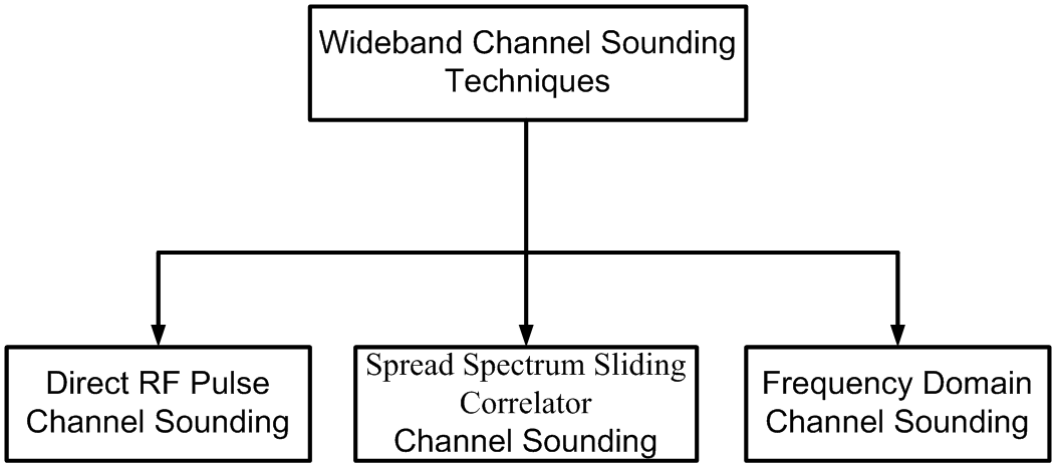

Figure 2.2 General classification of wideband channel sounding techniques.

2.2.2 Direct RF pulse channel sounding technique

2.2.2.1 Principles of operation

In the direct RF pulse channel sounding technique, a short duration periodic pulse having a given width of T_{bb} is used to excite the radio propagation channel. The pulse repetition period is usually rapid in order to allow observation of the time-varying behaviour of the radio propagation channel. At the receiver, the received signal is filtered with a wide bandpass filter of bandwidth $BW = 2/T_{bb}$; it is then amplified, detected with an envelope detector, and displayed on a digital storage oscilloscope (Rappaport 2002). The pulse duration T_{bb} determines the minimum resolvable delay between successive echo contributions. Details of the system architecture of this channel sounding technique are provided in Rappaport (2002). The advantage and disadvantages of this channel sounding technique are presented as follows:

2.2.2.2 Advantage

- A major advantage of this technique is the simplicity of the system architecture.

2.2.2.3 Disadvantages

- One drawback of this system is that a high transmitter peak power must be used because of the very short duration of the transmitted pulse. This may cause regulatory concerns.

- This system is also subjected to noise and interference, as a result of the wide bandpass filter needed at the receiver for multipath time resolution.

- Another drawback of this technique is that the phases of each multipath component are not received when an envelope detection method is used.

Some applications of this channel sounding technique are presented in the following section.

2.2.2.4 Applications

In the first study of the impulse response of mobile radio propagation channel (Young and Lacy 1950), a direct RF pulse channel sounder with a pulse duration of 0.5 μs was used to carry out measurements in New York city, at 450 MHz. A further study was carried out in San Francisco (Turin, Clapp et al. 1972), using a similar method. In this later experiment, simultaneous transmissions of 100 ns duration pulses at frequencies of 2920 MHz, 1280 MHz, and 488 MHz were made from a fixed site and their reception at a mobile van analysed. A statistical analysis of the data from the experiment has shown the results for the three frequencies to be almost similar and this has been used as a basis for a statistical model of urban multipath propagation.

In a similar experiment carried out in medium-size office building (Saleh and Valenzuela 1987), an RF oscillator was used to generate a 1.5 GHz continuous wave (CW) signal. This was then modulated by a train of 10 ns radar-like pulses having 600 ns repetition period. This radar-like signal was amplified and transmitted with a vertically polarised discone antenna having omnidirectional radiation pattern. At the receiver, the signal was detected with a sensitive square-law envelope detector and displayed on a computer-controlled digital storage oscilloscope. A delay spread up to about 200 ns and maximum rms values of 50 ns were obtained.

Using a similar technique (Rappaport and McGillem 1988), wideband multipath measurements were conducted at 1300 MHz in five operational factories in Indiana, United States. The delay profiles were measured by transmitting a 10 ns pulse at a 500 ns repetition rate, and receiving the attenuated and distorted version of the pulse on a digital storage oscilloscope. An rms delay spread in the range of 30 - 300 ns was observed.

Also using the same method to analyse the statistical characteristics of the indoor radio channel, a 910 MHz signal was modulated by a train of 3 ns pulses having 500 ns repetition period (Ganesh and Pahlavan 1991). The modulated carrier was then amplified and transmitted using a quarter-wave dipole antenna. Similar antenna was used at the receiver to capture the radio signal. The received signal was demodulated using an envelope detector; whose output was displayed on a computer-controlled digital storage oscilloscope. The transmitter was moved to various locations at each measurement site. A total of 472 multipath profiles were collected from measurements made at different locations in five areas on three different manufacturing floors and two office areas in a college campus. The manufacturing floors are characterised by large open areas, often with line-of-sight (LOS) paths, having various machinery and equipment of different sizes. Areas with a lot of machinery and less LOS paths between the transmitter and receiver had higher values of rms delay spread. The statistical parameters required for computer simulation of multipath profiles in these indoor radio environments are then determined. The results obtained show that the multipath arrivals form a modified Poisson process and the amplitude of the paths fit a log-normal distribution. The standard deviation and mean of the log-normal distribution were shown to fit decaying exponentials.

2.2.3 Frequency domain channel sounding technique

2.2.3.1 Principles of operation

As a result of the duple relationship between the frequency and time domain methods, it becomes possible to measure the channel impulse response (CIR) in the frequency domain and later convert to the time domain (Rappaport 2002). The most popular frequency domain technique is the swept-frequency method that is implemented using a vector network analyser (VNA).

Details of the system architecture of this wideband channel sounding technique are also provided in Rappaport (2002). The advantages and disadvantages of this channel sounding technique are presented as follows:

2.2.3.2 Advantages

- When using a VNA for wideband radio channel measurements, the measurement bandwidth which governs the multipath resolution can be chosen to be large enough so that significant multipath components can be resolved.

- This technique can also be used to provide both amplitude and phase responses.

2.2.3.3 Disadvantages

- The increase in measurement bandwidth required for high-resolution increases the measurement time of the channel transfer function. As a consequence, it becomes difficult to measure consecutive transfer functions for time varying channels. This is because the channel frequency response may change rapidly, causing erroneous channel impulse response measurements. This results in confinement to static environments when using the swept-frequency method.

- Another limitation of this technique is that the system needs careful synchronisation and calibration between the transmitter and receiver. This makes it useful for only very close measurements like indoor environments.

2.2.3.4 Applications

A channel sounding performed in the 1.7-2.2 GHz band using swept-frequency channel sounding, with 625 kHz frequency steps and sweep time of 400 ms, samples 801 points in each sweep (Degli-Esposti, Lombardi et al. 2001). The signal-to-noise ratio (SNR) was kept above 30 dB, by averaging on 10 sweeps to reduce noise effects. This has been shown to produce a maximum nonambiguous echo delay of $1.6\,\mu s$ and theoretical resolution of 2 ns. This measurement campaign was carried out in a single-floor building having offices and laboratories of a factory, which is located in an open, suburban zone without any neighbouring buildings.

In a similar experiment (Tholl, Fattouche et al. 1993), it was shown that the results from frequency domain measurement are similar to those using a time-domain measurement approach, based on a spread spectrum system with a sliding correlator at the receiver. In this experiment, a total of 120 impulse response functions were measured in a set order with the sliding correlator system, and another 120 transfer functions were measured, in the reverse order, using the VNA. The VNA measures the complex transfer function of the radio channel at 201 discrete frequency points between 900 and 1000 MHz over a time period of 100 ms.

Using a similar technique (Hashemi 1993a), measurements were carried out in two dissimilar office buildings with both LOS and NLOS transmissions between the transmitter and the receiver using two discone antennas. In this experiment, the network analyser swept-frequency band was 900 to 1300 MHz in 500 KHz steps (i.e. 801 points). The time interval per sweep was 400 ms, with 10 sweeps being averaged per measurement. This makes the actual time for each measurement to be 4 s. Measurements were conducted at night, or on weekends, when there were few people moving around in the vicinity of the measurement setup. A database of 12000 samples of the channel impulse responses was obtained. The time resolution of the channel impulse responses was estimated to be 5 ns. The values of the rms delay spread and the mean delay, for both dissimilar office buildings, were computed to be in the range of 10 to 50 ns and 20 to 30 ns respectively.

2.2.4 Spread spectrum sliding correlator channel sounding technique

2.2.4.1 Principles of operation

A well-known time domain channel sounding technique is the sliding correlator channel sounding (SCCS). This channel sounder has been utilised as a reference for this study. Block diagrams of the transmitter and receiver units, of this channel sounding technique, are shown in Figs. 2.3 and 2.4 respectively (Rappaport 2002).

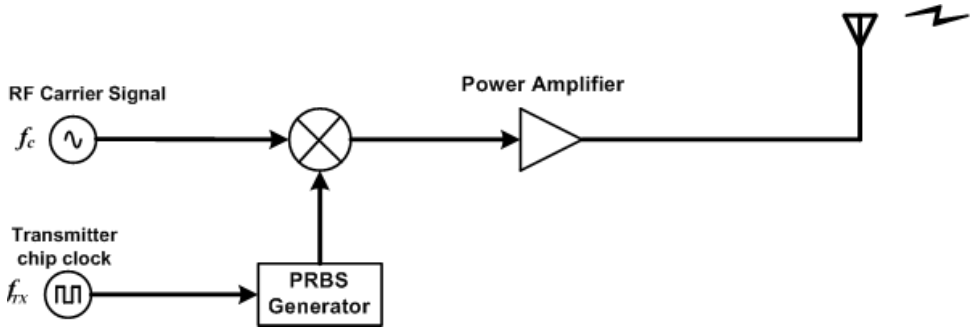

Figure 2.3 Transmitter unit of a sliding correlator channel sounding technique (Rappaport 2002).

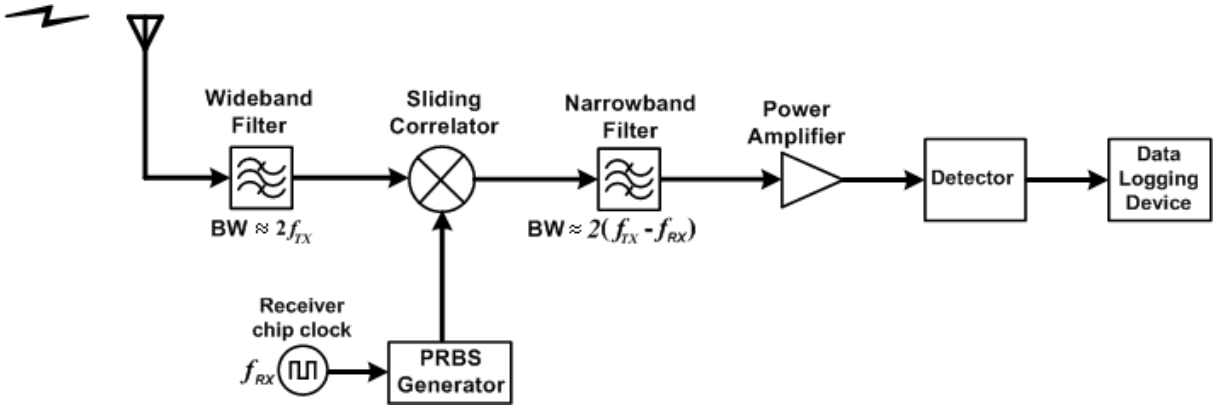

Figure 2.4 Receiver unit of a sliding correlator channel sounding technique (Rappaport 2002).

In sliding correlator channel sounding, a carrier signal is spread across a large bandwidth by mixing it with a binary pseudo-noise (PN) sequence having a given chip rate f_{TX} . The created binary phase shift keyed (BPSK) signal is then transmitted through a multipath channel. At the receiver, the spread spectrum signal is received, filtered, and dispread using a PN sequence generator identical to that used at the transmitter but runs at a somewhat slower rate than the transmitter chip clock. In practice, the difference between the receiver and transmitter chip clock rates, i.e. $f_{TX} - f_{RX}$, is of the order of a few kHz.

The result is that the transmitter PN sequence seems to slide across the receiver PN sequence, and therefore the name "sliding correlator." Whenever the PN code of the faster chip clock meets up with the PN code of the slower chip clock, the two chip sequences will be almost identically aligned, resulting in maximum correlation. Since the various incoming multipath components have different time-delays, they will hence maximally correlate with the receiver PN sequence at different times.

In order to understand how the sliding correlator works, the sliding actions are briefly explained. First it is assumed that the transmitted signal is not corrupted by multipath effects at the receiver. In this case, when there is maximum correlation between the transmitter and receiver PN sequences, then a voltage peak is produced at the output of the detector. Conversely, when the transmitter and receiver PN sequences are not aligned the correlation of the two sequences is at a minimum, and the output voltage of the detector will be low when compared to the peak voltage produced for maximum correlation.

Now when the sounding signal is corrupted by multipath effects, then an attenuated and delayed replica of the transmitted signal will be produced for each physical propagation path. As the receiver sequence aligns with each of the multipath signals, correlation peaks are produced at the output of the detector. The output voltage waveform of the detector then gives an estimate of the radio channel impulse response.

A sliding factor ν used in the SCCS is defined by

$$\nu = \frac{f_{TX}}{f_{TX} - f_{RX}}. \tag{2.4}$$

This sliding factor relates the measurement observation time, $t_{observed}$, to the actual propagation time t_{actual}, as follows

$$t_{actual} = \frac{t_{observed}}{\nu}. \tag{2.5}$$

This causes time dilation in the sliding correlator system since the propagation delays are expanded in time by the sliding correlator. The time interval ΔT, between maximal correlations, is given by (Rappaport 2002)

$$\Delta T = t_{TX} \nu G, \tag{2.6}$$

where

t_{TX} is the transmitter chip duration (s),

ν is the sliding factor (dimensionless),

$G = 2^n - 1$, where n is the number of shift registers used in the sequence generator.

The PN sequence period, $\tau_{PN} = t_{TX} G$, gives an estimate of the maximum unambiguous multipath signals time-delay range which can be measured with a sliding correlator channel sounder.

In this study, the multipath delay resolution is defined to be the minimum relative delay between any two paths such that these paths can be resolved by the SCCS system. For a channel with only a single path, the detected signal waveform of the channel sounder takes the form of a triangle with a base width of $2t_{TX}$ around the correlation peak. That is after accounting for the apparent dilation of the horizontal axis time scale caused by the sliding factor. In a multipath radio channel, the superposition of such triangular pulses, each of which is delayed according to the relative delays of the propagation paths, forms the output of the sliding correlator channel sounder system.

For example, given that $2t_{TX} = 100$ ns. Now if the occurrence of the first correlation peak (also used as the time reference) is at 50 ns, while the other correlation peaks are

described relative to the arrival time of this first correlation peak; then multipath components separated by 50 ns or more are resolved by the sounder system.

The output waveform of the channel sounder, in the absence of noise, can be expressed as

$$x(t) = \sum_{i=1}^{K} \alpha_{ic}\, p(\mathrm{t} - \tau_i), \tag{2.7}$$

where $p(\mathrm{t} - \tau_i)$ represents the correlation of the pseudo-random binary sequence (PRBS) at the transmitter and receiver, delayed by τ_i, while $\alpha_{ic} = \alpha_i e^{j\vartheta_i}$ denotes the complex amplitude of the i^{th} path. K represents the number of multipath components. α_i and ϑ_i is the amplitude and phase respectively of the i^{th} path. The advantages and disadvantages of this channel sounding technique are as follows:

2.2.4.2 Advantages

- One advantage of this system is the low transmitter power that is required, when compared with the direct RF pulse channel sounding, as a result of the inherent processing gain of spread spectrum systems.

- Another advantage of this system is that its sensitivity can be adjusted by changing the sliding factor and the post-correlator filter bandwidth.

- Also, the transmitter and receiver PN sequence synchronisation is eliminated by the sliding correlator.

2.2.4.3 Disadvantages

- A drawback of this technique is that the time needed to make power delay profile measurements can often be immoderate, because measurements are not made in real time but are accumulated as the PN codes slide past one another.

- Also, the phases of individual multipath components cannot be measured with this system.

2.2.4.4 Applications

The first published impulse response measurements of a mobile radio environment using a spread spectrum sliding correlator channel sounder, were recorded in a vehicle moving along several business and residential streets in suburban New Jersey at 910 MHz (Cox 1972). Similar experiment was also carried out in the heavily built-up urban mobile radio environment of New York City (Cox 1973a). In these experiments, a PRBS with a length of 511, and clocked at 10 MHz, was used to binary phase modulate a 70 MHz carrier. Then the modulated signal was translated to the sounding frequency by mixing it with an 840 MHz local oscillator. This modulated signal was amplified to 10 W and radiated from a vertical broadside collinear antenna array which has an omnidirectional radiation pattern. At the receiver, an identical maximal-sequence to that used in the transmitter, but clocked at a slightly slower rate of 9.998 MHz, was used to phase modulate a 70 MHz carrier. A resolution of 0.1 μs was obtained with the measuring equipment. The rms delay spreads in the suburban mobile radio environments of New Jersey were in the order of 0.25 μs, while that in urban environment of New York City were computed to be in the order of 2 - 2.5 μs.

A summary of some applications of these channel sounding techniques, published in the literature, is presented in the next section.

2.2.5 Summary of some channel sounding experiments

Many mobile radio channel measurements have been carried out and published in the literature. Table 2.1 presents a summary of some of these measurements (Cox 1973a; Devasirvatham 1987; Saleh and Valenzuela 1987; Rappaport and McGillem 1988; Pahlavan, Ganesh et al. 1989; Rappaport 1989; Takeuchi, Sako et al. 1990; Davies, Bensebti et al. 1991; Devasirvatham 1991; Turkami, Demery et al. 1991; Huang and Khayata 1992; Seidel, Rappaport et al. 1992; Bultitude, Melancon et al. 1993; Hashemi 1993a; Sheikh and Hau 2002; Neves, Matos et al. 2009; Siamarou and Al-Nuaimi 2010; Kim, Konishi et al. 2014).

Table 2.1 Summary of a number of mobile radio channel measurements published in the literature.

Authors	Frequency Band	Channel Sounding Technique	Channel Parameters	Environment
Cox D.C., 1973a	910 MHz	Swept-time delay cross correlator channel sounding.	$\tau_{rms} = 2 - 2.5\ \mu s$.	Urban location. New York City.
Devasirvatham D.M.J., 1987	850 MHz	Spread spectrum sliding correlator channel sounding.	τ_{rms} = under 100 ns, for LOS. Maximum τ_{rms} = 250 ns.	Large office building.
Saleh A.A.M. and Valenzuela R.A., 1987	1.5 GHz	Direct RF pulse channel sounding.	Median τ_{rms} = 25 ns. Maximum τ_{rms} = 50 ns.	Medium-size office building.
Pahlavan K., Ganesh R., et al., 1989	910 MHz	Direct RF pulse channel sounding.	Median τ_{rms} = 15.3 - 52.6 ns. Maximum τ_{rms} = 40 – 152 ns.	Factory environments.
Rappaport T.S., 1989	1300 MHz	Direct RF pulse channel sounding.	τ_{rms} = 30 – 300 ns. Median τ_{rms} = 96 ns, for LOS. 105 ns, for NLOS.	Factory environments.
Takeuchi T., Sako M., et al., 1990	1.5 GHz	Spread spectrum sliding correlator channel sounding.	τ_{rms} = under 90 ns.	Laboratory room on the 4th floor of a six-storey isolated building in Japan.

Davies R., Bensebti M., et al., 1991	1.7 GHz and 60 GHz	Direct RF pulse channel sounding, used in the 1.7 GHz. Swept-time delay cross correlator channel sounding, used in the 60 GHz.	τ_{rms} = under 50 ns, for the RF pulse technique. Under 40 ns, for the cross-correlation technique.	Variety of indoor locations in and around Bristol University, UK.
Devasirvatham D.M.J., 1991	850 MHz, 1.9 GHz, 4.0 GHz and 5.8 GHz	Spread spectrum sliding correlator channel sounding.	τ_{rms} = under 120 ns.	Large commercial building in New York.
Turkmani A.M.D., Demery D.A., et al., 1991	900 MHz	Swept-time delay cross correlator channel sounding.	τ_{rms} = 0.1 - 6 μs.	Urban locations. City of Liverpool.
Huang C. and Khayata R., 1992	910 MHz, 2.44 GHz, and 5.8 GHz (ISM Bands)	Spread spectrum sliding correlator channel sounding.	τ_{rms} = under 100 ns.	Various buildings within Columbia University, New York.
Seidel S.Y., Rappaport T.S. et al., 1992	915 MHz and 1900 MHz	Direct RF pulse channel sounding.	Median τ_{rms} = 67 - 94 ns. Maximum τ_{rms} = 112 - 1470 ns.	Three dissimilar large office buildings.
Bultitude R.J.C., Melancon P., et al., 1993	950 MHz and 900-1100 MHz	Spread spectrum sliding correlator channel sounding, used in the 950 MHz. Swept-frequency channel sounding, used in the 900-1100 MHz.	static τ_{rms} = 69.7 ns, for the cross-correlation technique. static τ_{rms} = 69.2 ns, for the swept frequency technique.	Open office and along a corridor in a three-storey office building.
Hashemi H., 1993a	900-1300 MHz	Frequency domain channel sounding using vector network analyser.	τ_m = 20 – 30 ns. τ_{rms} = 10 – 50 ns.	Two dissimilar office buildings. Calgary, Alberta, Canada.
Sheikh A.U.H. and Hau S.F., 2002	1.8 GHz	Spread spectrum sliding correlator channel sounding.	τ_{rms} = 0.149 - 0.257 μs.	Urban locations. Hung Hom, Hong Kong.

Neves F.F., Matos L.J., et al., 2009	1.88 GHz	Swept-time delay cross correlator channel sounding.	τ_m = 2.13 μs. τ_{rms} =1.32 μs.	Mixed vegetated environments and University buildings. Rio de Janeiro, Brazil.
Siamarou A.G. and Al-Nuaimi M., 2010	57-64 GHz	Swept-frequency channel sounding.	static τ_{rms} = under 70 ns.	Various picocell environments in a University campus. Corridors and teaching rooms.
Kim M., Konishi Y., et al., 2014	11 GHz	MIMO channel sounding, transmitting an unmodulated multitone signal.	τ_{rms} = under 50 ns, for LOS. 20 ns, for NLOS.	Various indoor environments in a University building.

2.3 Signal Parameter Estimation Techniques

2.3.1 Overview

Parameter estimation algorithms can be classified into two main categories; namely non-parametric and parametric-based approaches (Kay and Marple 1981; Marple 1987; Kay 1988; Krim and Viberg 1996; Stoica and Moses 1997).

Non-parametric techniques are Fourier-based methods of providing spectral estimates where no prior model is assumed, in the sense that no assumptions are made concerning the physical process that generated a given data. They are also known as the classical methods of spectral estimation. Generally, these methods require very long sequences of stationary data in order to yield the necessary frequency resolution that is needed in many applications (Proakis 1990; Therrien 1992).

In this first category, the discrete Fourier transform (DFT) has been reported useful for resolving the constituent components in multipath fields (Richter and Al-Nuaimi 1995). Their fast Fourier transform (FFT) implementation provides reduced computational

time. Although this approach of signal parameter estimation is computationally efficient, it however has limited frequency resolution. If the arrival times of the multipath components are much closer than the reciprocal of the analysis bandwidth, then this Fourier-based technique is ineffective (Lau, Austin et al. 1987). Given a measurement bandwidth of 31.25 MHz for example, the shortest delay which could be resolved using the Fourier-based approach is 32 ns (Ndzi, Austin et al. 2000). Consequently, the Fourier-based methods are unable to resolve closely spaced multipath components that might have significant effects in indoor mobile radio channels. These methods also suffer from spectral leakage effects that often mask weak signals. Prominent conclusions from these non-parametric techniques are that there is always a compromise in the bias-variance trade-off because both of these errors cannot be minimised simultaneously (Kay 1988; Krim and Viberg 1996; Stoica and Moses 1997).

Parametric-based methods can however be very useful in extracting high-resolution estimates, especially in applications where short data records are available due to transient phenomena, provided the signal structure is known (Kay 1988; Proakis 1990). These techniques are also known as model-based methods of spectral estimation, where a generating model with known functional form is assumed. The parameters in the assumed model are then estimated, and a signal's spectral characteristics of interest derived from the estimated model. Therefore, the estimated spectral characteristics are only as good as the underlying model. However, the model order selection is a difficult problem in practice. Choosing a model order that is too low can result in poor resolution, while the choice of a model order that is too high can give rise to spurious components in the parameter estimates.

The parametric-based estimation technique is reviewed in this study. Examples of these parametric-based methods includes the autoregressive (AR) process model (comprising the Yule-Walker (Walker 1931; Stoica and Moses 1997) and least squares methods (Stoica and Moses 1997)), the moving average (MA) process model, as well as the combined autoregressive moving average (ARMA) process model (Gersh 1970; Kinkel, Perl et al. 1979; Beex and Scharf 1981; Cadzow 1982; Marple 1987; Kay 1988; Stoica

and Moses 1997). A further example, of these parametric-based methods, is the space-alternating generalized expectation-maximization (SAGE) algorithm (Fleury, Tschudin et al. 1999). The SAGE algorithm is an elongation of the expectation-maximization (EM) algorithm (Feder and Weinstein 1988). The EM algorithm is an iterative procedure used to compute a maximum likelihood estimate when an observed data is regarded as incomplete (Therrien 1992).

Another class of these parametric-based estimation methods is the subspace-based technique. This method, also known as high-resolution or super-resolution techniques, generate frequency component estimates of a given signal based on the decomposition of an observation vector space into two subspaces; one associated with the signal and another associated only with the noise (Marple 1987; Therrien 1992). Each noise vector is assumed to be uncorrelated with the signal vectors and among other noise vectors. Then the functions corresponding to the vectors in the signal or noise subspaces can be used to create frequency estimators which when plotted, indicate sharp peaks at the frequency locations of interest. Pisarenko harmonic decomposition (PHD) algorithm (Marple 1987; Kay 1988; Stoica and Nehorai 1988; Stoica and Moses 1997) was the first of these methods, which consequently spurred many improved methods such as the multiple signal classification (MUSIC) algorithm (Schmidt 1981; Schmidt 1986). Other examples of these subspace-based techniques include the minimum norm method (Kumaresan and Tufts 1983) and estimation of signal parameters by rotational invariance techniques (ESPRIT) method (Paulraj, Roy et al. 1985; Paulraj, Roy et al. 1986; Roy 1987; Roy and Kailath 1989).

In subsequent sections, brief descriptions of a number of these parametric estimators are presented.

2.3.2 Prony-based algorithm

The most simplest of the parametric estimation techniques is autoregressive modelling of a signal (Therrien 1992; Stoica and Moses 1997). The Prony algorithm is an autoregressive parametric estimation technique which models sampled data as a linear

combination of exponentials (Marple 1987; Hewitt, Lau et al. 1989). It is a technique that can be used for identifying the frequencies, amplitudes, and phases of a signal (Kay 1988).

For example, given the following multipath channel impulse response model (Hewitt, Lau et al. 1989; Hashemi 1993a; Vaughan and Andersen 2003):

$$h(t) = \sum_{i=1}^{K} \alpha_i \delta(t - \tau_i), \tag{2.8}$$

where K is the number of multipath components, α_i is the amplitude of the i^{th} path with τ_i as the corresponding delay, while $\delta(\cdot)$ is the Dirac delta function.

The Fourier transform of this channel impulse response is given by:

$$H(\omega) = \sum_{i=1}^{K} \alpha_i exp(-j\omega\tau_i), \tag{2.9}$$

where $H(\omega)$ is the channel transfer function. At discrete frequencies, the sampled transfer function is given by (Hewitt, Lau et al. 1989):

$$H_n = \sum_{i=1}^{K} \alpha_i exp(-j\omega_n\tau_i), \qquad n = 0,1,2,\cdots,N-1, \tag{2.10}$$

where $\omega_n = 2\pi f_n$ is the n^{th} sample of the angular frequency ω, and N is the total number of samples. For sampling uniformly in frequency, $\omega_n = \omega_0 + n\Delta\omega$ where $\Delta\omega$ is the angular frequency spacing in rad/s, while ω_0 is the lowest angular frequency. Hence

$$H_n = \sum_{i=1}^{K} \{\alpha_i exp(-j\omega_0\tau_i) exp(-jn\Delta\omega\tau_i)\}. \tag{2.11}$$

If $\alpha_i exp(-j\omega_0\tau_i)$ is represented as β_i and $exp(-j\Delta\omega\tau_i)$ is represented as z_i, then the

transfer function samples can be written as

$$H_n = \sum_{i=1}^{K} \beta_i z_i^n \,, \tag{2.12}$$

where β_i are now referred to as the complex amplitudes. If the weighted sums, with weights $\{\lambda_m\}$, is represented by S_n, then (Hewitt, Lau et al. 1989)

$$S_n = \sum_{m=0}^{K} \lambda_m H_{n-m} \,. \tag{2.13}$$

Equation (2.13) can be expanded as follows:

$$S_n = \sum_{i=1}^{K} \left\{ \beta_i z_i^{n-K} \sum_{m=0}^{K} \lambda_m z_i^{K-m} \right\}, \tag{2.14}$$

$$= \sum_{i=1}^{K} \left\{ \beta_i z_i^{n-K} P_K(z_i) \right\}, \tag{2.15}$$

where $P_K(z)$ is a polynomial whose coefficients are the weights $\{\lambda_m\}$, and has roots z_i, that is

$$P_K(z) = \prod_{i=1}^{K} (z - z_i) = \sum_{m=0}^{K} \lambda_m z^{K-m} \,. \tag{2.16}$$

This polynomial is referred to as the predictor polynomial. If $\lambda_0 = 1$ and the sums $S_n = 0$, then (2.13) can be rewritten as

$$H_n = -\sum_{m=1}^{K} \lambda_m H_{n-m} \,. \tag{2.17}$$

Equation (2.17) shows that the channel transfer function samples H_n have an autoregressive structure, in which each sample can be expressed as a weighted sum of its neighbours. This equation is called the forward predictor and it relates H_n to its preceding K components, where K is the order of this predictor and $\{\lambda_m\}$ are called the

autoregressive coefficients.

Using similar analysis, a backward predictor which associates H_n to its succeeding K components can be obtained; by taking the weighted sums of the complex conjugate of H_n as follows:

$$H_n^* = -\sum_{m=1}^{K} \lambda_m H_{n+m}^* \ . \tag{2.18}$$

This procedure, which provides a means of processing H_n in order to derive the amplitudes α_i and the respective delays τ_i of the multipath components, is known as the Prony algorithm.

This algorithm can be summarised as follows:

- The weights $\{\lambda_m\}$ are estimated using (2.17) and (2.18).
- The predictor polynomial $P_K(z)$ is factorised to obtain the roots z_i.
- The path delays τ_i are obtained from z_i.
- The complex amplitudes β_i are estimated from (2.11) and (2.12).
- The actual amplitudes α_i are then obtained from β_i.

The Prony algorithm is inherently nonlinear in that the output parameters α_i and τ_i are not linear functions of the input samples H_n (Hewitt, Lau et al. 1989).

This algorithm has been reported useful for extracting the delays and amplitudes of constituent components in multipath fields (Hewitt, Lau et al. 1989; Lau, Austin et al. 1991). Hewitt et al. (1989) showed that while the Prony algorithm has the ability to resolve rays much closer than the Fourier-based limit, it also has a tendency to yield biased estimates of delays and amplitudes. An improved version of the Prony algorithm, named “singular value decomposition followed by prony-type root recovery,” and often

referred to as singular value decomposition prony (SVDP), has been used to extract the delays of constituent components in multipath fields (Ndzi, Austin et al. 2000). This SVDP algorithm has been shown to achieve a resolution of better than 5 ns, for a measurement bandwidth of 31.25 MHz (Ndzi, Austin et al. 2000). However the SNR value, at which the resolution of better than 5 ns was achieved, could not be ascertained in this paper. The SVDP algorithm has also been used to provide angle of arrival (AoA) information (Street, Lukama et al. 2000; Lukama, Street et al. 2001).

2.3.3 Space-alternating generalized expectation-maximization algorithm

The space-alternating generalized expectation-maximization (SAGE) algorithm is a low-complexity generalisation of the expectation-maximization algorithm. The SAGE algorithm, which iteratively approximates the maximum likelihood estimator, has been successfully used to estimate impinging waves' parameters in mobile radio environments (Fleury, Dahlhaus et al. 1996; Pedersen, Fleury et al. 1997). This algorithm breaks down a multi-dimensional optimisation process, necessary to compute the estimates of the parameters of a wave, into several separate, low-dimensional maximisation procedures, which are performed sequentially. This reduces the computational cost and is at an advantage when compared to the MUSIC algorithm. Rather than estimating all the parameters of a wave simultaneously which might predicate a slow convergence and difficult maximisation, as in the case of the EM algorithm, the SAGE algorithm estimates the parameters of a wave sequentially (Fessler and Hero 1994; Fleury, Tschudin et al. 1999).

The algorithm uses the underlying statistical structure of a problem to replace difficult numerical maximizations with simpler maximizations. Details of the theoretical framework underlying the derivation of the SAGE algorithm are given in Fessler and Hero (1994), and in Fleury, Tschudin et al (1999).

Furthermore, this algorithm overpowers the resolution limitation inherent in the Fourier or beam-forming methods (Fleury, Tschudin et al. 1999). However, the SAGE algorithm

depends on the assumption that a finite known number of waves characterised by their propagation delay, complex amplitude, and azimuthal incidence direction are impinging in the neighbourhood of a receiver. Under-estimating the number of impinging waves can result in poor resolution, while over-estimation can give rise to spurious components in the parameter estimates. As a consequence, the SAGE algorithm makes use of classical information theoretic methods for model order selection like Akaike's and Rissanen criteria (Marple 1987; Kay 1988). In the SAGE algorithm, the number of impinging waves is often fixed to a value large enough to capture all prominent impinging waves before their parameter vectors can be estimated.

This algorithm has been used for joint delay and azimuth estimation in time-invariant environments (Fleury, Dahlhaus et al. 1996), as well as for joint delay, azimuth, and Doppler frequency estimation in time-variant environments (Pedersen, Fleury et al. 1997). The high-resolution capability, convergence rate, and accuracy of the scheme have been assessed in synthetic and real macro- and pico-cellular channels (Fleury, Tschudin et al. 1999). The results obtained indicate that the convergence rate of the SAGE algorithm is slightly slower when it is applied to real measurement data than when it is used with synthetic data. Additionally, Monte Carlo simulations in synthetic environments show that the scheme is able to easily separate impinging waves as soon as one of their parameters differ by more than approximately half the intrinsic resolution of the measuring equipment.

2.3.4 Multiple signal classification algorithm

The MUSIC algorithm is a noise subspace based frequency estimator. It uses the noise-subspace eigenvectors of the data correlation matrix to form a null spectrum, the minima of which iteratively yield the signal parameter estimates (Wong and Zoltowski 2000). The MUSIC sinusoidal frequency estimator and delay pseudo-spectrum algorithm are discussed in this section.

Starting with the following weighted spectral estimate (Proakis 1990):

$$P(f) = \sum_{k=p+1}^{M} w_k \left| \boldsymbol{s}^H(f) \boldsymbol{v}_k \right|^2 , \tag{2.19}$$

where $\{\boldsymbol{v}_k\}_{k=p+1,\ldots,M}$ are the eigenvectors in the noise subspace, M is the size of these eigenvectors, p is the size of the signal subspace, H is the Hermitian transpose operator, while $\{w_k\}$ are set of positive weights. $\boldsymbol{s}(f)$ is a vector of complex sinusoids given as

$$\boldsymbol{s}(f) = \left[1 \quad e^{j2\pi f} \quad e^{j4\pi f} \quad \ldots \quad e^{j2\pi(M-1)f} \right]^T . \tag{2.20}$$

At any of the sinusoidal frequency components, $f = f_i$,

$$P(f_i) = 0 , \qquad i = 1,2,\ldots, p . \tag{2.21}$$

It is shown that

$$\frac{1}{P(f)} = \frac{1}{\sum_{k=p+1}^{M} w_k \left| \boldsymbol{s}^H(f) \boldsymbol{v}_k \right|^2} \tag{2.22}$$

is a sharply peaked function of frequency and offers a method for estimating the frequencies of the sinusoidal components. Theoretically $1/P(f)$ is infinite at $f = f_i$, in practice however, this results in finite values for $1/P(f)$ at all frequencies.

The MUSIC sinusoidal frequency estimator proposed by Schmidt (1986) equates the weights $w_k = 1$ for all k, so that

$$P_{MUSIC}(f) = \frac{1}{\sum_{k=p+1}^{M} \left| \boldsymbol{s}^H(f) \boldsymbol{v}_k \right|^2} . \tag{2.23}$$

In the same fashion, MUSIC can be used to compute the time delays τ_i by observing the locations of the peaks in the MUSIC delay pseudo-spectrum (Lo, Litva et al. 1993);

$$P_{MUSIC}(\tau) = \frac{1}{\sum_{k=p+1}^{M} \left| \boldsymbol{s}^H(\tau) \boldsymbol{v}_k \right|^2}, \tag{2.24}$$

where

$$\boldsymbol{s}(\tau) = \begin{bmatrix} 1 & e^{-j\Delta\omega\tau} & e^{-j2\Delta\omega\tau} & \dots & e^{-j(M-1)\Delta\omega\tau} \end{bmatrix}^T. \tag{2.25}$$

This delay searching vector, $\boldsymbol{s}(\tau)$, is akin to the frequency searching vector, $\boldsymbol{s}(f)$. However, the Dirichlet kernels are functions of the time-delays τ_i and are in conjugate form. Hence, the MUSIC delay pseudo-spectrum is plotted as a function of the time-delays τ_i.

The MUSIC algorithm was initially used for azimuth estimation (Schmidt 1986; Kowalski, Geffert et al. 1991). The algorithm was later applied to time-delay estimation (Lo, Litva et al. 1993). Although MUSIC was the first of the high-resolution algorithms to accurately exploit the underlying data model of signals that are buried in noise, the algorithm often has several limitations. For example, a complete knowledge of the array manifold is needed, and the search over parameter space is computationally expensive. The MUSIC algorithm gives better resolution than the autoregressive or Prony methods (Marple 1987). A previous study of wideband radio propagation, using the spread spectrum sliding correlator channel sounder with an intrinsic delay resolution of 50 ns, shows that the MUSIC delay pseudo-spectrum degrades below 16 ns at an SNR of 30 dB (Mossammaparast 1999). In another study, the MUSIC algorithm has been shown to give acceptable performance at SNRs above 16 dB (Kay 1988).

A polynomial-rooting version of the MUSIC technique, known as "root-MUSIC," is known to have similar asymptotic properties as the original MUSIC algorithm (Krim and Viberg 1996). Moreover, this root-MUSIC technique is plagued by spurious roots which cause problems in identifying the actual roots corresponding to the true signals (Therrien 1992).

A new variation of the MUSIC algorithm known as the "*gold*-MUSIC" has been recently proposed for obtaining accurate results in various forms of array geometries where the MUSIC algorithm is applied (Rangarao and Venkatanarasimhan 2013). Though the results obtained from this new variant of the MUSIC algorithm shows that this technique has quick convergence and gives accurate results under different SNR conditions, however the *gold*-MUSIC and conventional MUSIC algorithm requires an accurate estimate of the number of signals.

2.3.5 Estimation of signal parameters by rotational invariance technique

Estimation of signal parameters by rotational invariance technique (ESPRIT) is an extension of the MUSIC algorithm (Roy and Kailath 1989). The ESPRIT algorithm uses two or more arrays that bear a translation invariance relationship with respect to each other and then exploits the underlying rotational invariance among the signal subspaces to solve a generalised eigenvalue equation. This algorithm has two variants; the original ESPRIT method (Paulraj, Roy et al. 1985; Roy, Paulraj et al. 1986), and a total least squares (TLS) version of the original technique (Roy and Kailath 1989). These two variants of ESPRIT are known to give similar asymptotic estimation accuracy (Krim and Viberg 1996). However, the TLS version has lower bias in the frequency estimates. ESPRIT exhibits significantly low computational complexity over the MUSIC algorithm (Roy and Kailath 1989) and produces estimates that are asymptotically unbiased (Paulraj, Roy et al. 1985; Therrien 1992; Stoica and Moses 1997).

2.3.6 Summary of some signal parameter estimation techniques

A number of published results in the literature presented different assumptions and simplications to the complexity of signal parameter estimation problems from many different points of view. The advantages and disadvantages of some of these signal parameter estimation techniques are summarised in Table 2.2 (Kumaresan and Tufts 1980; Kay and Marple 1981; Kumaresan and Tufts 1983; Sakai 1984; Paulraj, Roy et al. 1985; Kaveh and Barabell 1986; Roy, Paulraj et al. 1986; Schmidt 1986; Lau, Austin et al. 1987; Marple 1987; Kay 1988; Stoica and Nehorai 1988; Hewitt, Lau et al. 1989; Roy and Kailath 1989; Therrien 1992; Fleury, Dahlhaus et al. 1996; Krim and Viberg 1996; Saariiisaari 1997; Stoica and Moses 1997; Fleury, Tschudin et al. 1999; Cristescu, Ristaniemi et al. 2000; Pourkhaatoun, Zekavat et al. 2007; Pourkhaatoun and Zekavat 2011; Rangarao and Venkatanarasimhan 2013).

Table 2.2 A summary of the advantages, and disadvantages, of some signal parameter estimation techniques.

Method	Advantages	Disadvantages
Yule-Walker Algorithm (Kay and Marple 1981; Marple 1987; Kay 1988; Stoica and Nehorai 1988).	(1) Computationally efficient. (2) Produces better resolution than FFT-based methods.	(1) The model order needs to be specified in advance of the analysis. (2) Performs relatively poorly for short data records.
Least Squares Method (Kay and Marple 1981; Marple 1987; Kay 1988; Stoica and Moses 1997).	(1) Has superior performance than the Yule-Walker algorithm. (Marple 1987; Kay 1988; Stoica and Moses 1997). (2) Yield statistically stable spectral estimates (Kay 1988).	(1) The model order needs to be specified in advance of the analysis. (2) The resolution for low SNR signals is comparable to that obtained from FFT-based methods.
Pisarenko Harmonic Decomposition (Kay and Marple 1981; Sakai 1984; Stoica and Nehorai 1988; Therrien 1992).	Computationally efficient (Stoica and Moses 1997).	(1) The performance is poor at low SNRs (Kay 1988; Stoica and Moses 1997). (2) The model order needs to be specified in advance of the analysis.

Extended Prony Algorithm (Kay and Marple 1981; Marple 1987; Kay 1988).	(1) Parameter estimates are less biased than those obtained from the Pisarenko method. (2) Can resolve delays to better than half the Fourier limit (Hewitt, Lau et al. 1989).	(1) The model order needs to be specified in advance of the analysis. (2) Resolution degrades at low SNR scenarios (Kay 1988).
MUSIC Algorithm (Schmidt 1986).	(1) Has better resolution than Prony-based algorithm. (2) Yields asymptotically unbiased parameter estimates (Schmidt 1986; Roy and Kailath 1989; Krim and Viberg 1996).	(1) High computational burden. (2) The model order needs to be specified in advance of the analysis. (3) Fails to resolve closely spaced signals at low SNRs (Kumaresan and Tufts 1983; Kay 1988; Krim and Viberg 1996).
Minimum Norm (Kumaresan and Tufts 1983).	(1) Has lower computational cost, and better resolution, than the MUSIC algorithm (Kaveh and Barabell 1986; Krim and Viberg 1996; Stoica and Moses 1997). (2) Optimises the separation of the spurious roots in the root-MUSIC (Therrien 1992).	Exhibit spurious peaks, and merging of spectral peaks, at low SNR values (Kumaresan and Tufts 1983).
TLS-ESPRIT (Paulraj, Roy et al. 1985; Roy and Kailath 1989; Therrien 1992; Saariiisaari 1997).	(1) Produces less biased estimates (Therrien 1992). (2) More accurate than conventional ESPRIT. (3) Manifests superior performance than the Pisarenko and Minimum-Norm methods (Therrien 1992; Stoica and Moses 1997).	(1) Requires an accurate estimate of the number of impinging waves. (2) Has higher computational cost than conventional ESPRIT.
SAGE Algorithm (Fleury, Dahlhaus et al. 1996).	(1) Has lower computational cost than the MUSIC algorithm. (2) Yields better resolution than FFT-based approaches (Fleury, Tschudin et al. 1999).	The number of impinging waves needs to be specified in advance of the analysis.
Independent Component Analysis (Cristescu, Ristaniemi et al. 2000; Pourkhaatoun, Zekavat et al. 2007).	(1) Lower sensitivity to SNRs, number-of-paths, and bandwidth, when compared with the MUSIC algorithm (Pourkhaatoun, Zekavat et al. 2007). (2) Has lower computational cost than the MUSIC algorithm (Pourkhaatoun, Zekavat et al. 2007).	Requires proper selection of a cost function (Pourkhaatoun, Zekavat et al. 2007).

***gold*-MUSIC Algorithm** (Rangarao and Venkatanarasimhan 2013).	(1) Low sensitivity to different SNR conditions. (2) Has quick convergence.	*gold*-MUSIC and conventional MUSIC algorithm follows the same steps, until the isolation of the noise eigenvectors, which requires an accurate estimate of the number of signals.

Over the last three decades, the advent of multiscale signal analysis based on wavelets has received much attention (Mallat 1989b; Rioul and Vetterli 1991; Daubechies 1992; Nason and Silverman 1995; Kyriakopoulos and Parish 2010). Wavelets cannot only be used to analyse stationary signals but can also be used to decompose non-stationary, time-varying or transient signals.

The next section presents a review of wavelet analysis. It starts with an historical overview of wavelets, and then a description of the discrete wavelet transform (DWT) and discrete stationary wavelet transform (SWT). This is followed by a discussion on wavelet packet analysis. Finally, some applications of wavelet analysis are presented.

2.4 Wavelet Analysis

2.4.1 Overview

Section 2.3 has shown that signal analysts already have at their disposal an efficient arsenal of tools for signal processing applications. One of such tool is Fourier analysis. Fourier-based methods break down a signal into its constituent sinusoids. Usually, the information that cannot be seen in the time-domain can be obtained in the frequency domain. Moreover, in transforming a time-domain signal into frequency-domain, the time information is lost.

Most signals encountered in practice are time-domain in their raw format. Fourier analysis provides the frequency contents of a signal with no indication about the time information at which a frequency component occurs. This time information is not

required when the time-domain signal is stationary, since the frequency content does not change in time. The Fourier transform is however not a desirable technique to analyse non-stationary signals. Fourier transform can be used for non-stationary signals, only if the spectral components are to be determined. However, if the time interval at which a spectral component occurs in non-stationary signals is to be determined, then Fourier transform is not the correct transform to use. When the time localisation of the spectral components is required, a transform that gives the time-frequency representation (TFR) of the signal is needed.

An alteration of the Fourier transform to enable analysis of non-stationary signals is the short-time Fourier transform (STFT). The STFT segments a signal into short pieces by moving a time-localised window across the signal, and then computing the Fourier transform for every windowed (i.e. time-localised) segment of the signal. Consequently, the STFT maps a signal into a two-dimensional function of frequency and time, and provides a form of compromise between the frequency and time based views of a signal. It gives information about the frequency contents of a signal and when the signal event occurs. The tilings of the time-frequency plane for STFT (Vetterli and Herley 1992; Herley, Kovacevic et al. 1993), is shown in Fig. 2.5.

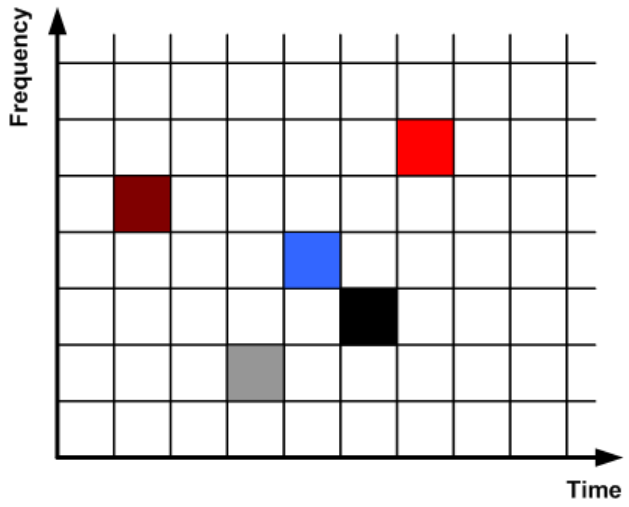

Figure 2.5 Tiling of the time-frequency plane for short-time Fourier transform.

These TFRs suffered from one major setback; once the size of a time window is chosen, this window shape remains the same in the entire analysis. STFT is able to analyse either high frequency components using narrow windows, resulting in good time resolution and poor frequency resolution, or low frequency components using wide windows giving poor time resolution and good frequency resolution. This technique is therefore not able to analyse signals that contain both slowly varying spectra and sharp transitions. The analysis of signals that exhibit short-duration high-frequency events and long-duration low-frequency events requires a windowing technique with variable-sized regions. The wavelet transform is a windowing technique of this type. These window functions are generated by dilation or compression of a prototype function. Many signals in practice require such a flexible approach, where the window size can be varied to ascertain more accurately either frequency or time. The underlying principles in wavelet analysis are presented in Appendix A.

This thesis explores the novel use of wavelet analysis as a post-processing technique to parameterise the multipath radio channel with a high-resolution. Wavelet analysis is a development of applied mathematics introduced in the 1980s (Mallat 1989a; Mallat 1989b). It evolved from earlier developments in Harmonic analysis. The tiling of the time-frequency plane for wavelet transform is shown in Fig. 2.6 (Vetterli and Herley 1992; Herley, Kovacevic et al. 1993).

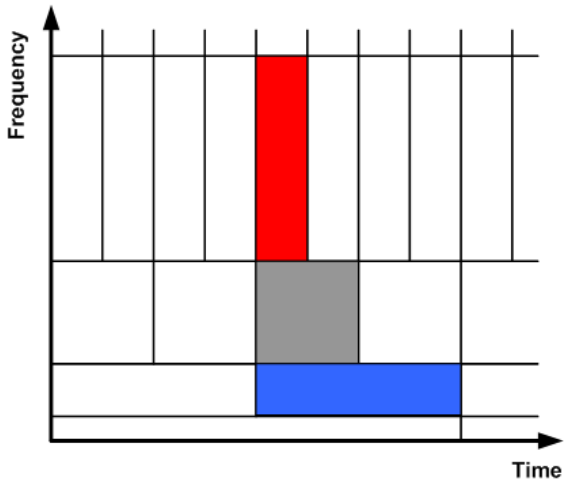

Figure 2.6 Tiling of the time-frequency plane for wavelet transform.

All the tiles in this case trade-off frequency resolution for time resolution and vice versa. Though the widths and heights of these tiles change, their area is constant. Each tile constitutes an equal portion of the time-frequency plane, but provides different ratios to time and frequency. At low frequencies, the height of the tilings are shorter corresponding to better frequency resolution, while their widths are longer corresponding to poor time resolution. At high frequencies however, the height of the tilings increases corresponding to poor frequency resolution, while their width decreases corresponding to good time resolution.

The wavelet transform of discrete-time signals can be discrete wavelet transform (DWT) or discrete stationary wavelet transform (SWT). The DWT and SWT procedure are discussed in the next section.

2.4.2 DWT versus SWT

In order to obtain the DWT, the parameters a and b in (1.1) are discretised (Daubechies 1992). The DWT of a discrete signal can also be obtained by iteratively applying low-pass and high-pass filters (Mallat 1989b; Mallat 1999), as shown in Fig. 2.7.

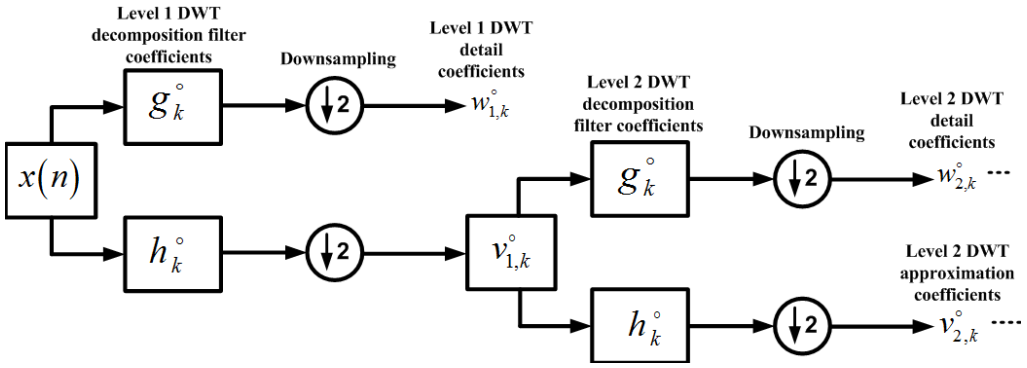

Figure 2.7 The discrete wavelet transform procedure.

In Fig. 2.7, the signal $x(n)$ to be analysed is passed through a high-pass filter with coefficients g_k° and a low-pass filter with coefficients h_k°, which splits this signal into two distinct subbands. The filter output is downsampled by two through discarding of

every other sample and therefore eliminating half of the original signal samples. This forms one level of decomposition. The output signal at this first level is represented by $v^{\circ}_{1,k}$, the approximation coefficients, and $w^{\circ}_{1,k}$, the corresponding detail coefficients. The symbol $\downarrow 2$ represents the downsampling operation.

Each decomposition level halves the time resolution of the input signal, but doubles the frequency resolution. The frequencies that are most prominent in the input signal appears as high amplitude wavelet coefficients in that region of the DWT that has those frequencies. While the frequency bands that are not outstanding in the original signal will have small amplitude wavelet coefficients, and this part of the DWT can be discarded without any vital loss of information; thus providing data reduction. This procedure is also known as subband coding (Ramchandran, Vetterli et al. 1996; Strang and Nguyen 1997; Akansu and Haddad 2001).

A well-known setback of the DWT is their sensitivity to translations (Liang and Parks 1996; Pesquet, Krim et al. 1996). That is, the DWT of a translated version of a signal is not the same as the translation of the DWT of the original signal (Percival and Walden 2000). This is as a result of the downsampling operation in the DWT, since downsampling is not a time-invariant operation (Strang and Nguyen 1997). This causes misalignments between features in a signal and features in a wavelet basis (Coifman and Donoho 1995). In order to reinstate the translation invariance, the stationary wavelet transform (SWT) is used (Nason and Silverman 1995).

The discrete stationary wavelet transform has been referred to in the wavelet literature under different names such as the shift invariant DWT (Beylkin 1992), the translation invariant DWT (Liang and Parks 1996), the time invariant DWT (Pesquet, Krim et al. 1996), and non-decimated DWT (Bruce and Gao 1996a).

In SWT, appropriate low-pass and high-pass filters are applied on a given signal to produce the approximation and detail coefficients, at the next level, without decimation such that the two new sequences each have the same length as the original signal. The

level 1 approximation coefficients is then applied to the upsampled versions of the level 1 decomposition filters, to produce the level 2 approximation and detail coefficients. This procedure is shown in Fig. 2.8, where $g_{j,k}$ are the decomposition high-pass filter coefficients, while $h_{j,k}$ are the decomposition low-pass filter coefficients. The levels of the SWT are denoted by j, while k are the translations of the wavelets at each level. The approximation coefficients are represented by $v_{j,k}$, and the detail coefficients by $w_{j,k}$.

Since shift-invariance is a desired property in feature extraction and detection applications, therefore the SWT is applied in this study to parameterise the multipath radio channel, in order to accurately detect the time-delays and number of multipath components.

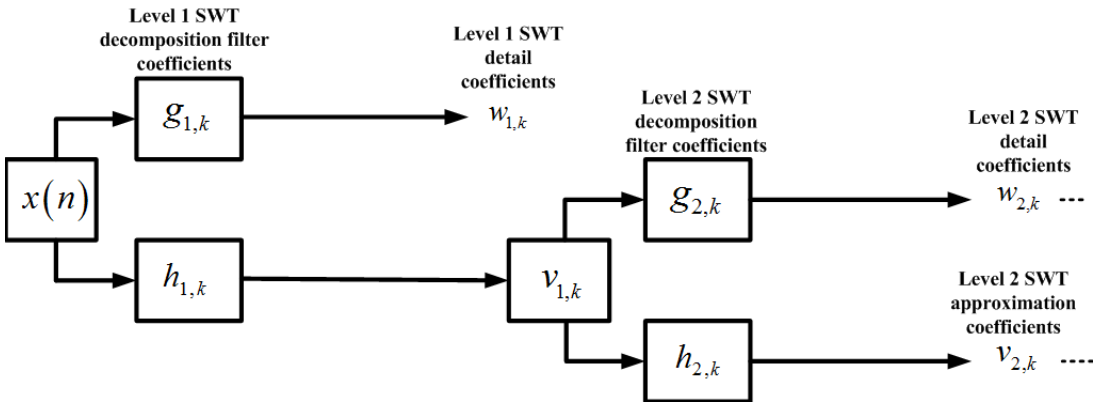

Figure 2.8 The stationary wavelet transform procedure.

2.4.3 Wavelet packet analysis

A well-known extension of wavelets and the DWT is wavelet packets (Wickerhauser 1994; Ramchandran, Vetterli et al. 1996; Percival and Walden 2000; Jensen and Cour-Harbo 2001). Wavelet packet analysis is a generalisation of wavelet analysis giving a richer decomposition procedure.

In the conventional wavelet decomposition paradigm, such as shown in Figs. 2.7 and 2.8, the generic step is to split the approximation coefficients into two parts. After splitting, another set of approximation coefficients and the detail coefficients are obtained at a coarser scale. Then, the next step consists in breaking up the new approximation coefficients; successive detail coefficients are not re-analysed. In the wavelet packet case, the detail coefficients are also decomposed into two parts using similar procedure as in the approximation coefficients splitting.

The wavelet packet transform (WPT) decomposition tree is shown in Fig. 2.9, where the symbols $\downarrow 2$, g_k^o, h_k^o, $w_{j,k}^o$ and $v_{j,k}^o$, are as defined in Fig. 2.7. The successive detail and approximation coefficients, resulting from splitting the detail coefficients, are denoted by $gw_{j,k}^\circ$ and $gv_{j,k}^\circ$ respectively.

Though this algorithm gives richer signal analysis, it however introduces higher complexities when compared with the conventional wavelet decomposition procedure (Coifman, Meyer et al. 1990; Coifman and Wickerhauser 1992; Daubechies 1992).

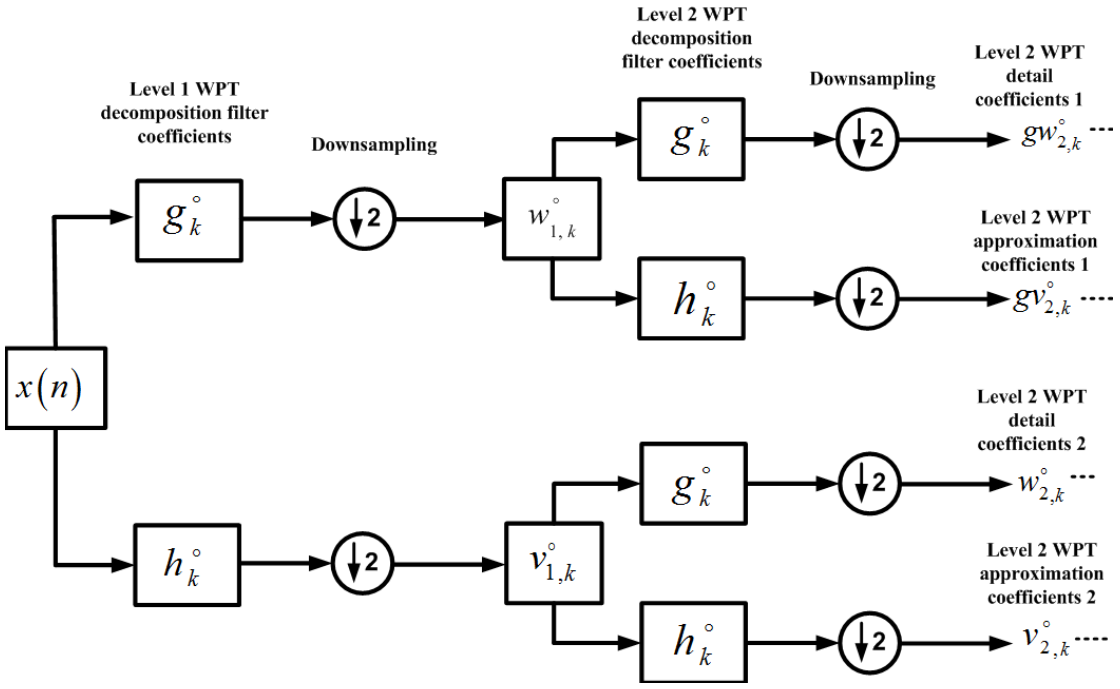

Figure 2.9 The wavelet packet transform decomposition tree.

2.4.4 Applications of wavelets

Wavelets have been used in a large number of fields; such as acoustics (Guillemain and Kronland-Martinet 1996), speech (Ramchandran, Vetterli et al. 1996), image processing (Mallat 1996), communication systems (Hetling, Medley et al. 1994; Wickert and Ionescu 1996; Wornell 1996; Ionescu and Wickert 1997; Quinquis and Boulinguez 1997; Akansu, Duhamel et al. 1998; Newlin 1998), astronomy (Bijaoui, Slezak et al. 1996), physics (Farge, Kevlahan et al. 1996), and biology (Unser and Aldroubi 1996).

Common utilisation of wavelets are related to data denoising (Donoho and Johnstone 1994; Coifman and Donoho 1995; Donoho and Johnstone 1995; Ainsleigh and Chui 1996), compression (Mallat 1989a; Mallat 1989b; Mallat 1996), feature extraction (Polikar, Greer et al. 1997), and discontinuity detection (Mallat 1991; Mallat and Hwang 1992).

Wavelets have been used in biomedical engineering for the analysis of electrocardiogram (ECG), i.e. electrical activity of the heart, for diagnosing cardiovascular disorders (Unser and Aldroubi 1996). It has also been used in the analysis of electroencephalogram (EEG), i.e. electrical activity of the brain, for diagnosing neurophysiological disorders such as epileptic seizure detection and Alzheimer disease (Unser and Aldroubi 1996; Polikar, Greer et al. 1997). Wavelets have been used, by the US Federal Bureau of Investigation (FBI), for digitised fingerprints compressions (Bradley and Brislawn 1994).

Wavelet packets have been used to improve the temporal resolution of underwater acoustic signals (Quinquis and Boulinguez 1997). In this experiment, arrays of sensors that receive PSK signals emitted by several sources were analysed. The transmitter and receiver system were situated in the Mediterranean Sea, and the closely-spaced acoustic ray paths resolved in order to determine their arrival times. The signals received by the sensors were sampled at 1600 Hz. They are then demodulated, filtered by a matched filter and subsampled at 400 Hz. A resolution of 10 ms was achieved. The results obtained with wavelet packets showed an improvement in resolution over the MUSIC

algorithm. However, the improvement in resolution obtained is unclear in this paper. Also although the closely spaced rays (i.e. those separated by less than 10 ms) are resolved in this experiment, the number of ray arrivals could not be precisely ascertained from the paper.

In another experiment, the performance of a wavelet in probing a multipath channel has been investigated (Wickert and Ionescu 1996). In this scheme, a properly shaped isolated pulse, having sufficient energy, is transmitted through a multipath channel. The demodulation process is assumed to be coherent. Wavelet analysis is then applied to decompose the noisy superposition of the delayed and attenuated versions of the transmitted pulse. The parameters of interest to be estimated are the attenuation factors and delay times of the different paths. Although the results obtained in the paper demonstrate the use of wavelets in multipath estimation, the resolution obtained is unclear in this paper. Also, the problem of translation sensitivity inherent in the conventional wavelet decomposition procedure (Liang and Parks 1996; Pesquet, Krim et al. 1996) was not adequately tackled.

Some areas of mathematics, science, and engineering that have contributed to the development of wavelets are shown in Fig. 2.10.

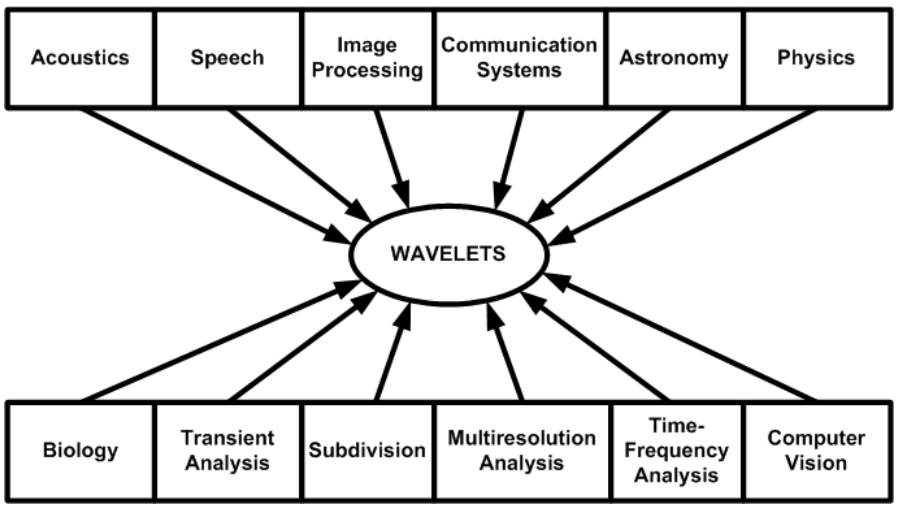

Figure 2.10 Some areas of mathematics, science, and engineering where wavelets have been used.

2.5 Summary

In this chapter, a survey of wideband channel sounding techniques and conventional signal parameter estimation algorithms has been presented.

The chapter began with a review of the operation, advantages, disadvantages, and applications of channel sounders used for wideband channel measurements. The wideband channel sounding techniques, surveyed, are generally classified as direct RF pulse channel sounding, spread spectrum sliding correlation channel sounding, and frequency domain measurements. This is then followed by a review of the conventional digital signal processing algorithms that are often used for signal parameter estimations. These parameter estimation algorithms are categorised as non-parametric and parametric-based techniques. The advantages and limitations of these signal parameter estimation algorithms were examined. It has been shown that the parametric-based methods can be very useful in extracting high-resolution estimates, especially in applications where short data records are available, provided the signal structure is known. However, the model order selection is often a difficult problem in most of these parametric-based methods.

An alternative high-resolution digital signal processing algorithm, based on wavelet analysis, is researched in this study. Therefore, an overview of wavelet analysis, the discrete wavelet transform, stationary wavelet transform, and wavelet packet analysis have been carried out. The justification for applying the stationary wavelet transform in this research, to parameterise the multipath channel, has been shown. Finally, the chapter concludes with a review of some applications of wavelet analysis, and the many areas of engineering, science, and mathematics that have led to the development of wavelets.

CHAPTER 3

PROPOSED ALGORITHM FOR MULTIPATH CHANNEL PARAMETER ESTIMATION

3.1 Introduction

As discussed in Section 2.1, a digital signal processing algorithm may be used to assist in resolving the multiple ray paths that are otherwise not individually identifiable for the purpose of mobile radio channel modelling. This chapter presents the development of a novel high-resolution digital signal processing algorithm, for use in resolving these multiple ray paths. This algorithm incorporates a novel wavelet family matched to the triangular output waveforms of the sliding correlator channel sounder, discussed in Section 2.2.4.

The chapter starts with the design procedure for customised mother wavelets, for use in this study. Since the determination of mobile radio channel parameters is usually impaired in the presence of noise, therefore, strategies that can be used in reducing noise through the use of wavelet analysis are shown next. These noise reduction schemes start with an investigation of how additive white Gaussian noise (AWGN) can influence the wavelet transform coefficients. This is followed by a presentation of the proposed noise reduction strategies. The SWT procedure, discussed in Section 2.4.2, has been applied in these schemes. Finally, this chapter concludes with the derivation of a novel amplitude

estimation algorithm, which can be used in estimating the amplitudes of the individual multipath components in synthetic mobile radio environments.

3.2 Building a Customised Wavelet

3.2.1 Desired signal model

The signal waveform at the receiver of the sliding correlator channel sounder, utilised as a reference for this study, can be generally modelled as follows:

$$y(t) = \sum_{i=1}^{K} \alpha_{ic}\, p(t-\tau_i) + \eta(t), \tag{3.1}$$

where $p(t-\tau_i)$ has a triangular shape, delayed by τ_i, formed from the correlation of the receiver and transmitter pseudo-random binary sequence. K represents the number of paths, α_{ic} denotes the complex amplitude of the i^{th} path, while $\eta(t)$ is the AWGN.

Now assuming that $K=1$, as in LOS transmissions, then the received signal $y(t)$ takes the form of a single triangle with a base width that is twice the chip clock period of the transmit PRBS. In this study, the clock period of the transmit PRBS is taken to be 50 ns. Therefore the actual base width of the output signal waveform is 100 ns. That is after accounting for the apparent dilation of the horizontal axis time scale caused by the sliding factor of the channel sounder. An example of a test signal profile containing a single path, without noise, is shown in Fig. 3.1. The peak amplitude of this triangular waveform has been assumed to be 1.0 V in this study. This research proposes to make use of the stationary wavelet transform to identify the peaks of each triangular waveform, thereby separating the individual propagation paths.

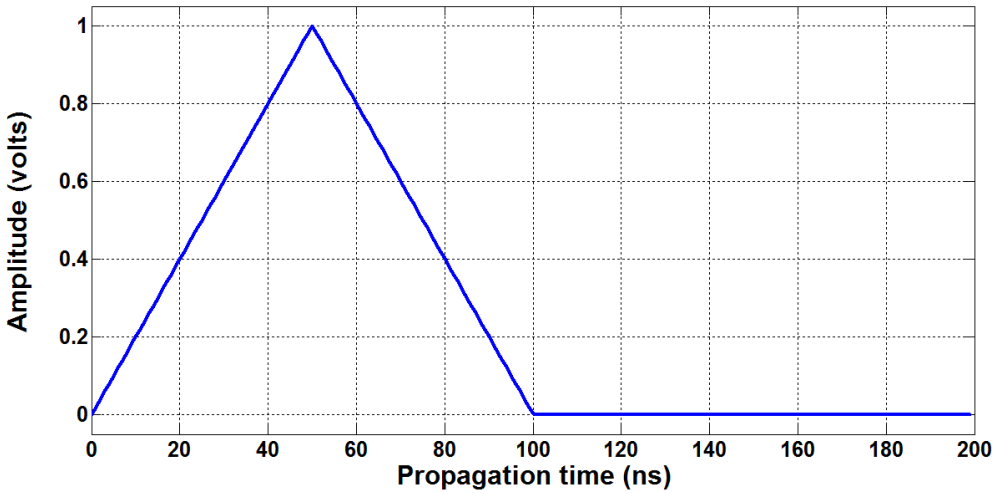

Figure 3.1 Simulated one-path test signal profile without noise.

In wavelet transform domain, the signal $y(t) \in V_j$ is projected into two subspaces V_{j+1} and W_{j+1}, where V_j and W_j are the approximation and detail spaces respectively at the j^{th} resolution level. The nesting of these subspaces is discussed in Section A.3 of Appendix A. The detail space W_j has basis functions $\{\psi_{j,k}(t)\}_{j\in\mathbb{Z},k\in\mathbb{Z}}$, called wavelets (Debnath 2003). These basis functions are translates and dilates of a prototype function, $\psi(t)$, known as the mother wavelet.

Generally, the best mother wavelet to use for a particular application depends on the nature of the signal to be analysed, as well as what is required from the analysis. For the single-path profile, shown in Fig. 3.1, the triangular waveform has discontinuities in the first derivative. A discontinuity in the first derivative can be detected by wavelets having at least 4 coefficients (Strang and Nguyen 1997). The discontinuity at time $t = 50\,ns$, i.e. the waveform peak, provides the time-delay information associated with each propagation path. A wavelet function is desirable in this study, therefore, if it matches the triangular waveform simulated in Fig. 3.1 and has filters with at least 4 coefficients.

The next section presents the design of customised mother wavelets for this research, to detect the peaks of the individual paths in a multipath delay profile, by use of finite-

duration impulse response (FIR) digital filter design technique (Oppenheim and Willsky 1997; Hayes 1999; Pollock 1999; Smith 1999; Smith 2003). One way of designing such a filter is by judicious placement of its zeros on the z-plane (Pollock 1999).

3.2.2 Novel wavelet design

As shown in the previous section, i.e. Section 3.2.1, a wavelet function of interest for this study must detect the peak of the triangular waveform shown in Fig. 3.1. Such a wavelet must also have linear phase effects (Hayes 1999; Pollock 1999).

A linear-phase condition can be defined as when (McClellan and Parks 1973; Hayes 1999):

$$h(n) = h(N-1-n), \quad n = 0,1,\ldots,N-1, \tag{3.2}$$

where $h(n)$ is the impulse response of an FIR filter with N number of coefficients. The z-transform of $h(n)$ becomes

$$H(z) = \sum_{n=0}^{N-1} h(n) z^{-n}, \tag{3.3}$$

where z is the z-transform variable. The transfer function, $H(z)$, can be expressed in terms of its zeros as

$$H(z) = \prod_{i=1}^{N} (z - z_i), \tag{3.4}$$

where z_i are the zeros of this FIR filter. In polynomial form (Smith 1999; Smith 2003):

$$H(z) = h_0 + h_1 z^{-1} + h_2 z^{-2} + h_3 z^{-3} + \cdots + h_N z^{-N}, \tag{3.5}$$

where $h_0, h_1, h_2, \cdots, h_N$ are the filter coefficients.

The impulse response of the filter can then be written in terms of the following transform pair (Oppenheim and Willsky 1997):

$$\delta(n+n_0) \Leftrightarrow z^{n_0}, \tag{3.6}$$

where $\Leftrightarrow$ denotes two way implications of the z-transform pair. Therefore,

$$h(n) = h_0\delta(n) + h_1\delta(n-1) + h_2\delta(n-2) + \cdots + h_N\delta(n-N). \tag{3.7}$$

For positive symmetry $h(n) = h(N-1-n)$, while for negative symmetry $h(n) = -h(N-1-n)$ (McClellan and Parks 1973; Hayes 1999). In this study, an FIR filter with odd length and positive symmetry is considered desirable. Three possible cases for such a symmetric wavelet filter, with at least 5 coefficients, are considered as follows:

Case 1

Starting with a single isolated triangular waveform, such as shown in Fig. 3.1, having the following scaling coefficients:

$$h_0 = 0,\ h_1 = 0.5,\ h_2 = 1,\ h_3 = 0.5,\ h_4 = 0.$$

Substituting these scaling coefficients into (3.5) gives the transfer function of the resulting low-pass FIR filter, in polynomial form, as

$$H(z) = 0.5z^{-1} + z^{-2} + 0.5z^{-3}. \tag{3.8}$$

Using (3.7), the impulse response of the low-pass filter is derived as

$$h(n) = 0.5\delta(n-1) + \delta(n-2) + 0.5\delta(n-3). \tag{3.9}$$

The corresponding high-pass filter coefficients are given by

$$g_k = (-1)^k h_{4-k}, \tag{3.10}$$

where

$$\sum_{k=0}^{4} g_k = 0, \tag{3.11}$$

as required for a wavelet. Equation (3.10) is known as the quadrature mirror filter relation (Strang and Nguyen 1997). Therefore

$$g_0 = 0,\ g_1 = -0.5,\ g_2 = 1.0,\ g_3 = -0.5,\ g_4 = 0.$$

The impulse response of the high-pass filter can then be written as

$$g(n) = -0.5\delta(n-1) + \delta(n-2) - 0.5\delta(n-3). \tag{3.12}$$

The mother wavelet, corresponding to the derived high-pass filter coefficients, is referred to as "Pathlet 5." This is because the number of coefficients associated with the low-pass and high-pass filters is 5. Pathlet 5 scaling function and mother wavelet is shown in Fig. 3.2. This scaling function approximates the triangular waveform in Fig. 3.1.

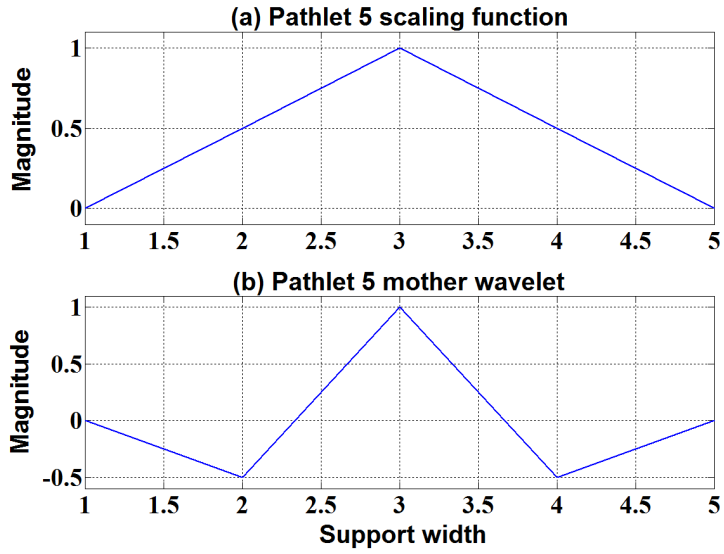

Figure 3.2 Plots of Pathlet 5 scaling function and mother wavelet.

The low-pass and high-pass filter coefficients satisfy the following single-shift orthogonality constraints:

$$\sum_{k=0}^{4} h_k g_{k-1} = 0, \tag{3.13}$$

$$\sum_{k=0}^{4} g_k h_{k-1} = 0. \tag{3.14}$$

The constraints in (3.13) and (3.14) leads to the single-shift orthogonality of the scaling function $\varphi(t)$ and the generated mother wavelet $\psi(t)$, defined as follows

$$\langle \varphi(t), \psi(t-1) \rangle = 0, \tag{3.15}$$

where $\langle \cdot\ ,\ \cdot \rangle$ denotes inner product operation. The maximum norm $\| \cdot \|_{\max}$ of h_k and g_k is unity, defined as

$$\begin{aligned} \|h_k\|_{\max} &= \max\{|h_k| : k = 0, \ldots 4\} \\ \|g_k\|_{\max} &= \max\{|g_k| : k = 0, \ldots 4\} \end{aligned}. \tag{3.16}$$

Case 2

In this case, the kernel function generated in case 1 is dilated to produce a new set of symmetric high-pass filter coefficients given by

$$g_0 = 0,\ g_1 = -0.1667,\ g_2 = -0.3333,\ g_3 = 1.0,\ g_4 = -0.3333,\ g_5 = -0.1667,\ g_6 = 0.$$

where

$$\sum_{k=0}^{6} g_k = 0. \tag{3.17}$$

The impulse response of this high-pass filter is then

$$g(n) = -0.1667\delta(n-1) - 0.3333\delta(n-2) + \delta(n-3) - 0.3333\delta(n-4) - 0.1667\delta(n-5). \quad (3.18)$$

Using the quadrature mirror filter relation, then the corresponding low-pass filter coefficients are given by

$$h_k = (-1)^k g_{6-k}. \quad (3.19)$$

Therefore

$$h_0 = 0,\ h_1 = 0.1667,\ h_2 = -0.3333,\ h_3 = -1.0,\ h_4 = -0.3333,\ h_5 = 0.1667,\ h_6 = 0.$$

This gives the impulse response of the low-pass filter as

$$h(n) = 0.1667\delta(n-1) - 0.3333\delta(n-2) - \delta(n-3) - 0.3333\delta(n-4) + 0.1667\delta(n-5). \quad (3.20)$$

These low-pass and high-pass filter coefficients also satisfy the single-shift orthogonality constraints. Therefore

$$h_1 g_0 + h_2 g_1 + h_3 g_2 + h_4 g_3 + h_5 g_4 + h_6 g_5 = 0, \quad (3.21)$$

and

$$\begin{aligned} \|h_k\|_{\max} &= \max\{|h_k| : k = 0,\ldots 6\} = 1 \\ \|g_k\|_{\max} &= \max\{|g_k| : k = 0,\ldots 6\} = 1 \end{aligned}. \quad (3.22)$$

The new mother wavelet generated in this case is referred to as “Pathlet 7,” because the number of coefficients associated with the low-pass and high-pass filters is 7. Pathlet 7 scaling function and mother wavelet is shown in Fig. 3.3.

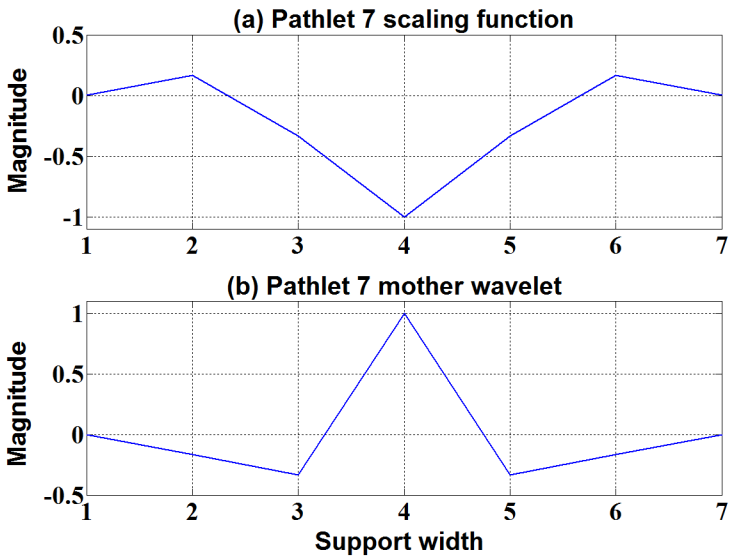

Figure 3.3 Plots of Pathlet 7 scaling function and mother wavelet.

Case 3

For this 3rd case, the kernel function generated in case 2 is dilated to produce another set of symmetric high-pass filter coefficients given by

$$g_0 = 0,\ g_1 = -0.08333,\ g_2 = -0.1667,\ g_3 = -0.25,\ g_4 = 1.0,$$
$$g_5 = -0.25,\ g_6 = -0.1667,\ g_7 = -0.08333,\ g_8 = 0,$$

such that

$$\sum_{k=0}^{8} g_k = 0. \tag{3.23}$$

Now the impulse response of this high-pass filter is then

$$g(n) = -0.08333\delta(n-1) - 0.1667\delta(n-2) - 0.25\delta(n-3) + \delta(n-4)$$
$$- 0.25\delta(n-5) - 0.1667\delta(n-6) - 0.08333\delta(n-7). \tag{3.24}$$

The corresponding low-pass filter coefficients, derived from the quadrature mirror filter relation, are

$$h_0 = 0,\ h_1 = 0.08333,\ h_2 = -0.1667,\ h_3 = 0.25,\ h_4 = 1.0,\ h_5 = 0.25,$$
$$h_6 = -0.1667,\ h_7 = 0.08333,\ h_8 = 0.$$

The impulse response of this low-pass filter is therfore

$$h(n) = 0.08333\delta(n-1) - 0.1667\delta(n-2) + 0.25\delta(n-3) + \delta(n-4) + 0.25\delta(n-5) - 0.1667\delta(n-6) + 0.08333\delta(n-7). \quad (3.25)$$

The mother wavelet generated is referred to as "Pathlet 9." Pathlet 9 scaling function and mother wavelet is shown in Fig. 3.4. This wavelet system also satisfy the single-shift orthogonality constraints, hence

$$h_1 g_0 + h_2 g_1 + h_3 g_2 + h_4 g_3 + h_5 g_4 + h_6 g_5 + h_7 g_6 + h_8 g_7 = 0, \quad (3.26)$$

and

$$\begin{aligned} \|h_k\|_{\max} &= \max\{|h_k| : k = 0,\ldots 8\} = 1 \\ \|g_k\|_{\max} &= \max\{|g_k| : k = 0,\ldots 8\} = 1 \end{aligned}. \quad (3.27)$$

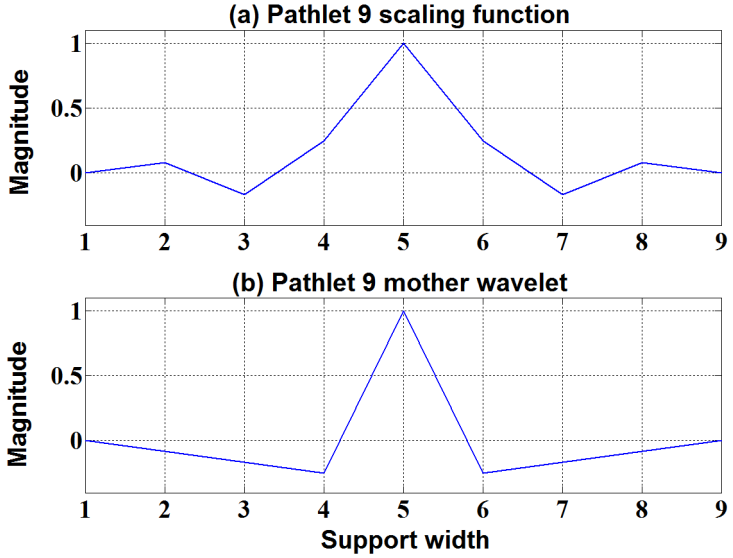

Figure 3.4 Plots of Pathlet 9 scaling function and mother wavelet.

Wavelets with compact support (in time), for high-resolution time-delay estimation, is essential for this study. Therefore, further dilations of the kernel function in case 3 to produce new set of high-pass filter coefficients are not considered suitable for use. The wavelet family generated, in cases 1-3, is referred to as "Pathlets" in this research.

The Pathlet wavelet family has the following properties:

1. Compact support.
2. Linear-phase filters.
3. Triangular (or near triangular) shapes.

Series of computer simulations are presented in Chapter 4, to demonstrate the performance of this new wavelet family in resolving the constituent components in multipath delay profiles. The stationary wavelet transform has been adopted in these simulations. The positive peaks in the SWT detail coefficients are used to provide information about the time-delays and number of propagation paths.

3.3 Noise Reduction Techniques

3.3.1 Noise analysis

Noise is an undesirable signal that disrupts the processing or communication of an information-bearing signal. It is one of the constraining factors in measurement systems. The ability to characterise and model the noise process, and also use the noise characteristics advantageously to distinguish a wanted signal from noise, is of paramount importance in any noise reduction technique. This section investigates how AWGN can influence the wavelet transform coefficients, using Pathlets 5, 7, 9, and a member of Daubechies' least-asymmetric wavelet family known as Symlet 2, as the analysing wavelets. Symlet 2 has been chosen for comparison with Pathlets, in these analyses, because Daubechies' least-asymmetric wavelets have near linear-phase filters and are compactly supported (Daubechies 1992; Mallat 1999; Tang, Yang et al. 2000). This wavelet family is more symmetric than the Daubechies' extremal phase wavelets.

The Daubechies' extremal phase filter coefficients are derived in Appendix B. Linear-phase filters and wavelets with compact support are some of the desired properties in the wavelets derived for use in this research, as discussed in Sections 3.2.1 and 3.2.2.

The decomposition low-pass and high-pass filter coefficients of Pathlets and Symlet 2, used in this study, are tabulated in Table 3.1. The maximum norm of Symlet 2 decomposition filter coefficients has been set to be unity, defined according to (3.16), so that a fair comparison can be made with Pathlets.

Table 3.1 Decomposition low-pass and high-pass filter coefficients of Pathlets 5, 7, 9, and Symlet 2.

Wavelet type	**Low-pass filter coefficients**	**High-pass filter coefficients**
Pathlet 5	0, 0.5, 1.0, 0.5, 0	0, -0.5, 1.0, -0.5, 0
Pathlet 7	0, 0.1667, -0.3333, -1.0, -0.3333, 0.1667, 0	0, -0.1667, -0.3333, 1.0, -0.3333, -0.1667, 0
Pathlet 9	0, 0.08333, -0.1667, 0.25, 1.0, 0.25, -0.1667, 0.08333, 0	0, -0.08333, -0.1667, -0.25, 1.0, -0.25, -0.1667, -0.08333, 0
Symlet 2	0.5774, 1.0, 0.2679, -0.1547	-0.1547, -0.2679, 1.0, -0.5774

Expressing the noisy signal, given in (3.1), as

$$y_N(n) = x_N(n) + \eta_N(n), \qquad n = 0,1,\ldots,N-1, \tag{3.28}$$

where $x_N(n)$ is the noiseless signal of interest, $\eta_N(n)$ is additive white Gaussian noise with an rms value of σ_η, while N is the length of the signal. This noisy signal $y_N(n)$ is assumed to be without band-limitations. The signal-to-noise ratio (SNR) is defined by

$$SNR = 20\log_{10}(\rho/\upsilon), \tag{3.29}$$

where ρ is the peak amplitude of a single triangular waveform set to be 1.0 V, taken to be the reference path in this study, while υ denotes the noise level.

Since the wavelet transform is a linear transformation, therefore the noisy signal $y_N(n)$ can be decomposed into wavelet transform domain as follows:

$$\langle \boldsymbol{y}, \boldsymbol{g} \rangle = \langle \boldsymbol{x}, \boldsymbol{g} \rangle + \langle \boldsymbol{\eta}, \boldsymbol{g} \rangle, \tag{3.30}$$

$$d_{j,k} = w_{j,k} + e_{j,k}, \qquad j = 1, 2, \ldots, J, \quad k = 0, 1, \ldots, N_j - 1, \tag{3.31}$$

where $\langle \cdot , \cdot \rangle$ is the inner product operation, while $d_{j,k}$, $w_{j,k}$, and $e_{j,k}$ are used to represent the wavelet transform detail coefficients of $y_N(n)$, $x_N(n)$, and $\eta_N(n)$, respectively, at the k^{th} coordinates and j^{th} level of wavelet transform. J represents the coarsest resolution level, $\boldsymbol{g}$ is the vector of the decomposition high-pass filter coefficients, while $\boldsymbol{y}$, $\boldsymbol{x}$, and $\boldsymbol{\eta}$ are vectors of $y_N(n)$, $x_N(n)$, and $\eta_N(n)$ respectively. N_j is the total number of samples at the j^{th} level.

The transform coefficients $d_{j,k}$, $w_{j,k}$, and $e_{j,k}$ are given by (Chidume 2003)

$$d_{j,k} = y_0 g_0 + y_1 g_1 + y_2 g_2 + \cdots + y_{N_j - 1} g_{N_j - 1}, \tag{3.32}$$

$$w_{j,k} = x_0 g_0 + x_1 g_1 + x_2 g_2 + \cdots + x_{N_j - 1} g_{N_j - 1}, \tag{3.33}$$

$$e_{j,k} = \eta_0 g_0 + \eta_1 g_1 + \eta_2 g_2 + \cdots + \eta_{N_j - 1} g_{N_j - 1}, \tag{3.34}$$

where $y_0, y_1, \ldots, y_{N_j - 1}$, $x_0, x_1, \ldots, x_{N_j - 1}$, $\eta_0, \eta_1, \ldots, \eta_{N_j - 1}$, and $g_0, g_1, \ldots, g_{N_j - 1}$ are elements of $\boldsymbol{y}$, $\boldsymbol{x}$, $\boldsymbol{\eta}$, and $\boldsymbol{g}$ respectively. In (3.34), the wavelet filter coefficients $g_0, g_1, \ldots, g_{N_j - 1}$ transform the noise source $\eta_N(n)$ into a new equivalent noise. Since the wavelet transform of the AWGN is also white and Gaussian distributed in the wavelet domain (Mallat and Hwang 1992; Debnath 2003), hence the detail coefficients,

$e_{j,k}$, are Gaussian random variables with a new standard deviation. When Pathlet 5 is used as the analysing wavelet, for example, then (3.34) becomes

$$e_{1,2} = \eta_0 g_0 + \eta_1 g_1 + \eta_2 g_2 + \eta_3 g_3 + \eta_4 g_4, \tag{3.35}$$

$$= -0.5\eta_1 + \eta_2 - 0.5\eta_3, \tag{3.36}$$

where $g_0 = 0$, $g_1 = -0.5$, $g_2 = 1.0$, $g_3 = -0.5$, $g_4 = 0$, $e_{1,2}$ is the wavelet transform coefficient at $j = 1$ and $k = 2$, while η_1, η_2, and η_3 are Gaussian random variables. This new noise term can be rewritten as

$$E = X + Y + Z, \tag{3.37}$$

where $E = e_{1,2}$, $X = -0.5\eta_1$, $Y = \eta_2$, and $Z = -0.5\eta_3$ are uncorrelated Gaussian random variables (Percival and Walden 2000). Their characteristic functions, $\Phi_\kappa(\omega)$, are defined as (Papoulis and Pillai 2002; Leon-Garcia 2008):

$$\Phi_\kappa(\omega) = \exp\left\{ j\xi_\kappa \omega - 0.5\sigma_\kappa^2 \omega^2 \right\}, \tag{3.38}$$

where κ can be E, X, Y, or Z random variable. ξ_κ and σ_κ^2 are the mean and variance respectively of the random variables. Hence

$$\Phi_X(\omega) = \Phi_{\eta_1}(-0.5\omega), \tag{3.39}$$

$$= \exp\left\{ -j0.5\xi_{\eta_1}\omega - 0.125\sigma_{\eta_1}^2 \omega^2 \right\}. \tag{3.40}$$

$$\Phi_Y(\omega) = \Phi_{\eta_2}(\omega), \tag{3.41}$$

$$= \exp\left\{ j\xi_{\eta_2}\omega - 0.5\sigma_{\eta_2}^2 \omega^2 \right\}. \tag{3.42}$$

$$\Phi_Z(\omega) = \Phi_{\eta_3}(-0.5\omega), \tag{3.43}$$

$$= \exp\left\{ -j0.5\xi_{\eta_3}\omega - 0.125\sigma_{\eta_3}^2 \omega^2 \right\}. \tag{3.44}$$

The joint characteristic function, $\Phi_E(\omega)$, of these random variables is given by (Papoulis and Pillai 2002):

$$\Phi_E(\omega) = \Phi_X(\omega) \times \Phi_Y(\omega) \times \Phi_Z(\omega), \tag{3.45}$$

$$= \exp\left\{ j\omega\left(-0.5\xi_{\eta_1} + \xi_{\eta_2} - 0.5\xi_{\eta_3}\right) - 0.5\omega^2\left(0.25\sigma_{\eta_1}^2 + \sigma_{\eta_2}^2 + 0.25\sigma_{\eta_3}^2\right)\right\}. \tag{3.46}$$

Comparing (3.38) and (3.46) gives

$$\xi_E = -0.5\xi_{\eta_1} + \xi_{\eta_2} - 0.5\xi_{\eta_3}, \tag{3.47}$$

$$\sigma_E^2 = 0.25\sigma_{\eta_1}^2 + \sigma_{\eta_2}^2 + 0.25\sigma_{\eta_3}^2. \tag{3.48}$$

If the original noise source, $\eta_N(n)$, has zero mean and variance of σ_η^2, then (3.47) and (3.48) become

$$\xi_E = 0, \tag{3.49}$$

$$\sigma_E^2 = 1.5\sigma_\eta^2. \tag{3.50}$$

The probability density function (PDF), $f_E(e)$, of the new Gaussian random variable E, is given by (Harris and Ledwidge 1974; Leon-Garcia 2008)

$$f_E(e) = \frac{1}{\sigma_E\sqrt{2\pi}} \exp\left[-\frac{(e-\xi_E)^2}{2\sigma_E^2}\right], \tag{3.51}$$

$$= \frac{1}{\sigma_E\sqrt{2\pi}} \exp\left[-\frac{e^2}{2\sigma_E^2}\right]. \tag{3.52}$$

By definition, the cumulative distribution function (CDF) $F_E(e)$, of E, is given by (Yates and Goodman 2005; Leon-Garcia 2008)

$$F_E(e) = \int_{-\infty}^{e} f_E(\gamma)\, d\gamma, \tag{3.53}$$

where $F_E(e)$ = probability that $E \le e$, $\quad e \in \mathbb{R}$.

Therefore

$$F_E(e) = \frac{1}{\sigma_E\sqrt{2\pi}} \int_{-\infty}^{e} \exp\left[-\frac{\gamma^2}{2\sigma_E^2}\right] d\gamma. \tag{3.54}$$

Let

$$\vartheta = \frac{\gamma}{\sigma_E}. \tag{3.55}$$

Then

$$d\gamma = \sigma_E d\vartheta. \tag{3.56}$$

Substituting (3.56) into (3.54) gives

$$F_E(e) = \frac{1}{\sqrt{2\pi}} \int_{-\infty}^{(e/\sigma_E)} \exp\left[-\frac{\vartheta^2}{2}\right] d\vartheta, \tag{3.57}$$

$$= 0.3989 \left\{ \int_{-\infty}^{0} \exp\left[-\frac{\vartheta^2}{2}\right] d\vartheta + \int_{0}^{(e/\sigma_E)} \exp\left[-\frac{\vartheta^2}{2}\right] d\vartheta \right\}, \tag{3.58}$$

$$= 0.3989 \left\{ 1.2533 + 1.2533\ erf\left[0.7071 \left(\frac{e}{\sigma_E} \right) \right] \right\}, \tag{3.59}$$

$$= 0.5 + 0.5\ erf\left[0.7071 \left(\frac{e}{\sigma_E} \right) \right]. \tag{3.60}$$

But from (3.50),

$$\sigma_E = 1.2248 \sigma_\eta. \tag{3.61}$$

Substituting (3.61) into (3.60) gives

$$F_E(e) = 0.5 + 0.5\ erf\left[0.7071 \left(\frac{e}{1.2248\sigma_\eta} \right) \right], \tag{3.62}$$

$$= 0.5 + 0.5\ erf\left[0.5773 \left(\frac{e}{\sigma_\eta} \right) \right], \tag{3.63}$$

where σ_η is the rms of the original AWGN source. Following similar procedure from (3.35) to (3.50) for Pathlet 5, but using the high-pass filter coefficients given in Table 3.1 for Pathlets 7, 9, and Symlet 2, then new equivalent noise variances have been derived as follows:

$$\sigma_Q^2 = 1.278 \sigma_\eta^2, \tag{3.64}$$

$$\sigma_R^2 = 1.1947 \sigma_\eta^2, \tag{3.65}$$

$$\sigma_U^2 = 1.4292\sigma_\eta^2. \tag{3.66}$$

Where σ_Q^2, σ_R^2, and σ_U^2 denote the variance of the new equivalent noise, using Pathlets 7, 9, and Symlet 2 respectively. σ_Q, σ_R, and σ_U are the corresponding rms values. Their CDFs are given by

$$F_Q(q) = 0.5 + 0.5\ erf\left[0.6255\left(\frac{q}{\sigma_\eta}\right)\right], \qquad q \in \mathbb{R}. \tag{3.67}$$

$$F_R(r) = 0.5 + 0.5\ erf\left[0.6469\left(\frac{r}{\sigma_\eta}\right)\right], \qquad r \in \mathbb{R}. \tag{3.68}$$

$$F_U(u) = 0.5 + 0.5\ erf\left[0.5915\left(\frac{u}{\sigma_\eta}\right)\right], \qquad u \in \mathbb{R}. \tag{3.69}$$

Let

$$F_S^c(s) = 1 - F_S(s), \qquad s \in \mathbb{R}, \tag{3.70}$$

where S can be the E, Q, R, or U random variable. Then, $F_S^c(s)$ = probability that $S > s$.

Equations (3.50), (3.64), (3.65), and (3.66) indicate that the variance σ_η^2 of the original noise source has been increased by factors of 1.5, 1.3, 1.2, and 1.4 after the wavelet analysis. Pathlets 5, 7, 9, and Symlet 2 respectively have been used as the analysing wavelets. The change in noise level, in dB, after wavelet transform is given in Table 3.2. The results show that Pathlet 5 is the least robust to noise, while Pathlet 9 is the most robust to noise, followed by Pathlet 7, and then Symlet 2.

Since the rms of the original AWGN source, i.e. σ_η, is usually unknown apriori in practice, then the estimates of σ_η can be determined as follows:

$$\hat{\sigma}_E = \frac{std\{d_{1,k}\}}{1.2248}, \qquad k = 0,1,\ldots,N-1, \tag{3.71}$$

$$\hat{\sigma}_Q = \frac{std\{d_{1,k}\}}{1.1305}, \tag{3.72}$$

$$\hat{\sigma}_R = \frac{std\{d_{1,k}\}}{1.093}, \tag{3.73}$$

$$\hat{\sigma}_U = \frac{std\{d_{1,k}\}}{1.1955}, \tag{3.74}$$

where $d_{1,k}$ are the SWT level 1 detail coefficients of the signal being analysed, while $std\{d_{1,k}\}$ denotes the standard deviation of $d_{1,k}$. $\hat{\sigma}_E$, $\hat{\sigma}_Q$, $\hat{\sigma}_R$, and $\hat{\sigma}_U$ are estimates of σ_η using Pathlets 5, 7, 9, and Symlet 2 respectively as the analysing wavelets.

Table 3.2 Values of the variance of the equivalent noise, and corresponding change in noise level in dB, derived from the wavelet analysis of a given noise source. Pathlets 5, 7, 9, and Symlet 2, are used as the analysing wavelets.

Wavelet type	**Original noise variance**	**New equivalent noise variance**	**Change in noise level (dB)**
Pathlet 5	σ_η^2	$1.5\sigma_\eta^2$	1.8
Pathlet 7	σ_η^2	$1.278\sigma_\eta^2$	1.1
Pathlet 9	σ_η^2	$1.1947\sigma_\eta^2$	0.8
Symlet 2	σ_η^2	$1.4292\sigma_\eta^2$	1.6

Computer simulation of an AWGN source, but with rms $\sigma_\eta = 0.05633$, is shown in Fig. 3.5 (a). The new equivalent noise after wavelet transform is shown in Figs. 3.5 (b-d); these are the level 1 detail coefficients. The results show that the rms σ_η of the original noise source has been increased approximately by factors of 1.23, 1.13, 1.09, and 1.20 after wavelet analysis using Pathlets 5, 7, 9, and Symlet 2 respectively. This increment is in agreement with the previous derivations in (3.50), (3.64), (3.65), and (3.66).

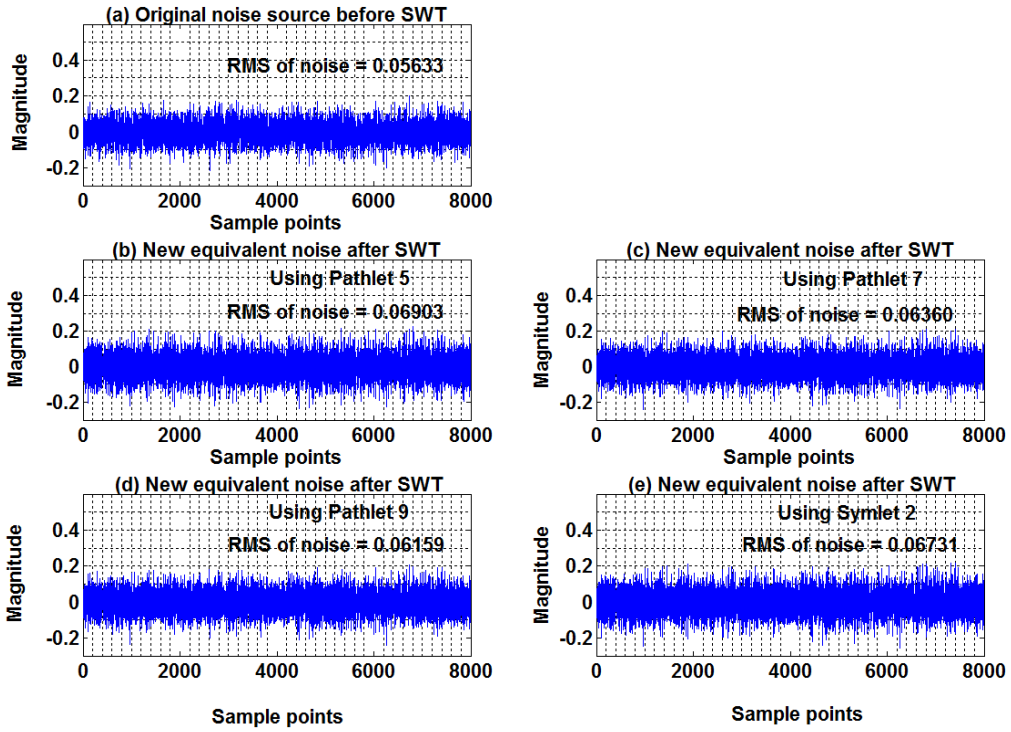

Figure 3.5 A simulated AWGN source before SWT and the equivalent noise after SWT, using Pathlets 5, 7, 9, and Symlet 2 as analysing wavelets.

The probability plots of the primary noise source and the transformed noise, for input SNR in the range 10-30 dB, has been derived in Fig. 3.6. These probability plots were derived using (3.70), for $F_S^c(0.15)$. These graphs show the probability distribution of the Gaussian random variable S, for magnitude greater than a noise threshold of $\Upsilon = 0.15$, and corresponding SNRs. The noise threshold has been arbitrarily chosen as a test threshold for use in this study.

These plots show that the probability of $S > \Upsilon$ is greatest when the equivalent noise derived with Pathlet 5 is used. This is followed by Symlet 2 equivalent noise, Pathlet 7 equivalent noise, Pathlet 9 equivalent noise, and then the primary noise source. These results are again in general agreement with the derivations in (3.50), (3.64), (3.65), and (3.66). It shows that Pathlet 9 is the most robust to noise in these analyses.

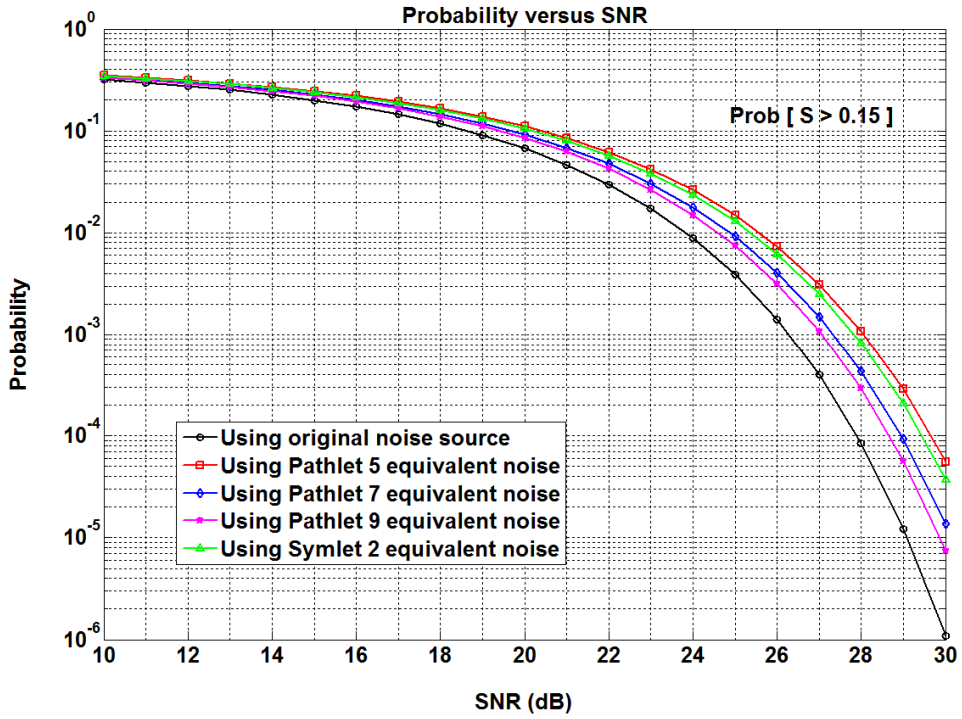

Figure 3.6 Probability plots of the equivalent noise derived with Pathlets 5, 7, 9, and Symlet 2, and the original noise source. For SNR range 10-30 dB.

3.3.2 Denoising using wavelet thresholding

In practice, the wavelet analysis of a noise corrupted signal may produce many undesirable wavelet transform coefficients attributed to noise, most especially at low SNRs, making it difficult to differentiate the wanted coefficients from the spurious ones. In order to remove the unwanted coefficients, noise needs to be suppressed.

One way to filter-out noise is through wavelet-based denoising by thresholding (Donoho and Johnstone 1994; Coifman and Donoho 1995; Donoho and Johnstone 1995). In this scheme, noise is removed from a signal as effectively as possible while preserving the signal features of interest. This is accomplished by selecting a wavelet that can be used to represent the signal features of interest, and performing a decomposition of the signal using the selected wavelet function. The resulting wavelet transform coefficients are then thresholded to remove those coefficients associated with noise while preserving those that are required to describe the signal of interest. Two well-known thresholding

procedures are the hard and soft thresholding techniques (Percival and Walden 2000; Jansen 2001). These thresholding schemes are discussed in Appendix C.

Since the noise variance σ^2 is unknown apriori, as in the case of applications, a procedure from the literature used to estimate this is based on the median absolute deviation (MAD) standard deviation estimate of noise (Percival and Walden 2000). This standard deviation estimator is defined, using the SWT, as follows;

$$\hat{\sigma}_{(mad)} = \frac{median\left\{\left|d_{1,0}\right|,\left|d_{1,1}\right|,\ldots,\left|d_{1,N-1}\right|\right\}}{0.6745}, \tag{3.75}$$

where $d_{1,0}, d_{1,1}, \ldots, d_{1,N-1}$ are used to represent the SWT level 1 detail coefficients of the signal to be analysed. N is the total number of detail coefficients. The factor 0.6745 in the denominator rescales the numerator so that $\hat{\sigma}_{(mad)}$ is a desirable estimator for the standard deviation of Gaussian white noise (Percival and Walden 2000). The level 1 detail coefficients, $d_{1,0}, d_{1,1}, \ldots, d_{1,N-1}$, are used to determine the noise variance σ^2 since these coefficients are mostly noise dominated, with the exception of few large values attributed to the signal of interest. Consequently, the variance of $d_{1,0}, d_{1,1}, \ldots, d_{1,N-1}$ would be mainly attributed to noise rather than to the wanted signal.

An estimate of the noise threshold, $\hat{\Upsilon}$, is then computed, using the universal noise threshold algorithm (Percival and Walden 2000; Jansen 2001), defined as

$$\hat{\Upsilon} = \hat{\sigma}_{(mad)}\sqrt{2\log N}\,. \tag{3.76}$$

This noise reduction procedure involves the following steps:

1. The noisy signal $y_N(n)$ is transformed into wavelet transform domain, as shown in (3.31).

2. A noise threshold level Υ is estimated by using (3.76).

3. After specifying the noise threshold value Υ, the noisy detail coefficients with values exceeding Υ in magnitude are left untouched while those coefficients with magnitude less than or equal to Υ are all set to zero. The detail coefficients $O_{j,k}$, after thresholding, are given by

$$O_{j,k} = \begin{cases} 0 & |d_{j,k}| \le \Upsilon \\ d_{j,k} & |d_{j,k}| > \Upsilon \end{cases}. \tag{3.77}$$

This procedure is known as hard thresholding. This thresholding technique is known to provide improved signal-to-noise ratio when compared with soft thresholding method (Resnikoff and Wells 1998; Ma, Zhou et al. 2002).

4. The denoised detail coefficients, $O_{j,k}$, are then used to determine the number of paths and time-delays in the noise corrupted signal profile.

3.3.3 Denoising using SWT multilevel products

This section describes a scheme for suppressing noise by exploiting the stationary wavelet transform multiscale dependencies. In this scheme, the adjacent stationary wavelet transform subbands are multiplied to form multiscale products where the features evolving with high magnitude across the SWT decomposition levels are amplified while the noise is diluted. This technique is referred to in this study as the "stationary wavelet transform multilevel products (SWTMP)."

As shown in the discussions in Sections 2.4.2, 2.4.3, and A.3, there exist dependencies between the wavelet transform coefficients. Denoising by wavelet thresholding, discussed in Section 3.3.2, describes an efficient way to reduce noise but it takes little or no advantage of the multiscale dependencies between the wavelet transform coefficients. In Fig. 3.7, the SWT detail coefficients at the first six resolution levels, for a sequence of

AWGN source, are illustrated. Pathlet 5 has been used as the analysing wavelet. Note that the local maxima in the detail coefficients rapidly decays across these six levels due to increased smoothing (Mallat and Zhong 1992; Mallat and Hwang 1992), in accordance with the multiscale decomposition given in (A.18). Mallat and Hwang (1992) observed that for the Gaussian white noise, the average number of local maxima at resolution level $j+1$ is half that at level j. The rms value of this AWGN source and that of the SWT levels 1-4 detail coefficients are shown in Fig. 3.8. These rms values are in general agreement with the previous derivations in Table 3.2.

Given the observations in Fig. 3.7, it is then expected that multiplying these SWT detail coefficients across adjacent levels would dilute the noise. Since the positive values of the detail coefficients are of interest in this study, therefore the first four resolution levels with the negative coefficients discarded are shown in Figs. 3.9 (b-e). The multilevel products, for Figs. 3.9 (b-e), are shown in Figs. 3.10 (b-e). The results from the multilevel products show that the original noise level in Fig. 3.10 (a) has been suppressed.

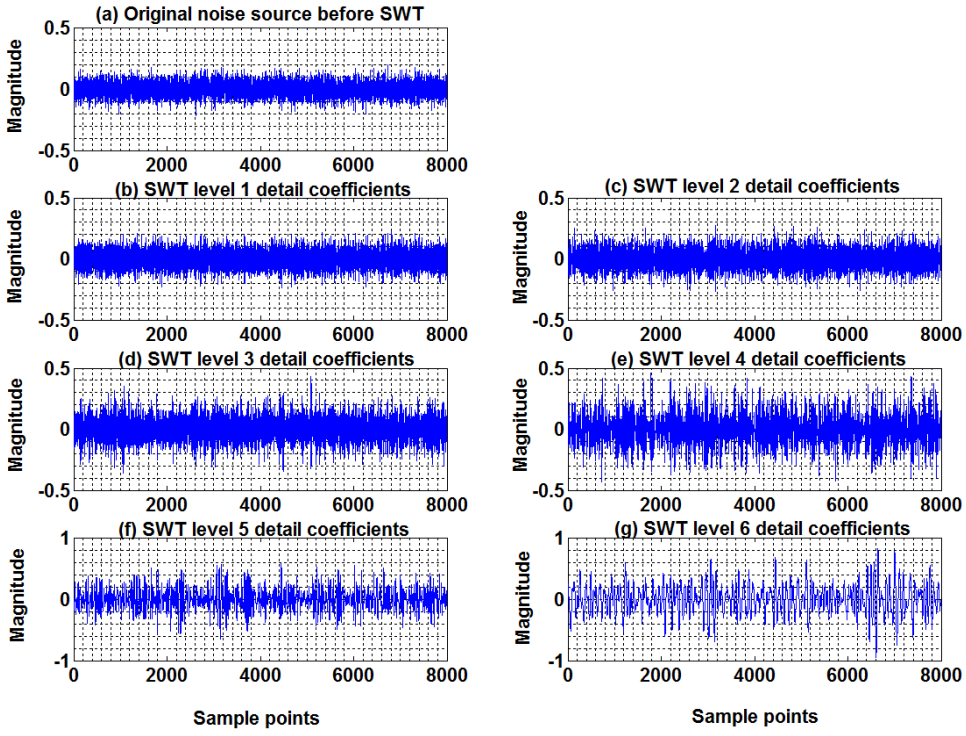

Figure 3.7 A simulated AWGN source and the SWT levels 1-6 detail coefficients, using Pathlet 5 as the analysing wavelet.

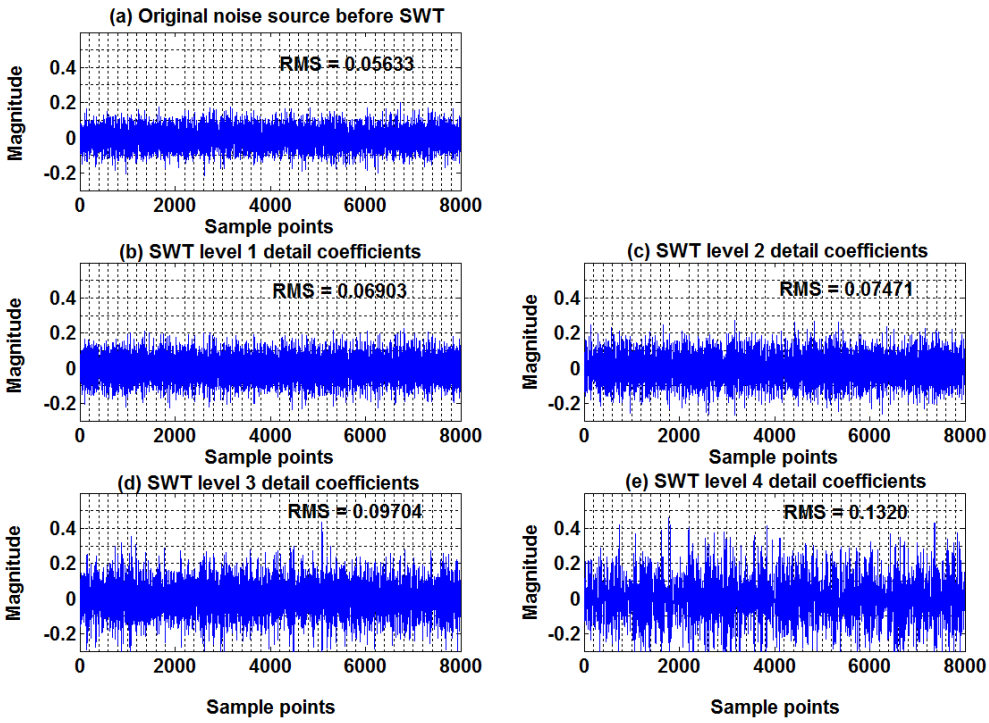

Figure 3.8 A simulated AWGN source and the SWT levels 1-4 detail coefficients, using Pathlet 5 as the analysing wavelet.

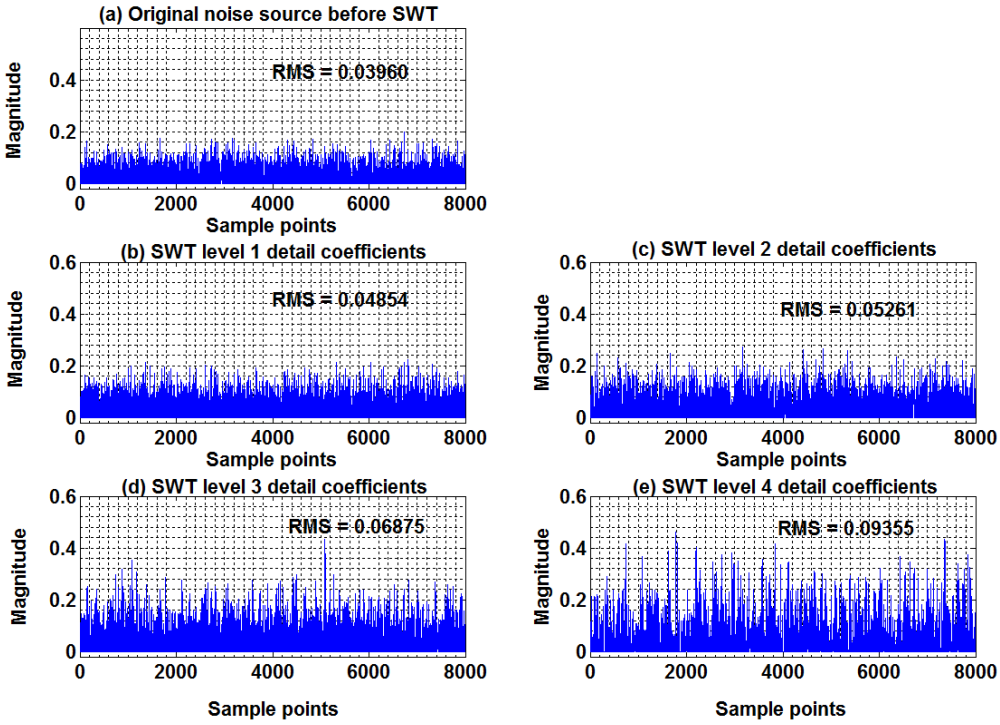

Figure 3.9 The simulated noise source in Fig. 3.8 and the SWT levels 1-4 detail coefficients, with the negative values discarded.

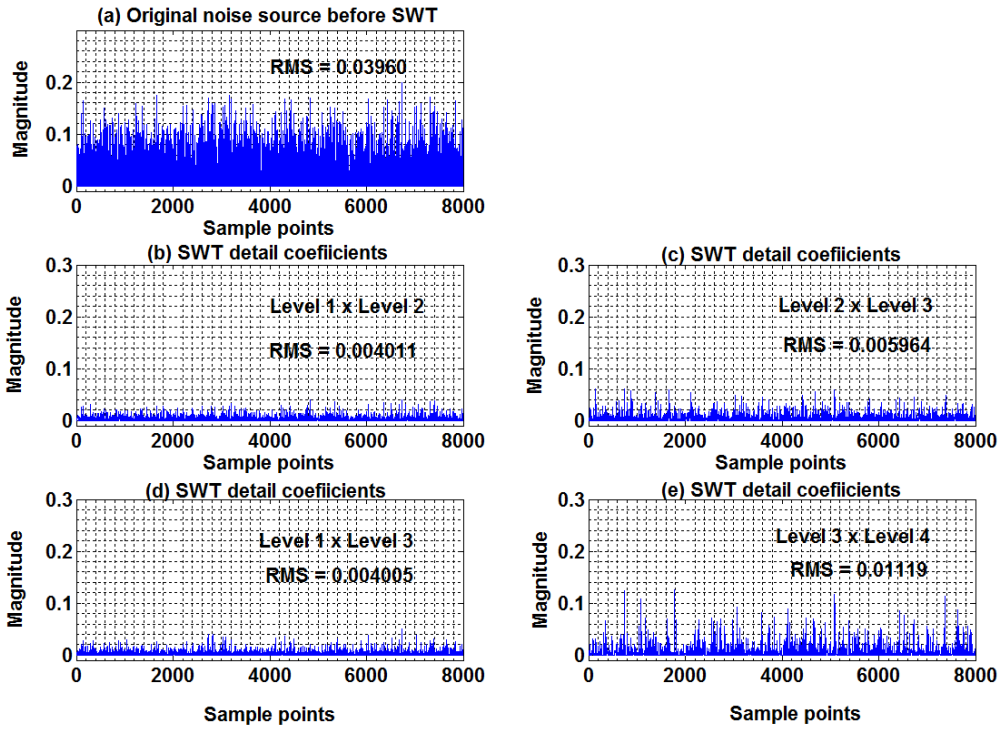

Figure 3.10 The stationary wavelet transform multilevel products (SWTMP) for Fig. 3.9, using Pathlet 5 as the analysing wavelet.

In Fig. 3.11, the SWT detail coefficients at the first four resolution levels, for a simulated noiseless test signal with four paths, are illustrated. Pathlet 5 has again been used as the analysing wavelet. Note that in this case, the local maxima in the detail coefficients propagate across the four SWT levels with observable peaks. With this evolution in the signal singularities, it is then expected that multiplying the SWT detail coefficients across adjacent levels would reinforce the edge structures. The edge structures, i.e. the signal singularities, are the transient events in the signal (Tang, Yang et al. 2000). These first four resolution levels with the negative coefficients discarded are shown in Figs. 3.12 (b-e).

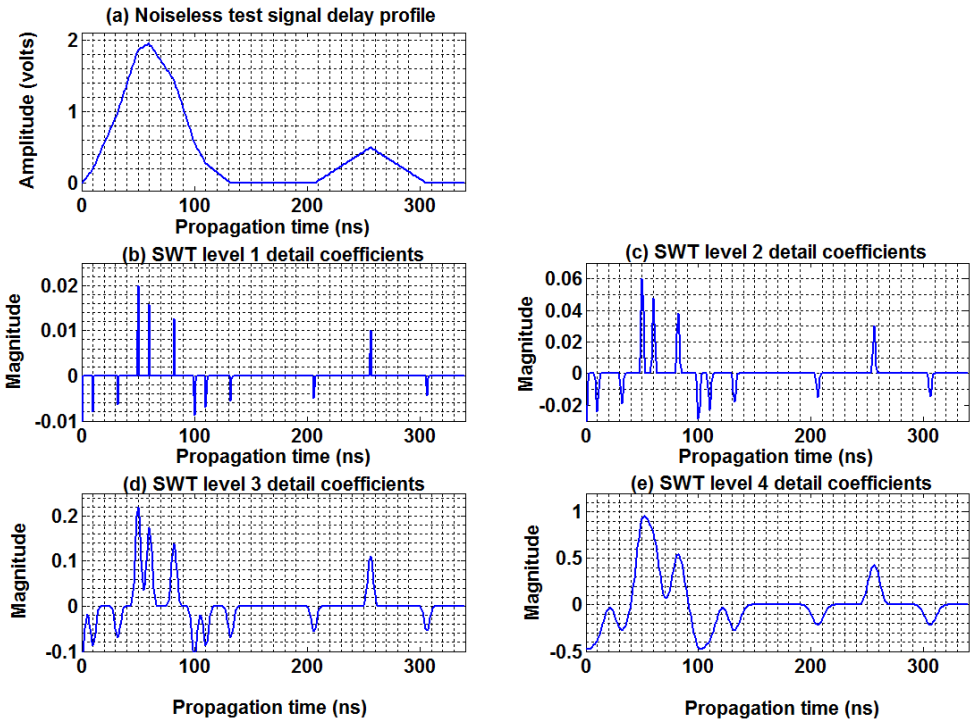

Figure 3.11 A simulated noiseless test signal and the SWT levels 1-4 detail coefficients, using Pathlet 5 as the analysing wavelet.

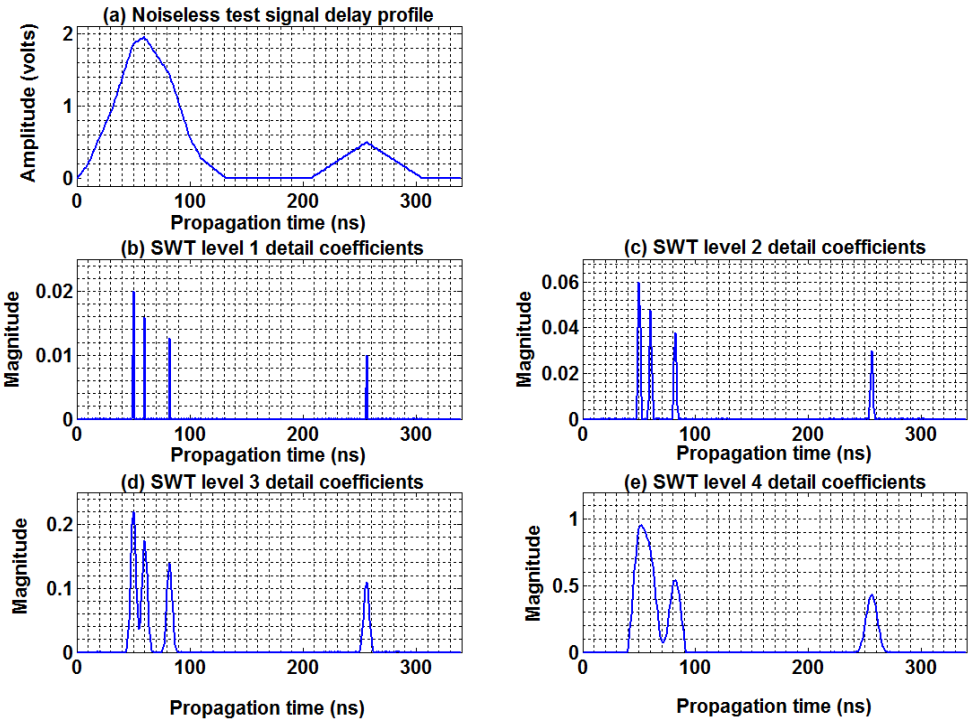

Figure 3.12 The simulated noiseless test signal and the SWT levels 1-4 detail coefficients, in Fig. 3.11, with the negative values discarded.

Given a noise corrupted signal, it is therefore expected that multiplying the SWT detail coefficients across adjacent levels would amplify the features of interest and suppress the noise. The denoised detail coefficients $\vec{\vec{O}}_{(r1\times r2),\,k}$ from applying the SWTMP, are defined by

$$\vec{\vec{O}}_{(r1\times r2),\,k} = \prod_{j=r1}^{r2} \vec{\vec{d}}_{\,j,k}\,, \qquad k = 0,1,\ldots,N_j - 1, \tag{3.78}$$

where $r1$ and $r2$ are two different non-negative integers, $\vec{\vec{d}}_{\,j,k}$ are non-negative noisy wavelet transform detail coefficients, while N_j represents the number of samples at the j^{th} level. The denoised detail coefficients, $\vec{\vec{O}}_{(r1\times r2),\,k}$, can then be used to provide information on the number of paths and time-delays in the input noise corrupted signal profile.

Once the number of paths, K, and relative time-delays τ_i, of the delay components have been successfully estimated from the denoised detail coefficients, then the amplitudes α_i of the individual paths can be subsequently determined. The amplitude estimation algorithm derived for use in this study is discussed in the next section.

3.4 Amplitude Estimation

The impulse response, $h(t)$, of a mobile radio channel can be modelled as (Lo, Litva et al. 1992; Lo, Litva et al. 1993; Vaughan and Andersen 2003)

$$h(t) = \sum_{i=1}^{K} \alpha_{ic}\,\delta(t - \tau_i) \;\Leftrightarrow\; H(\omega) = \sum_{i=1}^{K} \alpha_{ic}\,exp(-j\omega\tau_i), \tag{3.79}$$

where $\Leftrightarrow$ denotes two way implications of the Fourier transform pair. $H(\omega)$ is the channel transfer function while α_{ic} is the complex amplitude of the i^{th} path. K is the number of multipath components, while $\delta(\cdot)$ is the Dirac delta function. For discrete

angular frequencies ω_n, the sampled transfer function is given by (Lo, Litva et al. 1992; Lo, Litva et al. 1993)

$$H_n = \sum_{i=1}^{K} \alpha_{ic} exp\left(-j\omega_n \tau_i\right), \qquad n = 0,1,2,\ldots,N-1, \tag{3.80}$$

where N is the total number of samples. Assuming uniform sampling in frequency, with frequency spacing $\Delta\omega$ in rad/s, then the sampled transfer function becomes

$$H_n = \sum_{i=1}^{K} \alpha_{ic} exp\left(-jn\Delta\omega\tau_i\right). \tag{3.81}$$

Taking the complex conjugate of (3.81), gives

$$H_n^* = \sum_{i=1}^{K} \alpha_{ic} exp\left(jn\Delta\omega\tau_i\right). \tag{3.82}$$

In the presence of AWGN, then (3.82) becomes

$$M_n = H_n^* + \Re_n, \tag{3.83}$$

where M_n and $\Re_n$ denote the discrete signal and noise term, respectively. Equation (3.83) can be written in matrix form as

$$\mathbf{M} = \mathbf{\Gamma A} + \mathbf{\Re}, \tag{3.84}$$

where

$$\mathbf{M} = \left(M_0 \quad M_1 \quad \cdots \quad M_{N-1}\right)^{\mathrm{T}}, \tag{3.85}$$

$\mathbf{\Gamma}$ is $N \times K$ matrix given by

$$\mathbf{\Gamma} = \left(1 \quad e^{j\Delta\omega\tau_i} \quad e^{j2\Delta\omega\tau_i} \quad \cdots \quad e^{j(N-1)\Delta\omega\tau_i}\right)^{\mathrm{T}}, \qquad i = 1, 2, \ldots K, \tag{3.86}$$

$$\mathbf{A} = \left(\alpha_{1c} \quad \alpha_{2c} \quad \cdots \quad \alpha_{Kc}\right)^{\mathrm{T}}, \tag{3.87}$$

$$\mathbf{\Re} = \left(\eta_0 \quad \eta_1 \quad \cdots \quad \eta_{N-1}\right)^{\mathrm{T}}. \tag{3.88}$$

The superscript T denotes a transpose operation. Since the number of constituent multipath components K, and their delays τ_i, have already been determined from the denoised detail coefficients, then the amplitudes of the individual paths can be estimated by using least squares method as (Therrien 1992; Peracchi 2001)

$$\hat{\alpha}_{ic} = \left(\mathbf{\Gamma}^{\mathrm{T}}\mathbf{\Gamma}\right)^{-1}\mathbf{\Gamma}^{\mathrm{T}}\mathbf{M}, \tag{3.89}$$

where $\hat{\alpha}_{ic}$ is an estimate of α_{ic}, and $\hat{\alpha}_i = \left|\hat{\alpha}_{ic}\right|$.

The various steps involved in the proposed post-processing algorithm, required to extract the channel parameters, are shown in Fig. 3.13.

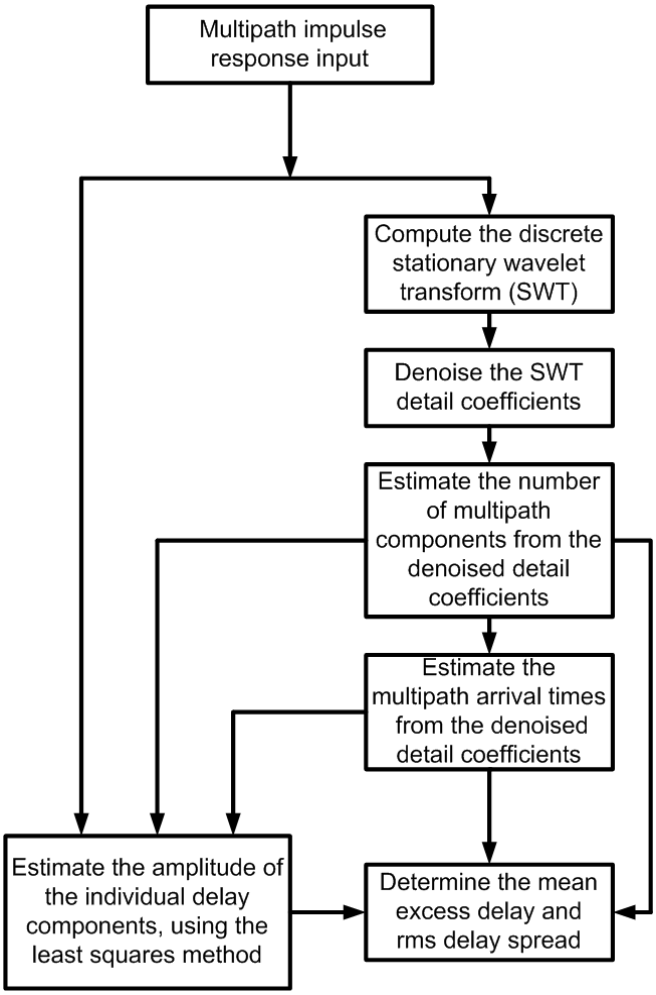

Figure 3.13 Proposed algorithm for post-processing multipath delay profiles.

3.5 Summary

In this chapter, the development of a novel digital signal post-processing algorithm for use in multipath channel parameter estimation has been presented. A new wavelet family named "Pathlet" has been derived and used in this algorithm. It has been shown that a desired wavelet in the current study must be symmetric, have a triangular (or a near triangular) shape, and compactly supported.

The probability plots of new equivalent noise sources, obtained after wavelet transform of a given original noise source using Pathlets 5, 7, 9, and Symlet 2 wavelets, have then been derived. It has been shown that Pathlet 9 is the most robust to noise in these analyses, followed by Pathlet 7, and then Symlet 2. Pathlet 5 is the least robust to noise amongst these wavelet family members considered.

Two noise reduction procedures are then presented. In the first noise reduction scheme, noise is suppressed by hard thresholding using the median absolute deviation standard deviation estimate of noise. This is accomplished by thresholding the wavelet transform coefficients to remove those coefficients associated with noise while preserving those that are required to describe the signal of interest. In the second noise reduction scheme, noise is suppressed by exploiting the multiscale dependencies inherent in the wavelet transform coefficients. In this denoising method, the adjacent wavelet transform subbands are multiplied to form multiscale products where the features evolving with high magnitude across different levels are reinforced while the noise is diluted. This second denoising technique has been referred to in this study as the "stationary wavelet transform multilevel products (SWTMP)." The denoised wavelet transform detail coefficients are used to predict the number of multipath components and time-delays. The estimated number of paths and relative time-delays are applied in a novel amplitude estimation algorithm, derived for use in this study, to determine the amplitudes of the individual paths.

CHAPTER 4

IMPLEMENTATION OF THE PROPOSED ALGORITHM IN SYNTHETIC MOBILE RADIO ENVIRONMENTS

4.1 Introduction

In this chapter, series of computer simulations are presented to demonstrate multipath components resolution using the digital signal processing algorithm proposed for this study in Chapter 3. In these high-resolution multipath channel parameter estimations, channel impulse response profiles similar to the triangular waveform shown in Fig. 3.1 are simulated. These simulated multipath delay profiles are assumed to be without band-limitations in this chapter. The effect of band-limitations is investigated in Chapter 5.

The stationary wavelet transform procedure is applied in transforming the simulated multipath delay profiles into wavelet transform domain. The novel wavelets named Pathlets, derived in Section 3.2.2, and Symlet 2 are used as the analysing wavelets. The wavelet transform detail coefficients are then used as an estimate of the number of multipath components and time-delays. In the presence of AWGN, the constituent multipath components that were not individually identifiable before post-processing are estimated from the detail coefficients after discarding the coefficients that are attributed to noise.

In order to denoise the noisy detail coefficients, performance comparison is made between the two noise reduction schemes proposed in Section 3.3; used to filter-out noise from the detail coefficients. In the first noise reduction technique, the SWTMP method given in (3.78) is applied. In this case, the product of levels 1 and 2 detail coefficients of the noisy delay profile are computed to get new coefficients with reduced noise. In the second noise reduction method, the wavelet thresholding scheme defined in (3.77) is applied. In this method, a denoising procedure that uses the hard thresholding technique based on the median absolute deviation standard deviation estimate of noise (Donoho and Johnstone 1994; Coifman and Donoho 1995; Donoho and Johnstone 1995; Percival and Walden 2000) is applied to remove the noisy detail coefficients.

Finally, the amplitude estimation algorithm, proposed in Section 3.4, is used to determine the amplitudes of the individual paths. Once the number of paths, time-delays, and amplitudes of the delay components has been successfully determined, then multipath delay statistics such as the mean excess delay and rms delay spread are calculated using (2.1) and (2.2) respectively.

This chapter starts with simulations of typical multipath radio channel scenarios considered in this research. Next, the digital signal post-processing algorithm developed in Chapter 3 is applied to resolve the constituent paths in the simulated multipath delay profiles. Multipath delay parameters such as the number of paths, time-delays, and amplitudes, as well as the mean excess delay, and rms delay spread are estimated in these simulations. Analyses are also carried out to determine the achievable multipath resolution that can be obtained in this study using the proposed algorithm. This chapter concludes, in Section 4.3, with a summary of these simulation results.

4.2 Estimation of Multipath Channel Parameters

4.2.1 Simulation model

A general system model of the multipath fading channel utilised in this research, based on the sliding correlator channel sounding discussed in Section 2.2.4, is shown in Fig. 4.1. The received multipath delay profile is as previously described in (3.1), while the wavelet-based digital signal processing algorithm is as shown in Fig. 3.13.

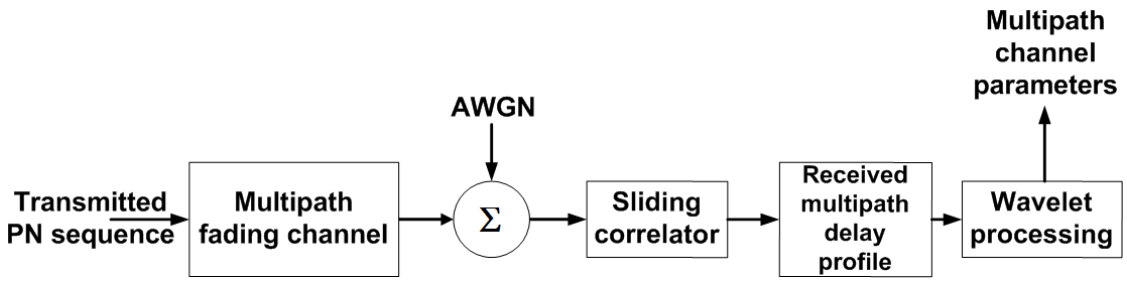

Figure 4.1 General system model of the multipath fading channel, and the wavelet-based digital signal processing, used in this study.

In the channel sounding simulations, the transmitter chip clock rate is assumed to be 20 MHz while the receiver chip clock rate is 19.996 MHz. The intrinsic delay resolution of the channel sounder is therefore 50 ns. Consequently, multipath components that are separated by 50 ns or more are resolved by the channel sounder. Applying (2.4) therefore gives the time sliding factor of the channel sounder to be 5000. This sliding factor relates the measurement observation time to the actual propagation time, according to (2.5).

As discussed in Section 3.2.1, the actual base width of the triangular signal waveform, formed by the correlation of the receiver and transmitter PRBS, is 100 ns for a single path. Also, the amplitudes of the multipath components are described relative to the path with the largest magnitude.

Simulated one- and two-path radio channel scenarios, corrupted with AWGN, are shown in Figs. 4.2 and 4.3 respectively. The two paths in Fig. 4.3 have equal amplitudes and

time-delays of 50 ns and 150 ns, a separation of 100 ns. Consequently, the two constituent paths in the radio channel are resolved by the channel sounder.

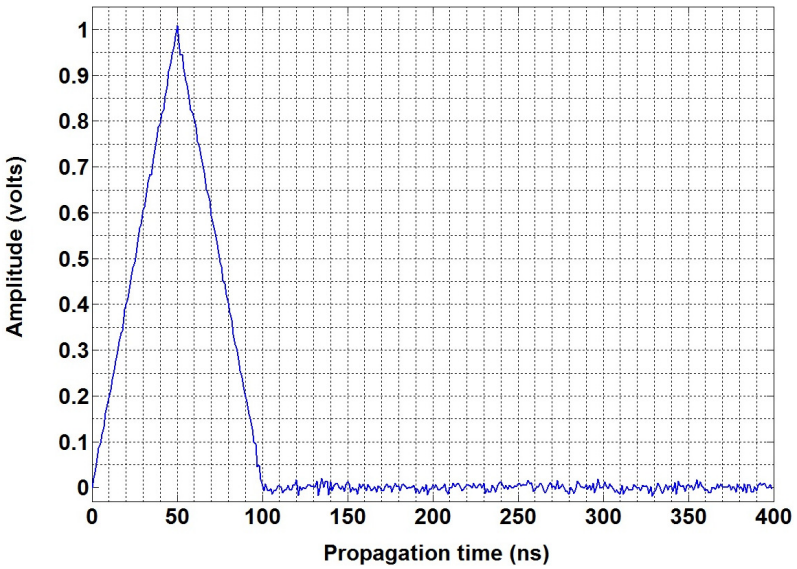

Figure 4.2 Simulated delay profile of a noisy one-path propagation channel.

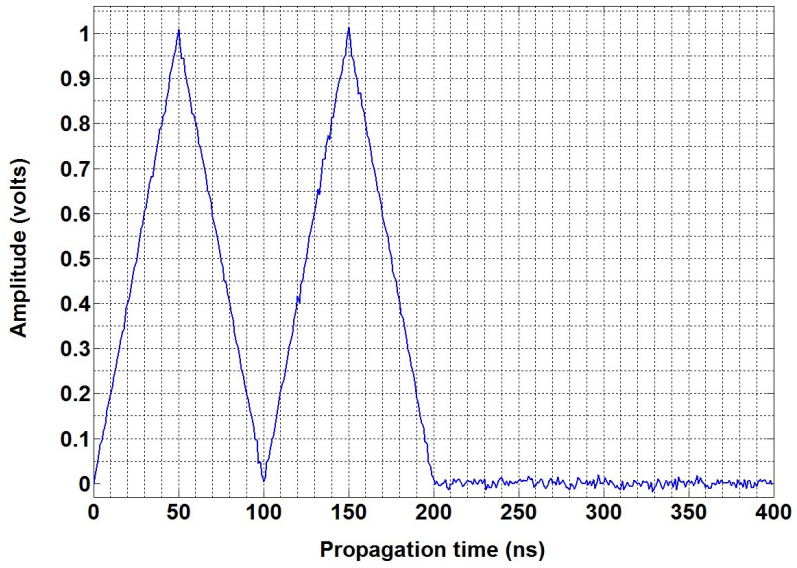

Figure 4.3 Simulated multipath delay profile of a noisy two-path propagation channel, with equal amplitudes and time-delays at 50 ns and 150 ns.

A scenario where the constituent multipath components, in the radio channel, are not resolved by the measuring equipment is simulated in Fig. 4.4. The two paths, in this propagation channel, have equal amplitudes and time-delays of 50 ns and 60 ns; a separation of 10 ns. Since this delay separation is less than the intrinsic delay resolution of the measuring equipment, i.e. less than 50 ns, therefore the channel sounder fails to resolve the two constituent paths in the propagation channel.

A situation where weaker rays are masked by the stronger rays is simulated in the four-path propagation channel shown in Fig. 4.5. The four paths in this propagation channel have differential amplitudes of 0 dB, -2 dB, -4 dB, and -6 dB and corresponding time-delays of 50 ns, 60 ns, 82 ns, and 256 ns respectively. The 3rd path, in this case, has been completely masked by the 1st and 2nd paths. Since the relative delay of the 2nd and 3rd paths is less than the intrinsic delay resolution of the channel sounder, it is hence impossible to identify these paths in the delay profile prior to post-processing. However the channel sounder can resolve the 4th path, at a relative delay of 206 ns, since this is greater than the intrinsic delay resolution of this measuring equipment.

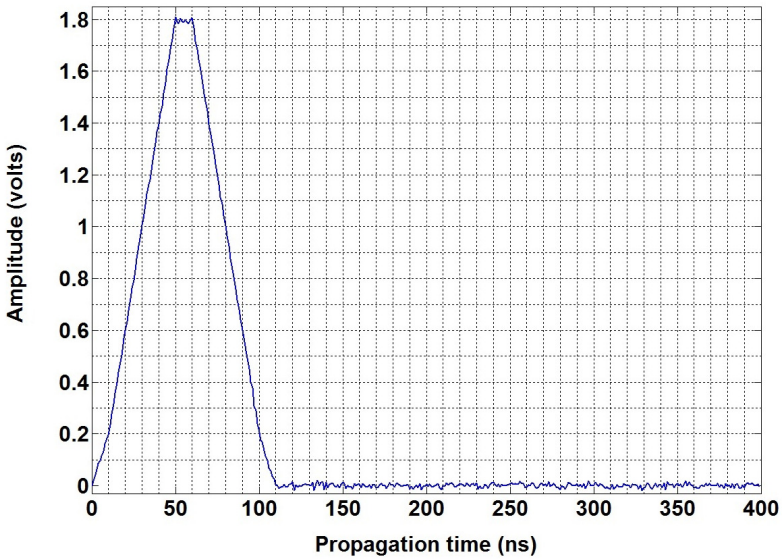

Figure 4.4 Simulated multipath delay profile of a noisy two-path propagation channel, with equal amplitudes and time-delays at 50 ns and 60 ns.

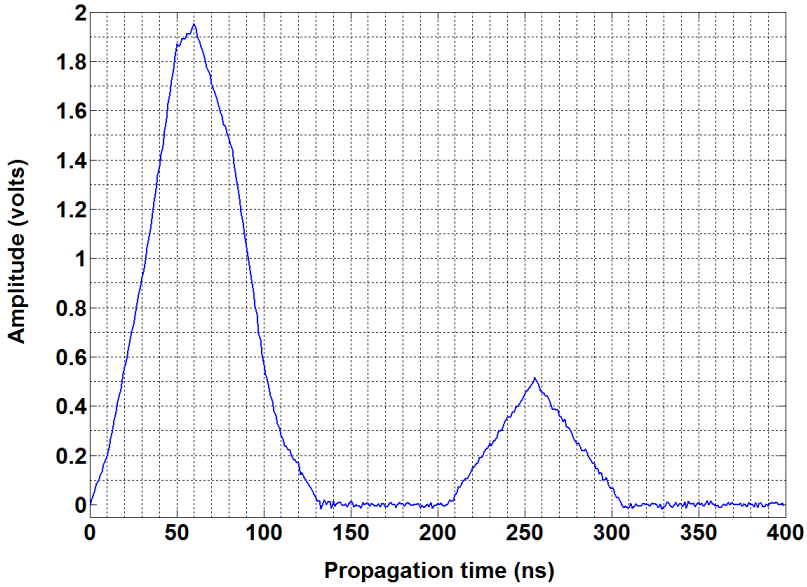

Figure 4.5 Simulated multipath delay profile of a noisy four-path propagation channel, with amplitudes of 0 dB, -2 dB, -4 dB, -6 dB, and delays at 50 ns, 60 ns, 82 ns, 256 ns respectively.

Multipath delay profiles, similar to the simulated scenarios in Figs. 4.2, 4.3, 4.4, and 4.5, have been developed as test signals in this chapter. Several captures of these multipath delay profiles, each of which has been corrupted by different noise sequences, have been produced and then averaged to obtain test signal waveforms that simulate the average output signal waveforms from the experimental SCCS system.

4.2.2 One-path delay profile

The wavelet analysis of a simulated one-path delay profile is discussed in this section. Pathlets 5, 7, 9, and Symlet 2 are used as the analysing wavelet to detect the single path in this delay profile.

The simulated one-path delay profile, in the absence of noise, is shown in Figs. 4.6 (a) – 4.9 (a), while the SWT levels 1 and 2 detail coefficients are shown in Figs. 4.6 (b-e) and 4.8 (b-e) respectively. The corresponding time-expanded views of these coefficients are given in Figs. 4.7 (b-e) and 4.9 (b-e). The locations of the positive peaks in these detail coefficients provide the arrival time of the multipath components. Table 4.1 shows the

magnitudes of the levels 1 and 2 detail coefficients. The magnitudes of these wavelet transform coefficients indicate that Pathlet 9 provides the best match with the multipath signals, while Pathlet 5 is the least match with this signal waveform. Furthermore, the magnitudes of these coefficients are increased as the wavelet transform level increases. These results also show that while both Pathlets and Symlet 2 can be successfully applied to detect the single peak in this propagation path, however the wavelet transform coefficients obtained with Symlet 2 are not exactly symmetric as observed in Figs. 4.7 (e) and 4.9 (e). As a consequence, the use of Symlet 2 in signal analyses may result in misalignments between features in a signal and features extracted by the basis functions.

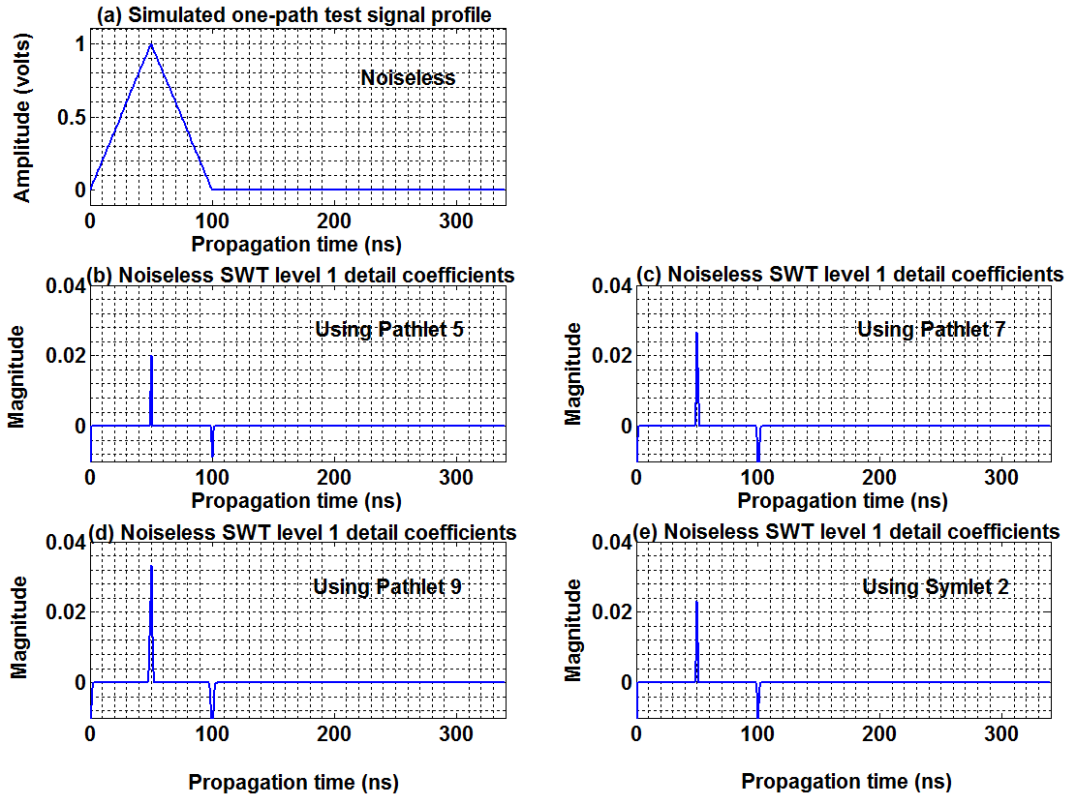

Figure 4.6 Noiseless test signal profile with one path and corresponding SWT level 1 detail coefficients using Pathlets 5, 7, 9, and Symlet 2 as the analysing wavelets.

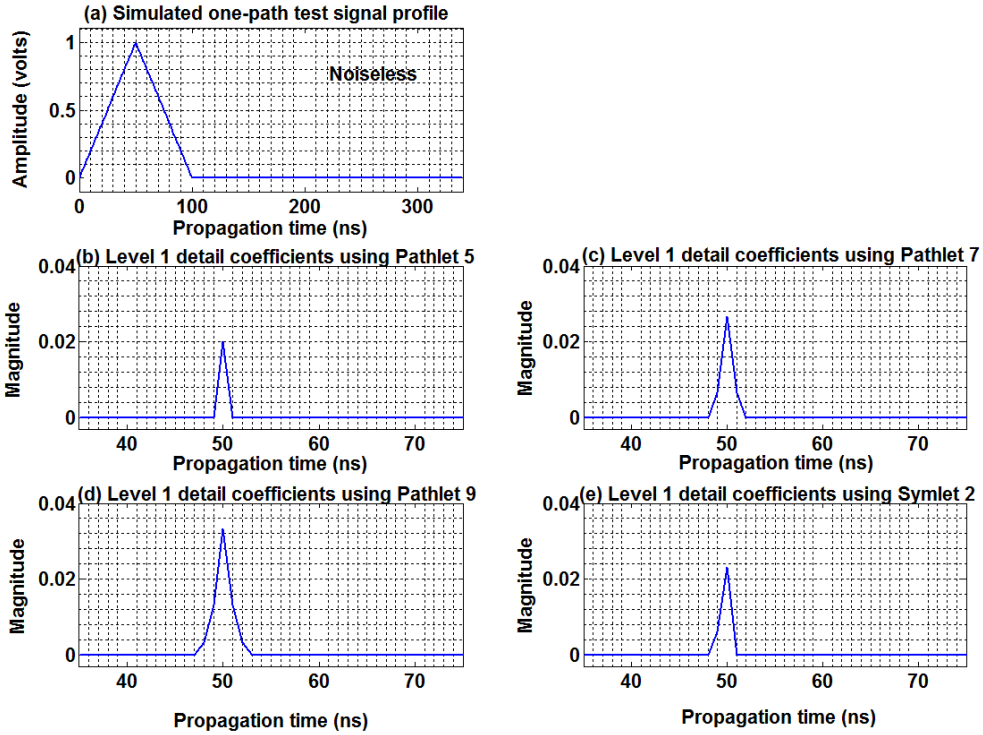

Figure 4.7 Time-expanded view of the noiseless SWT level 1 detail coefficients from Fig. 4.6.

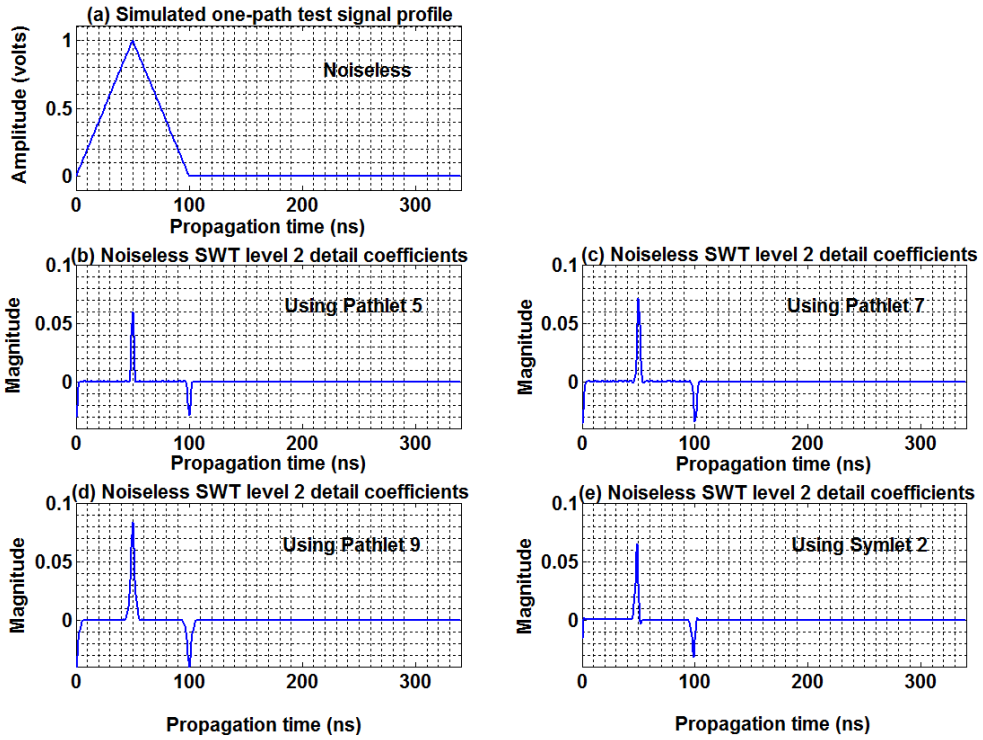

Figure 4.8 Noiseless test signal profile with one path and corresponding SWT level 2 detail coefficients using Pathlets 5, 7, 9, and Symlet 2 as the analysing wavelets.

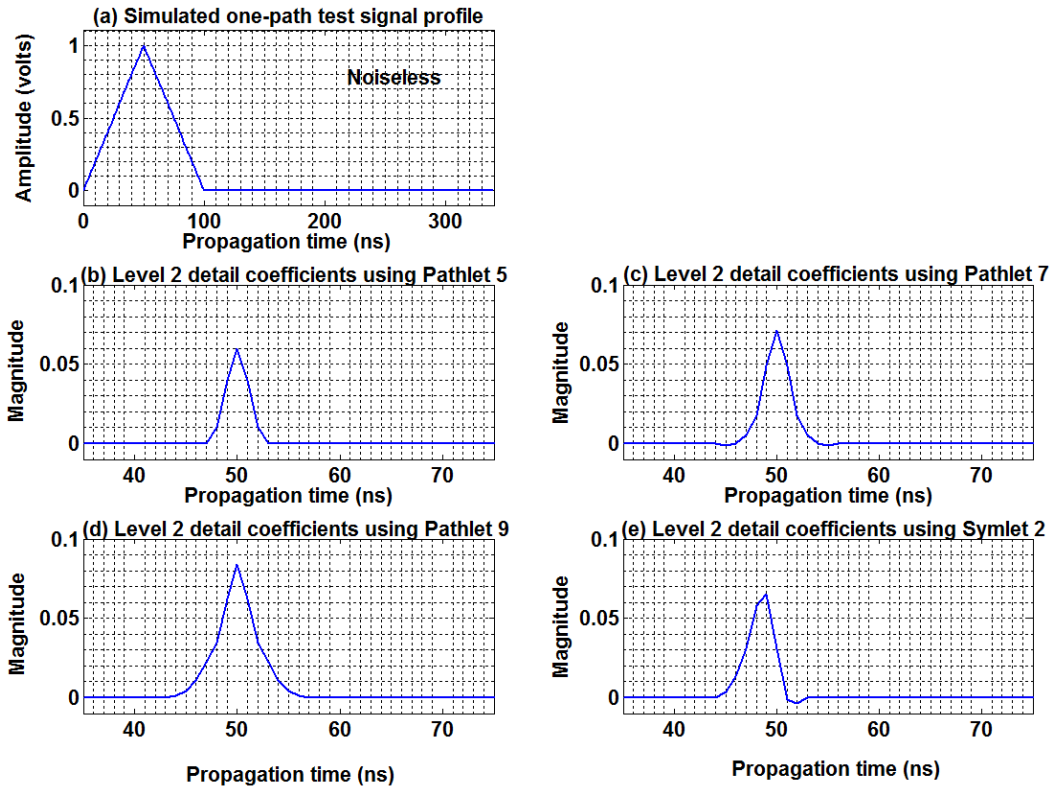

Figure 4.9 Time-expanded view of the noiseless SWT level 2 detail coefficients from Fig. 4.8.

Table 4.1 Magnitude of the SWT levels 1 and 2 detail coefficients for a noiseless one-path delay profile.

Wavelet type	**Magnitude of the noiseless detail coefficients**	
	Level 1	**Level 2**
Pathlet 5	0.020	0.060
Pathlet 7	0.027	0.071
Pathlet 9	0.033	0.084
Symlet 2	0.023	0.065

Now in the presence of AWGN, the SWT levels 1 and 2 detail coefficients of this one-path test signal profile are shown in Figs. 4.10 (b-e) and 4.11 (b-e) respectively. An SNR of 30 dB is assumed in these simulations. The dominant peak in these noisy wavelet transform coefficients, in this case, indicates the single path in the delay profile. The magnitude of this dominant peak increases, while the noise diminishes, as the wavelet transform decomposition level increases. This is in agreement with the observations in Section 3.3.3.

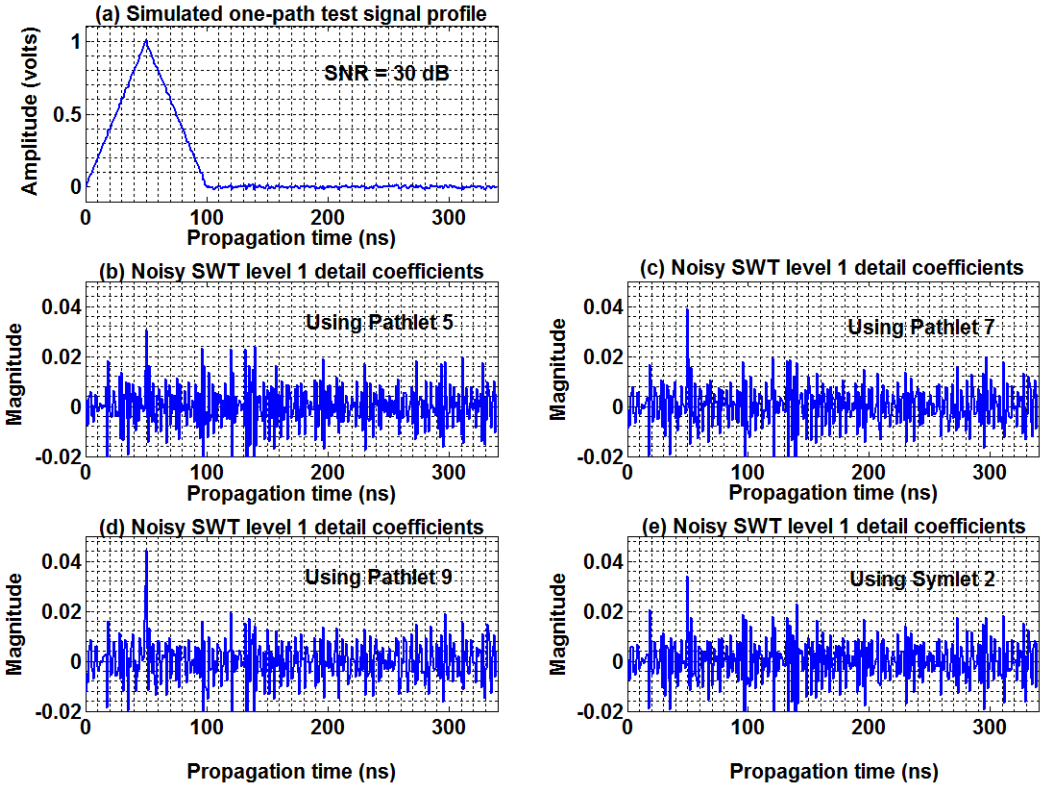

Figure 4.10 Noisy test signal profile with one path, at an SNR of 30 dB, and corresponding SWT level 1 detail coefficients using Pathlets 5, 7, 9, and Symlet 2 as the analysing wavelets.

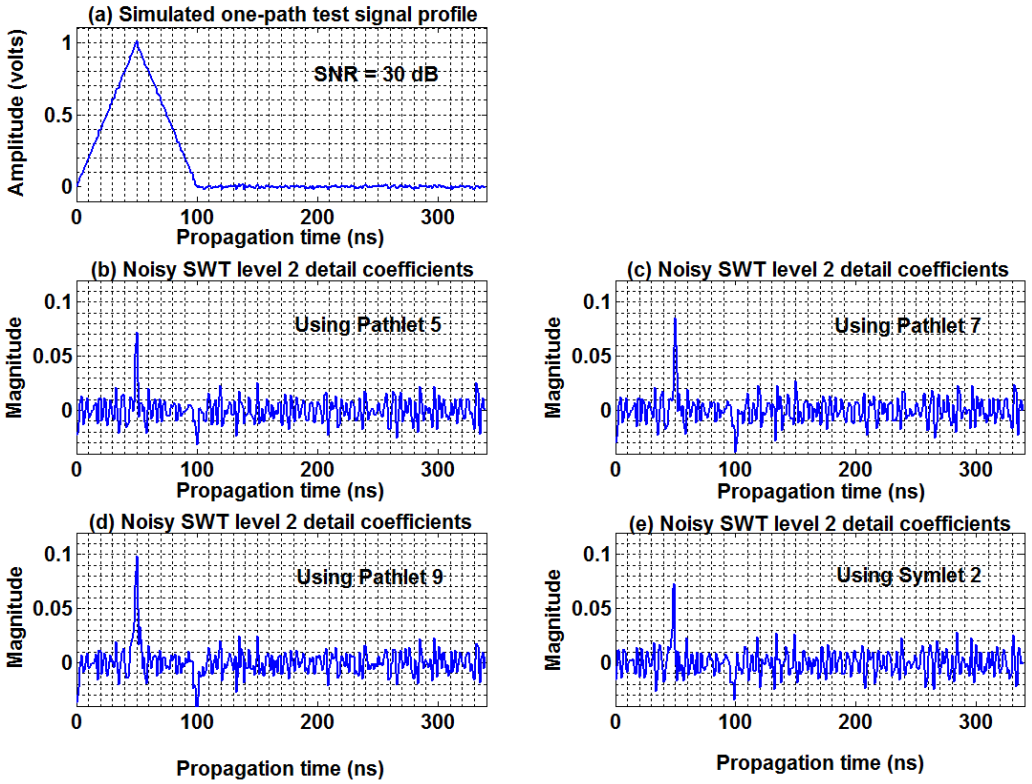

Figure 4.11 Noisy test signal profile with one path, at an SNR of 30 dB, and corresponding SWT level 2 detail coefficients using Pathlets 5, 7, 9, and Symlet 2 as the analysing wavelets.

4.2.3 Two-path delay profile with equal-amplitude paths

In this section, the algorithm proposed in Fig. 3.13 for post-processing multipath delay profiles is applied in a simulated two-path delay profile, having equal-amplitude paths and relative delay of 2 ns. Pathlets 5, 7, 9, and Symlet 2 are used as the analysing wavelets.

The parameters of this two-path delay profile are tabulated in Table 4.2. The time of arrival of the first path at 50 ns is taken to be the time reference, while the second path is at a delay of 2 ns relative to the arrival time of the first multipath component. Also, the amplitude of this first path is taken to be the reference amplitude.

Since the delay separation is less than the intrinsic delay resolution of the measuring equipment, i.e. less than 50 ns, therefore the two constituent paths in the propagation channel are not resolved. This multipath delay profile, in the absence of noise, is shown in Fig. 4.12.

Table 4.2 Parameters of a simulated two-path delay profile with equal-amplitude paths.

Paths	**Propagation time (ns)**	**Relative delay (ns)**	**Relative amplitude (dB)**
1st	50	0	0
2nd	52	2	0

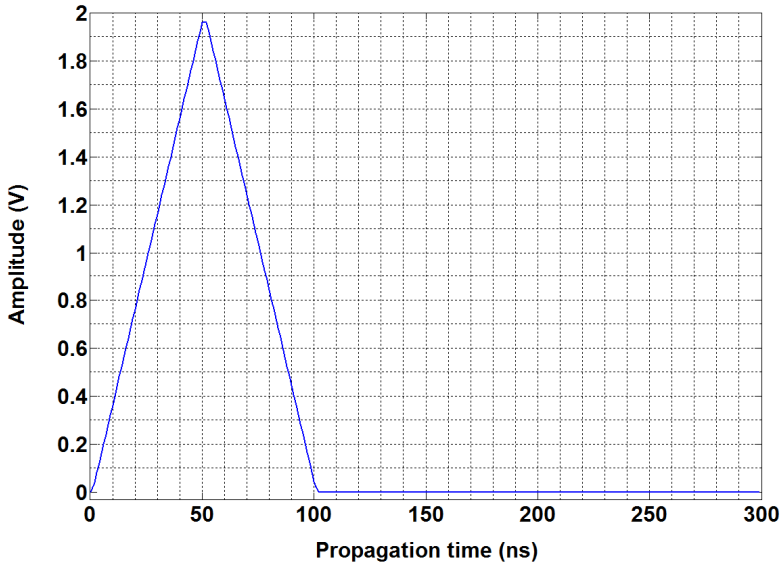

Figure 4.12 Simulated multipath delay profile of a noiseless two-path propagation channel, with equal amplitudes and time-delays at 50 ns and 52 ns.

The SWT levels 1 and 2 detail coefficients, of this noiseless test signal, are shown in Figs. 4.13 (c-f) and 4.15 (c-f) respectively. The actual multipath components are shown, for comparison, in Figs. 4.13 (b) and 4.15 (b). The time-expanded views of these detail coefficients, containing the two equal-amplitude paths, are given in Figs. 4.14 (c-f) and

4.16 (c-f). The time-expanded views of the actual multipath components are also shown, in Figs. 4.14 (b) and 4.16 (b).

The results in Figs. 4.14 (c-f) show that the two equal-amplitude paths are resolved after wavelet transform, at level 1, when Pathlets 5, 7, 9, and Symlet 2 are used. Pathlet 5 produces the best resolution of the two equal-amplitude paths when compared with the other wavelets used, while Pathlet 9 produces the least resolution of the two paths. The results in Figs. 4.16 (c-f) show that these noiseless two equal-amplitude paths are not resolved after wavelet transform at level 2, and hence for further higher wavelet transform levels, due to increased smoothing.

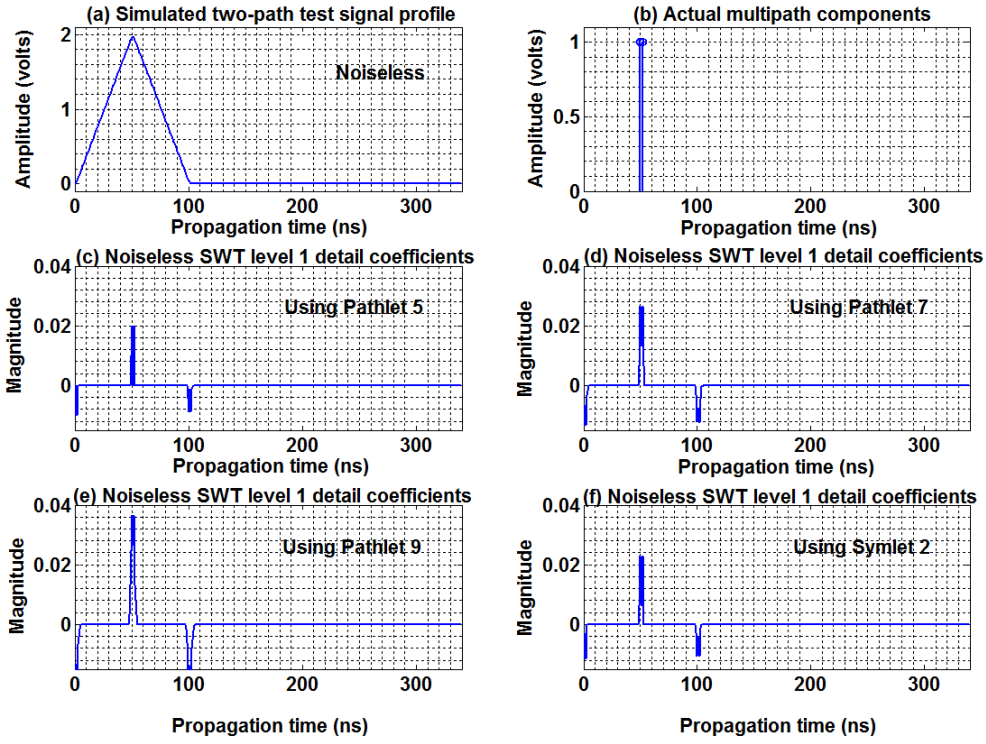

Figure 4.13 Noiseless test signal profile with two paths having equal amplitudes and corresponding SWT level 1 detail coefficients.

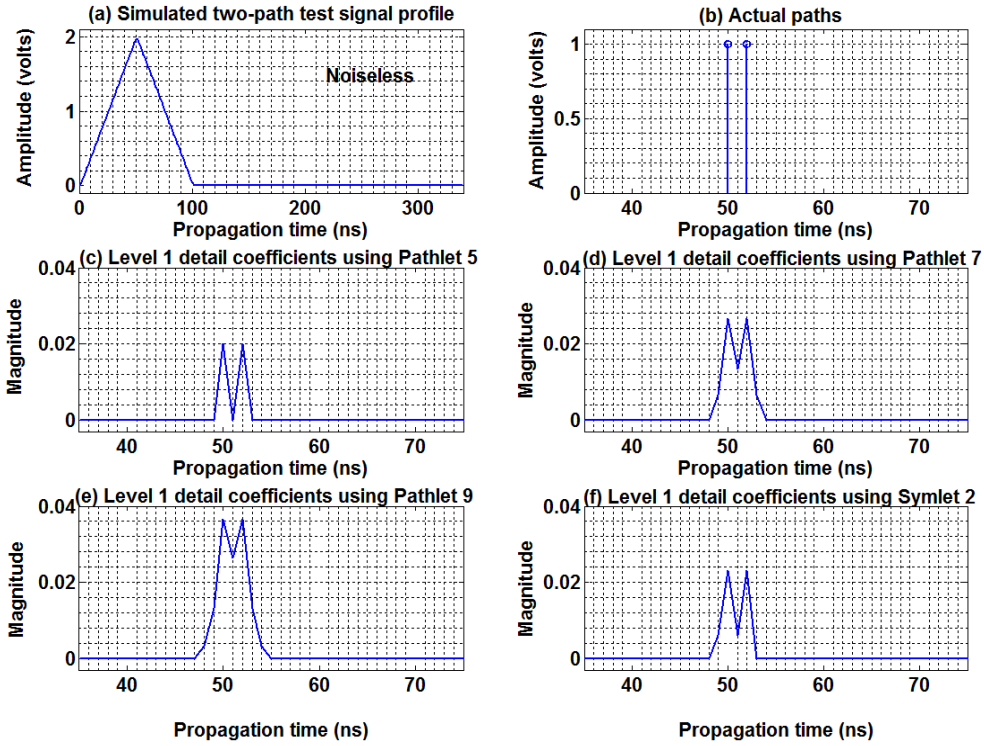

Figure 4.14 Time-expanded views of the two paths, and the noiseless SWT level 1 detail coefficients, from Fig. 4.13.

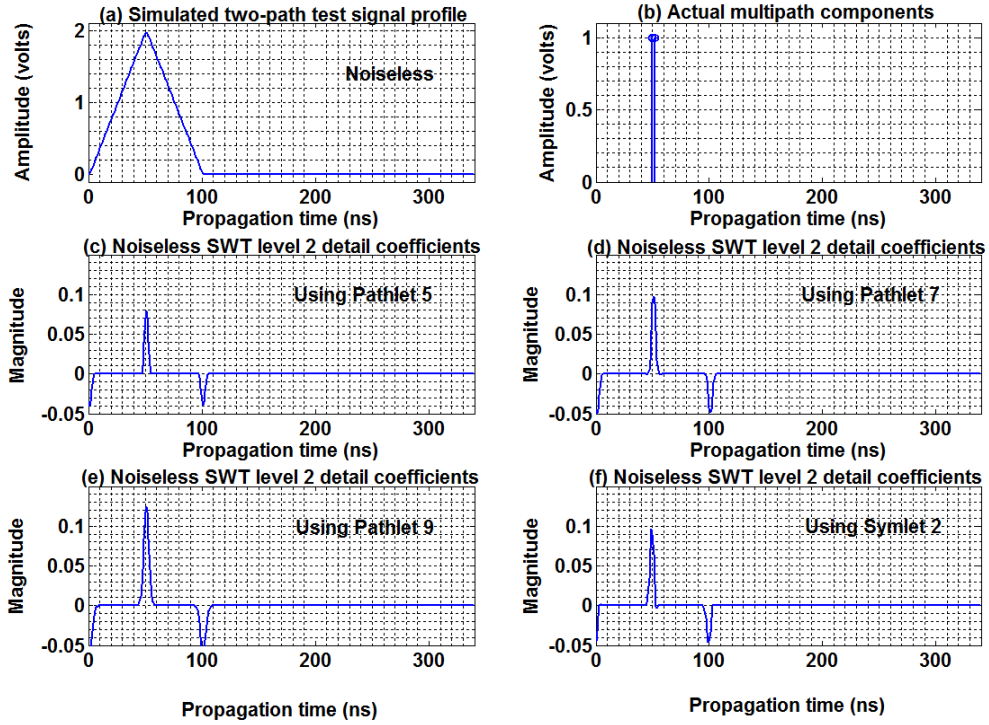

Figure 4.15 Noiseless test signal profile with two paths having equal amplitudes and corresponding SWT level 2 detail coefficients.

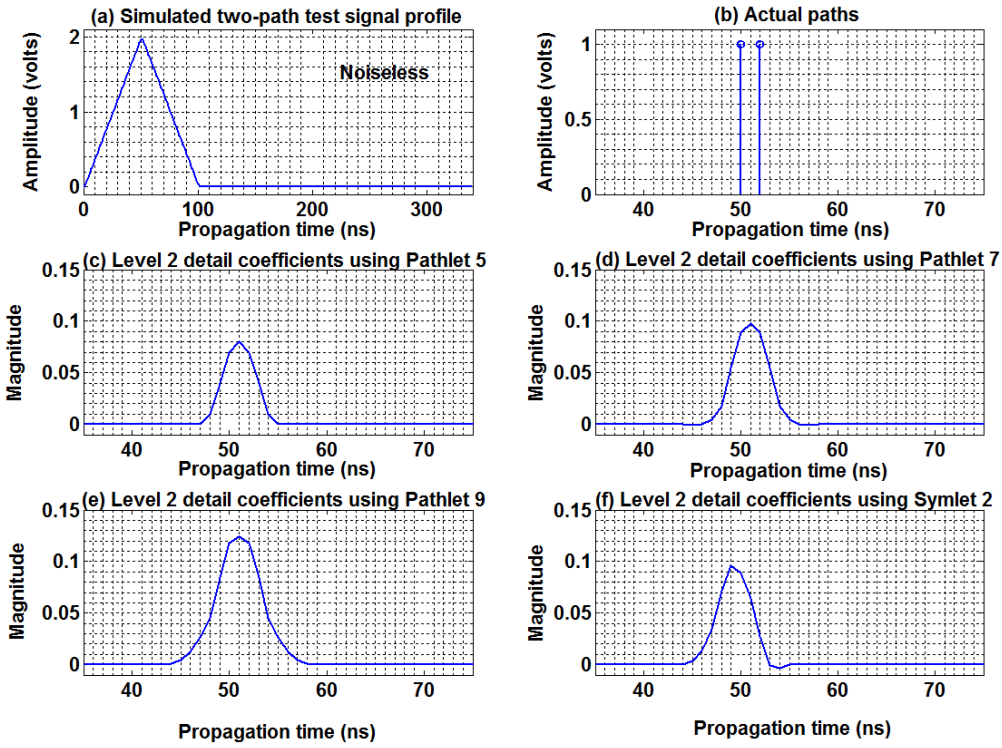

Figure 4.16 Time-expanded view of the two paths, and the noiseless SWT level 2 detail coefficients, from Fig. 4.15.

Next, the simulated two-path delay profile shown in Fig. 4.12 is corrupted with AWGN. An SNR of 40 dB is initially assumed. The SWT levels 1 and 2 detail coefficients of this test signal profile, in the presence of noise, are shown in Figs. 4.17 (c-f) and 4.19 (c-f) respectively. The corresponding time-expanded views of these noisy detail coefficients are given in Figs. 4.18 (c-f) and 4.20 (c-f). The actual multipath components are again shown, for comparison, in Figs. 4.18 (b) and 4.20 (b).

The results in Figs. 4.18 (c-f) show that though the two equal-amplitude paths have been resolved after wavelet transform at level 1, when Pathlets 5, 7, 9, and Symlet 2 are used, however the magnitudes of the wavelet transform coefficients observed in Figs. 4.14 (c-f) have been altered due to the influence of noise. Consequently, these noisy detail coefficients do not provide information about the amplitudes of the multipath components. These noisy two equal-amplitude paths are not resolved at level 2 of the wavelet transform, illustrated in Figs. 4.20 (c-f), and hence for further higher wavelet transform levels, as a result of the increased smoothing.

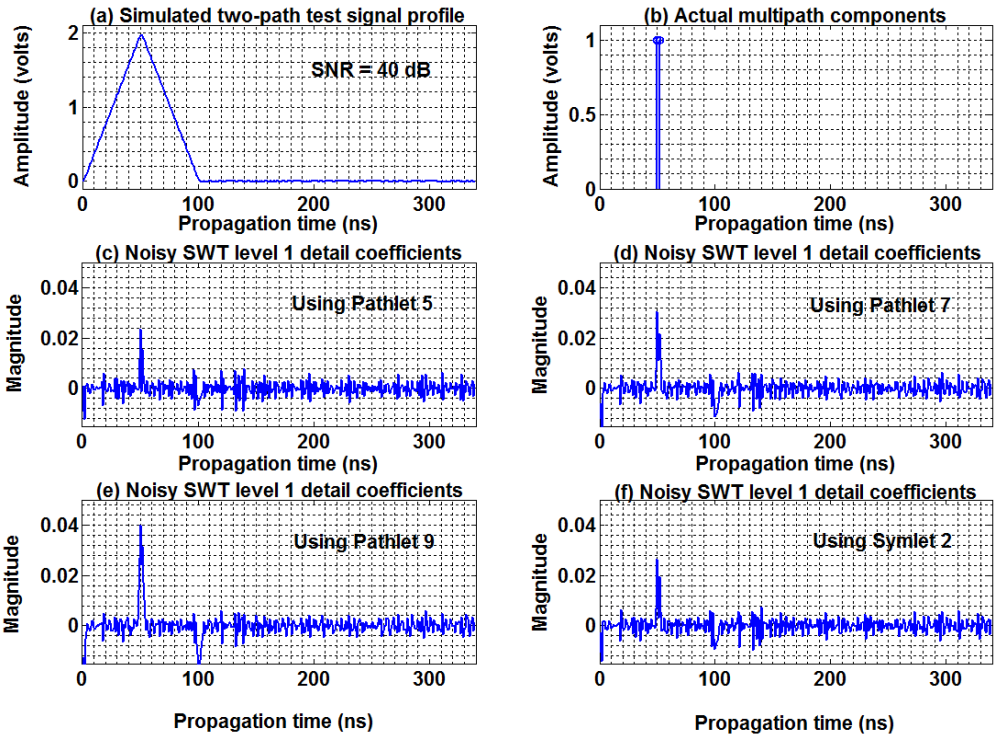

Figure 4.17 Noisy test signal profile with two paths having equal amplitudes, at an SNR of 40 dB, and corresponding SWT level 1 detail coefficients.

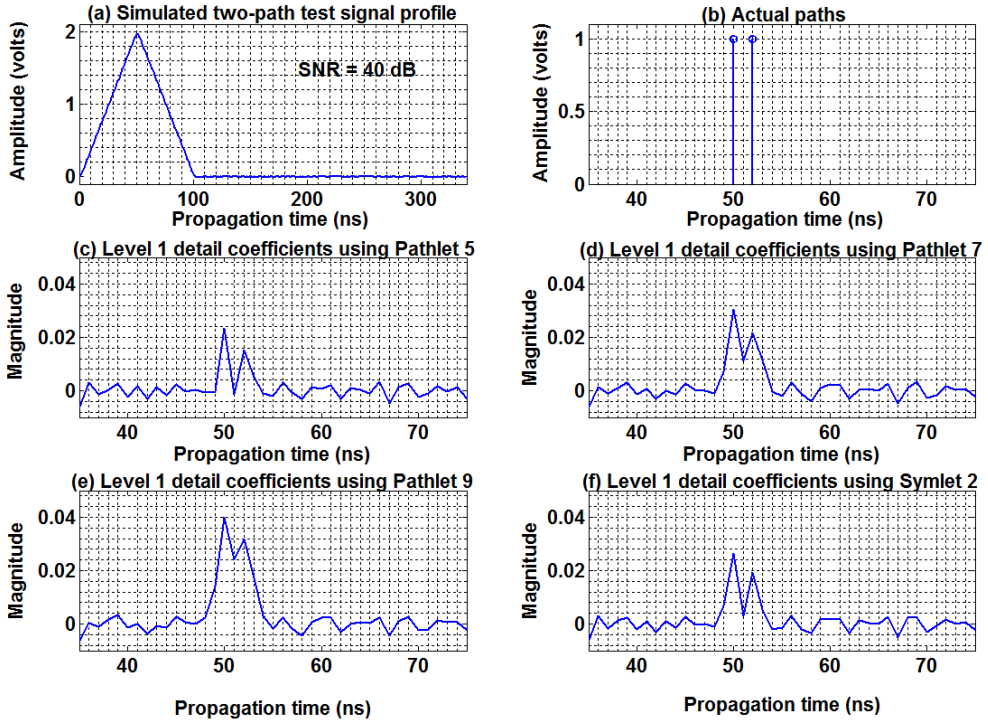

Figure 4.18 Time-expanded view of the two paths, and the noisy SWT level 1 detail coefficients, in Fig. 4.17.

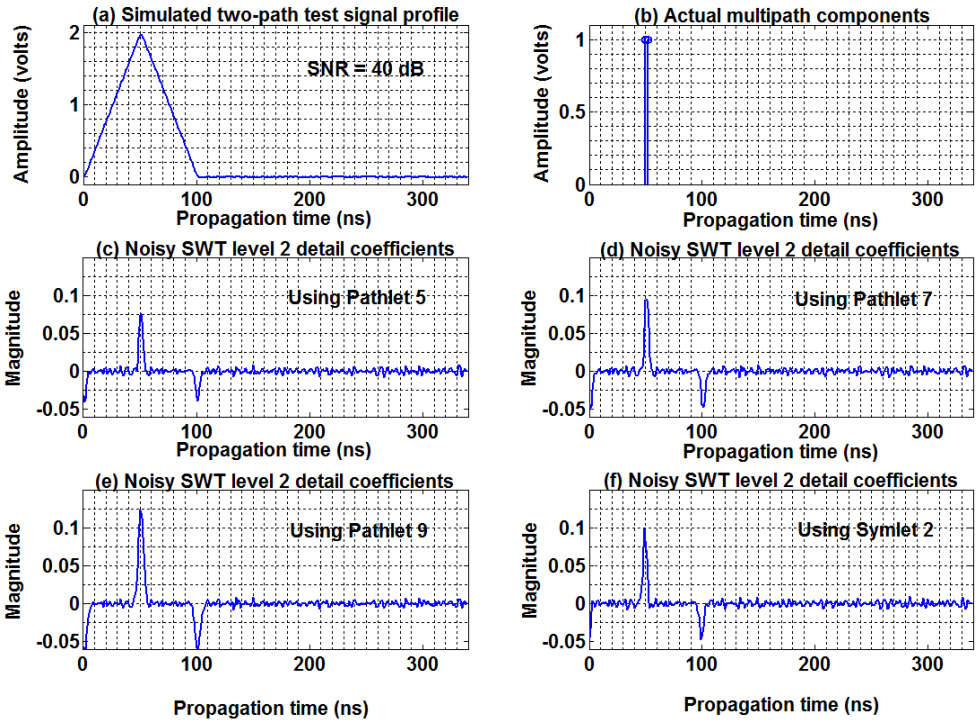

Figure 4.19 Noisy test signal profile with two paths having equal amplitudes, at an SNR of 40 dB, and corresponding SWT level 2 detail coefficients.

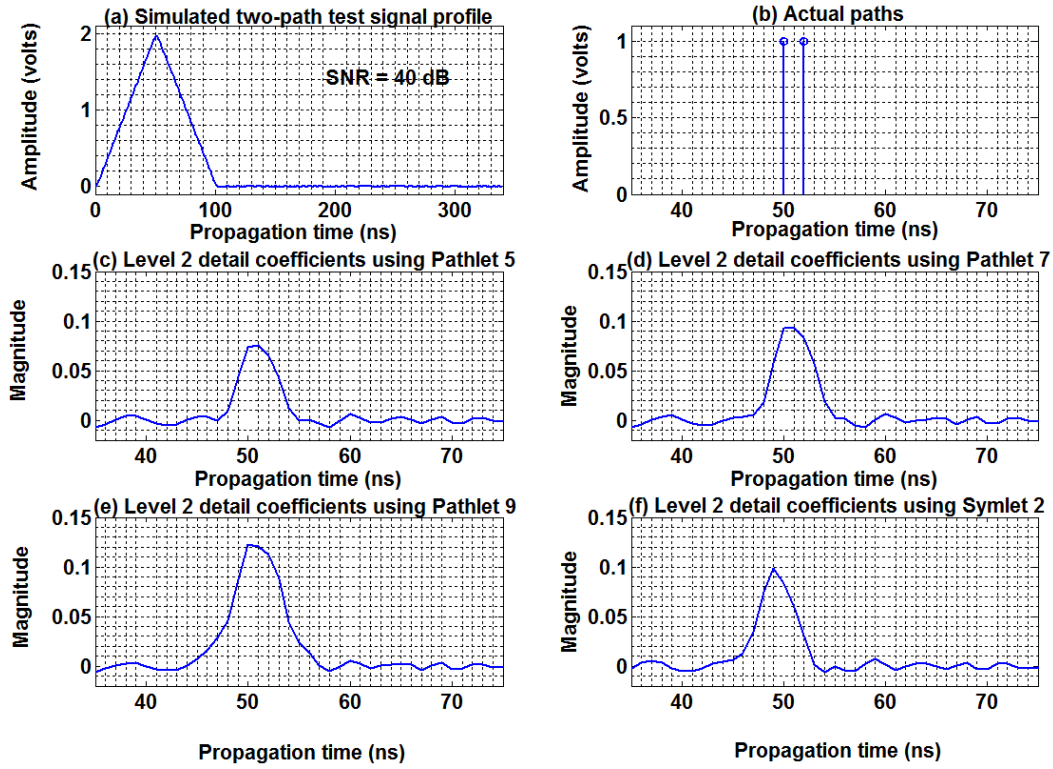

Figure 4.20 Time-expanded view of the two paths, and the noisy SWT level 2 detail coefficients, in Fig. 4.19.

In Section 3.3.3, it was shown that the local maxima in the detail coefficients, attributed to a noiseless signal of interest, propagate into the coarse SWT levels with observable peaks whereas the detail coefficients attributed to noise diminishes across these levels. This has been previously illustrated in Table 4.1, where the magnitudes of the noiseless detail coefficients are increased as the wavelet transform decomposition level increases. Since the level 1 detail coefficients are mostly noise dominated and have the greatest resolution, consequently the level 1 detail coefficients are multiplied with the detail coefficients at the next higher level (i.e. level 2), in order to dilute the noise without compromising too much multipath resolution.

In this study, the locations of the positive peaks in the SWT detail coefficients are used to provide information on the number of propagation paths, and time-delays of the constituent paths in a multipath delay profile. Hence, the negative detail coefficients are discarded prior to computing the multilevel products of the wavelet transform detail coefficients as discussed in Section 3.3.3 for the SWTMP procedure.

The product of levels 1 and 2 detail coefficients of the noisy delay profile are shown in Figs. 4.21 (c-f). These results show that the wavelet transform detail coefficients that were attributed to noise, originally observed in Figs. 4.17 (c-f) and 4.19 (c-f), have now been suppressed in Figs. 4.21 (c-f). These denoised coefficients are as defined in (3.78). The denoised detail coefficients can then be used as an estimate of the number of multipath components in the delay profile.

Another way to filter-out noise is through wavelet-based denoising by thresholding, using the median absolute deviation standard deviation estimate of noise (Percival and Walden 2000). In this method, the detail coefficients that are greater than a given threshold value are preserved while the remaining detail coefficients are set to zero. This procedure was discussed in Section 3.3.2, and now applied in Figs. 4.22 (c-f) to denoise the SWT level 1 detail coefficients. The hard thresholding technique (Percival and Walden 2000; Jansen 2001), discussed in Appendix C, has been adopted in this denoising scheme. The results obtained show that the wavelet transform detail

coefficients that were attributed to noise, in Figs. 4.17 (c-f) and 4.19 (c-f), have again been removed as observed in Figs. 4.22 (c-f). The thresholded coefficients are then used as estimates of the constituent multipath components.

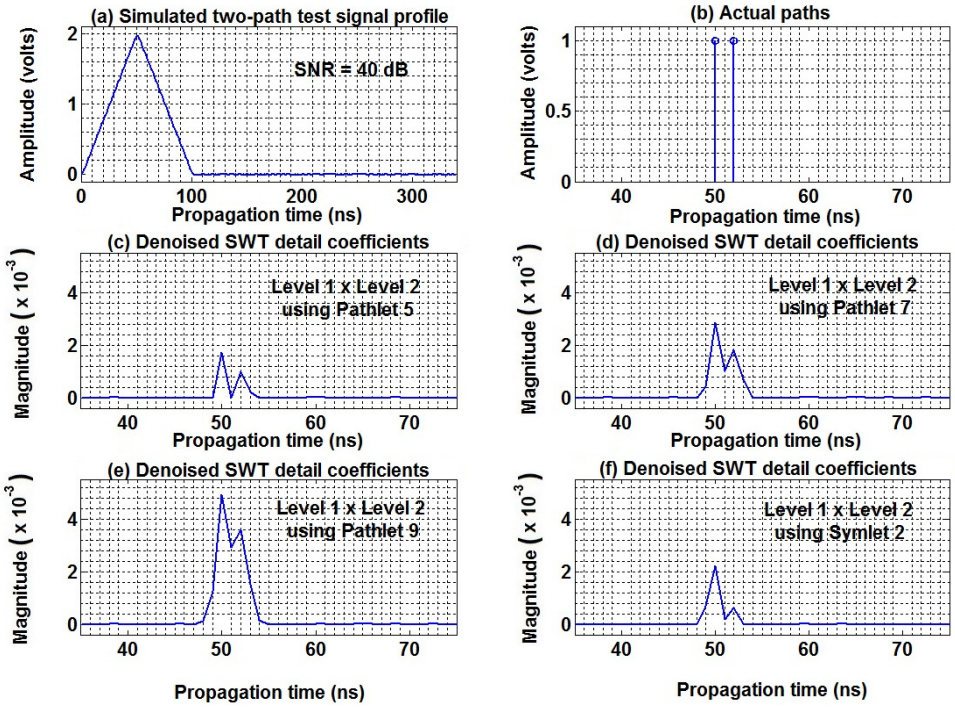

Figure 4.21 Noisy test signal profile with two paths having equal amplitudes, at an SNR of 40 dB, and the denoised SWT detail coefficients. Noise is suppressed by SWTMP using the levels 1 and 2 detail coefficients.

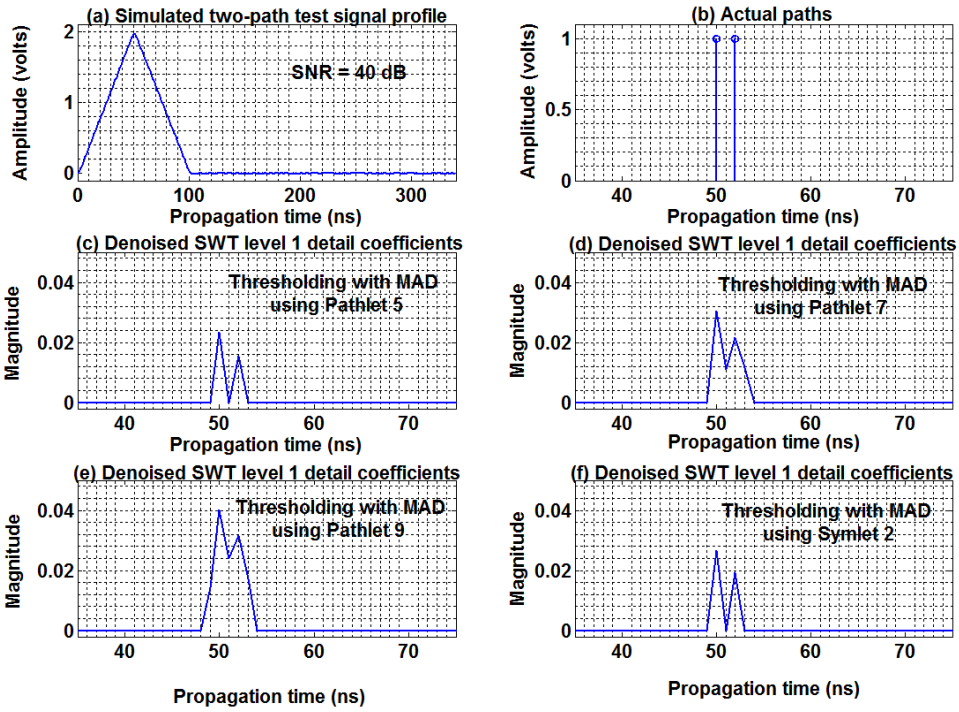

Figure 4.22 Noisy test signal profile with two paths having equal amplitudes, at an SNR of 40 dB, and the denoised SWT level 1 detail coefficients. Noise is removed by wavelet thresholding.

This simulated two-path delay profile shown in Fig. 4.12 is then corrupted with AWGN at an SNR of 30 dB. The SWT levels 1 and 2 detail coefficients of this noisy test signal profile are illustrated in Figs. 4.23 (c-f) and 4.25 (c-f) respectively, while the corresponding time-expanded views of these noisy detail coefficients are given in Figs. 4.24 (c-f) and 4.26 (c-f). The actual multipath components are shown, for comparison, in Figs. 4.24 (b) and 4.26 (b).

The results in Figs. 4.23 (c-f) and 4.24 (c-f) shows that only the first path can be indentified at level 1 of the wavelet transform, when Pathlets 5, 7, 9, and Symlet 2 are used. At level 2, the detail coefficients obtained, shown in the time-expanded view of Fig. 4.26 (c-f), suggests that there is at least one dominant path and the likelihood of a second path that has been masked by the first path; which is actually as a consequence of the effect of noise.

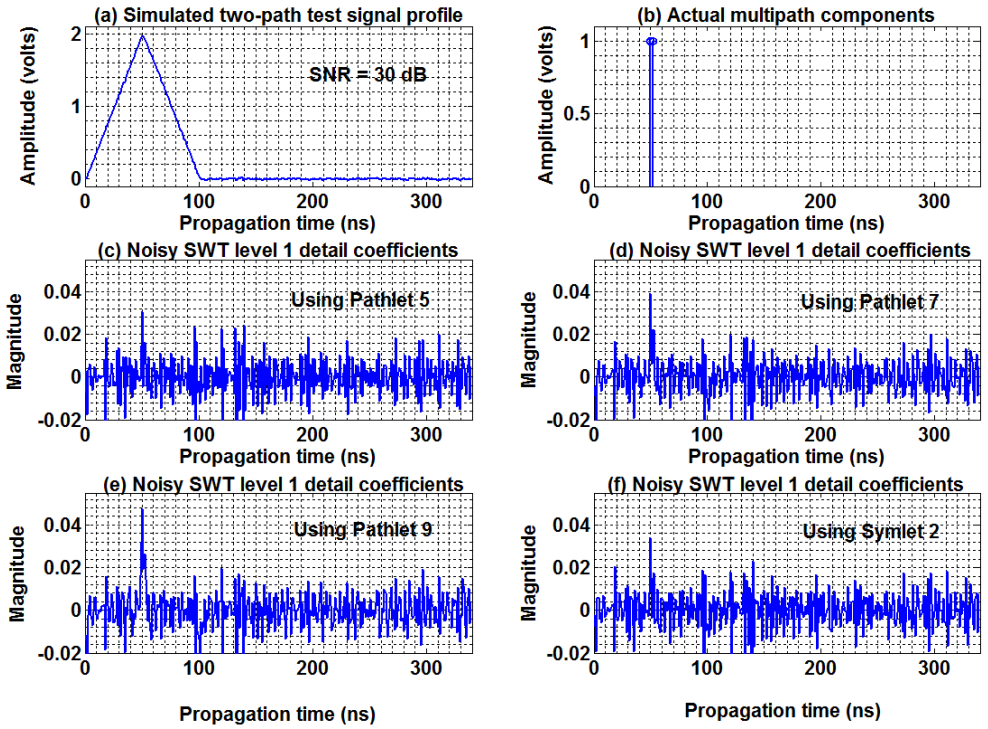

Figure 4.23 Noisy test signal profile with two paths having equal amplitudes, at an SNR of 30 dB, and corresponding SWT level 1 detail coefficients.

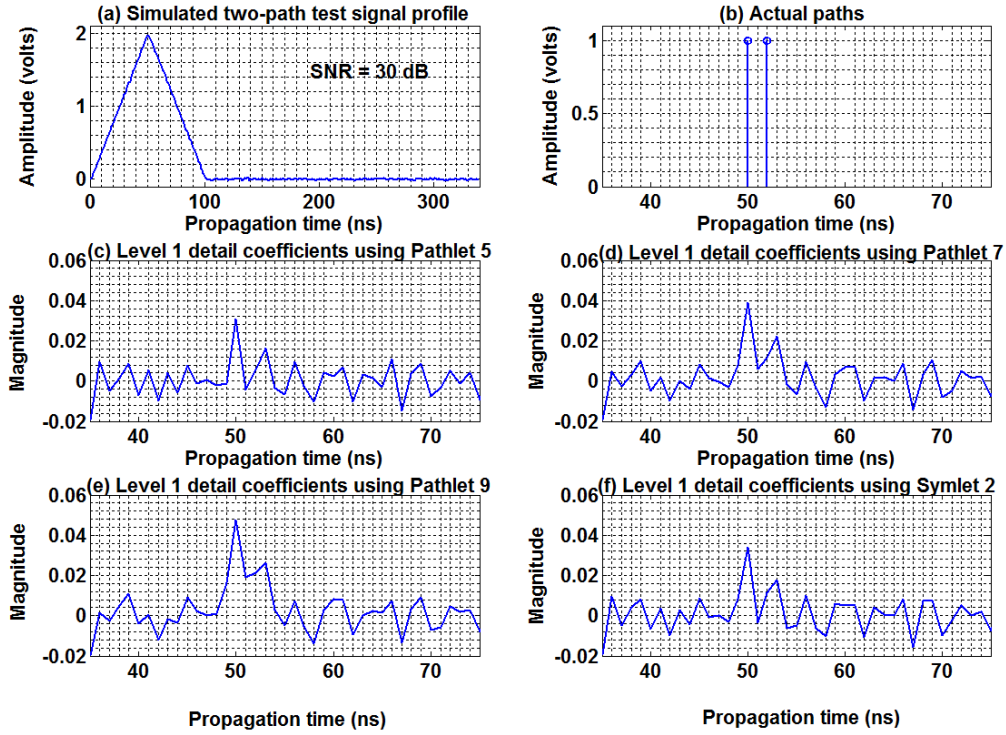

Figure 4.24 Time-expanded view of the two paths, and the noisy SWT level 1 detail coefficients, in Fig. 4.23.

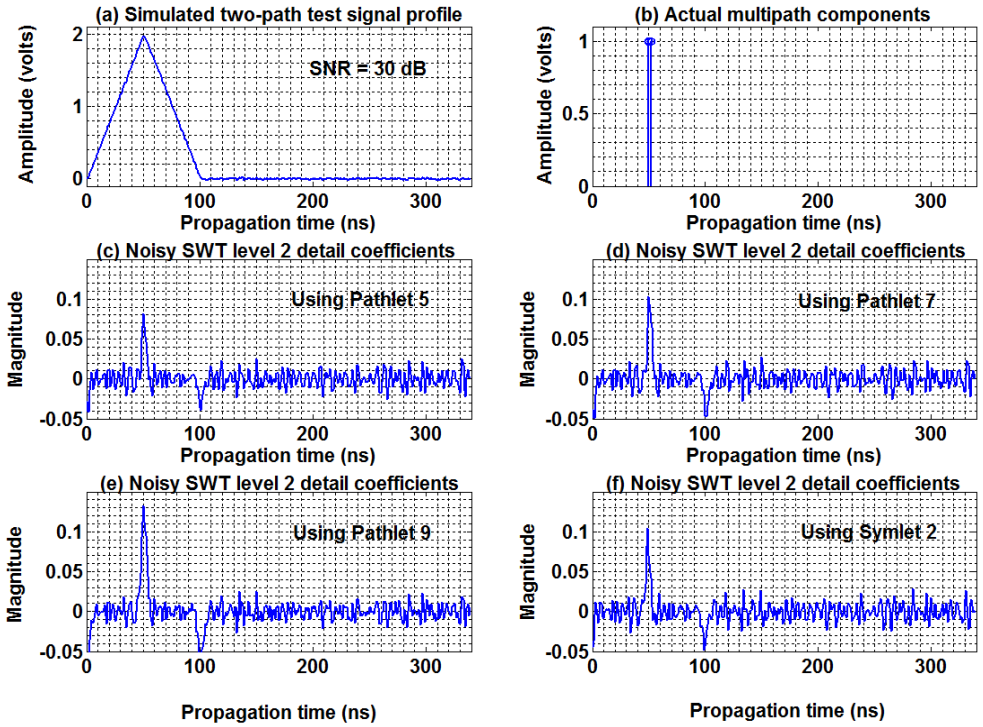

Figure 4.25 Noisy test signal profile with two paths having equal amplitudes, at an SNR of 30 dB, and corresponding SWT level 2 detail coefficients.

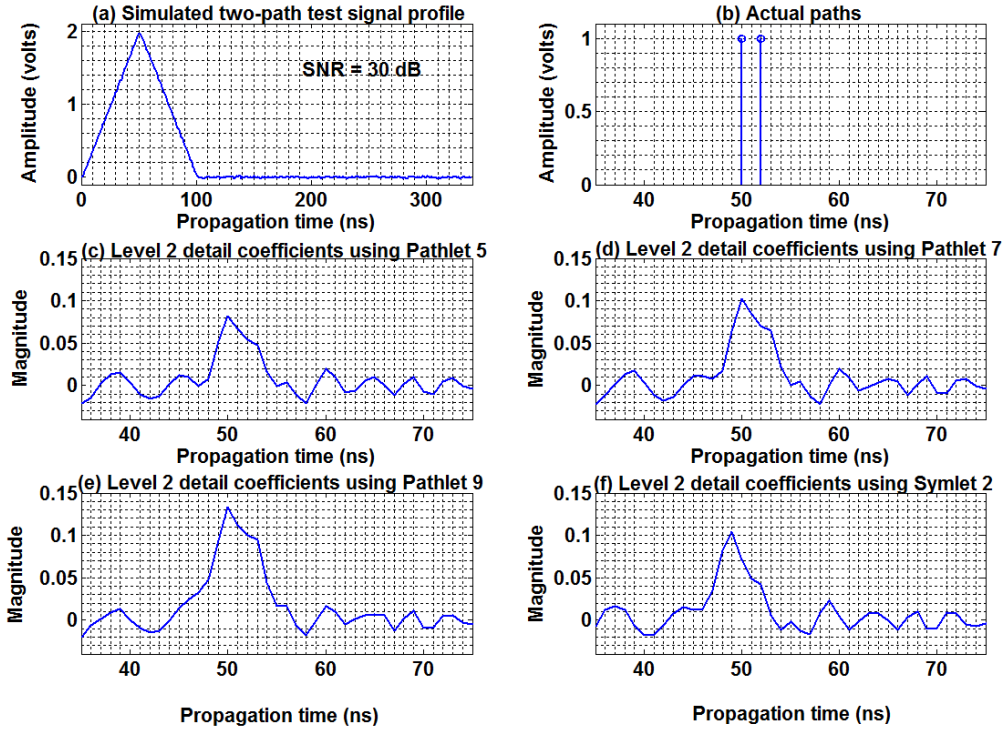

Figure 4.26 Time-expanded view of the two paths, and the noisy SWT level 2 detail coefficients, in Fig. 4.25.

The product of levels 1 and 2 detail coefficients of this noisy delay profile, defined according to (3.78), is shown in Figs. 4.27 (c-f). These results indicate that the wavelet transform detail coefficients that were attributed to noise, initially observed in Figs. 4.23 (c-f) and 4.25 (c-f), have now been suppressed in Figs. 4.27 (c-f).

The denoising scheme by wavelet thresholding, using hard thresholding and the MAD standard deviation estimate of noise, is then again applied to denoise the SWT level 1 detail coefficients of this noisy delay profile. The denoised detail coefficients are shown in Figs. 4.28 (c-f). The results obtained in this case show that only the first path can be detected at level 1 when Pathlets 7 and 9 are used. Pathlet 5 and Symlet 2 are, however, unable to detect either of the two paths due to the influence of noise. Therefore, at this SNR, the denoising method based on SWTMP using the levels 1 and 2 detail coefficients outperforms the denoising technique by wavelet thresholding procedure.

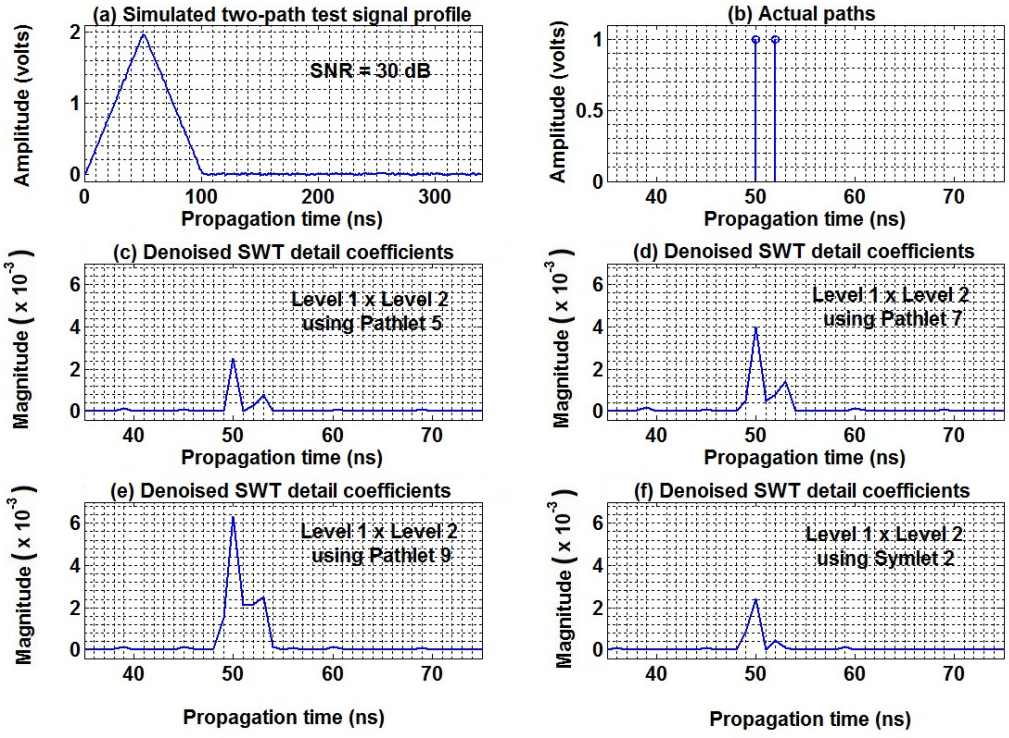

Figure 4.27 Noisy test signal profile with two paths having equal amplitudes, at an SNR of 30 dB, and the denoised SWT detail coefficients. Noise is suppressed by SWTMP using the levels 1 and 2 detail coefficients.

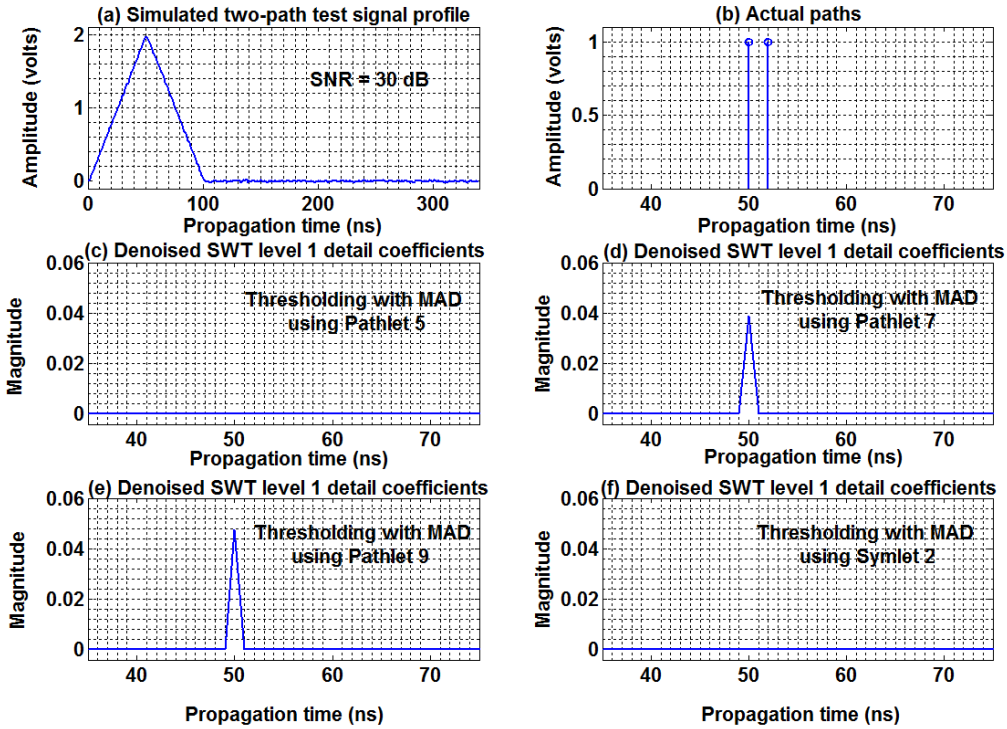

Figure 4.28 Noisy test signal profile with two paths having equal amplitudes, at an SNR of 30 dB, and the denoised SWT level 1 detail coefficients. Noise is removed by wavelet thresholding.

Once the number of paths and relative time-delays of the multipath components have been successfully estimated from the denoised detail coefficients, then the amplitudes of the individual paths can be determined. The amplitude estimation algorithm proposed in Section 3.4, has been applied to determine the amplitudes of the individual multipath components in the simulated noisy two-path delay profiles.

The actual and estimated delays, and amplitudes, of these two equal-amplitude paths at an SNR of 40 dB are shown in Table 4.3. The estimated number of paths and relative time-delays are based on the results obtained from using Pathlets 5, 7, 9, and Symlet 2 as the analysing wavelets, the denoised level 1 detail coefficients by thresholding, and the SWTMP.

These results show that the number of multipath components, as well as the relative delay and amplitude, are accurately estimated. Consequently, Pathlets 5, 7, 9, and

Symlet 2 can be successfully applied, in this research, to improve the resolution of impinging waves in synthetic mobile radio environments by more than a factor of ten.

Table 4.3 Actual and estimated delays, and amplitudes, of a simulated noisy test signal profile with two paths having equal amplitudes at an SNR of 40 dB.

Paths	Relative delay (ns)		Relative amplitude (dB)	
	Actual	Estimate	Actual	Estimate
1st	0	0	0	0
2nd	2	2	0	0

4.2.4 Four-path delay profile with differential amplitudes

In this section, the algorithm proposed for post-processing multipath delay profiles is applied in a test signal profile having four paths with differential amplitudes.

The parameters of this four-path delay profile are tabulated in Table 4.4. The multipath delay profile is as previously shown in Fig. 4.5. The amplitude of the first path is taken to be the reference amplitude, while the corresponding arrival time of this first path at 50 ns is taken to be the time reference. Pathlets 5, 7, 9, and Symlet 2 are again used as the analysing wavelets.

Table 4.4 Parameters of a simulated four-path delay profile with differential amplitudes.

Paths	Propagation time (ns)	Relative delay (ns)	Relative amplitude (dB)
1st	50	0	0
2nd	60	10	-2
3rd	82	32	-4
4th	256	206	-6

Since the relative delay of the 2nd and 3rd paths is less than the intrinsic delay resolution of the measurement system, it is therefore impossible to identify these paths in the delay profile. However, the 4th path at a relative delay of 206 ns can be clearly identified because this delay is greater than the intrinsic delay resolution of the channel sounder. This multipath delay profile, in the absence of noise, is shown in Figs. 4.29 (a) and 4.30 (a). The SWT levels 1 and 2 detail coefficients, of this noiseless test signal profile, are shown in Figs. 4.29 (c-f) and 4.30 (c-f) respectively. The actual multipath components are shown, for comparison, in Figs. 4.29 (b) and 4.30 (b).

The results in Figs. 4.29 (c-f) and 4.30 (c-f) shows that Pathlets 5, 7, 9, and Symlet 2 can be successfully applied to separate the constituent paths in this simulated four-path delay profile.

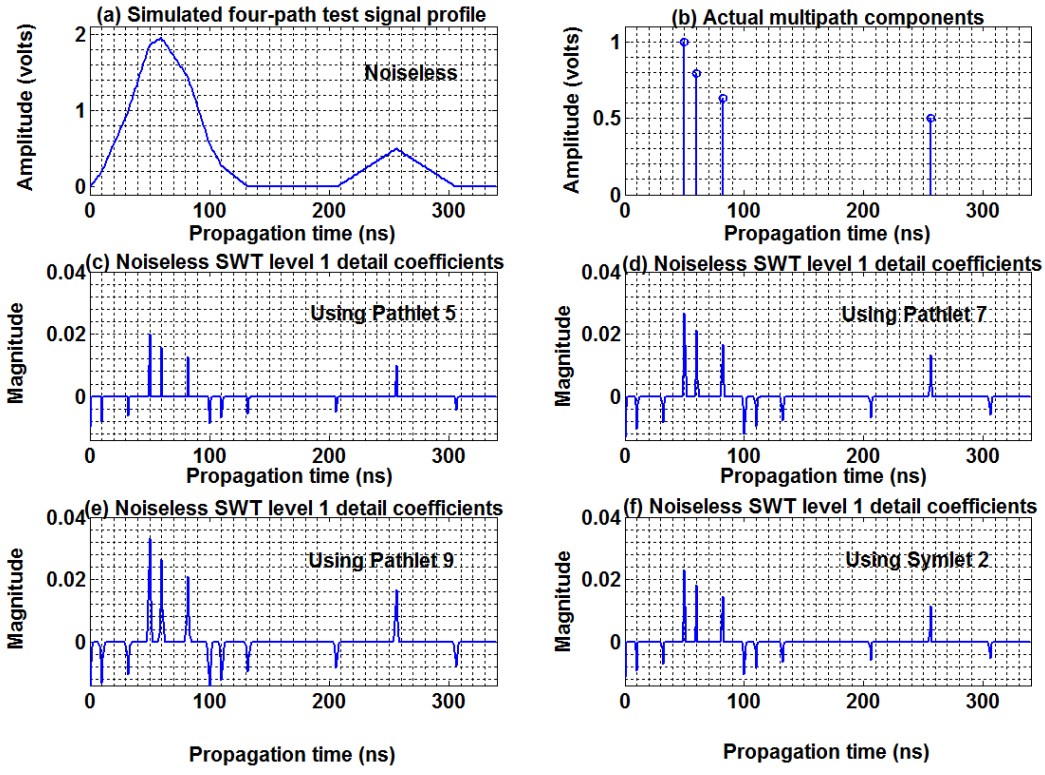

Figure 4.29 Noiseless test signal profile with four paths having differential amplitudes and corresponding SWT level 1 detail coefficients.

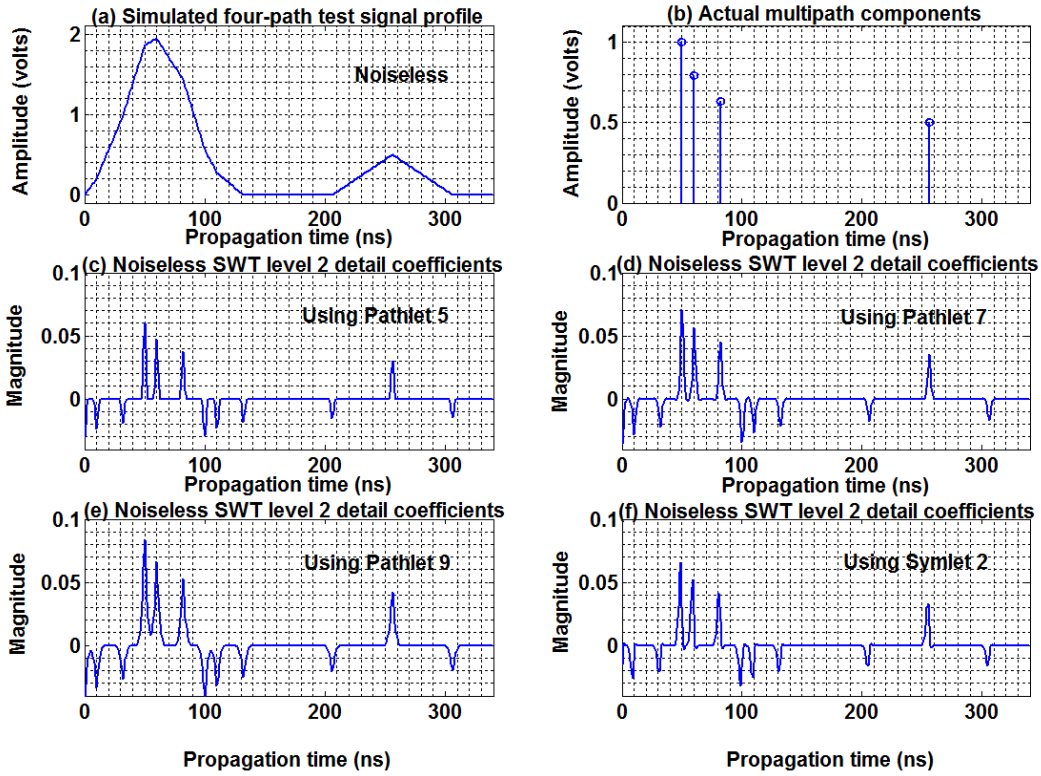

Figure 4.30 Noiseless test signal profile with four paths having differential amplitudes and corresponding SWT level 2 detail coefficients.

Next, AWGN is added to this simulated four-path delay profile. An SNR of 40 dB is, again, initially assumed. The SWT levels 1 and 2 detail coefficients of this noisy test signal profile are shown in Figs. 4.31 (c-f) and 4.32 (c-f) respectively. The dominant peaks in these noisy wavelet transform coefficients identify the actual constituent multipath components within the four-path delay profile. As expected, the magnitude of these dominant peaks is reinforced while the noise diminishes as the wavelet transform decomposition level increases.

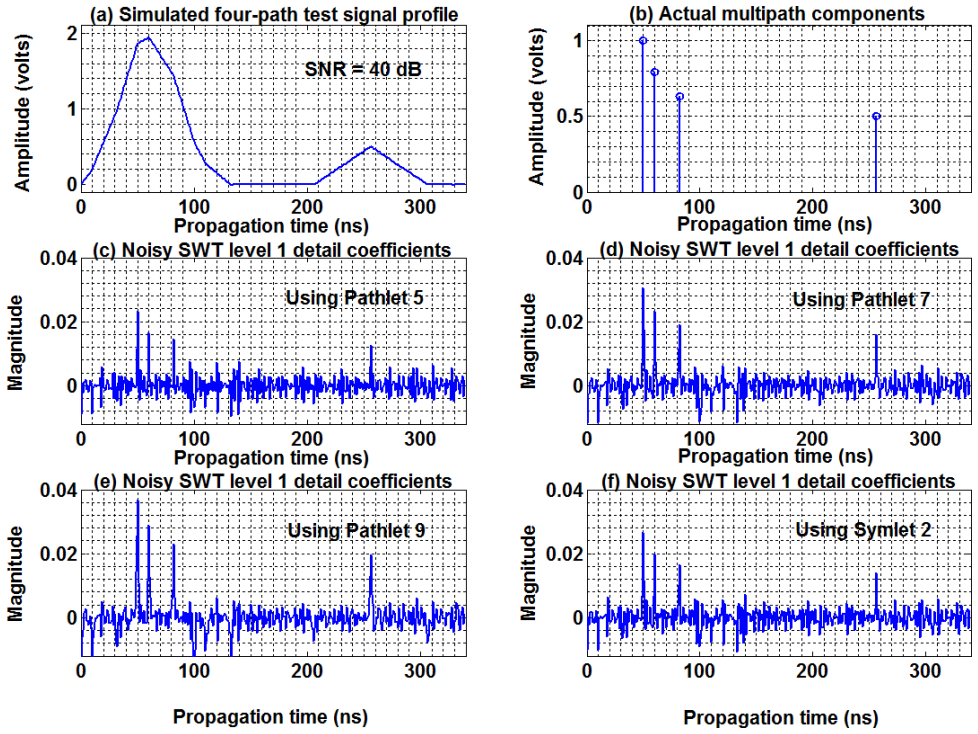

Figure 4.31 Noisy test signal profile with four paths having differential amplitudes, at an SNR of 40 dB, and corresponding SWT level 1 detail coefficients.

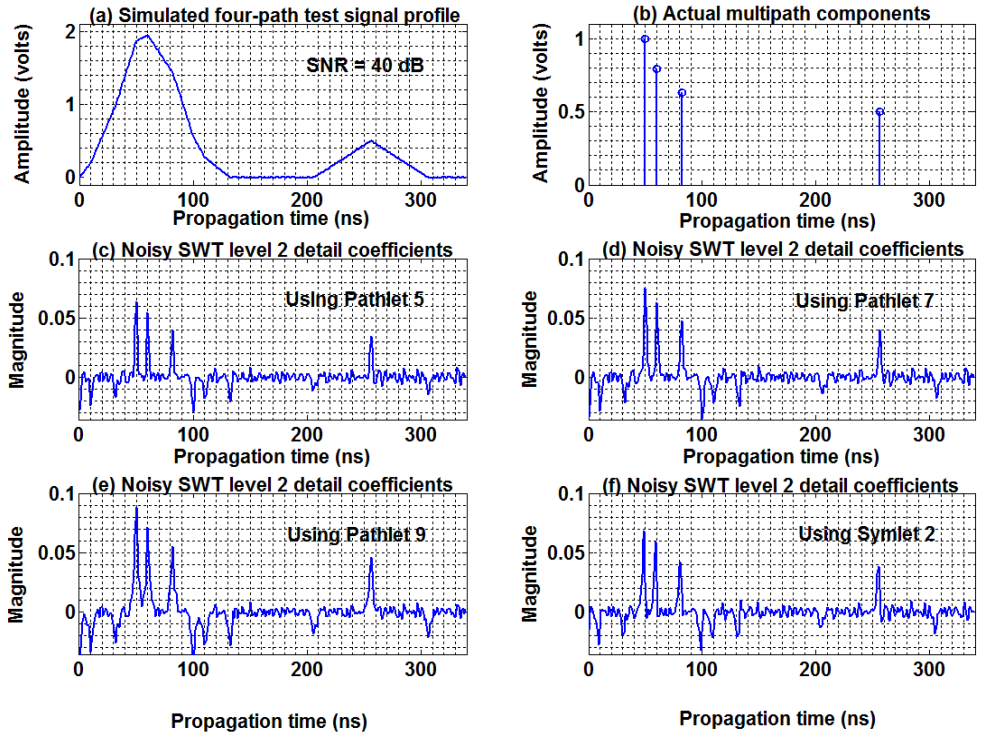

Figure 4.32 Noisy test signal profile with four paths having differential amplitudes, at an SNR of 40 dB, and corresponding SWT level 2 detail coefficients.

The results obtained from applying the SWTMP denoising strategy, using the levels 1 and 2 detail coefficients, are given in Figs. 4.33 (c-f). These show that the detail coefficients that were attributed to noise, in Figs. 4.31 (c-f) and 4.32 (c-f), have now been suppressed in Figs. 4.33 (c-f). As expected, Pathlet 9 is the most robust to noise; observed in Fig. 4.33 (e).

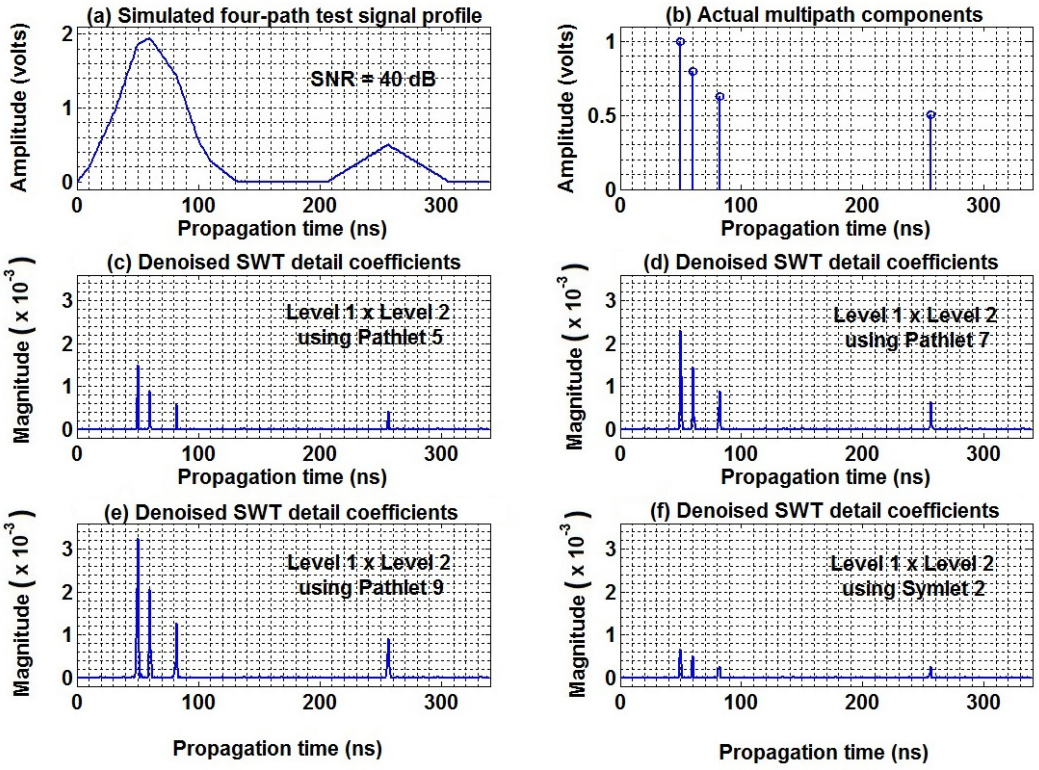

Figure 4.33 Noisy test signal profile with four paths having differential amplitudes, at an SNR of 40 dB, and the denoised SWT detail coefficients. Noise is suppressed by SWTMP using the levels 1 and 2 detail coefficients.

The denoising scheme by wavelet thresholding, using hard thresholding and the MAD standard deviation estimate of noise, is now applied to denoise the SWT levels 1 and 2 detail coefficients of this noisy four-path delay profile. The denoised detail coefficients are shown in Figs. 4.34 (c-f) and 4.35 (c-f). These results show that all the four constituent paths can be successfully extracted at levels 1 and 2 of the wavelet transform. The denoised detail coefficients can then be subsequently used as an estimate of the number of multipath components and the time-delays.

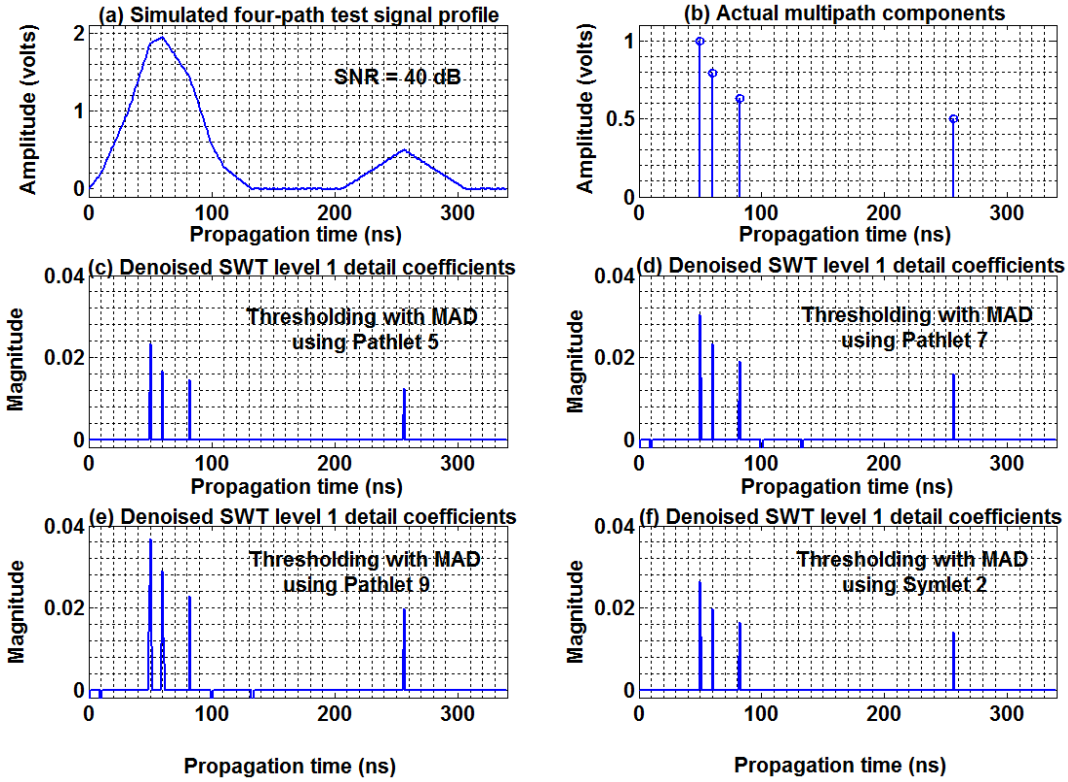

Figure 4.34 Noisy test signal profile with four paths having differential amplitudes, at an SNR of 40 dB, and the denoised SWT level 1 detail coefficients. Noise is removed by wavelet thresholding.

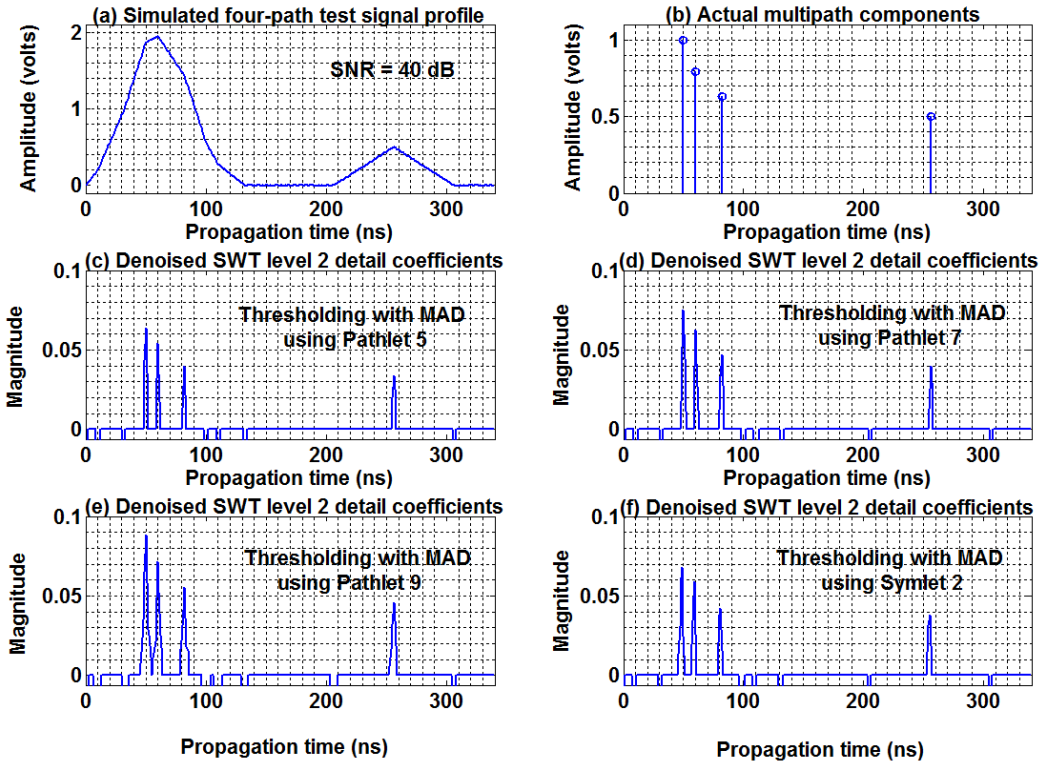

Figure 4.35 Noisy test signal profile with four paths having differential amplitudes, at an SNR of 40 dB, and the denoised SWT level 2 detail coefficients. Noise is removed by wavelet thresholding.

The SWT levels 1 and 2 detail coefficients of this noisy four-path delay profile at an SNR of 30 dB are shown in Figs. 4.36 (c-f) and 4.37 (c-f) respectively. In this case, the four constituent multipath components cannot be identified at level 1 prior to denoising. These four constituent paths appear as observable dominant peaks within the level 2 detail coefficients.

The SWTMP denoising technique, using the levels 1 and 2 detail coefficients, is now applied. The results obtained indicate that most of the detail coefficients that were attributed to noise, observed in Figs. 4.36 (c-f) and 4.37 (c-f), have been suppressed in Figs. 4.38 (c-f). Some spurious coefficients attributed to noise are also observed in Figs. 4.38 (c-f). Nevertheless, these results, again, demonstrate that Pathlet 9 is the most robust to the influence of noise when compared with the other analysing wavelets used in this study.

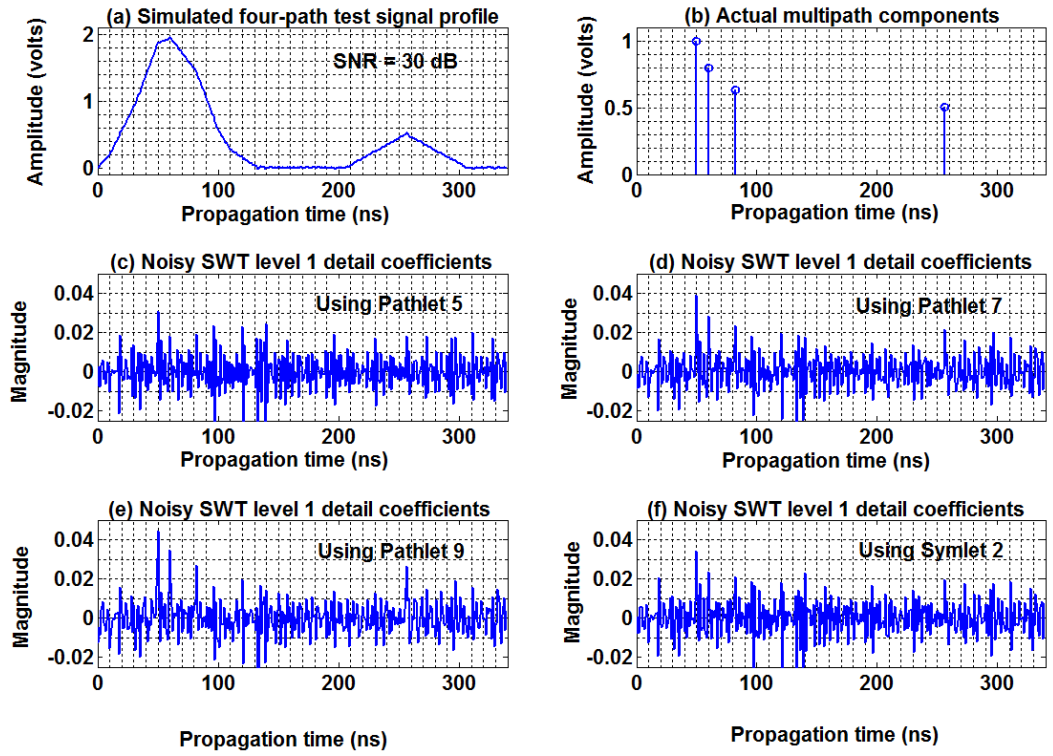

Figure 4.36 Noisy test signal profile with four paths having differential amplitudes, at an SNR of 30 dB, and corresponding SWT level 1 detail coefficients.

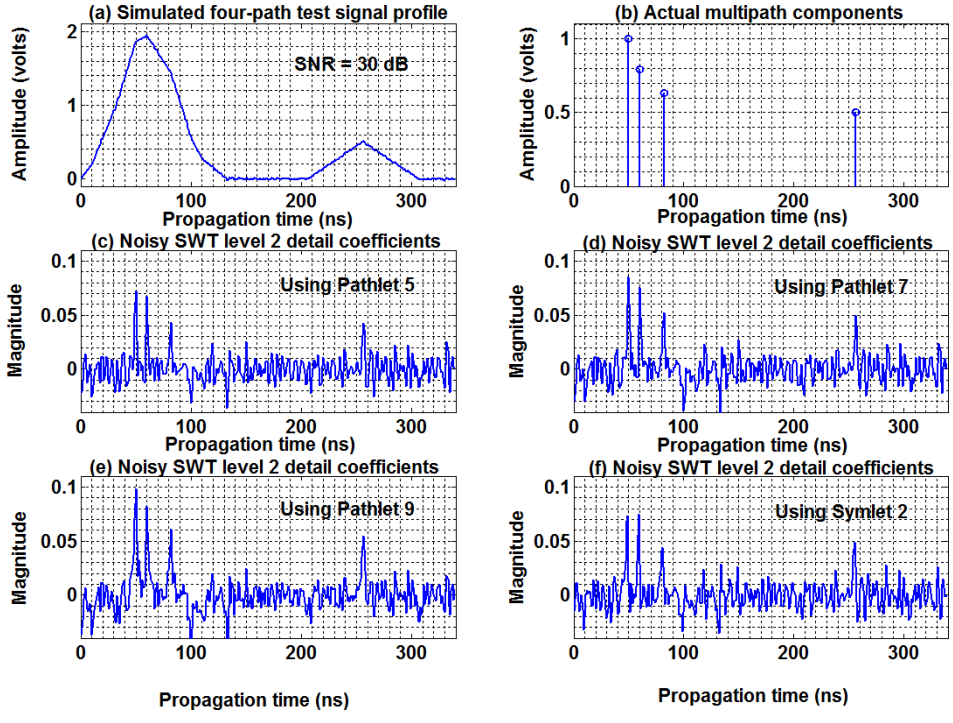

Figure 4.37 Noisy test signal profile with four paths having differential amplitudes, at an SNR of 30 dB, and corresponding SWT level 2 detail coefficients.

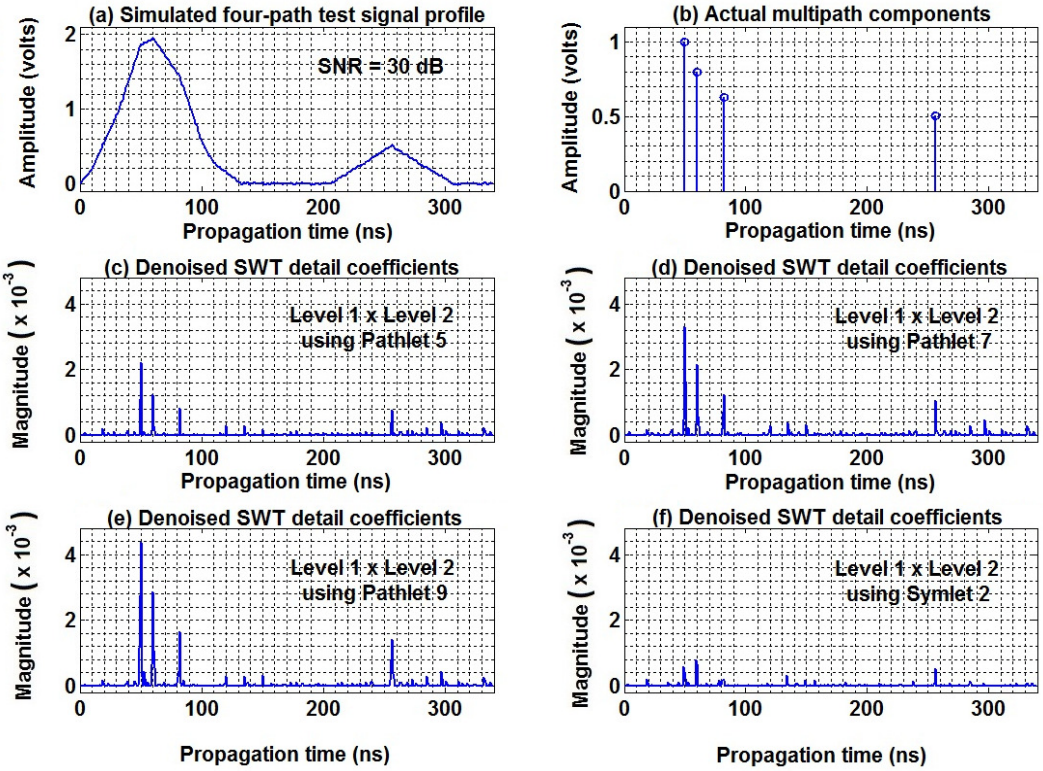

Figure 4.38 Noisy test signal profile with four paths having differential amplitudes, at an SNR of 30 dB, and the denoised SWT detail coefficients. Noise is suppressed by SWTMP using the levels 1 and 2 detail coefficients.

The denoised SWT levels 1 and 2 detail coefficients, based on wavelet thresholding, are shown in Figs. 4.39 (c-f) and 4.40 (c-f) respectively. The results obtained show that none of the constituent paths could be extracted at level 1 after denoising when Pathlet 5 and Symlet 2 are used. Only the 1st and 2nd paths were detected, at this level 1, when Pathlet 9 is used, while just the 1st path was detected when Pathlet 7 is used. Conversely, at level 2 all the four multipath components in this noisy test signal profile are successfully extracted with all the analysing wavelets used.

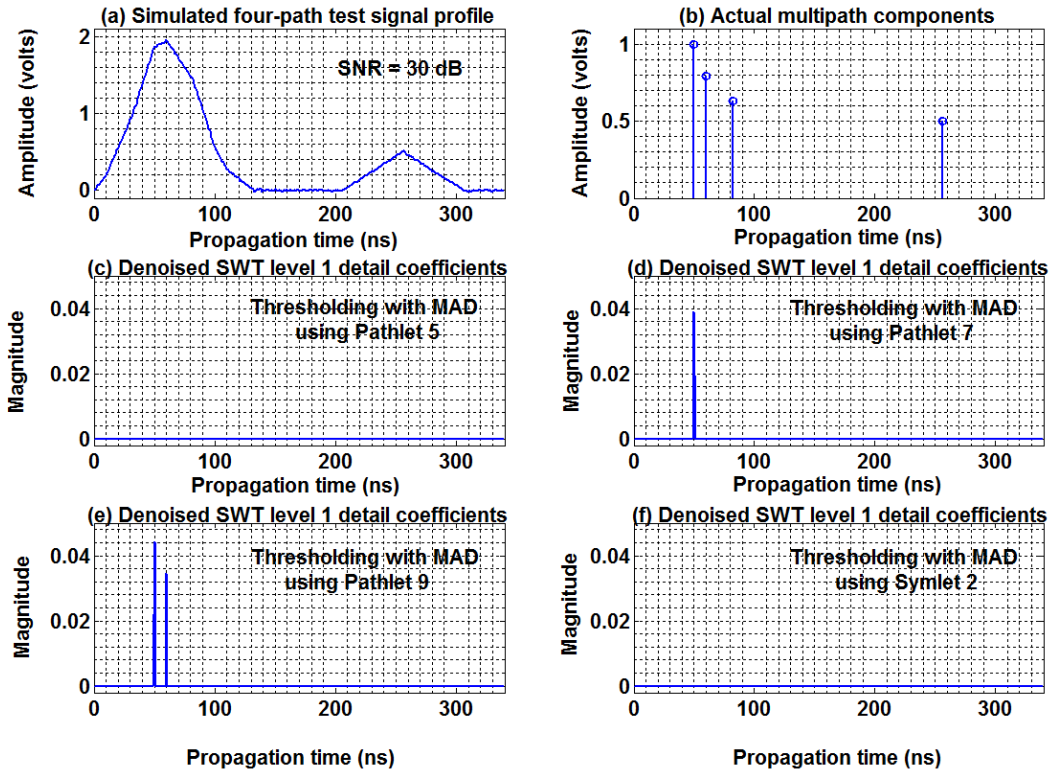

Figure 4.39 Noisy test signal profile with four paths having differential amplitudes, at an SNR of 30 dB, and the denoised SWT level 1 detail coefficients. Noise is removed by wavelet thresholding.

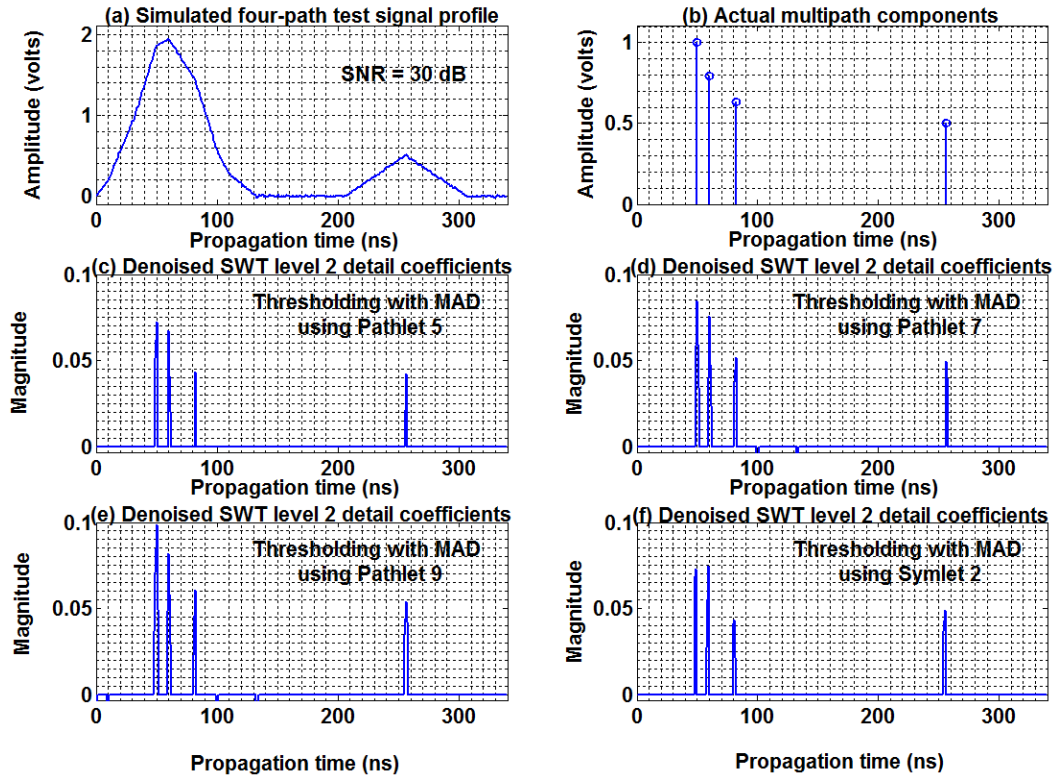

Figure 4.40 Noisy test signal profile with four paths having differential amplitudes, at an SNR of 30 dB, and the denoised SWT level 2 detail coefficients. Noise is removed by wavelet thresholding.

Finally, the SWT levels 1 and 2 detail coefficients of this four-path delay profile at an SNR of 25 dB are shown in Figs. 4.41 (c-f) and 4.42 (c-f) respectively. At this SNR, the constituent multipath components within the delay profile could not be identified from the levels 1 and 2 detail coefficients prior to denoising.

The results from applying the SWTMP denoising technique, using the levels 1 and 2 detail coefficients, are shown in Figs. 4.43 (c-f). In this case, though most of the detail coefficients that were attributed to noise, in Figs. 4.41 (c-f) and 4.42 (c-f), have been suppressed in Figs. 4.43 (c-f), however many spurious coefficients attributed to noise are also obtained.

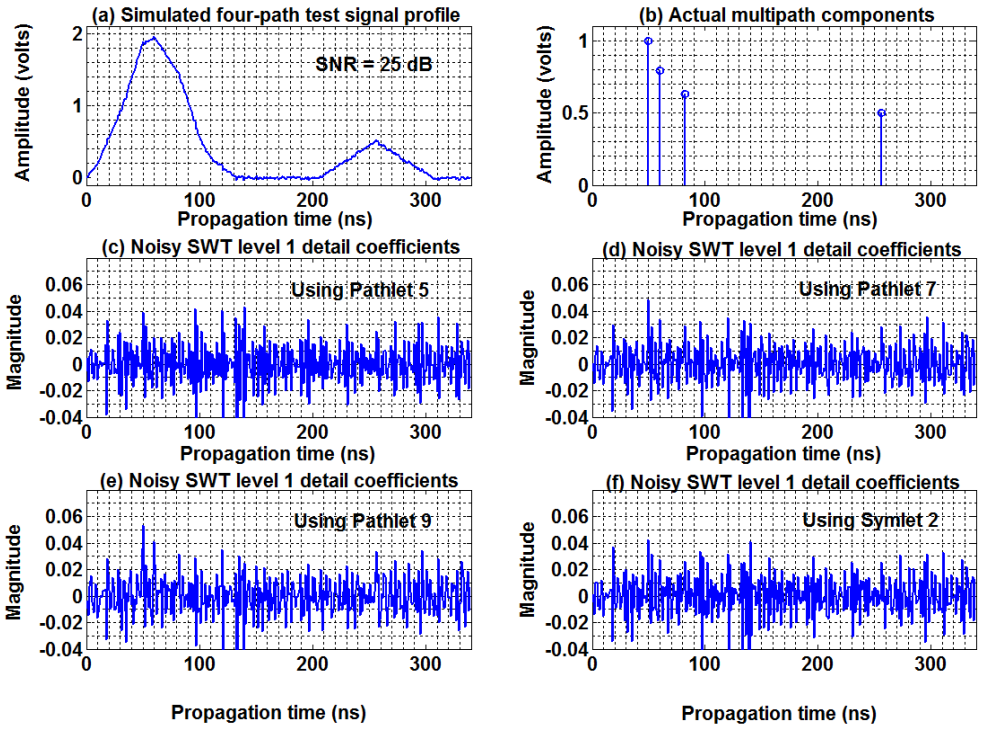

Figure 4.41 Noisy test signal profile with four paths having differential amplitudes, at an SNR of 25 dB, and corresponding SWT level 1 detail coefficients.

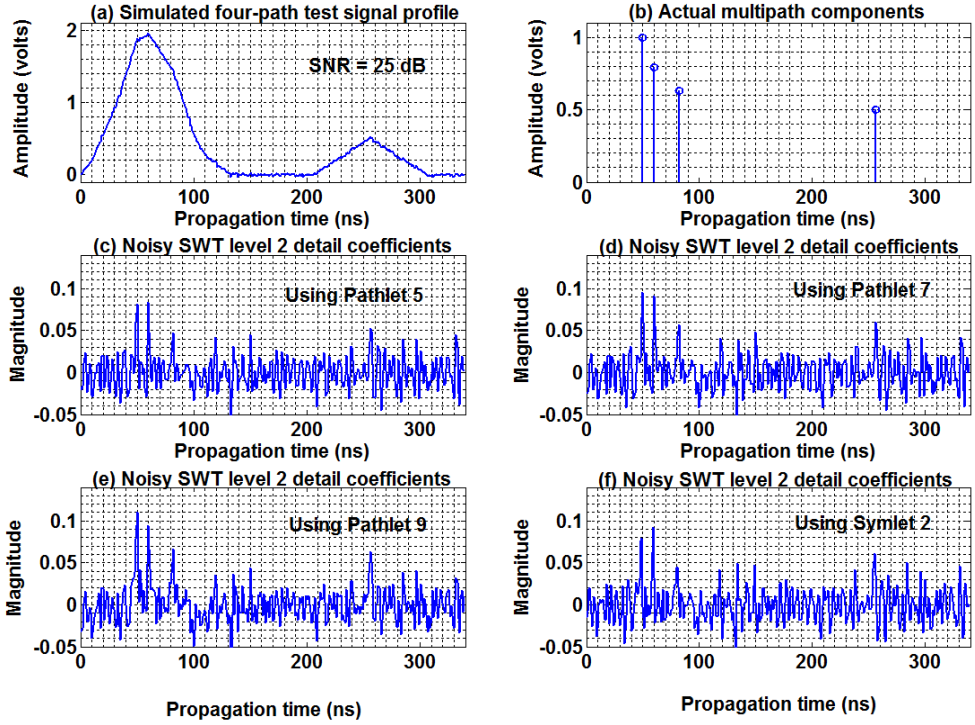

Figure 4.42 Noisy test signal profile with four paths having differential amplitudes, at an SNR of 25 dB, and corresponding SWT level 2 detail coefficients.

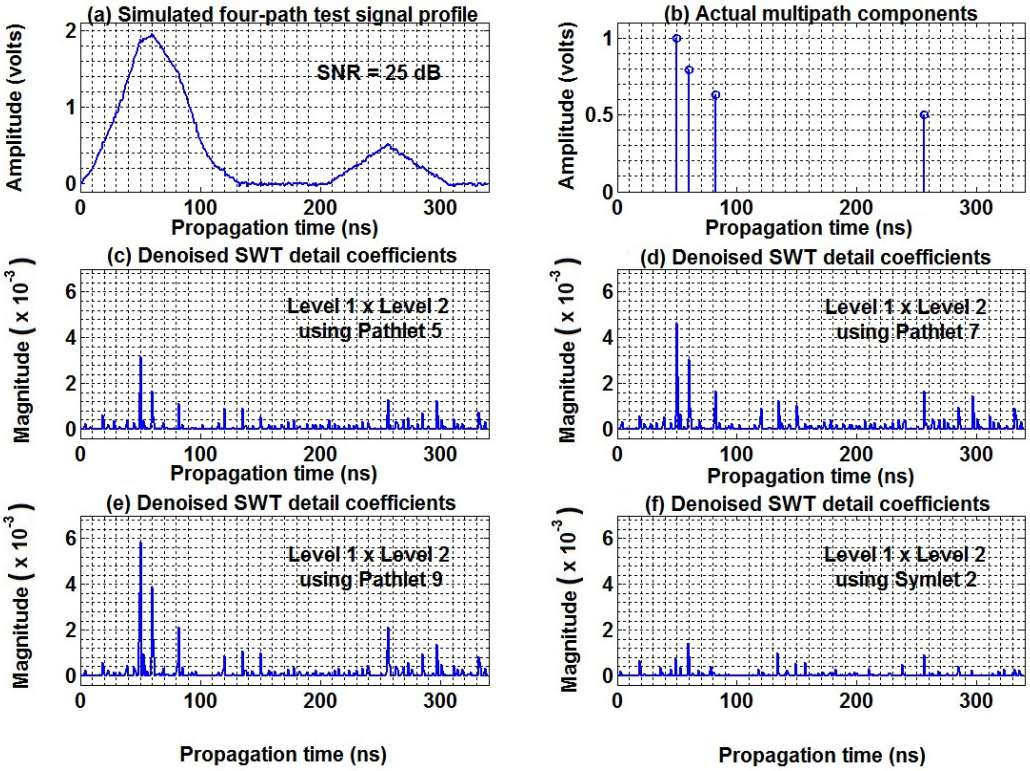

Figure 4.43 Noisy test signal profile with four paths having differential amplitudes, at an SNR of 25 dB, and the denoised SWT detail coefficients. Noise is suppressed by SWTMP using the levels 1 and 2 detail coefficients.

The denoised SWT levels 1 and 2 detail coefficients, based on thresholding, are shown in Figs. 4.44 (c-f) and 4.45 (c-f) respectively. The results obtained show that none of the four constituent paths could be detected at level 1 after denoising for all the wavelets used. Though the result from level 2 show an improvement over that of level 1, however only Pathlet 9 could extract all the four multipath components of this noisy test signal profile as seen in Fig. 4.45 (e). Pathlets 5 and 7, as well as Symlet 2, could only detect the 1st and 2nd paths at level 2 after thresholding.

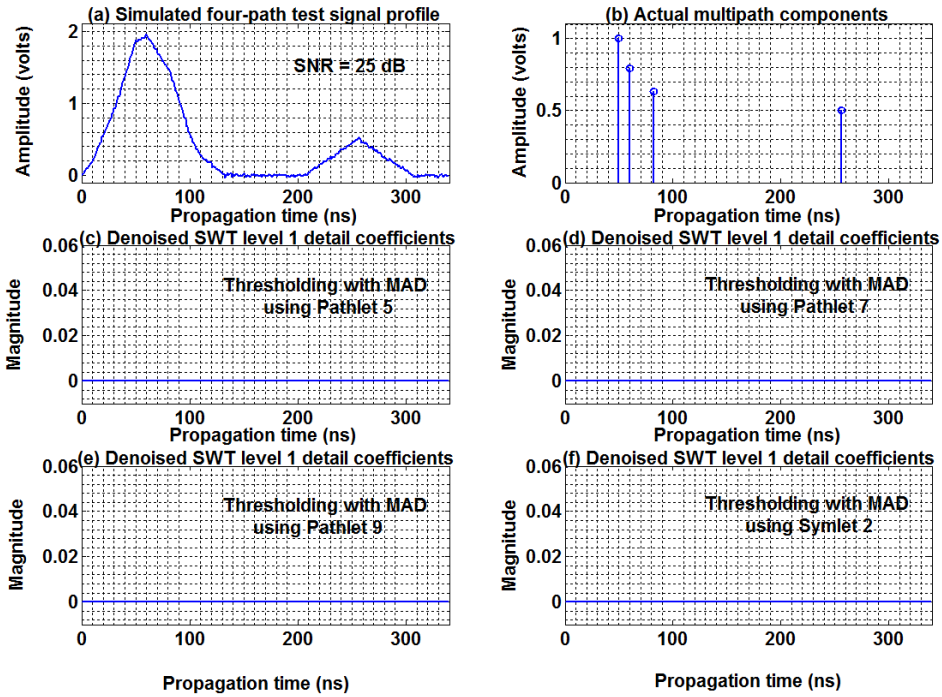

Figure 4.44 Noisy test signal profile with four paths having differential amplitudes, at an SNR of 25 dB, and the denoised SWT level 1 detail coefficients. Noise is removed by wavelet thresholding.

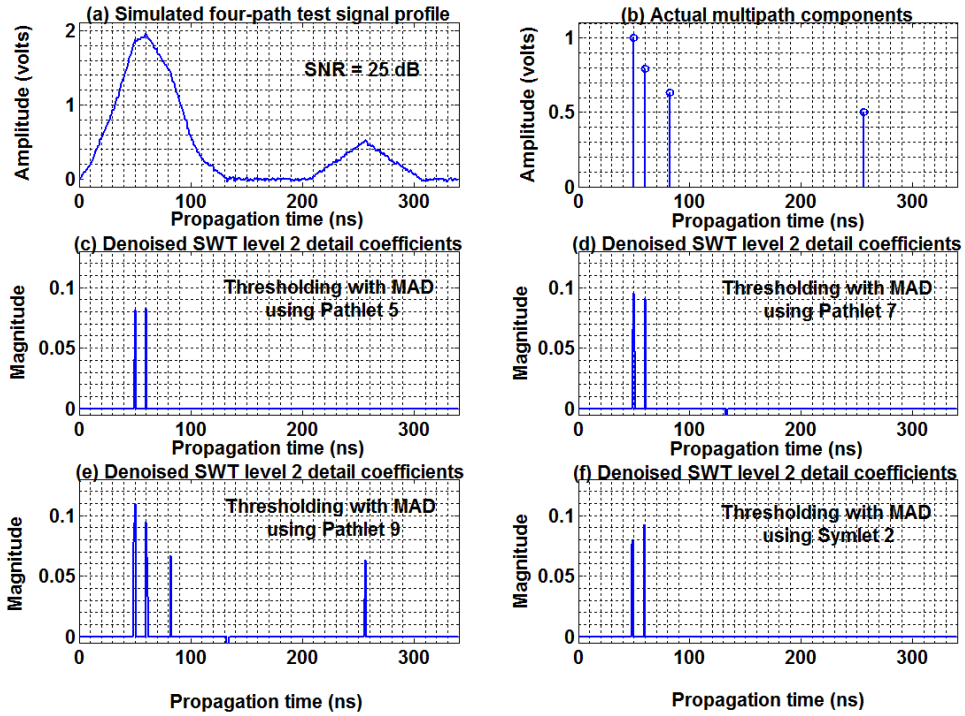

Figure 4.45 Noisy test signal profile with four paths having differential amplitudes, at an SNR of 25 dB, and the denoised SWT level 2 detail coefficients. Noise is removed by wavelet thresholding.

After the number of paths and relative time-delays of the constituent multipath components of the four-path test signal profile have been successfully estimated from the denoised detail coefficients, then the amplitudes of the individual paths can be determined. The amplitude estimation algorithm, derived in Section 3.4, has again been applied to determine the amplitudes of the individual multipath components. The actual and estimated delays, and amplitudes, of this test signal profile at an SNR of 25 dB are shown in Table 4.5. The estimated number of paths and relative time-delays are based on the results obtained from using Pathlet 9, and the denoised level 2 detail coefficients from thresholding. These results show that the delays and amplitudes of the four constituent paths are accurately estimated. These results are in general agreement with the conclusions in Section 4.2.3; that the proposed post-processing algorithm in this research can be successfully applied to improve the resolution of impinging waves in synthetic mobile radio environments by more than a factor of ten.

Then the mean excess delay and rms delay spread, for the synthetic four-path radio channel, are now computed using (2.1) and (2.2) respectively. The mean excess delay and rms delay spread (actual and estimated), are tabulated in Table 4.6. These results show that the estimated mean excess delay and rms delay spread deviates from the actual values by $10\ ps$. This illustrates the robustness of the algorithm proposed in Fig 3.13 in estimating the multipath channel parameters.

Table 4.5 Actual and estimated delays, and amplitudes, of a simulated noisy test signal profile having four paths with differential amplitudes at an SNR of 25 dB.

Paths	**Relative delay (ns)**		**Relative amplitude (dB)**	
	Actual	**Estimate**	**Actual**	**Estimate**
1st	0	0	0	0
2nd	10	10	-2	-2
3rd	32	32	-4	-4
4th	206	206	-6	-6

Table 4.6 Mean excess delay and rms delay spread of a simulated noisy test signal profile having four paths with differential amplitudes. The parameters of this test signal are shown in Table 4.5.

Mean excess delay (ns)		**RMS delay spread (ns)**	
Actual	**Estimate**	**Actual**	**Estimate**
31.05	31.04	62.59	62.60

4.3 Summary

The estimation of multipath channel parameters in synthetic mobile radio environment, using the algorithm proposed in Chapter 3, has been presented in this chapter. Noisy and noiseless synthetic mobile radio channel scenarios were simulated, and used in these analyses.

Multipath channel parameters such as the mean excess delay and rms delay spread provide a description of the mobile radio channels. One way of deriving these channel parameters, in practice, is through the use of a sliding correlator channel sounding technique. Consequently, typical multipath delay profiles obtained with this channel sounder are simulated as test signals in this study. The intrinsic delay resolution of this measurement system is assumed to be 50 ns.

Multipath delay profiles consisting of one, two, and four paths have been simulated. Performance comparison was then made between members of the newly derived family of wavelets called Pathlet in this study, and the Daubechies near symmetric wavelet family member known as Symlet 2, in resolving the constituent multipath components.

The simulation results for the one-path delay profile, in the absence of noise, show that Pathlets 5, 7, 9, and Symlet 2 can be successfully applied to detect the single path in the

delay profile, by observing the SWT detail coefficients. The levels 1 and 2 detail coefficients have been used in this case. The results obtained also show that the noiseless detail coefficients propagate across to the coarse SWT levels with larger peaks.

When this one-path delay profile is corrupted with AWGN at an SNR of 30 dB, the single path in the delay profile is seen as the dominant peak within the noisy SWT levels 1 and 2 detail coefficients. This dominant peak is reinforced, within the noisy detail coefficients, while the noise diminishes as the wavelet transform decomposition level increases.

Next, a two-path delay profile with equal-amplitude paths is simulated. The second path is at a delay of 2 ns relative to the arrival time of the first path. Since this delay separation is less than the intrinsic delay resolution of 50 ns, therefore these two paths are not distinguishable as distinct pulses prior to post-processing. The wavelet transform of this two-path delay profile, in the absence of noise, show that Pathlets 5, 7, 9, and Symlet 2 can be successfully applied to resolve the two equal-amplitude paths at level 1 by more than a factor of ten. These simulation results further show that Pathlet 9 has the best correlation with the multipath signals, since it produces detail coefficients with the largest magnitude. Moreover, this Pathlet family member has a lower resolution than the other wavelets used, due to its large support (in time). For example Pathlet 9 is unable to clearly separate the two peaks in the two equal-amplitude paths, as seen in the time-expanded view of Fig. 4.14 (e). Pathlet 5 gives the best multipath resolution, since it has the most compact support, as seen in the time-expanded view of Fig. 4.14 (c).

This two-path delay profile is now corrupted with AWGN, at SNRs of 40 dB and then 30 dB. Performance comparison was made between the two noise reduction strategies that are used in this study to filter-out noise from the detail coefficients. At an SNR of 40 dB, the results of the SWTMP denoising technique show that the detail coefficients attributed to noise are suppressed and the actual two constituent paths extracted. Similarly, when the denoising procedure based on thresholding using the MAD estimate is applied at level 1, the results obtained show that the detail coefficients that were

attributed to noise are removed and the two multipath components are extracted. Consequently 2 ns resolution can be achieved at high SNRs, when all the members of Pathlet family and Symlet 2 are used as analysing wavelets in resolving synthetic two equal-amplitude paths. These results also show that while both Pathlets and Symlet 2 can be successfully applied to resolve closely spaced multipath components in noise by more than a factor of ten, Pathlet 9 is however the most robust to the noise.

At an SNR of 30 dB, the results from the SWTMP denoising technique show that the detail coefficients that were attributed to noise are suppressed and the two constituent paths detected. However, when the denoising procedure based on thresholding is applied at level 1, the results obtained show that though the noisy detail coefficients have been removed, only one of the two closely-spaced paths could be identified after denoising.

Finally, a test signal profile having four paths with differential amplitudes is simulated. In this simulation, the arrival time of the first multipath component at 50 ns is taken to be the time reference while the other three multipath components are at delays of 10 ns, 32 ns, and 206 ns relative to the arrival time of the first multipath component. The results in the absence of noise show that Pathlets 5, 7, 9, and Symlet 2 can again be successfully applied to separate the constituent four paths in the delay profile by at least a factor of five.

This four-path delay profile is corrupted with AWGN, at SNRs of 40 dB, 30 dB, and 25 dB. Performance comparison is then made between the two noise reduction schemes used to filter-out noise from the detail coefficients in this research. At an SNR of 40 dB, the four constituent multipath components are detected in noise as the dominant peaks within the noisy SWT levels 1 and 2 detail coefficients, prior to denoising. These dominant peaks are also reinforced as the wavelet transform decomposition level increases. The results from the SWTMP denoising method show that the four constituent multipath components are extracted, while the wavelet transform detail coefficients that were attributed to noise are suppressed. The performance of Symlet 2 at detecting the four paths, in this case, is poor when compared with the members of Pathlet family.

When the denoising procedure based on thresholding is applied at levels 1 and 2, the results obtained shows that the four constituent multipath components are resolved and the detail coefficients that were attributed to noise removed after denoising. These results are in general agreement with the noiseless case.

At an SNR of 30 dB, the four constituent multipath components could only be identified as the dominant peaks within the noisy SWT level 2 detail coefficients prior to denoising. These four constituent multipath components are masked in noise at level 1 of the detail coefficients. The results from the SWTMP denoising scheme show that the four constituent multipath components are extracted by Pathlets 5, 7, and 9, while most of the detail coefficients that were attributed to noise are suppressed. The performance of Symlet 2 at detecting the four paths is again poor when compared with the members of Pathlet family. When the denoising procedure based on thresholding is applied, the results obtained show that all the four constituent multipath components are extracted at level 2 of the detail coefficients for all the wavelets used.

Meanwhile, a comparison with the results obtained from using conventional high-resolution algorithms such as the multiple signal classification algorithm, reviewed in Section 2.3.4, has been made. It shows that the MUSIC delay pseudo-spectrum degrades below 16 ns (that is about a factor of three) at an SNR of 30 dB. Consequently, multipath components with relative delays less than 16 ns could not be resolved by the MUSIC algorithm. This indicates that the wavelet-based approach proposed in this study overcomes the resolution limitation in the MUSIC algorithm, since a resolution of at least 5 ns can be achieved in this research.

At an SNR of 25 dB, the four constituent multipath components could not be clearly identified in noise at level 1 or 2, prior to denoising, because these four paths have been masked in noise. The results from the SWTMP denoising technique shows that whilst the peaks attributed to the actual multipath components are extracted by the Pathlet family, many spurious detail coefficients attributed to noise are also brought out. When the denoising scheme based on thresholding is applied, the results obtained show that

none of the four paths could be detected at level 1. All the four constituent multipath components are however extracted at level 2 of the detail coefficients after denoising, only when Pathlet 9 is used.

These results obtained from the wavelet analysis of the noisy one-path, two-path, and four-path delay profiles are in general agreement with the conclusions in Section 3.3.1. That is, Pathlet 9 is the most robust to noise, followed by Pathlet 7, Symlet 2, and Pathlet 5 as the least robust to noise. Furthermore, these results show that Pathlets 5, 7, 9, and Symlet 2 can be successfully applied, in this study, to improve the resolution of impinging waves in synthetic mobile radio environments by more than a factor of ten.

In practical implementations, it is suggested that Pathlets 7 and 9 be applied in the two noise reduction schemes; that are used to filter-out noise from the detail coefficients in this research. Pathlet 9 is robust to noise, while Pathlet 7 achieves a compromise between obtaining acceptable resolution of the multipath components and having a good dynamic range. Features that are extracted by both Pathlets 7 and 9 can therefore be regarded as the true parameter estimates.

A best paper award based on the results obtained from this research, as well as some published research papers on topics related to this study are shown in Appendix D.

CHAPTER 5

EFFECTS OF BANDWIDTH LIMITATION

5.1 Introduction

In Chapter 3, a novel wavelet family named "Pathlets" and wavelet-based denoising strategies have been developed for use in estimating the number of multipath components and time-delays. An amplitude estimation procedure, for the individual multipath components, has been subsequently derived. Series of computer simulations were then presented in Chapter 4 to show multipath components resolution using the stationary wavelet transform and wavelet-based denoising with Pathlets 5, 7, 9, and Symlet 2 as the analysing wavelets. The simulated multipath delay profiles, used in these analyses, have been assumed to be without band-limitations.

The output signals from the measurement systems in practice, which can be used to obtain experimental data for the purpose of channel modelling, are bandwidth limited to minimise the influence of noise. Consequently, the digital signal processing algorithm proposed in Chapter 3 is applied in this chapter to resolve the constituent multipath components in band-limited delay profiles. This is done to examine the effects of band-limitations in the implementation of the proposed wavelet-based algorithm.

The test signal models discussed in Section 4.2 have been initially analysed without considering the effect of bandwidth limitations. When band-limitation is incorporated, then (3.28) becomes

$$\tilde{y}_N(n) = \left(x_N(n) + \eta_N(n)\right) * \chi(n), \tag{5.1}$$

where $\tilde{y}_N(n)$ denotes the band-limited replica of $y_N(n)$, $*$ denotes the convolution operation, while $\chi(n)$ is the impulse response of the filter used in the band-limitation.

In wavelet transform domain, $\tilde{y}_N(n)$ becomes

$$\tilde{d}_{j,k} = \langle \tilde{\boldsymbol{y}}, \boldsymbol{g} \rangle, \qquad j = 1, 2, \ldots, J, \quad k = 0, 1, \ldots, N_j - 1, \tag{5.2}$$

where $\tilde{d}_{j,k}$ represents the wavelet transform detail coefficients of the band-limited signal $\tilde{\boldsymbol{y}}$, at the k^{th} coordinates and j^{th} level. N_j is the number of wavelet transform coefficients at the j^{th} level, $\boldsymbol{g}$ is the vector of the decomposition wavelet filter coefficients, $\tilde{\boldsymbol{y}}$ is the vector of $\tilde{y}_N(n)$, while J denotes the coarsest decomposition level.

The band-limited versions of the simulated multipath delay profiles in Sections 4.2.2, 4.2.3, and 4.2.4 have been used as test signals in this chapter, so that a comparison can be made with the case without band-limitations. Several captures of these band-limited multipath delay profiles, each of which has been corrupted by different noise sequences, have again been produced and then averaged to simulate the average output signal waveform from the experimental SCCS system.

In denoising the noisy detail coefficients of the band-limited signal, performance comparison is made between the two noise reduction strategies used to filter-out noise from the detail coefficients. In the first technique, the SWTMP denoising scheme given in (3.78) is applied. The levels 1 and 2 detail coefficients are used in this first scheme. In

the second noise reduction method, a denoising procedure that uses the hard thresholding technique given in (3.77) is applied to remove the noisy detail coefficients before extracting the multipath components of interest.

5.2 Simulation Results

5.2.1 Band-limited one-path delay profile

The wavelet analysis of a band-limited one-path delay profile is computed in this section. Pathlets 5, 7, 9, and Symlet 2 are used in the wavelet analysis to detect the single path in this band-limited delay profile.

This delay profile, in the absence of noise, is shown in Figs. 5.1 (a) and 5.2 (a). The corresponding SWT levels 1 and 2 detail coefficients of this test signal profile are shown in Figs. 5.1 (b-e) and 5.2 (b-e) respectively. Table 5.1 shows the magnitudes of the levels 1 and 2 detail coefficients. These results are in general agreement to the case without band-limitations given in Table 4.1; that Pathlet 9 provides the best match with the multipath signals, while Pathlet 5 is the least match with these waveforms. Additionally, the local maxima in these noiseless detail coefficients evolve with larger peaks as the SWT decomposition level increases.

Now when this test signal is corrupted with AWGN at an SNR of 30 dB, and then band-limited, the resulting SWT levels 1 and 2 detail coefficients are shown in Figs. 5.3 (b-e) and 5.4 (b-e) respectively. The dominant peak in these noisy wavelet transform coefficients identifies the single path within the delay profile. Furthermore, as the wavelet transform decomposition level increases this observable peak is amplified.

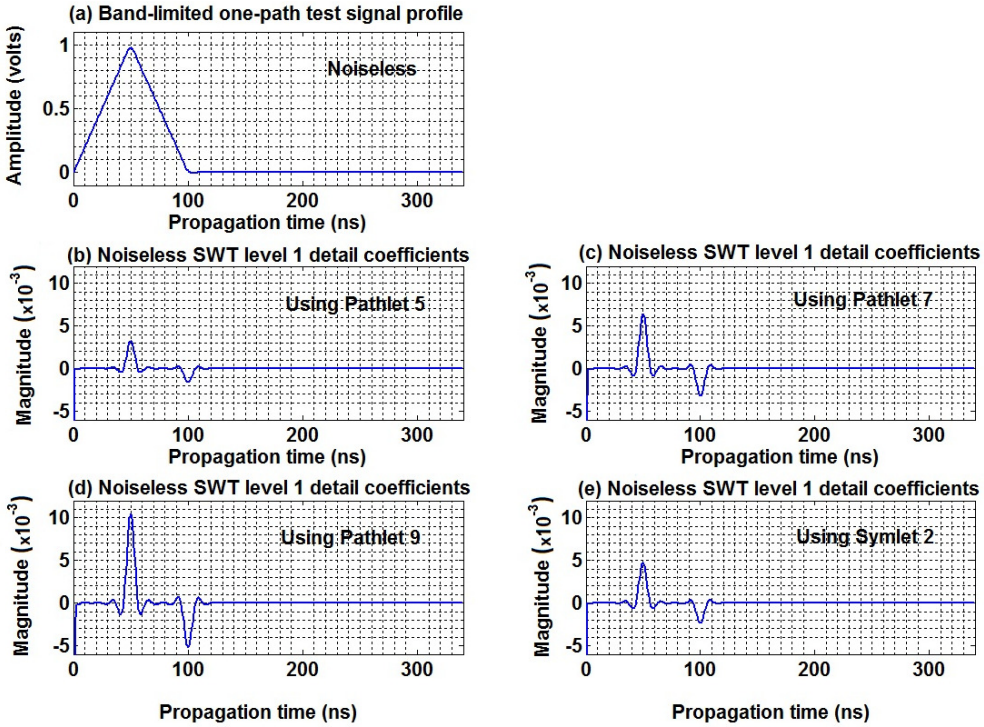

Figure 5.1 Band-limited one-path test signal profile, without noise, and corresponding SWT level 1 detail coefficients.

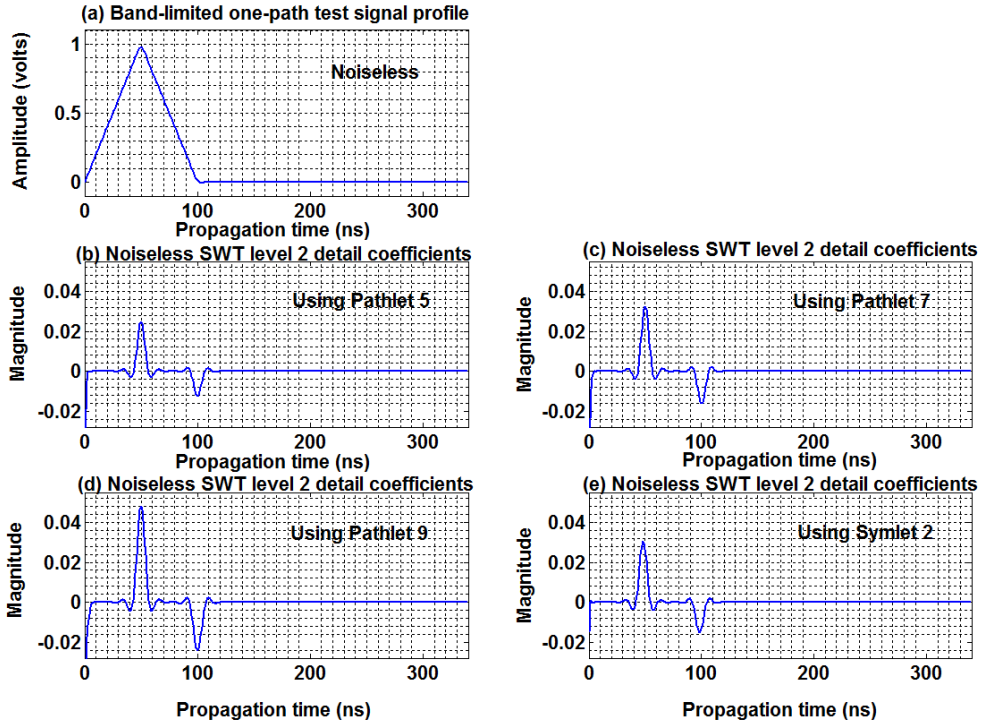

Figure 5.2 Band-limited one-path test signal profile, without noise, and corresponding SWT level 2 detail coefficients.

Table 5.1 Magnitude of the SWT levels 1 and 2 detail coefficients for a band-limited one-path delay profile without noise.

Wavelet type	Magnitude of the noiseless detail coefficients	
	Level 1	Level 2
Pathlet 5	0.00327	0.0249
Pathlet 7	0.00642	0.0325
Pathlet 9	0.0104	0.0482
Symlet 2	0.00473	0.0304

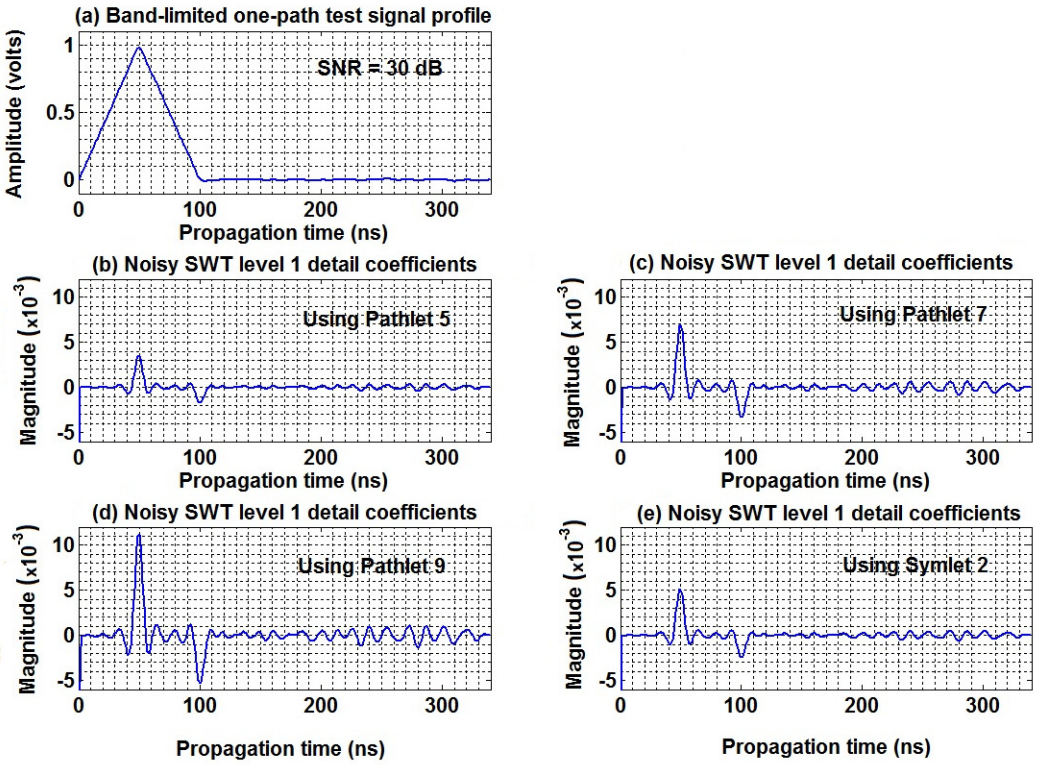

Figure 5.3 Band-limited one-path test signal profile corrupted with noise, at an SNR of 30 dB, and corresponding SWT level 1 detail coefficients.

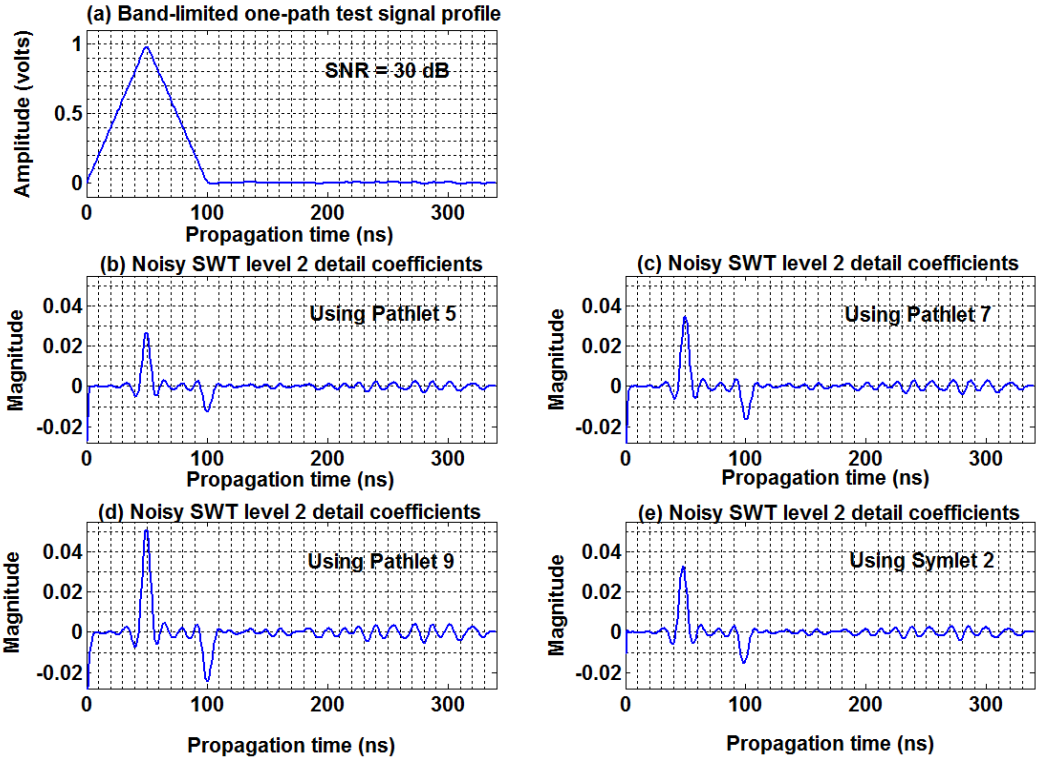

Figure 5.4 Band-limited one-path test signal profile corrupted with noise, at an SNR of 30 dB, and corresponding SWT level 2 detail coefficients.

5.2.2 Band-limited two-path delay profile with equal-amplitude paths

In this section, the constituent multipath components in a band-limited two-path delay profile with equal-amplitude paths and relative delay of 2 ns, are estimated with the algorithm proposed in Fig. 3.13 for post-processing multipath delay profiles. The parameters of this two-path delay profile have been previously shown in Table 4.2.

This band-limited delay profile, in the absence of noise, is given in Fig. 5.5 (a). It shows that the two constituent paths in the propagation channel appears as a single peak and are not resolved prior to wavelet decomposition. The SWT level 1 detail coefficients, of this band-limited test signal profile, are shown in Figs. 5.5 (b-e). These results show that the noiseless two equal-amplitude paths are not resolved at level 1 of the wavelet transform, and hence at subsequent higher wavelet transform levels.

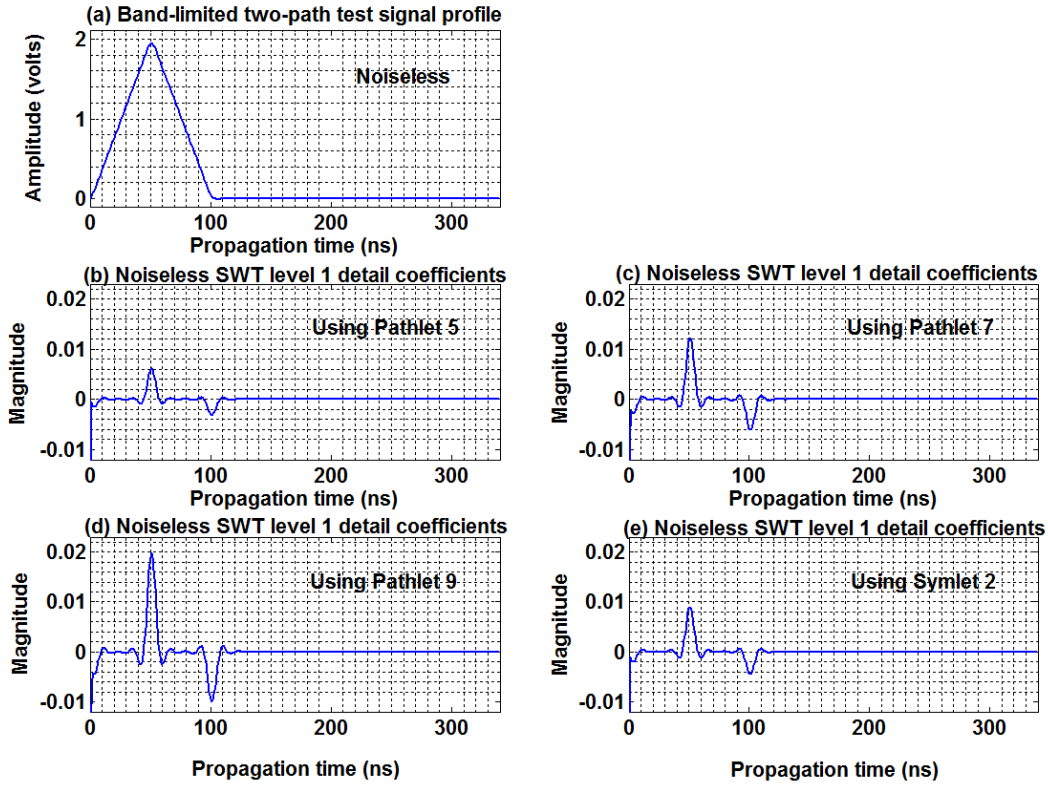

Figure 5.5 Band-limited test signal profile with two paths having equal amplitudes, without noise, and corresponding SWT level 1 detail coefficients.

Next, this two-path delay profile is corrupted with the AWGN at an SNR of 30 dB and then band-limited. The resulting SWT levels 1 and 2 detail coefficients are shown in Figs. 5.6 (b-e) and 5.7 (b-e) respectively. These results show that these noisy two equal-amplitude paths are again not resolved after wavelet transform at levels 1 and 2, and hence at subsequent higher wavelet transform levels.

A comparison of Figs. 4.23 (c-f) and 5.6 (b-e) shows that most of the detail coefficients that were attributed to noise, observed in Figs. 4.23 (c-f), have been filtered out in Figs. 5.6 (b-e) due to band-limitation. This gating of the noise is therefore advantageous in that the multipath signals of interest, which could have been otherwise immersed in noise, can be better extracted. However, this band-limitation causes the roundness of the edges on the triangular correlation functions, as seen in Fig. 5.6 (a), thereby resulting in lower resolution. Hence, there is a certain degree of uncertainty in estimating the exact relative arrival times of the multipath components.

Therefore, in actual practical measurement scenario, it is expected that the wavelet transform coefficients of an experimental data would have reduced noise due to the band-limitation in the measurement system. This reduction in noise level will be dependent on the extent of bandwidth limitations in the measurement system. The relative arrival times of the multipath component can then be estimated to a certain degree of accuracy.

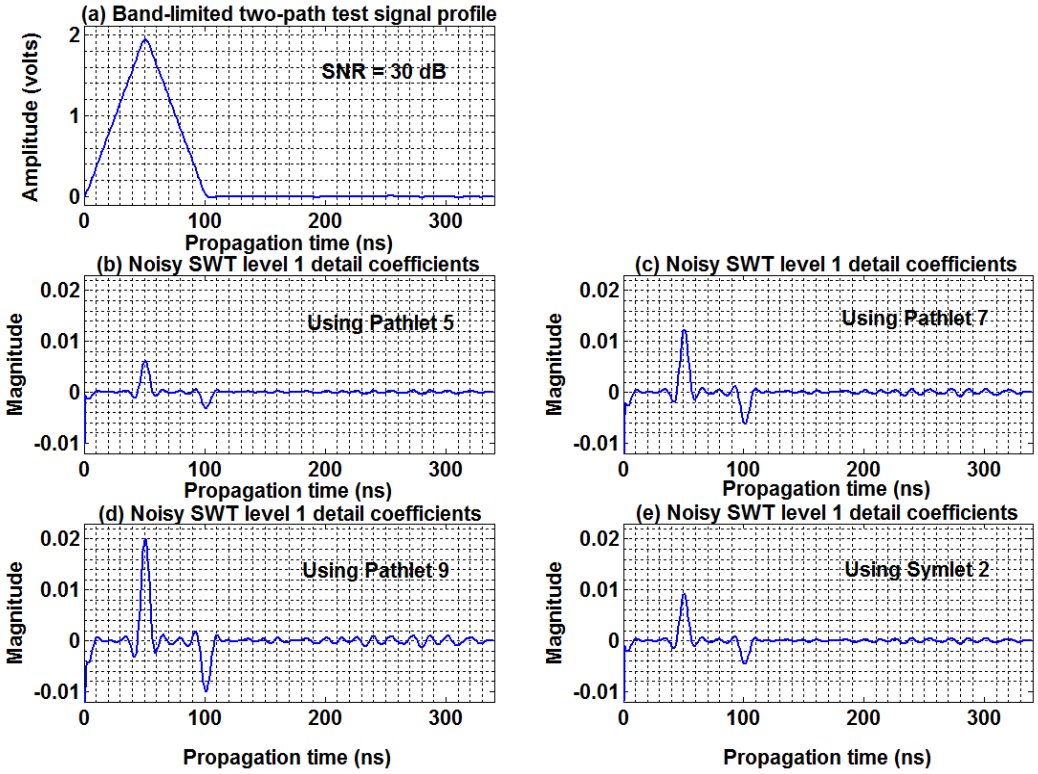

Figure 5.6 Band-limited test signal profile with two paths having equal amplitudes corrupted with noise, at an SNR of 30 dB, and corresponding SWT level 1 detail coefficients.

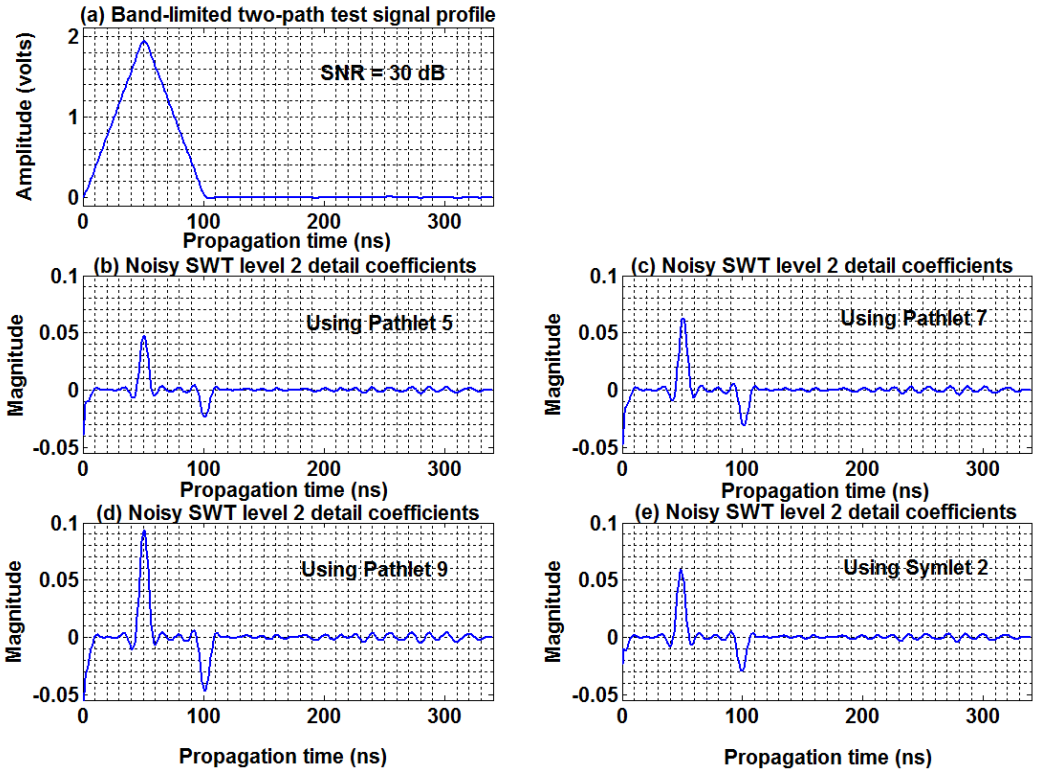

Figure 5.7 Band-limited test signal profile with two paths having equal amplitudes corrupted with noise, at an SNR of 30 dB, and corresponding SWT level 2 detail coefficients.

The results from applying the SWTMP denoising technique, using the levels 1 and 2 detail coefficients, are shown in Figs. 5.8 (b-e). The denoised coefficients by wavelet thresholding are shown in Figs. 5.9 (b-e). These results illustrate that the wavelet transform coefficients that were attributed to noise have been removed in Figs. 5.8 (b-e) and 5.9 (b-e). However the resolution has been degraded by band-limitation and so the two constituent paths, at 2 ns delay and SNR of 30 dB, are not separated.

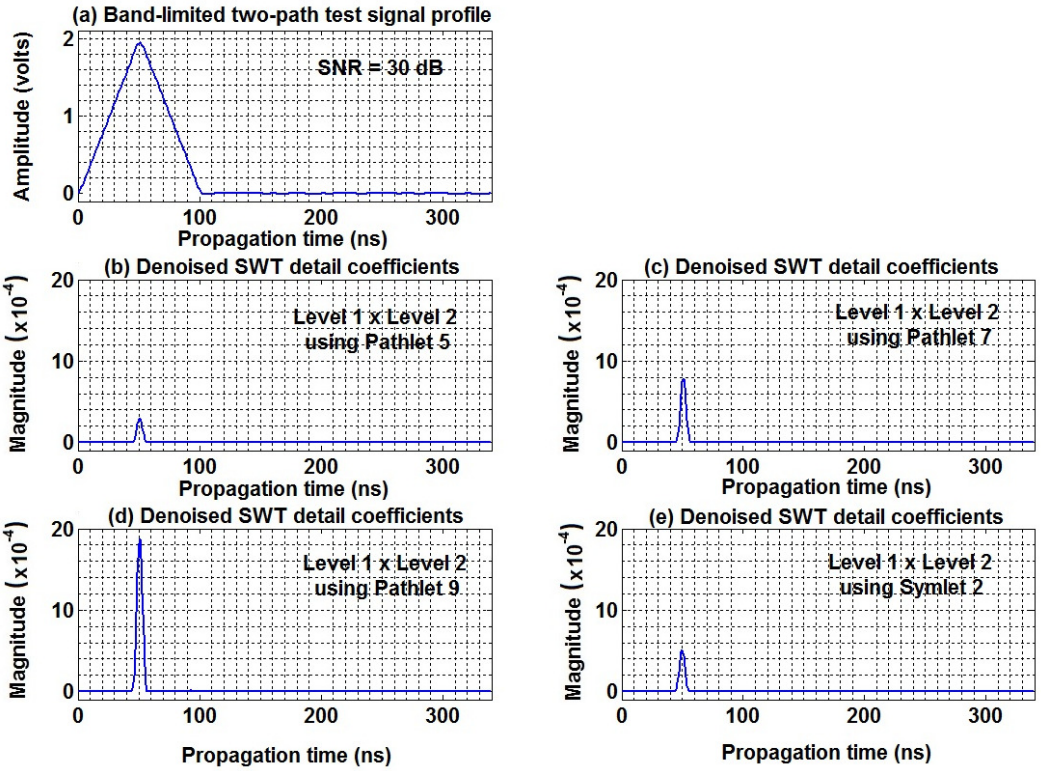

Figure 5.8 Band-limited test signal profile with two paths having equal amplitudes corrupted with noise, at an SNR of 30 dB, and the denoised SWT detail coefficients. Noise is suppressed by SWTMP using the levels 1 and 2 detail coefficients.

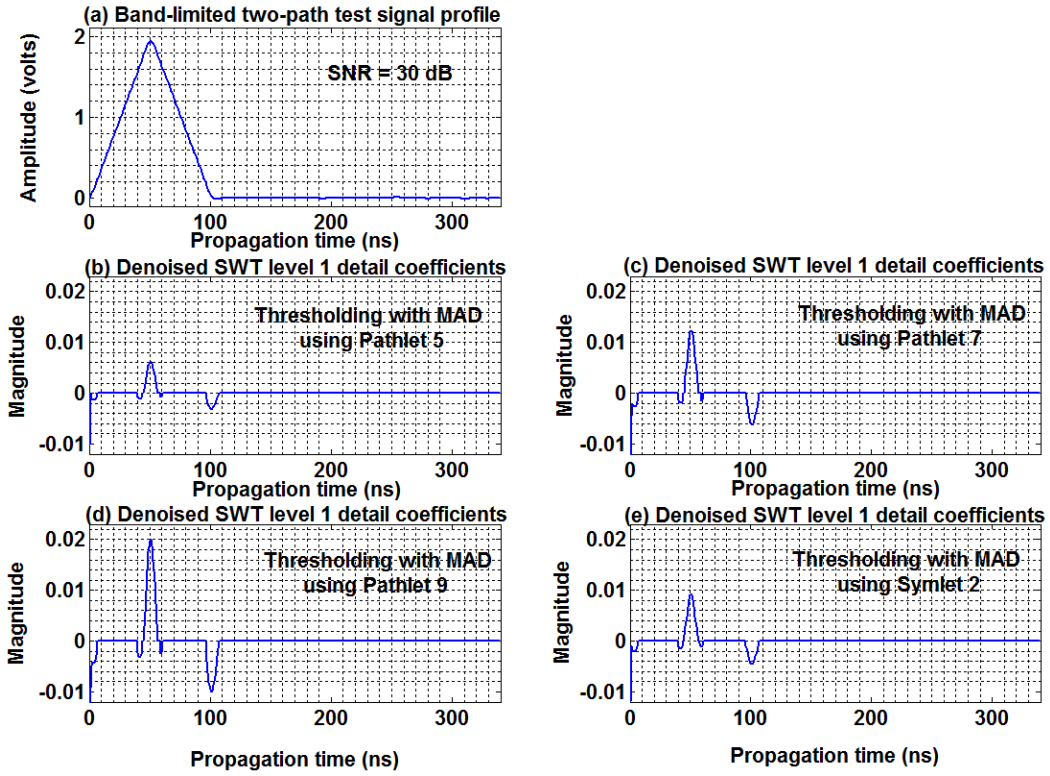

Figure 5.9 Band-limited test signal profile with two paths having equal amplitudes corrupted with noise, at an SNR of 30 dB, and the denoised SWT level 1 detail coefficients. Noise is removed by wavelet thresholding.

5.2.3 Band-limited four-path delay profile with differential amplitudes

The band-limited replica of the test signal profile having four paths with differential amplitudes, discussed in Section 4.2.4, is simulated in this section. The constituent multipath components of this band-limited four-path delay profile are then estimated with the algorithm proposed for post-processing multipath delay profiles.

The parameters of this four-path delay profile are as previously shown in Table 4.4. This band-limited delay profile, in the absence of noise, is shown in Figs. 5.10 (a) and 5.11 (a). The SWT levels 1 and 2 detail coefficients, of this noiseless test signal profile, are shown in Figs. 5.10 (b-e) and 5.11 (b-e) respectively. These noiseless results show that Pathlets 5, 7, 9, and Symlet 2 can be successfully applied to separate the constituent paths within the band-limited four-path delay profile by at least a factor of five.

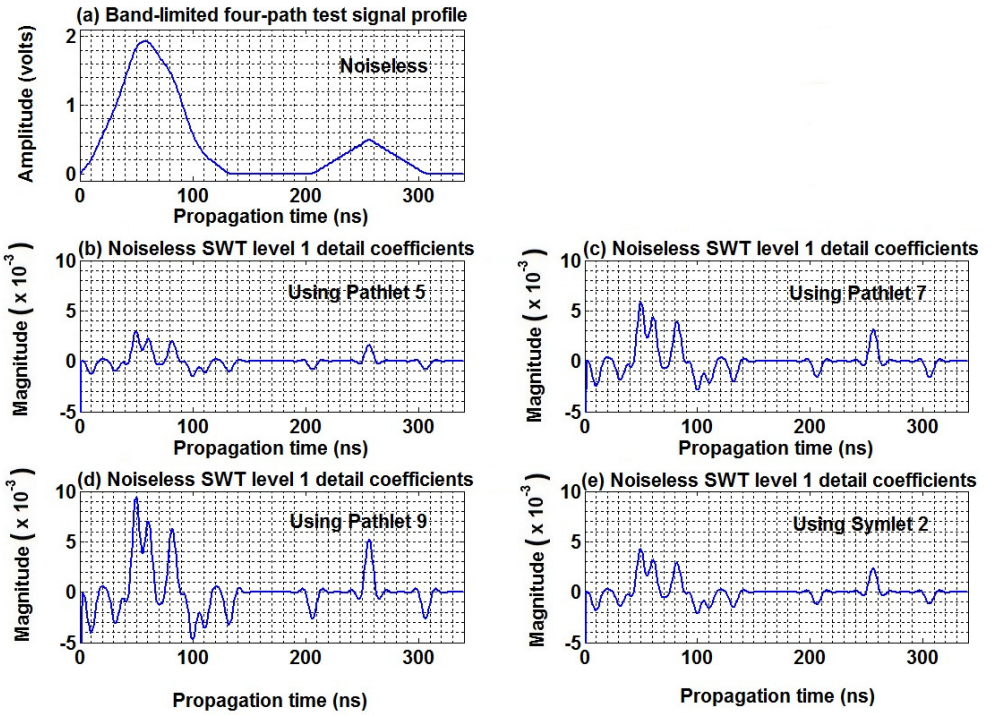

Figure 5.10 Band-limited test signal profile with four paths having differential amplitudes, without noise, and the SWT level 1 detail coefficients.

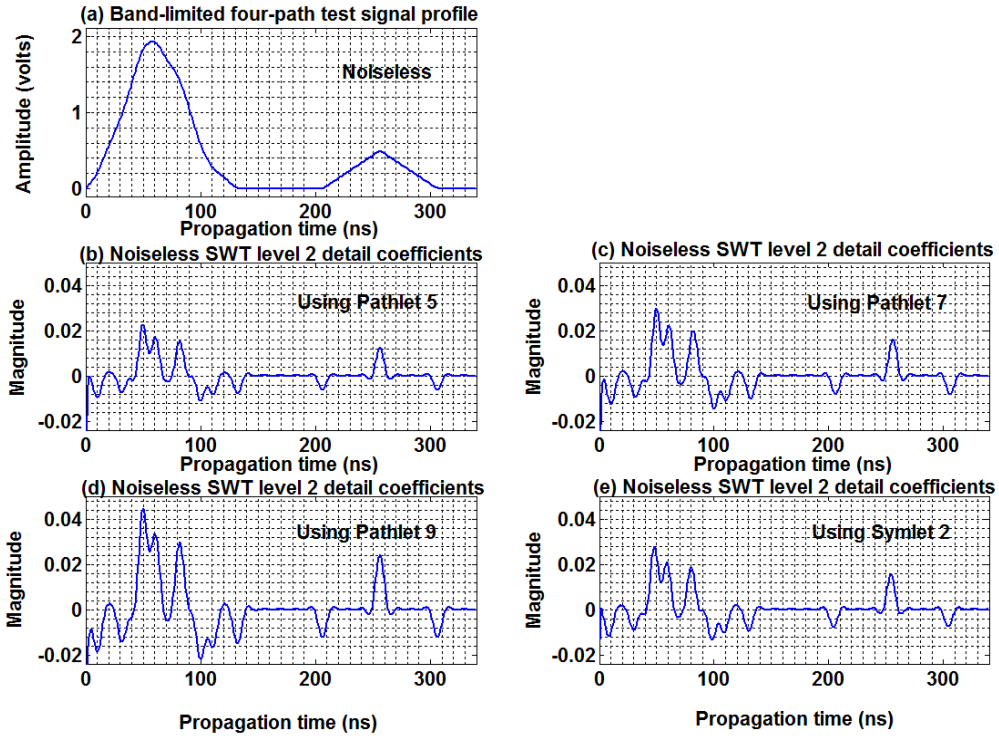

Figure 5.11 Band-limited test signal profile with four paths having differential amplitudes, without noise, and the SWT level 2 detail coefficients.

Next, this four-path delay profile is corrupted with AWGN at an SNR of 30 dB and then band-limited. The resulting SWT levels 1 and 2 detail coefficients are shown in Figs. 5.12 (b-e) and 5.13 (b-e) respectively. The dominant peaks in these noisy wavelet transform detail coefficients detect the constituent multipath components within the band-limited four-path delay profile. As expected, the magnitude of these dominant peaks is reinforced as the wavelet transform decomposition level increases.

A comparison of Figs. 4.36 (c-f) and 4.37 (c-f), with Figs. 5.12 (b-e) and 5.13 (b-e), respectively, shows that most of the detail coefficients that were attributed to noise have been filtered out in Figs. 5.12 (b-e) and 5.13 (b-e), due to the band-limitation. Again, suggesting that the band-limitation facilitates the extraction of the multipath signals of interest.

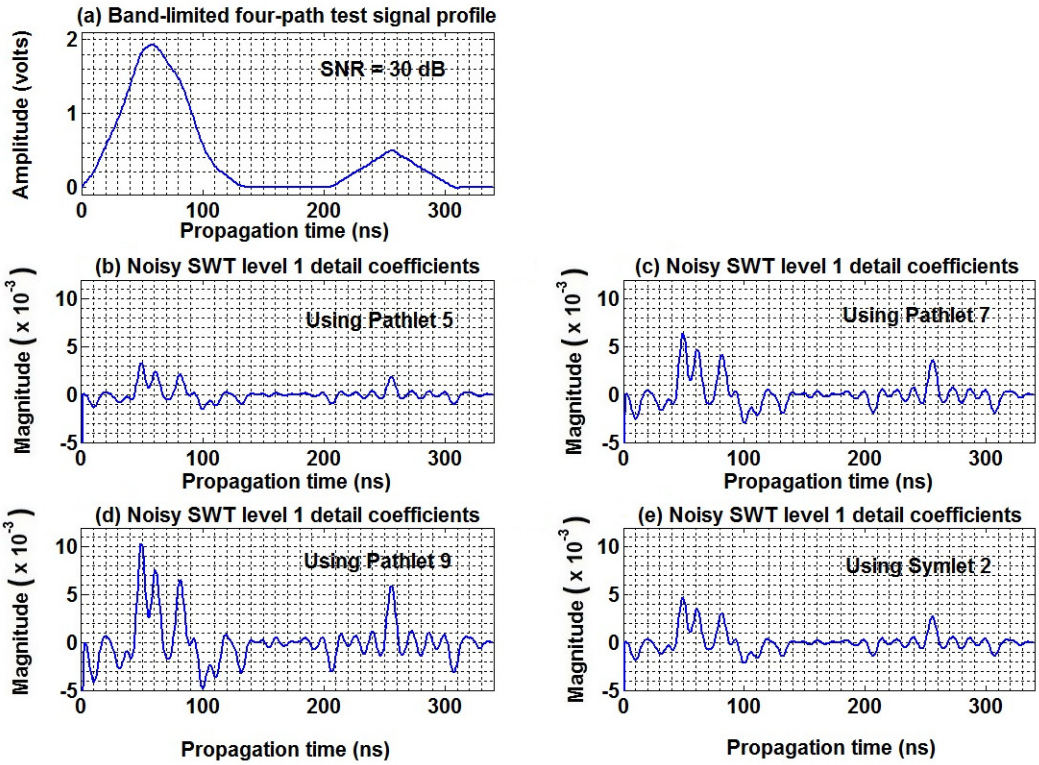

Figure 5.12 Band-limited test signal profile with four paths having differential amplitudes corrupted with noise, at an SNR of 30 dB, and corresponding SWT level 1 detail coefficients.

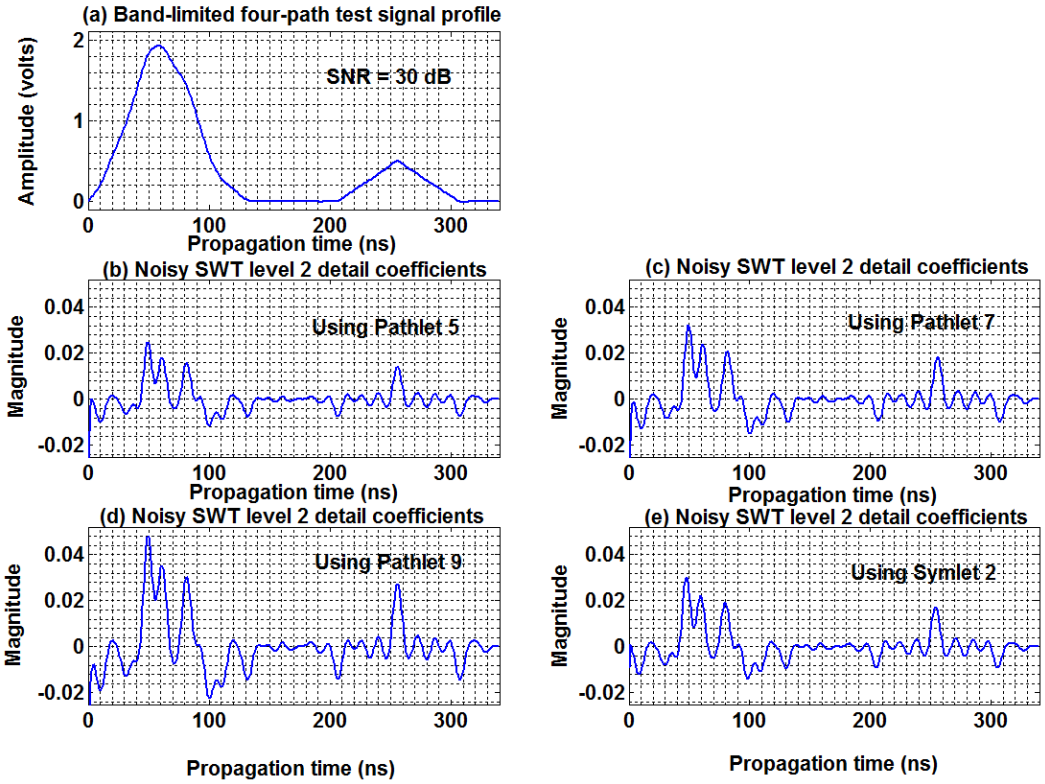

Figure 5.13 Band-limited test signal profile with four paths having differential amplitudes corrupted with noise, at an SNR of 30 dB, and corresponding SWT level 2 detail coefficients.

The results from applying the SWTMP denoising technique, using the levels 1 and 2 detail coefficients, are shown in Figs. 5.14 (b-e). This denoising technique computes the product of the non-negative levels 1 and 2 detail coefficients. These results show that the detail coefficients that were attributed to noise in Figs. 5.12 (b-e) and 5.13 (b-e), have now been suppressed in Figs. 5.14 (b-e). The results from using Pathlet 9, shown in Fig. 5.14 (d), is the most robust to noise, while the results from using Pathlet 5, shown in Fig. 5.14 (b), is the least robust to noise.

Furthermore, a comparison with the results from applying the SWTMP denoising technique for the case without band-limitation given in Figs. 4.38 (c-f), shows that the results from the band-limited case given in Figs. 5.14 (b-e) suppresses the noise better. These denoised detail coefficients can then be used as an estimate of the number of multipath components and time-delays.

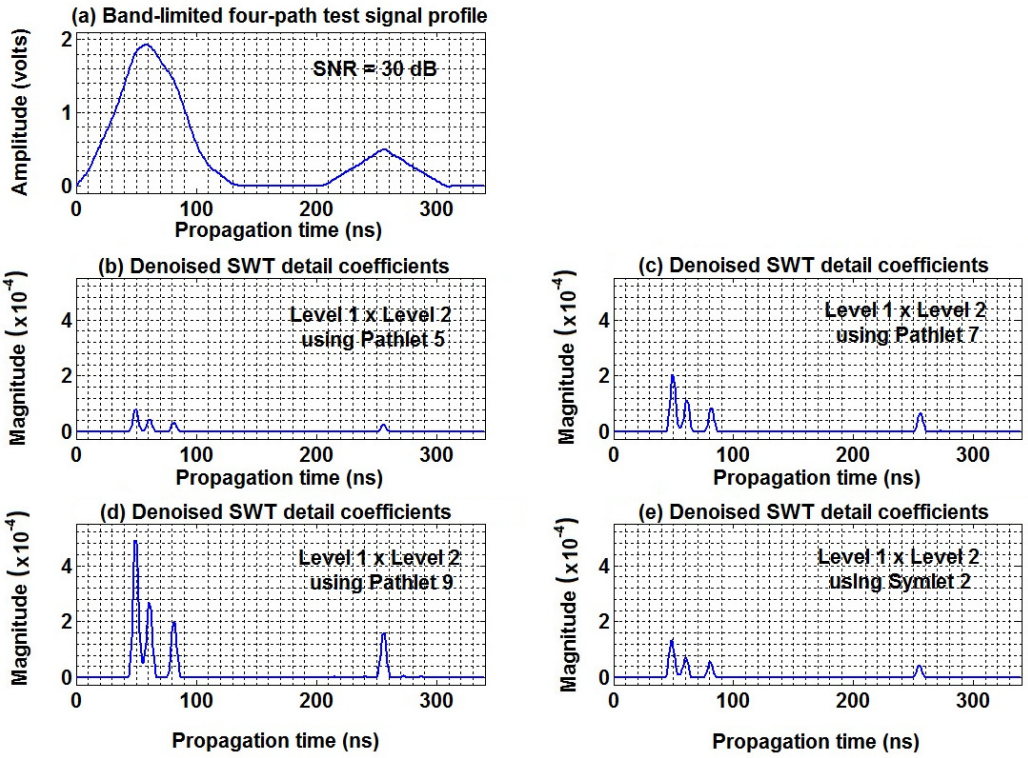

Figure 5.14 Band-limited test signal profile with four paths having differential amplitudes corrupted with noise, at an SNR of 30 dB, and the denoised SWT detail coefficients. Noise is suppressed by SWTMP using the levels 1 and 2 detail coefficients.

The denoised levels 1 and 2 detail coefficients, using hard thresholding and the median absolute deviation standard deviation estimate of noise, are shown in Figs. 5.15 (b-e) and 5.16 (b-e) respectively. These results show that all the four constituent paths, in this band-limited test signal profile with an SNR of 30 dB, can be detected at levels 1 and 2 of the wavelet transform for all the analysing wavelets used. These denoised detail coefficients is then used as an estimate of the number of multipath components and time-delays.

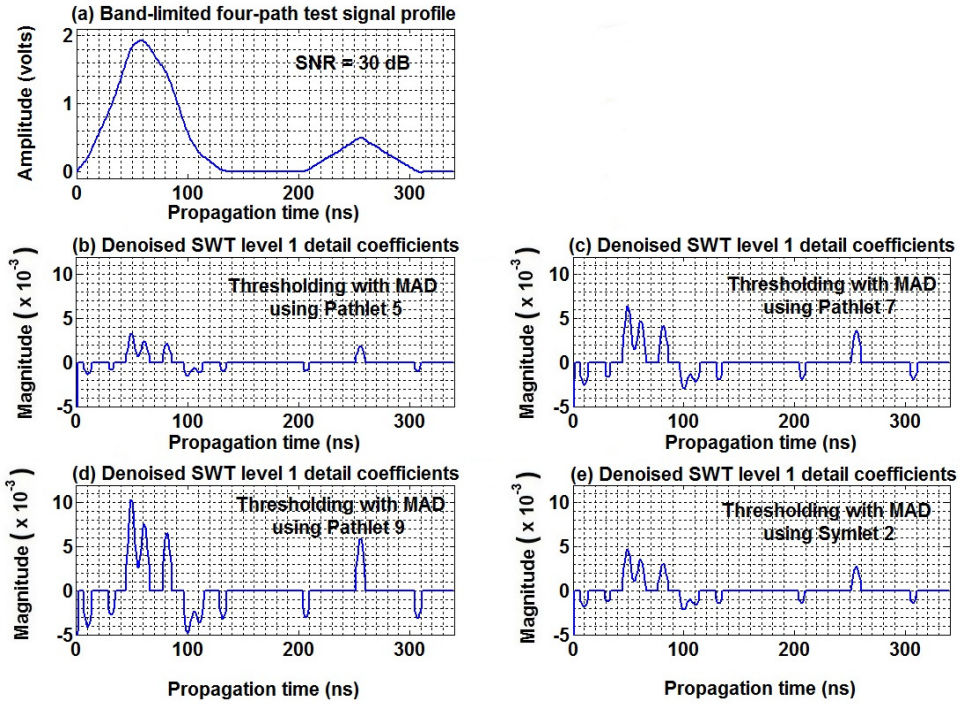

Figure 5.15 Band-limited test signal profile with four paths having differential amplitudes corrupted with noise, at an SNR of 30 dB, and the denoised SWT level 1 detail coefficients. Noise is removed by wavelet thresholding.

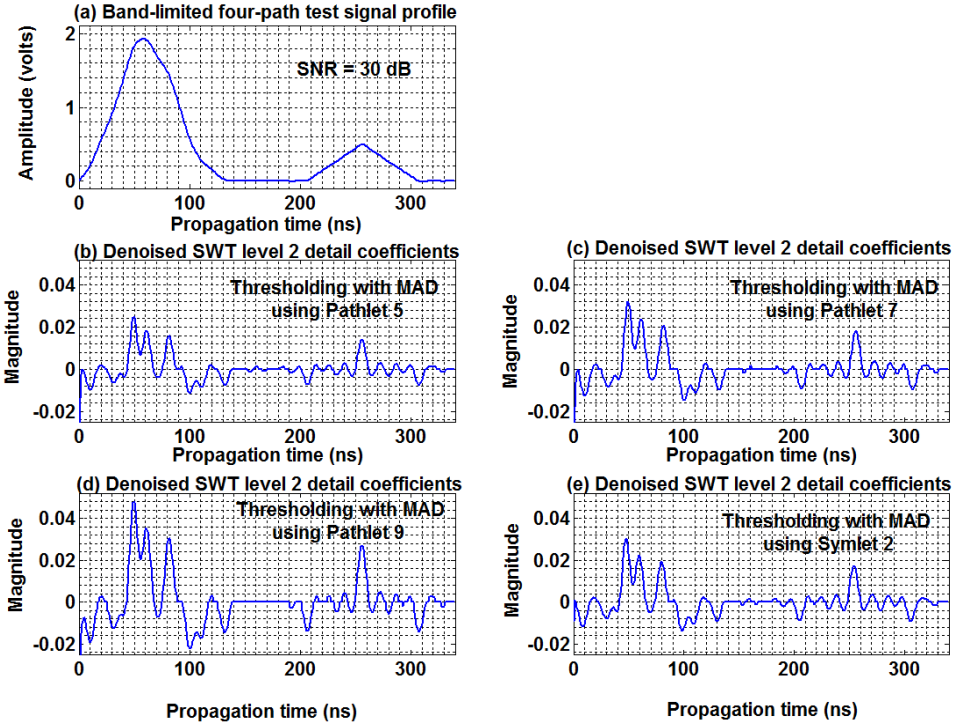

Figure 5.16 Band-limited test signal profile with four paths having differential amplitudes corrupted with noise, at an SNR of 30 dB, and the denoised SWT level 2 detail coefficients. Noise is removed by wavelet thresholding.

Finally, this four-path delay profile is corrupted with AWGN at SNRs of 25 dB and then 20 dB. The delay profiles are subsequently band-limited. At 25 dB SNR, the resulting noisy SWT levels 1 and 2 detail coefficients are shown in Figs. 5.17 (b-e) and 5.18 (b-e) respectively. The dominant peaks in these noisy detail coefficients again identify the constituent multipath components. As expected, these dominant peaks are increased in magnitude as the wavelet transform decomposition level increases.

At an SNR of 20 dB, the resulting SWT levels 1 and 2 detail coefficients are shown in Figs. 5.19 (b-e) and 5.20 (b-e) respectively. The dominant peaks within these noisy detail coefficients detect the constituent multipath components. Moreover, many spurious peaks are also now obtained at this SNR; which may be attributed to the correlations in the noise samples after band-limitations.

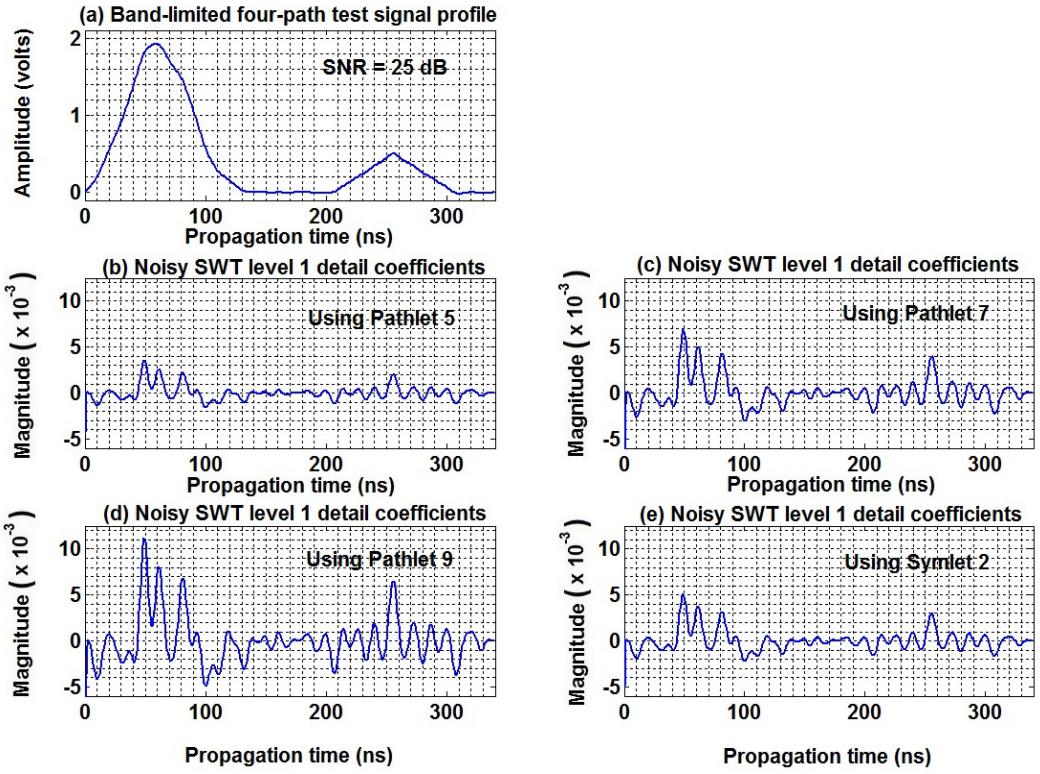

Figure 5.17 Band-limited test signal profile with four paths having differential amplitudes corrupted with noise, at an SNR of 25 dB, and corresponding SWT level 1 detail coefficients.

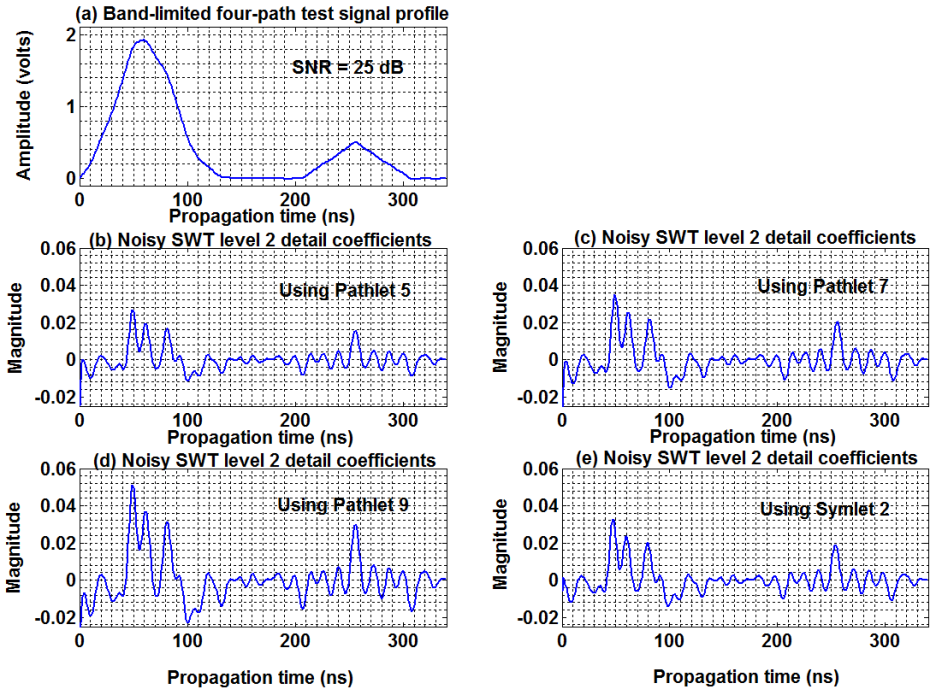

Figure 5.18 Band-limited test signal profile with four paths having differential amplitudes corrupted with noise, at an SNR of 25 dB, and corresponding SWT level 2 detail coefficients.

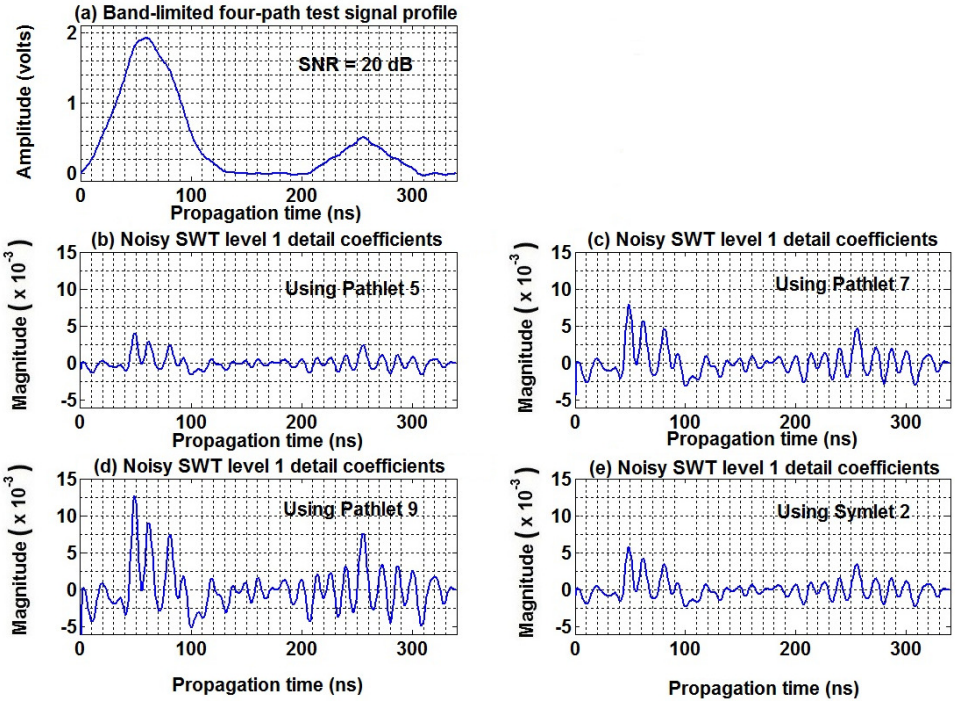

Figure 5.19 Band-limited test signal profile with four paths having differential amplitudes corrupted with noise, at an SNR of 20 dB, and corresponding SWT level 1 detail coefficients.

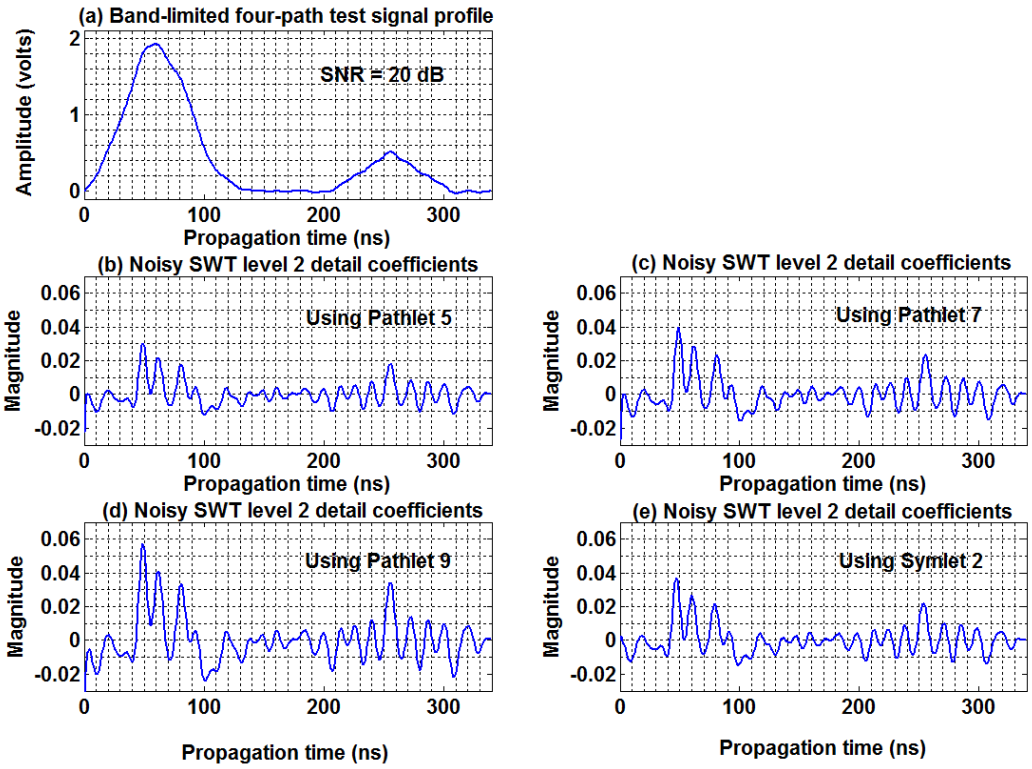

Figure 5.20 Band-limited test signal profile with four paths having differential amplitudes corrupted with noise, at an SNR of 20 dB, and corresponding SWT level 2 detail coefficients.

The results from applying the SWTMP denoising scheme, using the levels 1 and 2 detail coefficients, are shown in Figs. 5.21 (b-e) and 5.22 (b-e). These results show that the detail coefficients that were attributed to noise have now been suppressed. The results from using Pathlet 9, shown in Figs. 5.21 (d) and 5.22 (d), is also the most robust to the noise. A comparison with the results obtained from applying the SWTMP denoising technique for the case without band-limitation given in Figs. 4.43 (c-f), shows that the corresponding results from the band-limited case given in Figs. 5.21 (b-e) suppresses the noise better. These denoised detail coefficients can then be used as an estimate of the number of multipath components and time-delays.

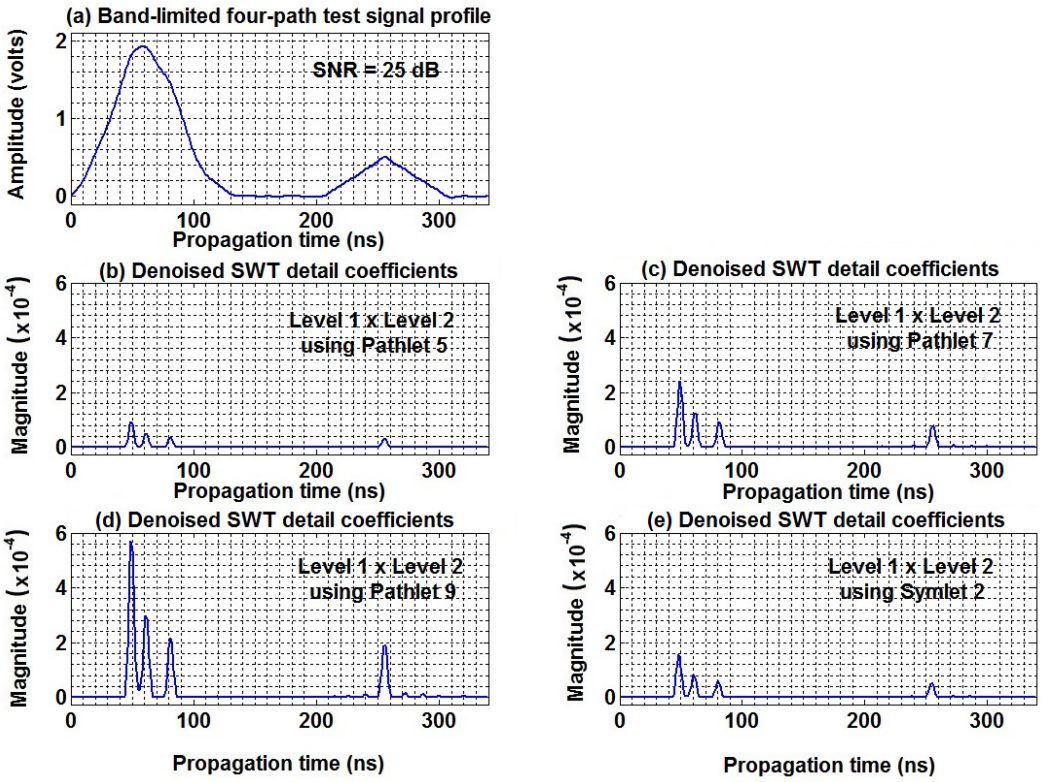

Figure 5.21 Band-limited test signal profile with four paths having differential amplitudes corrupted with noise, at an SNR of 25 dB, and the denoised SWT detail coefficients. Noise is suppressed by SWTMP using the levels 1 and 2 detail coefficients.

At an SNR of 25 dB, the denoised levels 1 and 2 detail coefficients by wavelet thresholding are shown in Figs. 5.23 (b-e) and 5.24 (b-e) respectively. These results show that the four constituent paths, in this band-limited test signal profile, can be detected at levels 1 and 2 of the wavelet transform for all the analysing wavelets used. Some spurious peaks, attributed to noise, are also obtained in the level 2 denoised coefficients. The denoised detail coefficients at level 1, however, contain none of these spurious coefficients. Consequently, the denoised level 1 detail coefficients can be used as true estimate of the number of multipath components and time-delays.

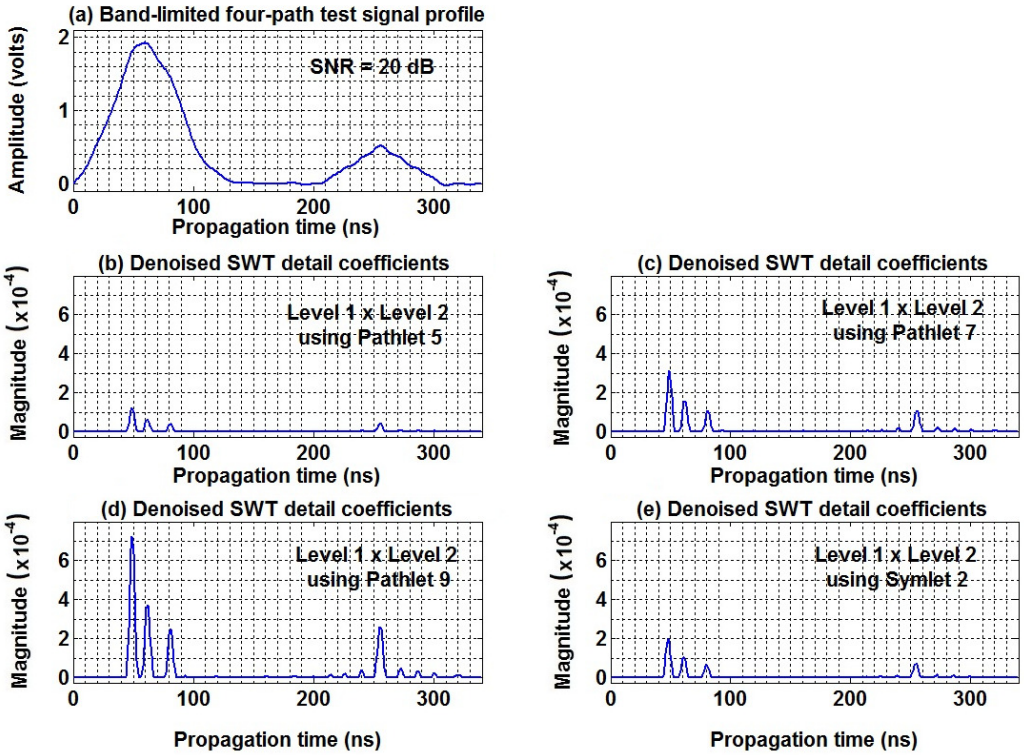

Figure 5.22 Band-limited test signal profile with four paths having differential amplitudes corrupted with noise, at an SNR of 20 dB, and the denoised SWT detail coefficients. Noise is suppressed by SWTMP using the levels 1 and 2 detail coefficients.

At an SNR of 20 dB, the denoised levels 1 and 2 detail coefficients by wavelet thresholding are shown in Figs. 5.25 (b-e) and 5.26 (b-e) respectively. The results in this case show that while all the four constituent paths, in this band-limited test signal profile, can be extracted at both levels 1 and 2, many spurious peaks attributed to noise are also now obtained at level 2. The presence of these spurious peaks may be attributed to the correlations in the noise samples after band-limitations. The denoised detail coefficients at level 1, however, do not contain these spurious coefficients. Consequently, these coefficients can be used as true estimate of the number of multipath components and time-delays.

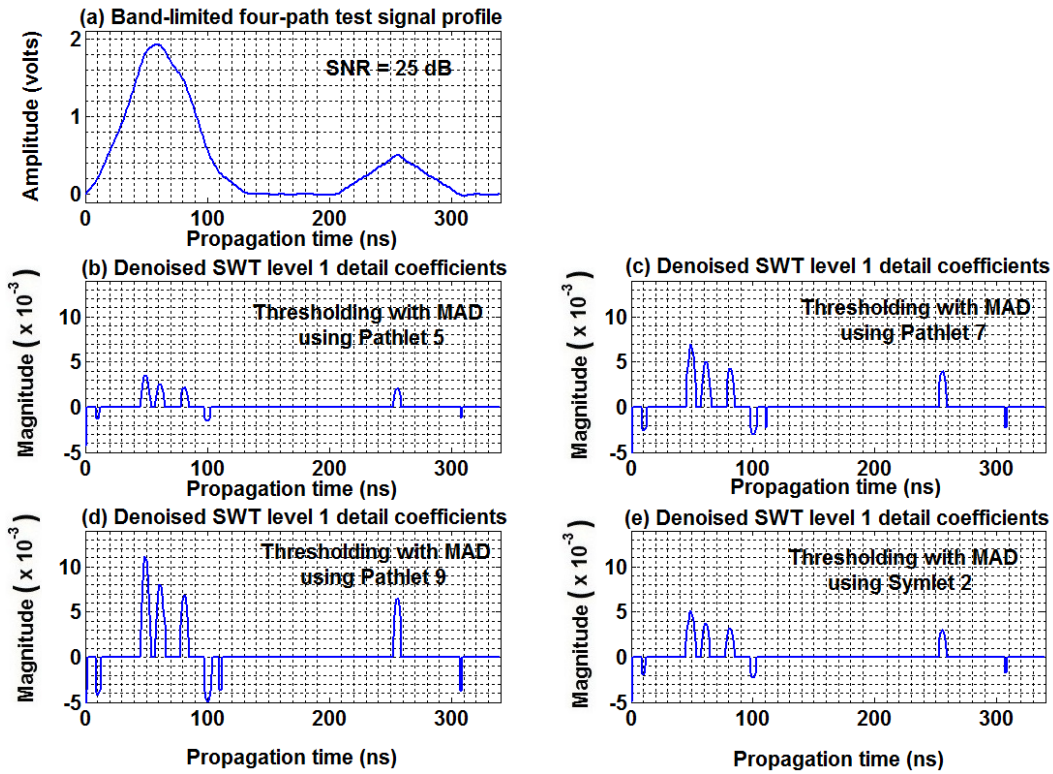

Figure 5.23 Band-limited test signal profile with four paths having differential amplitudes corrupted with noise, at an SNR of 25 dB, and the denoised SWT level 1 detail coefficients. Noise is removed by wavelet thresholding.

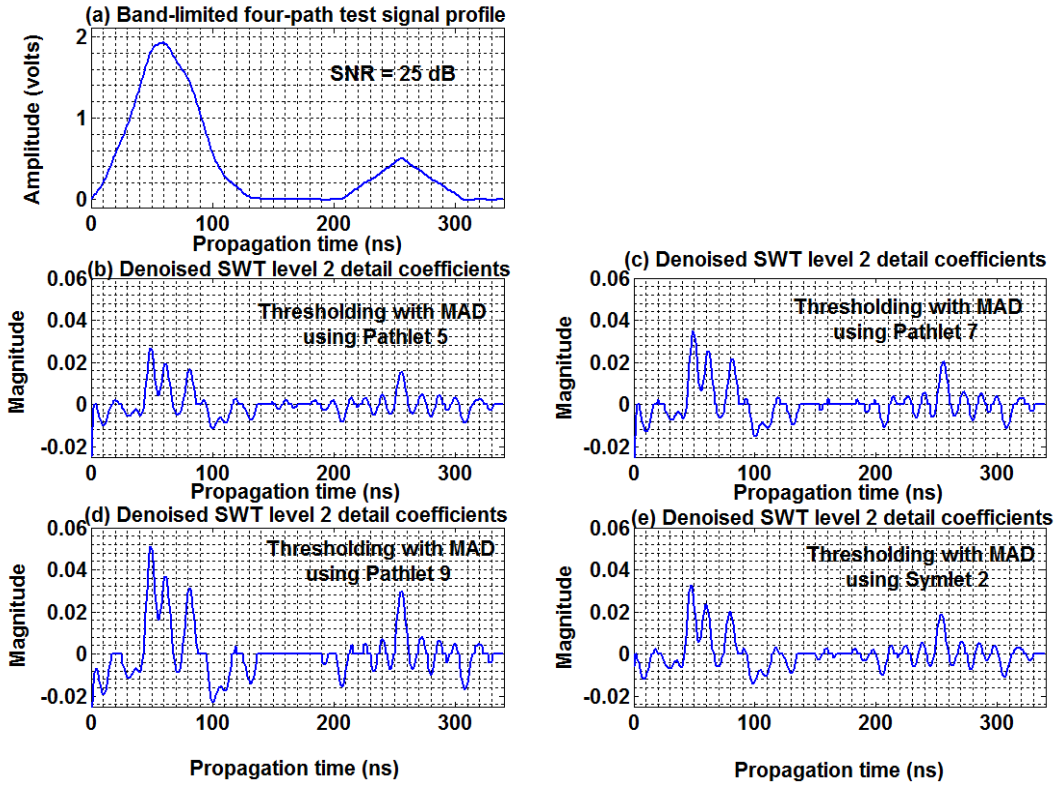

Figure 5.24 Band-limited test signal profile with four paths having differential amplitudes corrupted with noise, at an SNR of 25 dB, and the denoised SWT level 2 detail coefficients. Noise is removed by wavelet thresholding.

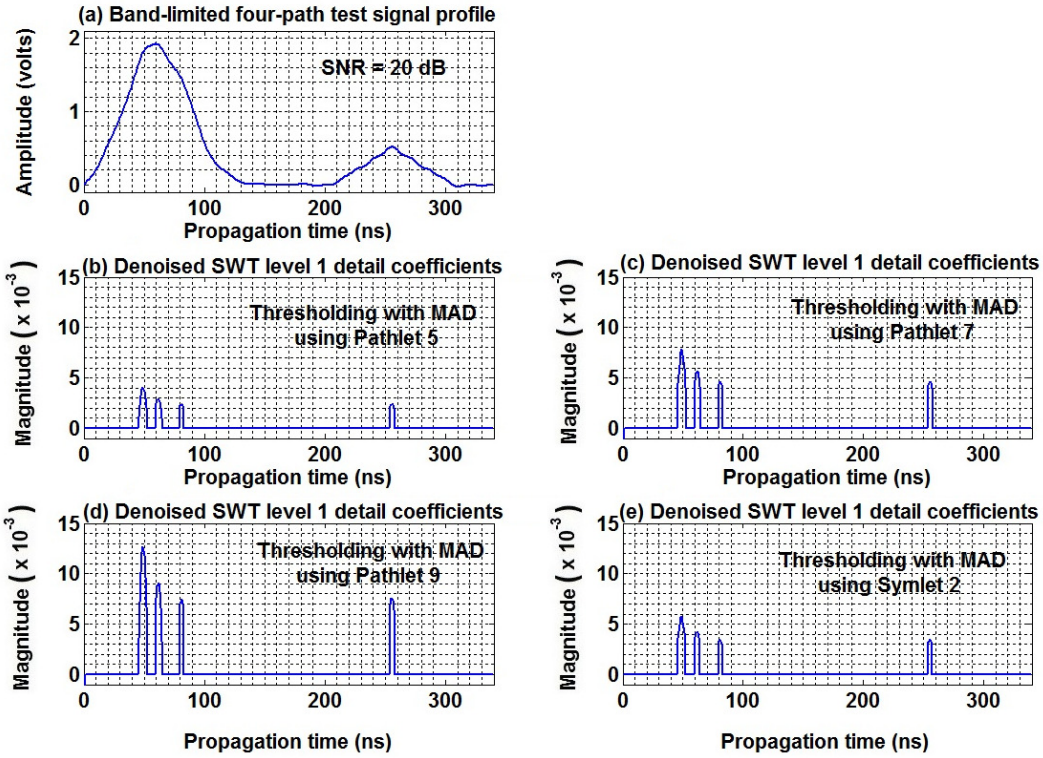

Figure 5.25 Band-limited test signal profile with four paths having differential amplitudes corrupted with noise, at an SNR of 20 dB, and the denoised SWT level 1 detail coefficients. Noise is removed by wavelet thresholding.

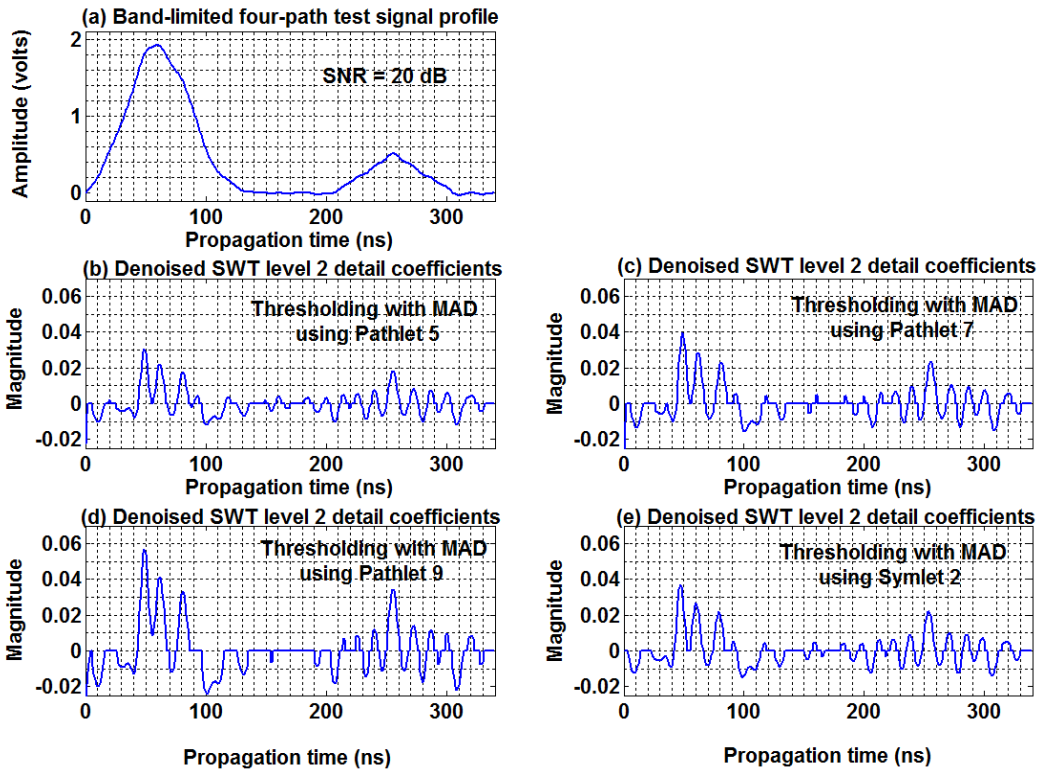

Figure 5.26 Band-limited test signal profile with four paths having differential amplitudes corrupted with noise, at an SNR of 20 dB, and the denoised SWT level 2 detail coefficients. Noise is removed by wavelet thresholding.

5.3 Summary

In this chapter, series of computer simulations have been carried out to examine the effect on time resolution, caused by bandwidth limitations, in wavelet-based multipath channel parameter estimation. The band-limited replica of the simulated multipath delay profiles in Sections 4.2.2, 4.2.3, and 4.2.4 have been developed as test signals so that a comparison can be made with the results obtained from the delay profiles without band-limitations.

A comparison of the SWT detail coefficients for the simulated multipath delay profiles without band-limitations, with those for the band-limited delay profiles, show that most of the noisy detail coefficients are filtered out after band-limitation. It is therefore expected that in actual experimental measurement scenario, the wavelet analysis of an experimental data would have coefficients with reduced noise level as a consequence of the inherent bandwidth limitations.

Performance comparison was also made between the two noise reduction strategies used to filter-out noise from the band-limited detail coefficients so that the constituent multipath components that are buried in noise can be extracted. In the first technique, the product of the non-negative values of levels 1 and 2 detail coefficients are computed so as to suppress noise. This denoising procedure has been referred to as the "stationary wavelet transform multilevel products (SWTMP)" in Section 3.3.3. In this first scheme, the denoised detail coefficients are as defined in (3.78). In the second noise reduction scheme, a denoising procedure that uses the hard thresholding technique based on the median absolute deviation standard deviation estimate of noise is applied to remove the noisy detail coefficients. In this second case, the denoised detail coefficients are as defined in (3.77).

The result obtained from the first noise reduction technique is found to be comparable to the results obtained for the second method when applied to the SWT level 1 detail coefficients, for SNR $\geq$ 20 dB. In these two noise reduction schemes, the use of Pathlet

9 is found to be the most robust to noise, followed by Pathlet 7, Symlet 2, and Pathlet 5 as the least robust to noise. Again, in actual practical implementations, it is suggested that both Pathlets 7 and 9 be applied in the two noise reduction strategies that are used to filter-out noise from the detail coefficients. Features that are extracted by both Pathlets 7 and 9, in these two denoising schemes, can then be regarded as the true parameter estimates.

Finally, the results in this chapter have shown that though band-limitation reduces the effect of noise, however this is at the expense of multipath resolution. For example, while the two paths with equal amplitudes and 2 ns delay in Fig. 5.5 (a) could not be resolved at the SWT level 1 detail coefficients shown in Figs. 5.5 (b-e) after band-limitations; these two paths are however separated in the absence of bandwidth limitations as seen in Figs. 4.14 (c-f). There is, therefore, a compromise between obtaining acceptable resolution of the multipath components and reducing the effect of noise. Nevertheless, these results demonstrate that the wavelet-based algorithm proposed in this thesis can still be successfully applied to resolve the multipath components, even in the presence of band-limitations.

CHAPTER 6

EXPERIMENTAL RESULTS

6.1 Introduction

This chapter presents the description, and wavelet analysis, of the channel impulse response profiles captured with an experimental portable channel sounder used for wideband indoor radio propagation measurements in the 900 MHz band (Mossammaparast, Afifi et al. 1997; Mossammaparast 1999). This portable channel sounder is based on the sliding correlation technique previously discussed in Section 2.2.4.

The transmitter unit of this channel sounder uses a pseudorandom binary sequence to binary phase modulate a sinusoidal carrier signal at 914 MHz. The output binary phase shift keyed signal is subsequently amplified and transmitted through a radio channel. At the receiver, an identical PRBS generator similar to that used at the transmitter, but clocked at a somewhat slower rate, is utilised. This slower PRBS is used to modulate a locally generated sinusoidal carrier. Then the received BPSK signal is mixed with the locally generated BPSK to give a crosscorrelated signal at an intermediate frequency (IF) of 45 MHz. This crosscorrelated signal is further converted into the in-phase (I) and quadrature-phase (Q) components, at zero IF. These baseband I and Q waveforms have a maximum output voltage swing of $\pm$ 5V and bandwidth of 4 kHz. These waveforms are captured with a digital oscilloscope for further post-processing to obtain estimates of the

multipath delay parameters. The transmitter and receiver units of this channel sounder are shown in Fig. 6.1, while a summary of the experimental channel sounder parameters is presented in Table 6.1.

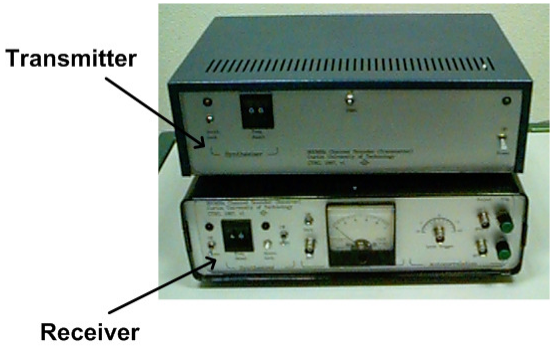

Figure 6.1 The transmitter and receiver units of the sliding correlator channel sounder used in the wideband radio propagation measurements in the 900 MHz band.

Table 6.1 Summary of the sliding correlator channel sounder parameters, used in the wideband radio propagation measurements in the 900 MHz band.

Parameter	Value
Transmitter chip clock rate	20 MHz
Receiver chip clock rate	19.996 MHz
Multipath delay resolution	50 ns
Time sliding factor	4500 ~ 5500
Transmit output power	13 dB
RF bandwidth	40 MHz

6.2 Data Processing and Analysis

As discussed in Section 1.1, a large bandwidth is required for high-resolution measurements with a channel sounder. However, legal transmission bandwidth restrictions place an upper bound on such large bandwidth. As a result of this limited resolution capability of the experimental channel sounder, the close-in multipath delay components with delays less than the intrinsic time resolution overlap each other. Consequently, these individual delay components are not resolved. Additionally, when adjacent multipath components have very different amplitudes, then a strong ray may mask a weaker ray. When this happens, then the output waveform from the channel sounder appears as a single pulse which is spread in time. The captured multipath delay profiles are hence subjected to post-processing, to resolve the multiple ray paths that have been otherwise not individually identifiable.

This section describes the wavelet analysis of measured multipath delay profiles obtained by connecting the transmitter and receiver units of an experimental sliding correlator channel sounder back-to-back, using RG142 50Ω coaxial cables. The experiment was carried out in a previous wideband indoor radio propagation study at Curtin University. A sample of the back-to-back experimental data, containing two unresolved propagation paths, is presented in Table 6.2. Further details about this experiment are provided in Mossammaparast (1999). The wavelet-based digital signal processing algorithm proposed for this study in Chapter 3 is applied in these analyses. Pathlets 7 and 9 have been used as the analysing wavelets.

Examples of multipath delay profiles, obtained from these back-to-back measurements, are shown in Figs. 6.2 and 6.3. There are two paths in each of these delay profiles. Note that the time axis in these plots has not been scaled to take the sliding factor of the measurement system into consideration, but rather displayed in terms of the data points to show the actual experimental data.

Table 6.2 Sample of the experimental data with two unresolved paths, obtained from back-to-back measurements, using the sliding correlator channel sounder system shown in Fig. 6.1.

4.00E-02	2.40E-01	2.80E+00	-2.80E-01	-2.40E-01
4.00E-02	2.80E-01	2.68E+00	-3.20E-01	-2.40E-01
0.00E+00	3.20E-01	2.64E+00	-3.20E-01	-2.40E-01
0.00E+00	3.60E-01	2.64E+00	-3.60E-01	-2.40E-01
4.00E-02	4.80E-01	2.56E+00	-3.20E-01	-2.80E-01
8.00E-02	5.60E-01	2.56E+00	-3.60E-01	-3.20E-01
8.00E-02	6.80E-01	2.48E+00	-2.80E-01	-2.40E-01
8.00E-02	8.00E-01	2.48E+00	-2.80E-01	-2.40E-01
0.00E+00	9.20E-01	2.44E+00	-2.80E-01	-2.80E-01
0.00E+00	1.04E+00	2.36E+00	-2.80E-01	-2.80E-01
4.00E-02	1.12E+00	2.32E+00	-2.80E-01	-2.40E-01
4.00E-02	1.20E+00	2.20E+00	-2.80E-01	-2.40E-01
8.00E-02	1.28E+00	2.08E+00	-2.40E-01	-2.40E-01
0.00E+00	1.36E+00	2.00E+00	-2.40E-01	-2.40E-01
4.00E-02	1.52E+00	1.88E+00	-2.80E-01	-2.80E-01
4.00E-02	1.56E+00	1.72E+00	-2.40E-01	-2.40E-01
4.00E-02	1.72E+00	1.56E+00	-2.40E-01	-2.40E-01
4.00E-02	1.72E+00	1.40E+00	-2.00E-01	-2.80E-01
4.00E-02	1.88E+00	1.24E+00	-2.40E-01	-2.80E-01
0.00E+00	1.88E+00	1.12E+00	-2.80E-01	-2.40E-01
4.00E-02	2.00E+00	1.04E+00	-2.40E-01	-2.80E-01
4.00E-02	2.12E+00	8.80E-01	-2.40E-01	-2.40E-01
4.00E-02	2.28E+00	8.00E-01	-2.40E-01	-2.00E-01
8.00E-02	2.36E+00	6.80E-01	-2.00E-01	-2.40E-01
4.00E-02	2.48E+00	6.00E-01	-2.40E-01	-2.40E-01
8.00E-02	2.60E+00	5.20E-01	-2.80E-01	-2.40E-01
8.00E-02	2.64E+00	4.40E-01	-2.40E-01	-2.80E-01
4.00E-02	2.76E+00	3.60E-01	-2.40E-01	-2.40E-01
8.00E-02	2.88E+00	3.60E-01	-2.80E-01	-2.40E-01
1.20E-01	3.00E+00	3.20E-01	-2.80E-01	-2.80E-01
8.00E-02	3.00E+00	2.40E-01	-2.40E-01	-2.40E-01
8.00E-02	3.08E+00	2.00E-01	-2.80E-01	-2.40E-01
8.00E-02	3.12E+00	1.60E-01	-2.80E-01	-2.80E-01
8.00E-02	3.16E+00	8.00E-02	-3.20E-01	-2.40E-01
8.00E-02	3.12E+00	4.00E-02	-2.80E-01	-2.40E-01
8.00E-02	3.12E+00	0.00E+00	-2.80E-01	-2.40E-01
8.00E-02	3.08E+00	-8.00E-02	-2.40E-01	-2.40E-01
1.20E-01	3.04E+00	-8.00E-02	-2.40E-01	-2.40E-01
1.20E-01	2.96E+00	-1.60E-01	-2.40E-01	-2.40E-01
1.60E-01	2.88E+00	-2.00E-01	-2.80E-01	-2.40E-01
2.00E-01	2.80E+00	-2.40E-01	-2.80E-01	-2.40E-01

Two scenarios are illustrated in these examples. In the first scenario, shown in Fig. 6.2, the delay difference of the two constituent paths in the measured delay profile is less than the intrinsic delay resolution of the experimental channel sounder used; so that the two paths could not be individually identified prior to post-processing. A sample of the experimental data obtained in this case has been shown in Table 6.2. In the second scenario, shown in Fig. 6.3, the delay difference of the two constituent paths is greater than the intrinsic delay resolution of the channel sounder so that these two paths can be clearly identified prior to post-processing.

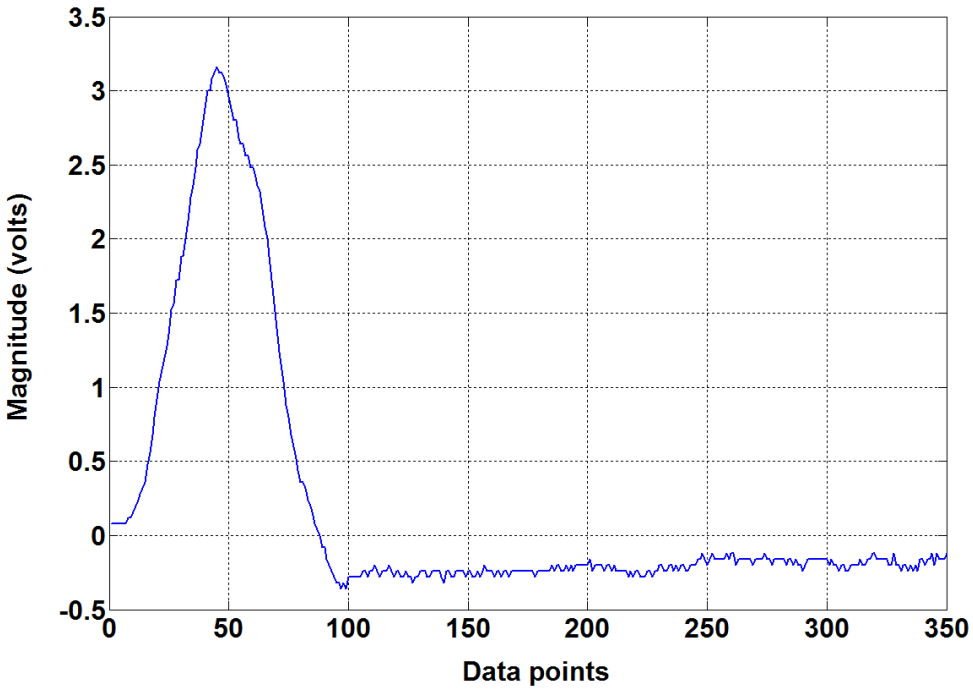

Figure 6.2 An example of measured multipath delay profile having two unresolved paths, from back-to-back measurements, obtained using the sliding correlator channel sounder system shown in Fig. 6.1.

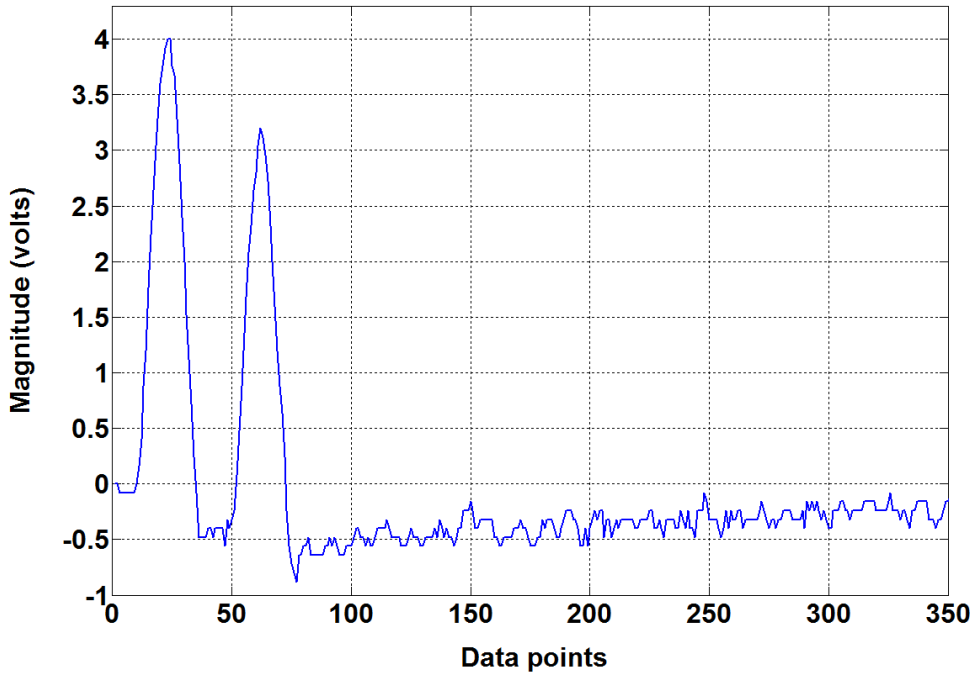

Figure 6.3 An example of measured multipath delay profile having two resolved paths, from back-to-back measurements, obtained using the sliding correlator channel sounder system shown in Fig. 6.1.

In Fig. 6.2, a two-way splitter has been used to split an RF signal from the transmitter unit of the channel sounder into two coaxial cables of different lengths. The outputs from the two cables, delayed and attenuated, were later combined at the receiver front-end. The delay difference, formed by these two coaxial cables, is less than the channel sounder's intrinsic delay resolution of 50 ns. These two paths could not therefore be individually indentified, prior to post-processing, and appear as a single pulse which is spread in time. In Fig. 6.3, however, the delay difference formed by the two coaxial cables is greater than the channel sounder's intrinsic delay resolution. These two paths can therefore be individually indentified, prior to post-processing. The wavelet transform of these channel impulse response profiles is now computed.

First, the SWT is applied in Fig. 6.2. The SWT levels 1-4 detail coefficients of this measured multipath delay profiles are shown in Figs. 6.4 (b-e) and 6.5 (b-e), using Pathlets 7 and 9 as the analysing wavelets respectively. These results show that the two

constituent multipath components are identified, and separated, at levels 3 and 4. As expected, Pathlet 7 achieves a compromise between obtaining acceptable resolution of the multipath components, and having a good dynamic range. Also, in agreement with the discussions in Section 3.3.3, the two multipath components of interest evolves with high magnitude as the SWT decomposition level increases while the noise decays.

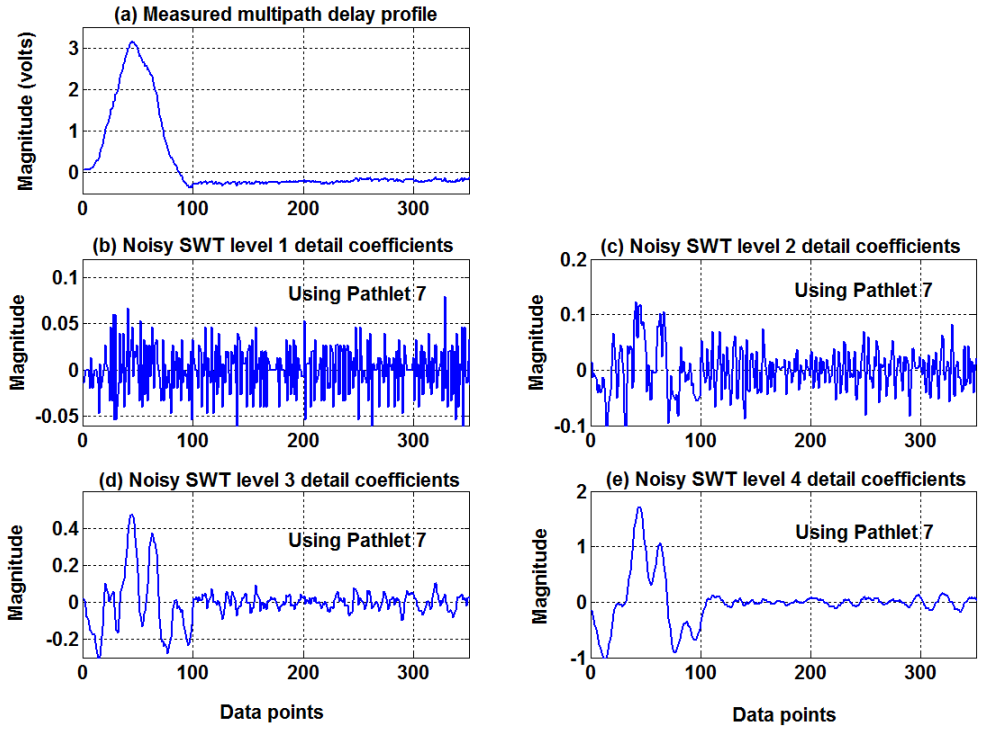

Figure 6.4 Measured multipath delay profile, having two unresolved paths, and corresponding SWT levels 1-4 detail coefficients. Pathlet 7 is used as the analysing wavelet.

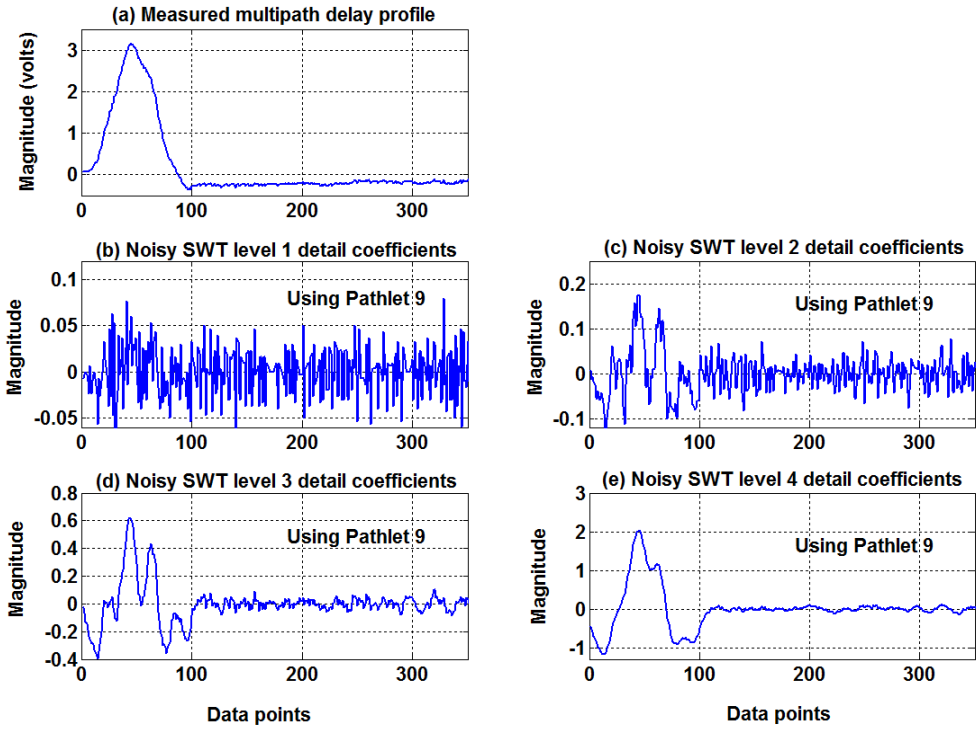

Figure 6.5 Measured multipath delay profile, having two unresolved paths, and corresponding SWT levels 1-4 detail coefficients. Pathlet 9 is used as the analysing wavelet.

The results from applying the SWTMP denoising technique given by (3.78), using the levels 3 and 4 detail coefficients, are shown in Figs. 6.6 (b & c). These results indicate that the detail coefficients that were attributed to noise, observed in Figs. 6.4 (b-e) and 6.5 (b-e), have been suppressed in Figs. 6.6 (b & c). The two paths which have been previously unresolvable in Fig. 6.6 (a) are now separated by both Pathlets 7 and 9. The location, in time, of the denoised peaks can then be used as estimates of the relative arrival times of the multipath components.

The denoised levels 3 and 4 detail coefficients, using hard thresholding and the median absolute deviation standard deviation estimate of noise given in (3.77), are shown in Figs. 6.7 (b & c) and 6.8 (b & c) respectively. These results also show that most of the noisy detail coefficients have been removed, and the two multipath components which have been previously unresolvable are now separated by both Pathlets 7 and 9.

These results are in general agreement with the simulation examples, in Chapters 4 and 5, that Pathlets 7 and 9 can be successfully applied to resolve closely spaced multipath components immersed in noise.

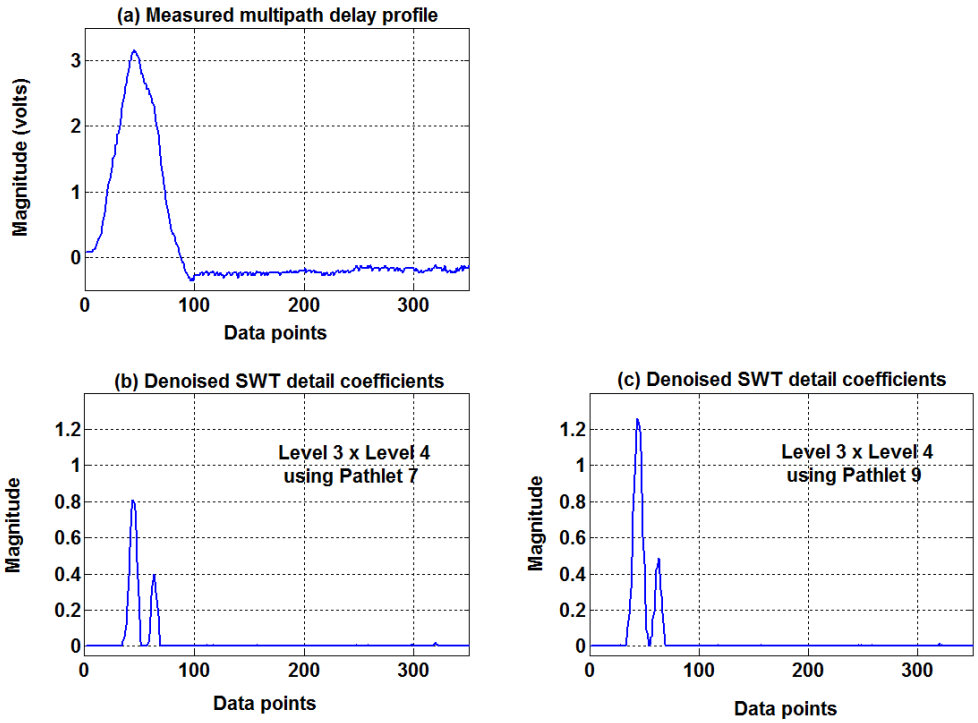

Figure 6.6 Measured multipath delay profile, having two unresolved paths, and the denoised SWT detail coefficients. Noise is suppressed by SWTMP using the levels 3 and 4 detail coefficients, with Pathlets 7 and 9 as the analysing wavelets.

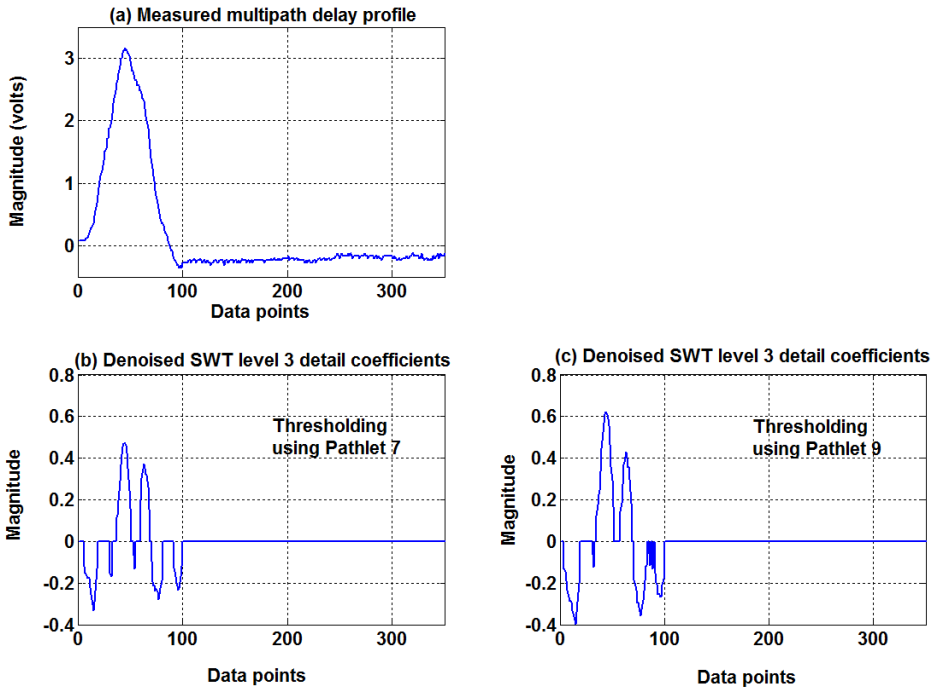

Figure 6.7 Measured multipath delay profile, having two unresolved paths, and the denoised SWT level 3 detail coefficients. Noise is removed by wavelet thresholding, with Pathlets 7 and 9 as the analysing wavelets.

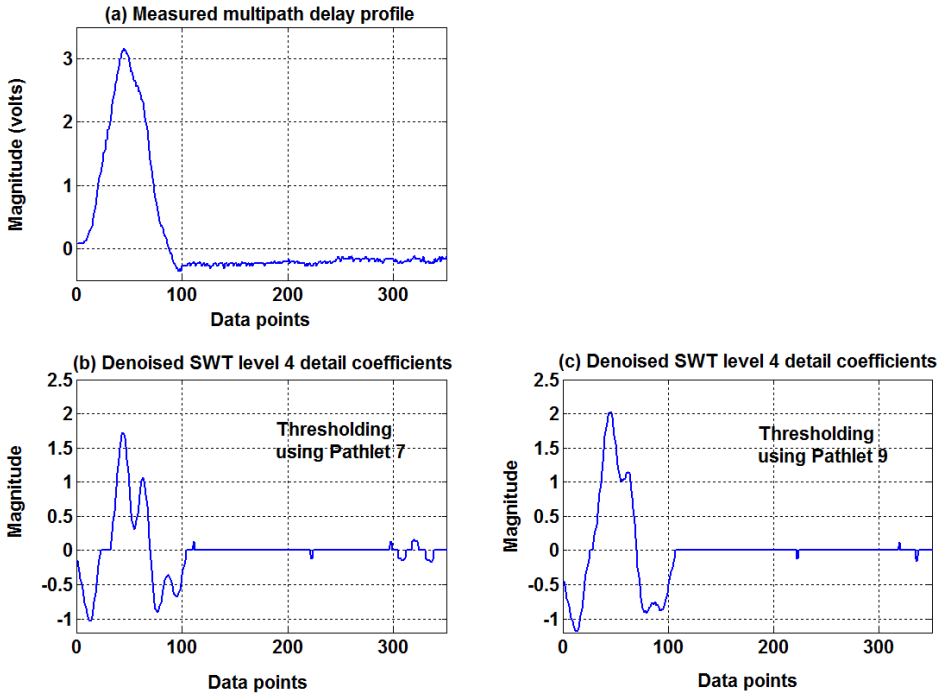

Figure 6.8 Measured multipath delay profile, having two unresolved paths, and the denoised SWT level 4 detail coefficients. Noise is removed by wavelet thresholding, with Pathlets 7 and 9 as the analysing wavelets.

Next, the SWT is applied in Fig. 6.3. The SWT levels 1-4 detail coefficients of this measured multipath delay profiles are shown in Figs. 6.9 (b-e) and 6.10 (b-e), using Pathlets 7 and 9 as the analysing wavelets respectively. In this case, the two multipath components can be individually indentified prior to wavelet processing as seen in Figs. 6.9 (a) and 6.10 (a). These results from the SWT again illustrate that the two constituent paths are identified as the dominant peaks at levels 3 and 4, in agreement with the discussions in Section 3.3.3, since the noise has decayed at these levels.

Finally, the SWTMP denoising technique given by (3.78) is applied using the levels 3 and 4 detail coefficients. The denoised detail coefficients are shown in Figs. 6.11 (b & c). These results show that the detail coefficients that were attributed to noise, observed in Figs. 6.9 (b-e) and 610 (b-e), have once more been suppressed in Figs. 6.11 (b & c). The location, in time, of the denoised peaks can then be used as estimates of the relative arrival times of the multipath components.

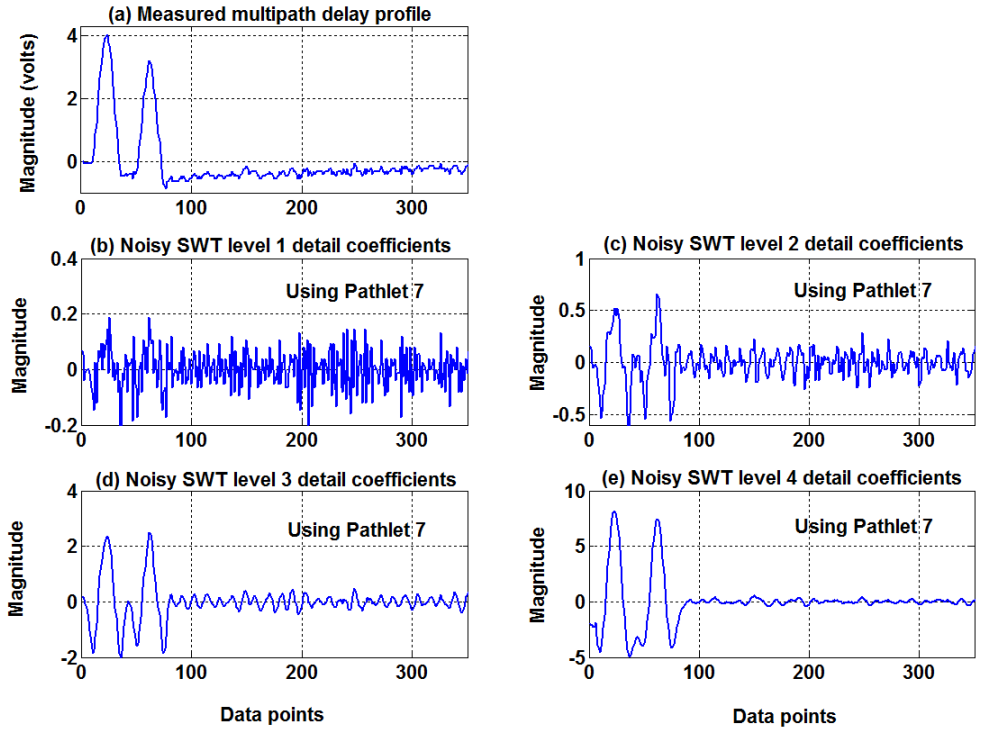

Figure 6.9 Measured multipath delay profile, having two resolved paths, and corresponding SWT levels 1-4 detail coefficients. Pathlet 7 is used as the analysing wavelet.

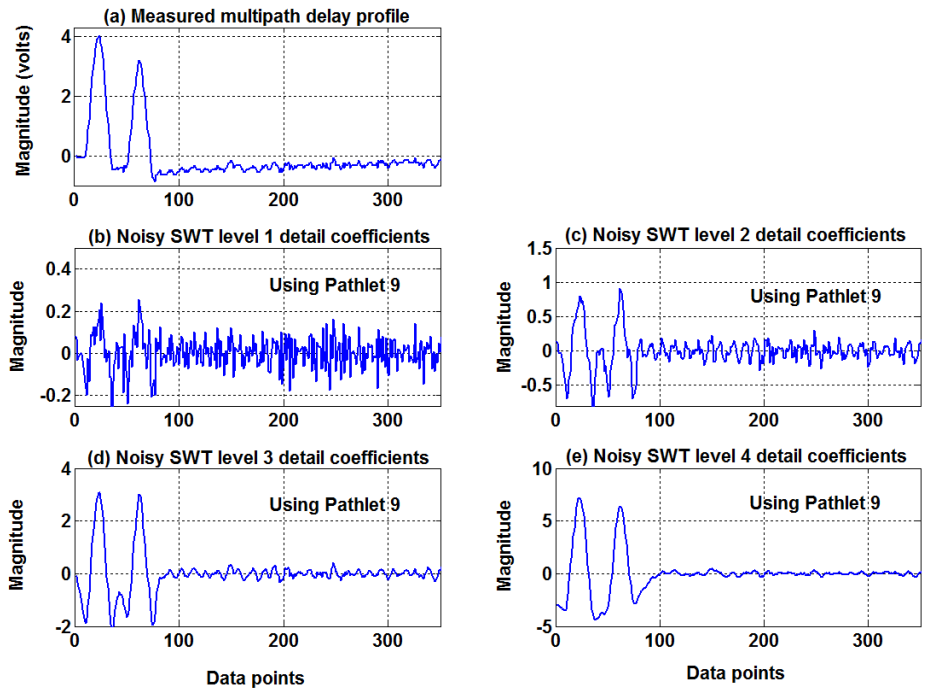

Figure 6.10 Measured multipath delay profile, having two resolved paths, and corresponding SWT levels 1-4 detail coefficients. Pathlet 9 is used as the analysing wavelet.

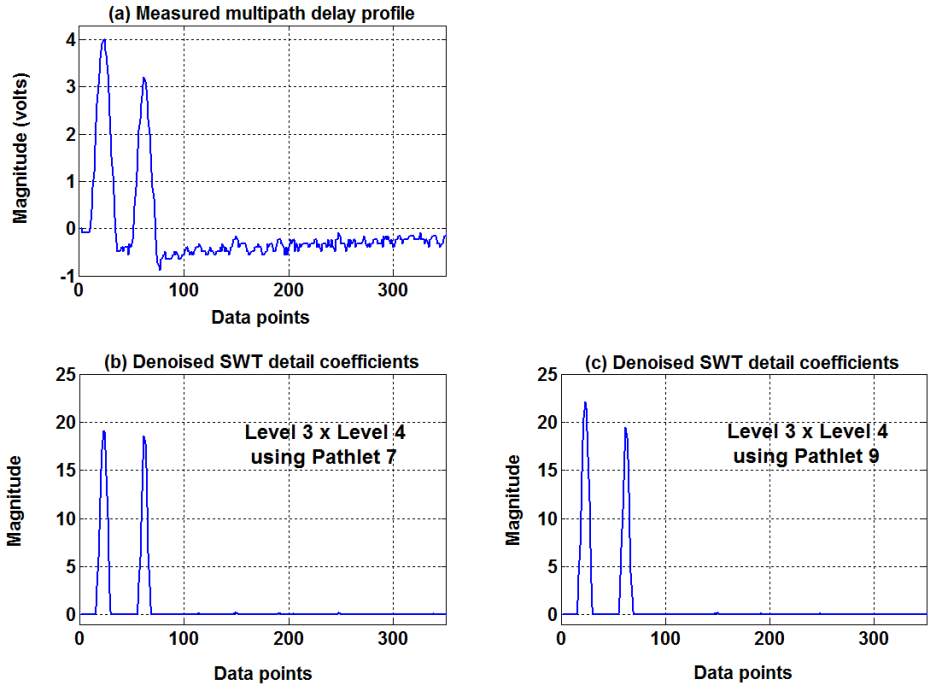

Figure 6.11 Measured multipath delay profile, having two resolved paths, and the denoised SWT detail coefficients. Noise is suppressed by SWTMP using the levels 3 and 4 detail coefficients, with Pathlets 7 and 9.

6.3 Summary

In this chapter, the wavelet analysis of measured channel impulse response profiles has been presented. These channel impulse response profiles were obtained by connecting the transmitter and receiver units of an experimental sliding correlator channel sounder, back-to-back using RG142 50Ω coaxial cables.

Two scenarios were examined. In the first scenario, the delay difference of the two constituent paths in a measured delay profile is less than the intrinsic delay resolution of the experimental channel sounder used; so that these two paths could not be identified prior to wavelet processing. In the second scenario, however, the delay difference of the constituent paths is greater than the intrinsic delay resolution of the channel sounder so that these paths can be clearly identified prior to the wavelet processing. The algorithm proposed in Chapter 3 for multipath resolution, is then applied to extract the multipath components.

The results obtained for the first scenario show agreement with the discussions in Section 3.3.3; that the features of interest evolves with high magnitude as the SWT decomposition level increases while the noise decays. Additionally, Pathlet 7 achieves a compromise between obtaining acceptable resolution of the multipath components and having a good dynamic range; in agreement with the simulation examples in Chapters 4 and 5.

Futhermore, the results from applying the SWTMP denoising scheme in Fig. 6.2, using the levels 3 and 4 detail coefficients, show that the wavelet transform detail coefficients that were attributed to noise are suppressed and the two constituent paths extracted after denoising. When the denoising procedure based on thresholding using the MAD estimate is applied, the results obtained show that the detail coefficients that were attributed to noise are also removed and the two paths successfully separated at levels 3 and 4. Pathlet 7 gives a better resolution.

Finally, the results obtained in the second scenario as well show that Pathlets 7 and 9 successfully detected the two paths in the channel impulse response profile at levels 3 and 4 of the wavelet transform. Moreover, these multipath components of interest are reinforced within the detail coefficients as the SWT decomposition level increases while the noise diminishes, in accordance with the wavelet transform multiscale dependencies given in (A.18).

CHAPTER 7

CONCLUSIONS AND RECOMMENDATIONS FOR FUTURE RESEARCH

7.1 Summary of Results and Conclusions

The subject of the research described in this thesis has been the identification and development of a novel wavelet-based high-resolution digital signal processing algorithm, for multipath channel parameter estimation. The thesis has been organised into seven chapters. The first chapter presents the introduction and original contributions of the thesis. The second chapter reviews various wideband channel sounding and signal parameter estimation techniques. This included a description of wavelet analysis and some applications. The third chapter presents the design of novel mother wavelets for use in this research and the proposed multipath channel parameter estimation procedure. The fourth chapter details the implementation of the algorithm developed in the third chapter, for multipath channel parameter estimation, through computer simulations. The fifth chapter presents series of computer simulations which were carried out to examine the effect on time resolution, caused by bandwidth limitations, in the wavelet-based multipath channel parameter estimation technique. Finally in Chapter 6, the algorithm developed in this research has been applied to resolve the multipath components in measured channel impulse response profiles, obtained by connecting the transmitter and receiver units of an experimental sliding correlator channel sounder back-to-back.

As previously discussed in Section 2.1, a major prerequisite to the design and specification of any wideband digital mobile radio system is a complete cognition of the multipath geometries of the radio channel. This is achieved by resolving the multipath field into its constituent components. Moreover, the resolution of very closely spaced multipath components requires channel measurements with huge bandwidth. Hence, the intrinsic delay resolution of channel sounding equipments is more easily enhanced through the use of digital signal post-processing algorithms. A review of such digital signal processing techniques has been given in Section 2.3. It has been shown that the model order selection is often the most difficult problem in the parametric-based methods of signal parameter estimation. The main contribution of this thesis is, therefore, in the development of a novel wavelet-based digital signal post-processing algorithm for estimating the number of impinging waves and time-delays in mobile radio environments. The results obtained in this research have shown that this wavelet-based procedure can be successfully applied to improve the intrinsic delay resolution of channel sounding equipments by more than a factor of ten.

In Chapter 3, the development of a new wavelet family for resolving the constituent components in a multipath channel has been presented. The results obtained have shown the desired properties of a wavelet used in this research as symmetry, compact support, and triangular (or near triangular) shape. That is, the shape of the wavelet function used should reflect the type of features to be extracted. This novel wavelet family has been named “Pathlet.” Two noise reduction schemes were then proposed using Pathlets 5, 7, 9, and a member of Daubechies near symmetric wavelet family called Symlet 2, as the analysing wavelets. The probability distributions of the equivalent noise, obtained from the wavelet analysis of a Gaussian white noise source using Pathlets 5, 7, 9, and Symlet 2 as analysing wavelets, have also been derived. Finally, an amplitude estimation algorithm was developed.

Chapter 4 investigates the use of the stationary wavelet transform in estimating the number, and time-delays, of the impinging waves in synthetic mobile radio environments. Two noise reduction schemes are implemented in the SWT. The first

noise reduction scheme is based on using hard thresholding and the MAD standard deviation estimate (Donoho and Johnstone 1994; Donoho 1995; Donoho and Johnstone 1995; Percival and Walden 2000). An alternative denoising procedure was also proposed, based on exploiting the stationary wavelet transform multiscale dependencies. This scheme has been named the "stationary wavelet transform multilevel products (SWTMP)." In general, the results obtained from using these two denoising strategies have been found to be comparable. The denoised detail coefficients provide information about the number of impinging waves, and time-delays, in synthetic mobile radio environments.

A measure of multipath resolution of equal-amplitude paths show that 2 ns resolution can be obtained at high SNRs, when Pathlet family members and Symlet 2 are used as analysing wavelets. The estimated number of paths and arrival times are then used to determine the amplitudes of the individual delay components, using the amplitude estimation algorithm developed as part of this study. Estimates of multipath delay statistics such as mean excess delay and rms delay spread have been subsequently determined.

In Chapter 5, series of computer simulations were carried out to examine the effect of bandwidth limitations on multipath resolution using the algorithm proposed in this study. The results obtained shows that the wavelet-based algorithm proposed in this research can still be successfully applied to resolve the multipath components, even after band-limitations. Moreover, these results indicate that there is a compromise between obtaining acceptable resolution of the multipath components and noise reduction.

Chapter 6 presents the description, and wavelet analysis, of the channel impulse response profiles captured with an experimental portable channel sounder used for wideband radio propagation measurements.

7.2 Study Limitations and Recommendations

7.2.1 Number of impinging waves and time-delay estimation

Throughout this study, a lot of issues have been brought to light. Not all of these issues can be considered to have been fully exhausted by the author. One such subject is the influence of bandwidth limitations and low SNR conditions in the estimation of the number and time-delays of impinging waves. Traditionally, the number of impinging waves in mobile radio environments is often set to a value large enough to capture all the significant impinging waves before their parameter vectors can be estimated. This study has presented a novel algorithm for estimating the time-delays and number of these impinging waves. This wavelet-based algorithm, proposed in the study, gives good estimates of the multipath delay statistics at high SNRs. However, more studies are required to investigate the influence of band-limitation and very low SNRs on such estimates of the time-delays and number of impinging waves.

7.2.2 Reduction of noise

This study has also presented a new noise reduction procedure, based on exploiting the stationary wavelet transform multiscale dependencies. The performance of this noise reduction technique has been found to be comparable, under high SNRs, to that based on the conventional wavelet thresholding method. However much lower SNRs may be encountered in practice and hence more studies is required to investigate schemes for reducing noise at very low SNRs.

7.2.3 Field tests

Another recommendation for further study is the performance, in real mobile radio environments, of the algorithm proposed in this thesis through extensive field tests.

REFERENCES

Ainsleigh, P. L., & Chui, C. K. (1996). A B-Wavelet-Based Noise-Reduction Algorithm. *IEEE Transactions on Signal Processing*, **44**(5), 1279-1284. doi: 10.1109/78.502342

Akansu, A. N., Duhamel, P., Lin, X., & Courville, M. d. (1998). Orthogonal Transmultiplexers in Communication: A Review. *IEEE Transactions on Signal Processing*, **46**(4), 979-995. doi: 10.1109/78.668551

Akansu, A. N., & Haddad, R. A. (2001). *Multiresolution signal decomposition: transforms, subbands, and wavelets*. San Diego, CA: Academic Press.

Beex, A. A., & Scharf, L. L. (1981). Covariance sequence approximation for parametric spectrum modeling. *IEEE Transactions on Acoustics, Speech, and Signal Processing*, **29**(5), 1042-1052. doi: 10.1109/TASSP.1981.1163680

Beylkin, G. (1992). On the Representation of Operators in Bases of Compactly Supported Wavelets. *SIAM Journal on Numerical Analysis*, **29**(6), 1716-1740.

Bijaoui, A., Slezak, E., Rue, F., & Lega, E. (1996). Wavelets and the Study of the Distant Universe. *Proceedings of the IEEE*, **84**(4), 670-679. doi: 10.1109/5.488706

Bradley, J. N., & Brislawn, C. M. (1994, 30 May - 2 June). *The Wavelet / Scalar Quantization Compression Standard for Digital Fingerprint Images*. IEEE International Symposium on Circuits and Systems, London. doi: 10.1109/ISCAS.1994.409142

Bruce, A. G., & Gao, H.-Y. (1996a). *Applied Wavelet Analysis with S-PLUS*. New York: Springer.

Bultitude, R. J. C., Mahmoud, S. A., & Sullivan, W. A. (1989). A Comparison of Indoor Radio Propagation Characteristics at 910 MHz and 1.75 GHz. *IEEE Journal on Selected Areas in Communications*, **7**(1), 20-30. doi: 10.1109/49.16840

Bultitude, R. J. C., Melancon, P., Zaghloul, H., Morrison, G., & Prokki, M. (1993). The Dependence of Indoor Radio Channel Multipath Characteristics on Transmit/Receive Ranges. *IEEE Journal on Selected Areas in Communications*, **11**(7), 979-990. doi: 10.1109/49.233211

Cadzow, J. A. (1982). Spectrum estimation: An overdetermined rational model equation approach. *Proceedings of the IEEE*, **70**(9), 907-939. doi: 10.1109/PROC.1982.12424

Chidume, C. E. (2003). *Applicable functional analysis, fundamental theorems with applications*. Trieste, Italy: International Centre for Theoretical Physics.

Coifman, R. R., & Donoho, D. L. (1995). Translation-Invariant De-Noising. In A. Antoniadis & G. Oppenheim (Eds.), *Wavelets and Statistics: Lecture Notes in Statistics* (pp. 125-150). New York, NY: Springer.

Coifman, R. R., Meyer, Y., Quake, S., & Wickerhauser, M. V. (1990). Signal Processing and Compression With Wavelet Packets. In Y. Meyer & S. Roques (Eds.), *Progress in Wavelet Analysis and Applications* (pp. 77-93). France: Atlantica Séguier Frontières.

Coifman, R. R., & Wickerhauser, M. V. (1992). Entropy-Based Algorithms for Best Basis Selection. *IEEE Transactions on Information Theory*, **38**(2), 713-718. doi: 10.1109/18.119732

Cox, D. C. (1972). Delay-doppler characteristics of multipath propagation at 910 MHz in a suburban mobile radio environment. *IEEE Transactions on Antennas and Propagation*, **20**(5), 625-635. doi: 10.1109/TAP.1972.1140277

Cox, D. C. (1973a). 910 MHz Urban Mobile Radio Propagation: Multipath Characteristics in New York City. *IEEE Transactions on Communications*, **21**(11), 1188-1194. doi: 10.1109/TCOM.1973.1091571

Cristescu, R., Ristaniemi, T., Joutsensalo, J., & Karhunen, J. (2000, September). *CDMA delay estimation using fast ICA algorithm*. The 11th IEEE International Symposium on Personal, Indoor and Mobile Radio Communications, London. doi: 10.1109/PIMRC.2000.881593

Daubechies, I. (1992). *Ten Lectures on wavelets*. Philadelphia, PA: Society for Industrial and Applied Mathematics (SIAM).

Davies, R., Bensebti, M., Beach, M. A., & McGeehan, J. P. (1991, May). *Wireless Propagation Measurements in Indoor Multipath Environments at 1.7 GHz and 60 GHz for Small Cell Systems*. IEEE Vehicular Technology Conference, Saint Louis, Missouri. doi: 10.1109/VETEC.1991.140560

Debnath, L. (2003). *Wavelets and Signal Processing*. Boston, Massachusetts: Birkhauser.

Degli-Esposti, V., Lombardi, G., Passerini, C., & Riva, G. (2001). Wide-Band Measurement and Ray-Tracing Simulation of the 1900 MHz Indoor Propagation Channel: Comparison Criteria and Results. *IEEE Transactions on Antennas and Propagation*, **49**(7), 1101-1110. doi: 10.1109/8.933490

Devasirvatham, D. M. J. (1987). A Comparison of Time Delay Spread and Signal Level Measurements Within Two Dissimilar Office Buildings. *IEEE Transactions on Antennas and Propagation*, **35**(3), 319-324. doi: 10.1109/TAP.1987.1144106

Devasirvatham, D. M. J. (1991, September). *Multi-Frequency Propagation Measurements and Models in a Large Metropolitan Commercial Building For Personal Communications*. IEEE International Symposium on Personal, Indoor and Mobile Radio Communications, London. doi: 10.1109/PIMRC.1991.571472

Donoho, D. L. (1995). De-Noising by Soft-Thresholding. *IEEE Transactions on Information Theory*, **41**(3), 613-627. doi: 10.1109/18.382009

Donoho, D. L., & Johnstone, I. M. (1994). Ideal Spatial Adaptation by Wavelet Shrinkage. *Biometrika*, **81**(3), 425-455. doi: 10.2307/2337118

Donoho, D. L., & Johnstone, I. M. (1995). Adapting to unknown smoothness via wavelet shrinkage. *Journal of the American Statistical Association*, **90**(432), 1200-1224.

Farge, M., Kevlahan, N., Perrier, V., & Goirand, E. (1996). Wavelets and Turbulence. *Proceedings of the IEEE* **84**(4), 639-669. doi: 10.1109/5.488705

Feder, M., & Weinstein, E. (1988). Parameter Estimation of Superimposed Signals Using the EM Algorithm. *IEEE Transactions on Acoustics, Speech, and Signal Processing*, **36**(4), 477-489. doi: 10.1109/29.1552

Fessler, J. A., & Hero, A. O. (1994). Space-Alternating Generalized Expectation-Maximization Algorithm. *IEEE Transactions on Signal Processing*, **42**(10), 2664-2677. doi: 10.1109/78.324732

Fleury, B. H., Dahlhaus, D., Heddergott, R., & Tschudin, M. (1996, September). *Wideband angle of arrival estimation using the SAGE algorithm*. IEEE 4th International Symposium on Spread Spectrum Techniques and Applications, Mainz, Germany. doi: 10.1109/ISSSTA.1996.563747

Fleury, B. H., Tschudin, M., Heddergott, R., Dahlhaus, D., & Pedersen, K. L. (1999). Channel parameter estimation in mobile radio environments using the SAGE algorithm. *IEEE Journal on selected areas in communications*, **17**(3), 434-450. doi: 10.1109/49.753729

Ganesh, R., & Pahlavan, K. (1991). Statistical modelling and computer simulation of indoor radio channel. *IEE Proceedings-I*, **138**(3), 153-161.

Gersh, W. (1970). Estimation of the autoregressive parameters of mixed autoregressive moving-average time series. *IEEE Transactions on Automatic Control*, **15**(5), 583-588. doi: 10.1109/TAC.1970.1099560

Guillemain, P., & Kronland-Martinet, R. (1996). Characterization of Acoustic Signals Through Continuous Linear Time-Frequency Representations. *Proceedings of the IEEE*, **84**(4), 561-585. doi: 10.1109/5.488700

Harris, R. W., & Ledwidge, T. J. (1974). *Introduction to noise analysis*. London: Pion Limited.

Hashemi, H. (1993a). Impulse Response Modeling of Indoor Radio Propagation Channels. *IEEE Journal on Selected Areas in Communications*, **11**(7), 967-978. doi: 10.1109/49.233210

Hayes, M. H. (1999). *Schaum's Outline of Theory and Problems of Digital Signal Processing*: McGraw-Hill Companies, Inc.

Herley, C., Kovacevic, J., Ramchandran, K., & Vetterli, M. (1993). Tilings of the Time-Frequency Plane: Construction of Arbitrary Orthogonal Bases and Fast Tiling Algorithms. *IEEE Transactions on Signal Processing*, **41**(12), 3341-3359. doi: 10.1109/78.258078

Hetling, K., Medley, M., Saulnier, G., & Das, P. (1994, October). *A PR-QMF (Wavelet) Based Spread Spectrum Communications System*. IEEE Military Communications Conference, Fort Monmouth, NJ. doi: 10.1109/MILCOM.1994.473869

Hewitt, A., Lau, W. H., Austin, J., & Vilar, E. (1989). An Autoregressive Approach to the Identification of Multipath Ray Parameters from Field Measurements. *IEEE Transactions on Communications*, **37**(11), 1136-1143. doi: 10.1109/26.46507

Huang, C.-C., & Khayata, R. (1992, June). *Delay spreads and channel dynamics measurements at ISM bands*. IEEE International Conference on Communications, Chicago, IL. doi: 10.1109/ICC.1992.268046

Ionescu, D. M., & Wickert, M. A. (1997, May). *On the performance of a CDMA system with user signatures based on packet wavelets in multipath channels*. IEEE 47th Vehicular Technology Conference, Phoenix, AZ. doi: 10.1109/VETEC.1997.596387

Jansen, M. (2001). *Noise Reduction by Wavelet Thresholding*. New York: Springer-Verlag Inc.

Jensen, A., & Cour-Harbo, A. l. (2001). *Ripples in Mathematics: The Discrete Wavelet Transform*. Berlin: Springer-Verlag.

Kashyap, R. L. (1980). Inconsistency of the AIC Rule for Estimating the Order of Autoregressive Models. *IEEE Transactions on Automatic Control*, **25**(5), 996-998. doi: 10.1109/TAC.1980.1102471

Kaveh, M., & Barabell, A. J. (1986). The Statistical Performance of the MUSIC and the Minimum-Norm Algorithms in Resolving Plane Waves in Noise. *IEEE Transactions on Acoustics, Speech, and Signal Processing*, **34**(2), 331-341. doi: 10.1109/TASSP.1986.1164815

Kay, S. M. (1988). *Modern Spectral Estimation: Theory and Application*. Englewood Cliffs, New Jersey: Prentice-Hall Inc.

Kay, S. M., & Marple, S. L. (1981). Spectrum Analysis - A Modern Perspective. *Proceedings of the IEEE*, **69**(11), 1380-1419. doi: 10.1109/PROC.1981.12184

Kim, M., Konishi, Y., Chang, Y., & Takada, J.-i. (2014). Large Scale Parameters and Double-Directional Characterization of Indoor Wideband Radio Multipath Channels at 11 GHz. *IEEE Transactions on Antennas and Propagation*, **62**(1), 430-441. doi: 10.1109/TAP.2013.2288633

Kinkel, J. F., Perl, J., Scharf, L., & Stubberud, A. (1979). A note on covariance-invariant digital filter design and autoregressive-moving average spectrum analysis. *IEEE Transactions on Acoustics, Speech, and Signal Processing*, **27**(2), 200-202. doi: 10.1109/TASSP.1979.1163220

Kowalski, P., Geffert, T., & Veve, M. (1991, November). *MUSIC algorithm implementation for shipboard HF radio direction finding*. IEEE Military Communications Conference, McLean, VA, USA. doi: 10.1109/MILCOM.1991.258407

Krim, H., & Viberg, M. (1996, July 1996). Two decades of array signal processing research. *IEEE Signal Processing Magazine*67-94.

Krim, H., & Viberg, M. (1996, July). Two decades of array signal processing research: the parametric approach. *IEEE Signal Processing Magazine*, *13*(4), 67-94. doi: 10.1109/79.526899

Kumaresan, R., & Tufts, D. W. (1980). Improved Spectral Resolution III: Efficient Realization. *Proceedings of the IEEE*, **68**(10), 1354-1355. doi: 10.1109/PROC.1980.11867

Kumaresan, R., & Tufts, D. W. (1983). Estimating the Angles of Arrival of Multiple Plane Waves. *IEEE Transactions on Aerospace and Electronic Systems*, **AES-19**(1), 134-139. doi: 10.1109/TAES.1983.309427

Kyriakopoulos, K. G., & Parish, D. J. (2010). Applying wavelets for the controlled compression of communication network measurements. *IET Communications*, **4**(5), 507-520. doi: 10.1049/iet-com.2009.0050

Lau, W. H., Austin, J., Hewitt, A., Vilar, E., & Martin, L. (1991). Analysis of the Time-Variant Structure of Microwave Line-of-Sight Multipath Phenomena. *IEEE Transactions on Communications*, **39**(6), 847-855. doi: 10.1109/26.87174

Lau, W. H., Austin, J., & Vilar, E. (1987). Improved Prony Algorithm to identify Multipath Components. *Electronics Letters*, **23**(20), 1059-1060. doi: 10.1049/el:19870740

Leon-Garcia, A. (2008). *Probability, Statistics, and Random Processes for Electrical Engineering*. Upper Saddle River, NJ: Pearson/Prentice Hall.

Liang, J., & Parks, T. W. (1996). A Translation-Invariant Wavelet Representation Algorithm with Applications. *IEEE Transactions on Signal Processing*, **44**(2), 225-232. doi: 10.1109/78.485919

Lo, T., Litva, J., & Bultitude, R. J. C. (1992, June). *High-resolution spectral analysis techniques for estimating the impulse response of indoor radio channels*. IEEE International Conference on Selected Topics in Wireless Communications, Vancouver, BC, Canada. doi: 10.1109/ICWC.1992.200712

Lo, T., Litva, J., & Leung, H. (1993). Estimating the impulse response of indoor radio channels using signal subspace techniques. *IEE Proceedings-I*, **140**(3), 203-210.

Lukama, L., Street, A. M., Konstantinou, K., Edwards, D. J., & Jenkins, A. P. (2001, April). *Characterization of Wideband Mobile Radio Channels using Singular Value Decomposition-Prony (SVDP) Algorithm at 2.4 GHz*. 11th International Conference on Antennas and Propagation, Manchester, UK. doi: 10.1049/cp:20010337

Ma, X., Zhou, C., & Kemp, I. J. (2002, March/April). Automated wavelet selection and thresholding for PD detection. *IEEE Electrical Insulation Magazine*, *18*(2), 37-45. doi: 10.1109/57.995398

Mallat, S. (1991). Zero-Crossings of a Wavelet Transform. *IEEE Transactions on Information Theory*, **37**(4), 1019-1033. doi: 10.1109/18.86995

Mallat, S. (1996). Wavelets for a Vision. *Proceedings of the IEEE*, **84**(4), 604-614. doi: 10.1109/5.488702

Mallat, S., & Zhong, S. (1992). Characterization of Signals from Multiscale Edges. *IEEE Transactions on Pattern Analysis and Machine Intelligence*, **14**(7), 710-732. doi: 10.1109/34.142909

Mallat, S. G. (1989a). Multifrequency Channel Decompositions of Images and Wavelet Models. *IEEE Transactions on Acoustics, Speech and Signal Processing*, **37**(12), 2091-2110. doi: 10.1109/29.45554

Mallat, S. G. (1989b). A Theory for Multiresolution Signal Decomposition: The Wavelet Representation. *IEEE Transactions on Pattern Analysis and Machine Intelligence*, **11**(7), 674-693. doi: 10.1109/34.192463

Mallat, S. G. (1999). *A wavelet tour of signal processing*. San Diego, California: Academic Press.

Mallat, S. G., & Hwang, W. L. (1992). Singularity Detection and Processing with Wavelets. *IEEE Transactions on Information Theory*, **38**(2), 617-643. doi: 10.1109/18.119727

Marple, S. L. (1987). *Digital Spectral Analysis with Applications*. Englewood Cliffs, New Jersey: Prentice-Hall Inc.

McClellan, J. H., & Parks, T. W. (1973). A Unified Approach to the Design of Optimum FIR Linear-Phase Digital Filters. *IEEE Transactions on Circuit Theory*, **20**(6), 697-701. doi: 10.1109/TCT.1973.1083764

Mossammaparast, M. (1999). *High Resolution Time Delay Spread Measurement*. (M.Eng Thesis). Curtin University of Technology, Bentley, WA.

Mossammaparast, M., Afifi, N., & Chung, K. S. (1997). Portable Channel Characterisation Sounder. In T. Wysocki, H. Razavi & B. Honary (Eds.), *Digital Signal Processing for Communication Systems* (pp. 141-146). New York, NY: Springer Science+Business Media.

Nason, G. P., & Silverman, B. W. (1995). The stationary wavelet transform and some statistical applications. In A. Antoniadis & G. Oppenheim (Eds.), *Wavelets and Statistics: Lecture Notes in Statistics* (pp. 281-300). New York, NY: Springer.

Ndzi, D., Austin, J., & Vilar, E. (2000, April). *Indoor channel characterisation using hyper-resolution impulse response*. AP2000 Millennium Conference on Antennas & Propagation, Davos, Switzerland.

Neves, F. F., Matos, L. J., & Siqueira, G. L. (2009, November). *Wideband Characterization of the Mobile Radio Signal in a Vegetated Environment*. SBMO/IEEE MTT-S International Microwave and Optoelectronics Conference, Belem, Brazil. doi: 10.1109/IMOC.2009.5427571

Newlin, H. M. (1998, October). *Developments in the use of wavelets in communication systems*. IEEE Military Communications Conference, Boston, MA. doi: 10.1109/MILCOM.1998.722601

Oppenheim, A. V., & Willsky, A. S. (1997). *Signals and Systems*. New Jersey: Prentice-Hall.

Pahlavan, K., Ganesh, R., & Hotaling, T. (1989). Multipath Propagation Measurements on Manufacturing Floors at 910 MHz. *Electronics Letters*, **25**(3), 225-227. doi: 10.1049/el:19890161

Papoulis, A., & Pillai, S. U. (2002). *Probability, random variables, and stochastic processes*. Boston: McGraw-Hill.

Parsons, D. (1992). *The Mobile Radio Propagation Channel*. London: Pentech Press.

Parsons, J. D., Demery, D. A., & Turkami, A. M. D. (1991). Sounding techniques for wideband mobile radio channels: a review. *IEE Proceedings-I*, **138**(5), 437-446.

Paulraj, A., Roy, R., & Kailath, T. (1985, November). *Estimation of Signal Parameters via Rotational Invariance Techniques - ESPRIT*. 19th Asilomar Conference on Circuits, Systems and Computers, Pacific Grove, CA, USA. doi: 10.1109/ACSSC.1985.671426

Paulraj, A., Roy, R., & Kailath, T. (1986). A subspace rotation approach to signal parameter estimation. *Proceedings of the IEEE*, **74**(7), 1044-1046. doi: 10.1109/PROC.1986.13583

Pedersen, K. I., Fleury, B. H., & Mogensen, P. E. (1997, September). *High resolution of electromagnetic waves in time-varying radio channels*. The 8th IEEE International Symposium on Personal, Indoor and Mobile Radio Communications, Helsinki, Finland. doi: 10.1109/PIMRC.1997.631112

Peracchi, F. (2001). *Econometrics*. Chichester, England: John Wiley & Sons Ltd.

Percival, D. B., & Walden, A. T. (2000). *Wavelet Methods for Time Series Analysis*. Cambridge: Cambridge University Press.

Pesquet, J.-C., Krim, H., & Carfantan, H. (1996). Time-Invariant Orthonormal Wavelet Representations. *IEEE Transactions on Signal Processing*, **44**(8), 1964-1970. doi: 10.1109/78.533717

Polikar, R., Greer, M. H., Udpa, L., & Keinert, F. (1997, 30 Oct. - 2 Nov.). *Multiresolution Wavelet Analysis of ERPs for the Detection of Alzheimer's Disease*. 19th Annual International Conference of the IEEE Engineering in Medicine and Biology Society, Chicago, IL. doi: 10.1109/IEMBS.1997.756614

Pollock, D. S. G. (1999). *A handbook of time-series analysis, signal processing and dynamics*. San Diego, California; London: Academic Press.

Pourkhaatoun, M., & Zekavat, S. A. (2011). High-resolution independent component analysis based time-of-arrival estimation for line-of-sight multipath environments. *IET Communications*, **5**(10), 1440-1452. doi: 10.1049/iet-com.2010.0289

Pourkhaatoun, M., Zekavat, S. A., & Pourrostam, J. (2007, April). *A Novel High Resolution ICA-Based TOA Estimation Technique*. IEEE Radar Conference Boston, MA. doi: 10.1109/RADAR.2007.374235

Proakis, J. G. (1990). Model-Based Spectrum Estimation. In J. G. McWhirter (Eds.), *Mathematics in Signal Processing II* (pp. 281-282). New York: Oxford University Press.

Quinquis, A., & Boulinguez, D. (1997). Multipath Channel Identification with Wavelet Packets. *IEEE Journal of Oceanic Engineering*, **22**(2), 342-346. doi: 10.1109/48.585953

Ramchandran, K., Vetterli, M., & Herley, C. (1996). Wavelets, Subband Coding, and Best Bases. *Proceedings of the IEEE*, **84**(4), 541-560. doi: 10.1109/5.488699

Rangarao, K. V., & Venkatanarasimhan, S. (2013). gold-MUSIC: A Variation on MUSIC to Accurately Determine Peaks of the Spectrum. *IEEE Transactions on Antennas and Propagation*, **61**(4), 2263-2268. doi: 10.1109/TAP.2012.2232893

Rappaport, T. S. (1989). Characterization of UHF Multipath Radio Channels in Factory Buildings. *IEEE Transactions on Antennas and Propagation*, **37**(8), 1058-1069. doi: 10.1109/8.34144

Rappaport, T. S. (2002). *Wireless Communications: Principles and Practice*. Upper Saddle River, New Jersey: Prentice-Hall Inc.

Rappaport, T. S., & McGillem, C. D. (1988, 28 Nov. - 1 Dec.). *UHF Multipath and Propagation Measurements in Manufacturing Environments*. IEEE Global Telecommunications Conference, Hollywood, FL. doi: 10.1109/GLOCOM.1988.25954

Resnikoff, H. L., & Wells, R. O. (1998). *Wavelet analysis: the scalable structure of information*. New York: Springer-Verlag.

Richter, J., & Al-Nuaimi, M. O. (1995). Resolution of constituent components in multipath field using DFT. *Electronics Letters*, **31**(17), 1415-1416. doi: 10.1049/el:19951033

Rioul, O., & Vetterli, M. (1991, October). Wavelets and Signal Processing. *IEEE Signal Processing Magazine*, *8*(4), 14-38. doi: 10.1109/79.91217

Rissanen, J. (1978). Modeling by Shortest Data Description. *Automatica*, **14**(5), 465-471.

Roy, R., & Kailath, T. (1989). ESPRIT-Estimation of Signal Parameters via Rotational Invariance Techniques. *IEEE Transactions on Acoustics, Speech and Signal Processing*, **37**(7), 984-995. doi: 10.1109/29.32276

Roy, R., Paulraj, A., & Kailath, T. (1986). ESPRIT - A Subspace Rotation Approach to Estimation of Parameters of Cisoids in Noise. *IEEE Transactions on Acoustic, Speech and Signal Processing*, **34**(5), 1340-1342. doi: 10.1109/TASSP.1986.1164935

Roy, R. H. (1987). *ESPRIT - Estimation of signal parameters via rotational invariance techniques*. (Doctoral dissertation). Stanford University, Stanford, CA.

Saariiisaari, H. (1997, May). *TLS-ESPRIT in a time delay estimation*. IEEE 47th Vehicular Technology Conference, Phoenix, Arizona, USA. doi: 10.1109/VETEC.1997.605832

Sakai, H. (1984). Statistical Analysis of Pisarenko‘s Method for Sinusoidal Frequency Estimation. *IEEE Transactions on Acoustics, Speech, and Signal Processing*, **32**(1), 95-101. doi: 10.1109/TASSP.1984.1164273

Saleh, A. A. M., & Valenzuela, R. A. (1987). A Statistical Model for Indoor Multipath Propagation. *IEEE Journal on Selected Areas in Communications*, **5**(2), 128-137. doi: 10.1109/JSAC.1987.1146527

Schmidt, R. O. (1981). *A Signal Subspace Approach to Multiple Emitter Location and Spectral Estimation*. (Doctoral dissertation). Stanford University, Stanford, California.

Schmidt, R. O. (1986). Multiple Emitter Location and Signal Parameter Estimation. *IEEE Transactions on Antennas and Propagation*, **34**(3), 276-280. doi: 10.1109/TAP.1986.1143830

Seidel, S. Y., Rappaport, T. S., Feuerstein, M. J., Blackard, K. L., & Grindstaff, L. (1992, May). *The Impact of Surrounding Buildings on Propagation for Wireless In-Building Personal Communications System Design*. IEEE Vehicular Technology Conference, Denver, CO. doi: 10.1109/VETEC.1992.245301

Sheikh, A. U. H., & Hau, S. F. (2002). Channel Impulse Response: Measurements and Interpretations. *Wireless Personal Communications*, **21**(2), 219-228.

Siamarou, A. G., & Al-Nuaimi, M. (2010). A Wideband Frequency-Domain Channel-Sounding System and Delay-Spread Measurements at the License-Free 57- to 64-GHz Band. *IEEE Transactions on Instrumentation and Measurement*, **59**(3), 519-526. doi: 10.1109/TIM.2009.2023105

Smith, S. W. (1999). *The Scientist and Engineer's Guide to Digital Signal Processing*. San Diego, CA: California Technical Publishing.

Smith, S. W. (2003). *Digital Signal Processing: A Practical Guide for Engineers and Scientists*. Burlington, MA: Elsevier Science.

Stoica, P., & Moses, R. (1997). *Introduction to Spectral Analysis*. Upper Saddle River, N.J: Prentice Hall.

Stoica, P., & Nehorai, A. (1988). Study of the statistical performance of the Pisarenko harmonic decomposition method. *IEE Proceedings F*, **135**(2), 161-168. doi: 10.1049/ip-f-1:19880022

Strang, G., & Nguyen, T. (1997). *Wavelets and Filter Banks*. Wellesley, MA: Wellesley-Cambridge Press.

Street, A. M., Lukama, L., & Edwards, D. J. (2000). Radio imaging using SVD Prony. *Electronics Letters*, **36**(13), 1150-1152. doi: 10.1049/el:20000803

Takeuchi, T., Sako, M., & Yoshida, S. (1990, May). *Multipath Delay Estimation for Indoor Wireless Communication*. IEEE Vehicular Technology Conference, Orlando, FL. doi: 10.1109/VETEC.1990.110355

Tang, Y. Y., Yang, L. H., Liu, J., & Ma, H. (2000). *Wavelet Theory and Its Application to Pattern Recognition*. Singapore: World Scientific Publishing.

Therrien, C. W. (1992). *Discrete Random Signals and Statistical Signal Processing*. Englewood Cliffs, New Jersey: Prentice-Hall Inc.

Tholl, D., Fattouche, M., Bultitude, R. J. C., Melancon, P., & Zaghloul, H. (1993). A Comparison of Two Radio Propagation Channel Impulse Response Determination Techniques. *IEEE Transactions on Antennas and Propagation*, **41**(4), 515-517. doi: 10.1109/8.220988

Turin, G. L., Clapp, F. D., Johnson, T. L., Fine, S. B., & Lavry, D. (1972). A Statistical Model of Urban Multipath Propagation. *IEEE Transactions on Vehicular Technology*, **21**(1), 1-9. doi: 10.1109/T-VT.1972.23492

Turkami, A. M. D., Demery, D. A., & Parsons, J. D. (1991). Measurement and modelling of wideband mobile radio channels at 900 MHz. *IEE Proceedings I*, **138**(5), 447-457.

Unser, M., & Aldroubi, A. (1996). A Review of Wavelets in Biomedical Applications. *Proceedings of the IEEE*, **84**(4), 626-638. doi: 10.1109/5.488704

Vaughan, R., & Andersen, J. B. (2003). *Channels, Propagation And Antennas For Mobile Communications*. London: Institution of Electrical Engineers.

Vetterli, M., & Herley, C. (1992). Wavelets and Filter Banks: Theory and Design. *IEEE Transactions on Signal Processing*, **40**(9), 2207-2232. doi: 10.1109/78.157221

Walker, G. (1931). On Periodicity in Series of Related Terms. *Proceedings of the Royal Society of London*, **131**(818), 518-532.

Wax, M., & Kailath, T. (1985). Detection of Signals by Information Theoretic Criteria. *IEEE Transactions on Acoustics, Speech and Signal Processing*, **33**(2), 387-392. doi: 10.1109/TASSP.1985.1164557

Wickerhauser, M. V. (1994). *Adapted Wavelet Analysis from Theory to Software*. Wellesley, MA: A K Peters.

Wickert, M. A., & Ionescu, D. M. (1996, 28 April - 1 May). *Multipath Channel Parameter Estimation Using the Wavelet Transform*. IEEE Vehicular Technology Conference, Atlanta, GA. doi: 10.1109/VETEC.1996.503431

Wong, K. T., & Zoltowski, M. D. (2000). Self-Initiating MUSIC-Based Direction Finding and Polarization Estimation in Spatio-Polarizational Beamspace. *IEEE Transactions on Antennas and Propagation*, **48**(8), 1235-1245. doi: 10.1109/8.884492

Wornell, G. W. (1996). Emerging Applications of Multirate Signal Processing and Wavelets in Digital Communications. *Proceedings of the IEEE*, **84**(4), 586-603. doi: 10.1109/5.488701

Yates, R. D., & Goodman, D. J. (2005). *Probability and Stochastic Processes: A Friendly Introduction for Electrical and Computer Engineers*. Hoboken, NJ: John Wiley & Sons.

Young, W. R., & Lacy, L. Y. (1950). Echoes in Transmission at 450 Megacycles from Land-to-Car Radio Units. *Proceedings of the IRE*, **38**(3), 255-258. doi: 10.1109/JRPROC.1950.230736

APPENDIX A

BASIC PRINCIPLES OF WAVELET ANALYSIS

A.1 Wavelet Basis Functions

The word "wavelet" essentially means "a small wave" that oscillates with a zero net area. Wavelets provide sets of basis functions for function spaces. A wavelet basis function is a set of complete and linearly independent functions generated from a prototype wavelet. The case where the set is over complete leads to frames. What makes wavelet bases especially interesting is their self-similarity; every function in a wavelet basis is a dilated and translated replica of a prototype function.

Some important properties of a wavelet system include:

- Orthogonality
- Compact support
- Symmetry
- Smoothness

Orthogonality

A wavelet system is orthogonal if

$$\langle \varphi(t),\, \psi(t) \rangle = 0, \tag{A.1}$$

where $\varphi(t)$ and $\psi(t)$ are the scaling and wavelet functions respectively, while $\langle \cdot\,,\, \cdot \rangle$ denotes inner product operation. Orthogonality is a desired property in signal analyses.

Compact support

This property is a function of the filter length. If the scaling and wavelet functions are compactly supported, then the corresponding low-pass and high-pass filters are finite impulse response filters. A compact wavelet (in time) has good time resolution but poor frequency resolution, while a broad wavelet function has poor time resolution and good frequency resolution. Wavelets with compact support allow reduced computational complexities.

Symmetry

When the scaling and wavelet functions are symmetric, then the corresponding filters will have generalised linear phase. The absence of symmetry can lead to phase distortion, especially in signal processing applications.

Smoothness

This property is determined by the number of vanishing moments in a wavelet. The larger the number of vanishing moments, the smoother is the wavelet. This is useful in compression applications.

A.2 Translation and Dilation of Wavelets

Consider a real-valued function $\gamma(t)$. The translation of $\gamma(t)$ yields a new function $\gamma_{0,k}(t)$, where

$$\gamma_{0,k}(t) = \gamma(t-k), \qquad -\infty < t < \infty,\ k \in \mathbb{Z}. \tag{A.2}$$

$\mathbb{Z}$ denotes the set of all integer values.

Dyadic dilation, i.e. scaling in multiple powers of 2, yields $\gamma_{j,0}(t)$ as

$$\gamma_{j,0}(t) = 2^{-j/2}\gamma\left(2^{-j}t\right), \qquad -\infty < t < \infty, \quad j = 1, 2, \ldots . \tag{A.3}$$

The factor $2^{-j/2}$ ensures that if $\gamma(t)$ is a member of $L^2(\mathbb{R})$ with a squared norm given by

$$\left\|\gamma(t)\right\|^2 = \int_{-\infty}^{\infty} \left|\gamma(t)\right|^2 dt, \tag{A.4}$$

then $\left\|\gamma_{1,0}(t)\right\|^2 = \left\|\gamma(t)\right\|^2$, i.e. the norm is preserved regardless of the scale. $L^2(\mathbb{R})$ denotes a Hilbert space of square integrable functions.

A translation and dilation of $\gamma(t)$ is then given by

$$\gamma_{j,k}(t) = 2^{-j/2}\gamma\left(2^{-j}t - k\right), \qquad -\infty < t < \infty, \quad j = 1, 2, \ldots . \tag{A.5}$$

A.3 Multiresolution Analysis

Early on in the history of wavelet development, it was a non-trivial task to find a function $\psi(t)$ to ensure that

$$\left\{\psi_{j,k}(t) = 2^{-j/2}\psi\left(2^{-j}t - k\right)\right\}_{j\in\mathbb{Z},k\in\mathbb{Z}}, \tag{A.6}$$

is an orthonormal basis of $L^2(\mathbb{R})$. Such functions were discovered in the 1980s, and consequently a standard procedure to construct wavelet bases was developed. Multiresolution analysis (MRA) describes a mathematical framework for analysing functions at various levels of resolution, and may be likened to a chain of subspaces. It provides simultaneous information on time and frequency of the signal characteristics, in terms of the projection of a signal at multiple resolutions. From the literature, a sequence

of subspaces $\{V_j\}_{j\in\mathbb{Z}}$ of $L^2(\mathbb{R})$ is said to be a multiresolution analysis when the following properties are satisfied:

$$f(t)\in V_j \Leftrightarrow f(t-k)\in V_j\ , \qquad j\in\mathbb{Z},\ k\in\mathbb{Z}\,. \tag{A.7}$$

$$V_{j+1}\subset V_j\ . \tag{A.8}$$

$$f(t)\in V_j \Leftrightarrow f\left(2^{-1}t\right)\in V_{j+1}. \tag{A.9}$$

$$\lim_{j\to+\infty} V_j = \bigcap_{j\in\mathbb{Z}} V_j = \{0\}\,. \tag{A.10}$$

$$\lim_{j\to-\infty} V_j = \overline{\bigcup_{j\in\mathbb{Z}} V_j} = L^2(\mathbb{R})\,. \tag{A.11}$$

Property (A.7) implies that V_j is invariant by any translation, where $\Leftrightarrow$ stands for two way implications. V_j is known as the approximation subspace.

Property (A.8) is a causality property showing that an approximation at the resolution 2^{-j} bears all information to compute an approximation at a coarser resolution $2^{-(j+1)}$. The information lost between any two successive approximations is captured in the detail subspace, or wavelet space, W_j.

Property (A.9) shows that dilating functions in V_j by 2 defines an approximation at a coarser resolution $2^{-(j+1)}$.

Properties (A.10) and (A.11) define an approximation of a function as a sequence of closed and embedded approximation subspaces whose intersection is empty and whose closure converges to $L^2(\mathbb{R})$. In particular, (A.10) implies that when the resolution 2^{-j} goes to 0, then all the signal details are lost. (A.11) shows that when the resolution goes to $+\infty$, then the signal approximation converges to the original signal.

Whenever a collection of closed subspaces fulfils above conditions, then there exists an orthonormal wavelet basis $\{\psi_{j,k}; j,k \in \mathbb{Z}\}$. At a given resolution, there exists a unique scaling function $\varphi_j(t)$ that can be written as

$$\varphi_j(t) = 2^{-j/2}\varphi\left(2^{-j}t\right). \tag{A.12}$$

A scaling function $\varphi(t)$, such that its entire integer translates form a basis of V_0, is defined by

$$\varphi(t) \in V_0 \Leftrightarrow \varphi(t-k) \in V_0. \tag{A.13}$$

Since the subspace $W_j \subset V_{j-1}$ is the orthogonal complement of V_j in V_{j-1}, then

$$V_{j-1} = V_j \oplus W_j. \tag{A.14}$$

By iteration, this means that

$$V_j = V_{j+1} \oplus W_{j+1}, \tag{A.15}$$

$$V_{j+1} = V_{j+2} \oplus W_{j+2}, \tag{A.16}$$

$$\vdots$$

$$V_{J-1} = V_J \oplus W_J. \tag{A.17}$$

Therefore

$$V_{j-1} = W_j \oplus W_{j+1} \oplus W_{j+2} \oplus W_{j+3} \oplus \cdots \oplus W_J \oplus V_J, \tag{A.18}$$

$\leftarrow$ *fine scale* *coarse scale* $\rightarrow$

where J denotes the coarsest resolution level, while $\oplus$ represents a direct sum operator.

APPENDIX B

DERIVATION OF THE DAUBECHIES EXTREMAL PHASE FILTER COEFFICIENTS

The most frequently used orthogonal wavelets are the Daubechies wavelets. The Daubechies' extremal phase low-pass filter and wavelet coefficients are derived in this appendix. This wavelet family is commonly abbreviated as dbN where N denotes the wavelet order and number of vanishing moments. They are family of orthogonal wavelets supported on an interval of length $\mathrm{P}-1$, where $\mathrm{P}=2\mathrm{N}$.

The low-pass filter and wavelet coefficients are derived, in this appendix, such that orthogonality and moment conditions are guaranteed.

Starting with a four-coefficient scaling equation described by

$$2^{-1/2}\varphi\left(2^{-1}t\right)=\sum_{k=0}^{\mathrm{P}-1}h_k\varphi\left(t-k\right),\qquad \mathrm{P}=4, \tag{B.1}$$

where $h_k\varphi\left(t-k\right)$ is a replica of the scaling function $\varphi\left(2^{-1}t\right)$, but at a different resolution, translated along the time axis by an integer step k and factored by the scaling coefficients h_k.

Assume that the coefficients of the scaling function, i.e. h_k, are normalised such that

$$\sum_{k=0}^{\mathrm{P}-1}h_k=\sqrt{2}\,. \tag{B.2}$$

For orthogonality, these scaling coefficients must satisfy the following constraints;

$$\sum_{k=0}^{P-1} h_k h_{k+2\zeta} = \begin{cases} 1 & \zeta = 0 \\ 0 & \zeta \neq 0 \end{cases}. \tag{B.3}$$

The m^{th} moment of the corresponding wavelet function, in terms of the scaling coefficients h_k, is defined as follows:

$$\sum_{k=0}^{P-1} (-1)^k h_{(P-1)-k} k^m = 0, \qquad m = 0, \ldots, N-1, \tag{B.4}$$

where N is the number of vanishing wavelet moments. Therefore,

$$\sum_{k=0}^{3} (-1)^k h_{3-k} = 0, \qquad \text{for } m = 0, \tag{B.5}$$

$$\sum_{k=0}^{3} (-1)^k h_{3-k} k = 0, \qquad \text{for } m = 1. \tag{B.6}$$

The orthogonality requirement and moment condition, with normalised scaling coefficients, results in the following equations:

$$h_0 + h_1 + h_2 + h_3 = \sqrt{2}, \tag{B.7}$$
$$-h_0 + h_1 - h_2 + h_3 = 0, \tag{B.8}$$
$$-3h_0 + 2h_1 - h_2 = 0, \tag{B.9}$$
$$h_0^2 + h_1^2 + h_2^2 + h_3^2 = 1. \tag{B.10}$$

Putting (B.7) - (B.9) into matrix of the form

$$\begin{pmatrix} 1 & 1 & 1 \\ -1 & 1 & -1 \\ -3 & 2 & -1 \end{pmatrix} \begin{pmatrix} h_0 \\ h_1 \\ h_2 \end{pmatrix} = \begin{pmatrix} \sqrt{2} - h_3 \\ -h_3 \\ 0 \end{pmatrix}. \tag{B.11}$$

This gives

$$h_0 = 0.25\sqrt{2} - h_3 . \tag{B.12}$$

$$h_1 = 0.5\sqrt{2} - h_3 , \tag{B.13}$$

$$h_2 = 0.25\sqrt{2} + h_3 . \tag{B.14}$$

Substituting (B.12) – (B.14) into (B.10) results in the following two sets of solutions:

$$h_0 = 0.4830 ,\ h_1 = 0.8365 ,\ h_2 = 0.2241 ,\ h_3 = -0.1294 ,$$

and

$$h_0 = -0.1294 ,\ h_1 = 0.2241 ,\ h_2 = 0.8365 ,\ h_3 = 0.4830 .$$

The first set leads to $\varphi(t)$ while the second set leads to $\varphi(-t)$.

The wavelet filter coefficients associated with the first set of scaling coefficients is given by the quadrature mirror filter relation:

$$g_k = (-1)^k h_{P-1-k} , \tag{B.15}$$

where $P = 4$. Hence

$$g_0 = -0.1294 ,\ g_1 = -0.2241 ,\ g_2 = 0.8365 ,\ g_3 = -0.4830 .$$

These are the Daubechies 2, i.e. db2, wavelet coefficients. Following the same procedure from (B.1) to (B.15), the scaling filter coefficients and the corresponding wavelet filter coefficients for a six-coefficient scaling equation can also be obtained.

Expressing the wavelet function as a moment condition, described by (B.4) but for $P=6$ gives

$$\sum_{k=0}^{5}(-1)^k h_{5-k}=0, \qquad \text{for } m=0, \tag{B.16}$$

$$\sum_{k=0}^{5}(-1)^k h_{5-k}k=0, \qquad \text{for } m=1, \tag{B.17}$$

$$\sum_{k=0}^{5}(-1)^k h_{5-k}k^2=0, \qquad \text{for } m=2. \tag{B.18}$$

Applying the orthogonality and moment conditions, with normalised scaling coefficients, results in the following equations:

$$h_0+h_1+h_2+h_3+h_4+h_5=\sqrt{2}, \tag{B.19}$$
$$-h_0+h_1-h_2+h_3-h_4+h_5=0, \tag{B.20}$$
$$-5h_0+4h_1-3h_2+2h_3-h_4=0, \tag{B.21}$$
$$-25h_0+16h_1-9h_2+4h_3-h_4=0, \tag{B.22}$$
$$h_0h_2+h_1h_3+h_2h_4+h_3h_5=0, \tag{B.23}$$
$$h_0^2+h_1^2+h_2^2+h_3^2+h_4^2+h_5^2=1. \tag{B.24}$$

Putting (B.19) – (B.22) into matrix of the form

$$\begin{pmatrix} 1 & 1 & 1 & 1 \\ -1 & 1 & -1 & 1 \\ -5 & 4 & -3 & 2 \\ -25 & 16 & -9 & 4 \end{pmatrix}\begin{pmatrix} h_0 \\ h_1 \\ h_2 \\ h_3 \end{pmatrix}=\begin{pmatrix} \sqrt{2}-h_4-h_5 \\ h_4-h_5 \\ h_4 \\ h_4 \end{pmatrix}. \tag{B.25}$$

Then solving for the scaling coefficients h_k gives the solution of $\varphi(t)$ as

$h_0=0.3327$, $h_1=0.8069$, $h_2=0.4599$, $h_3=-0.1350$, $h_4=-0.0854$, $h_5=0.0352$.

The wavelet coefficients associated with these scaling coefficients can be obtained by applying (B.15), where $\mathrm{P}=6$. Therefore

$g_0=0.0352,\ g_1=0.0854,\ g_2=-0.1350,\ g_3=-0.4599,\ g_4=0.8069,\ g_5=-0.3327.$

These are the Daubechies 3, i.e. db3, wavelet coefficients. In the same way, the scaling and wavelet coefficients can be obtained for db4 through to db10.

The Daubechies wavelets have the following properties:

1. Compact support.
2. Asymmetric for length of filter greater than 2.
3. Orthogonality.
4. N vanishing moments.
5. Increasing smoothness as N increases.

These Daubechies low-pass filter coefficients $\{h_k\}$, for $db1 \sim db10$ from the literature, are listed in Tables B.1 through B.5. The coefficients $\{h_k\}$ have been normalised such that $\sum h_k=\sqrt{2}$, where $k=0,\ldots,(\mathrm{P}-1)$.

Table B.1 Daubechies low-pass filter coefficients of orders 1 to 4.

Order	k	**Low-pass filter coefficients** h_k
db1	0	0.7071067811865475
	1	0.7071067811865475
db2	0	0.4829629131445341
	1	0.8365163037378077
	2	0.2241438680420134
	3	-0.1294095225512603
db3	0	0.3326705529500827
	1	0.8068915093110928
	2	0.4598775021184915
	3	-0.1350110200102546
	4	-0.0854412738820267
	5	0.0352262918857096
db4	0	0.2303778133074431
	1	0.7148465705484058
	2	0.6308807679358788
	3	-0.0279837694166834
	4	-0.1870348117179132
	5	0.0308413818353661
	6	0.0328830116666778
	7	-0.0105974017850021

Table B.2 Daubechies low-pass filter coefficients of orders 5 to 6.

Order	k	**Low-pass filter coefficients** h_k
db5	0	0.1601023979741930
	1	0.6038292697971898
	2	0.7243085284377729
	3	0.1384281459013204
	4	-0.2422948870663824
	5	-0.0322448695846381
	6	0.0775714938400459
	7	-0.0062414902127983
	8	-0.0125807519990820
	9	0.0033357252854738
db6	0	0.1115407433501094
	1	0.4946238903984530
	2	0.7511339080210954
	3	0.3152503517091980
	4	-0.2262646939654399
	5	-0.1297668675672624
	6	0.0975016055873224
	7	0.0275228655303053
	8	-0.0315820393174862
	9	0.0005538422011614
	10	0.0047772575109455
	11	-0.0010773010853085

Table B.3 Daubechies low-pass filter coefficients of orders 7 to 8.

Order	k	**Low-pass filter coefficients** h_k
db7	0	0.0778520540850081
	1	0.3965393194819136
	2	0.7291320908462368
	3	0.4697822874052154
	4	-0.1439060039285293
	5	-0.2240361849938538
	6	0.0713092192668312
	7	0.0806126091510820
	8	-0.0380299369350125
	9	-0.0165745416306664
	10	0.0125509985560993
	11	0.0004295779729214
	12	-0.0018016407040474
	13	0.0003537137999745
db8	0	0.0544158422431049
	1	0.3128715909143031
	2	0.6756307362972904
	3	0.5853546836541907
	4	-0.0158291052563816
	5	-0.2840155429615702
	6	0.0004724845739124
	7	0.1287474266204837
	8	-0.0173693010018083
	9	-0.0440882539307952
	10	0.0139810279173995
	11	0.0087460940474061
	12	-0.0048703529934518
	13	-0.0003917403733770
	14	0.0006754494064506
	15	-0.0001174767841248

Table B.4 Daubechies low-pass filter coefficients of order 9.

Order	k	**Low-pass filter coefficients** h_k
db9	0	0.0380779473638791
	1	0.2438346746125939
	2	0.6048231236901156
	3	0.6572880780512955
	4	0.1331973858249927
	5	-0.2932737832791761
	6	-0.0968407832229524
	7	0.1485407493381306
	8	0.0307256814793395
	9	-0.0676328290613302
	10	0.0002509471148340
	11	0.0223616621236805
	12	-0.0047232047577520
	13	-0.0042815036824636
	14	0.0018476468830564
	15	0.0002303857635232
	16	-0.0002519631889427
	17	0.0000393473203163

Table B.5 Daubechies low-pass filter coefficients of order 10.

Order	k	**Low-pass filter coefficients** h_k
db10	0	0.0266700579005546
	1	0.1881768000776863
	2	0.5272011889317202
	3	0.6884590394536250
	4	0.2811723436606485
	5	-0.2498464243272283
	6	-0.1959462743773399
	7	0.1273693403357890
	8	0.0930573646035802
	9	-0.0713941471663697
	10	-0.0294575368218480
	11	0.0332126740593703
	12	0.0036065535669880
	13	-0.0107331754833036
	14	0.0013953517470692
	15	0.0019924052951930
	16	-0.0006858566949566
	17	-0.0001164668551285
	18	0.0000935886703202
	19	-0.0000132642028945

APPENDIX C

WAVELET THRESHOLDING

Thresholding of the wavelet transform coefficients can be used to separate a wanted signal from noise. A common formulation of threshold functions is that, if the magnitude of the wavelet transform coefficient, say Q_n, is less than a given threshold value $L > 0$, then this wavelet transform coefficient is set to zero.

Consider a noisy signal given by

$$y_N(n) = x_N(n) + \eta_N(n), \qquad n = 0,1,\ldots,N-1, \tag{C.1}$$

where $x_N(n)$ is an unknown signal of interest to be separated from noise, N is the length of the signal, and $\eta_N(n)$ is an additive white Gaussian noise term. A thresholding scheme for estimating $x_N(n)$ then consists of three main steps as follows:

(1) Determine the wavelet transform coefficients, $\boldsymbol{Q} = W_{j,k}$, of $y_N(n)$.

(2) Define the thresholded coefficients to be a vector $\boldsymbol{Q}^{(t)}$ with n^{th} element $Q_n^{(t)}$ given by

$$Q_n^{(t)} = \begin{cases} 0 & |Q_n| \le L \\ nonzero\ value & otherwise \end{cases}, \tag{C.2}$$

where L is the noise threshold level.

(3) Estimate $x_N(n)$ from the thresholded coefficients $\boldsymbol{Q}^{(t)}$.

This form of thresholding is also known as global thresholding. There are several possibilities for coefficients that exceed the threshold level L. A common scheme from the literature is the hard thresholding, for which the thresholded coefficients $\boldsymbol{Q}^{(t)}$ are defined to be a vector $\boldsymbol{Q}^{(ht)}$ with the following elements

$$Q_n^{(ht)} = \begin{cases} 0 & |Q_n| \le L \\ Q_n & otherwise \end{cases}. \tag{C.3}$$

That is the coefficients with magnitudes that exceed L are unmodified, while those less than or equal to L are thrown away. The mapping from Q_n to $Q_n^{(ht)}$ is known as hard thresholding.

Another type of thresholding scheme in common usage is the soft thresholding, for which $\boldsymbol{Q}^{(t)}$ is defined to be a vector $\boldsymbol{Q}^{(st)}$, with n^{th} element $Q_n^{(st)}$ such that

$$Q_n^{(st)} = sign\{Q_n\}\left(|Q_n| - L\right)_+, \tag{C.4}$$

where

$$sign\{Q_n\} \equiv \begin{cases} +1 & Q_n > 0 \\ 0 & Q_n = 0, \\ -1 & Q_n < 0 \end{cases} \tag{C.5}$$

and

$$\left(\Lambda\right)_+ \equiv \begin{cases} \Lambda & \Lambda \ge 0 \\ 0 & \Lambda < 0 \end{cases}. \tag{C.6}$$

In this case, coefficients that exceed L in magnitude are shrink toward zero by L, while those less than L are replaced with zero. The mapping from Q_n to $Q_n^{(st)}$ is known as soft

thresholding. Hard thresholding produces an improved signal to noise ratio in comparison with soft thresholding.

Finally, a compromise between hard and soft thresholding is the mid thresholding. This acts like hard thresholding when $|Q_n| \geq 2L$ and interpolates between hard and soft thresholding when $L \leq |Q_n| \leq 2L$. Therefore, $\boldsymbol{Q}^{(t)}$ is defined to be a vector $\boldsymbol{Q}^{(mt)}$ with elements

$$Q_n^{(mt)} = sign\{Q_n\}\left(|Q_n| - L\right)_{++}, \tag{C.7}$$

where

$$\left(|Q_n| - L\right)_{++} \equiv \begin{cases} 2\left(|Q_n| - L\right)_{+} & |Q_n| < 2L \\ |Q_n| & otherwise \end{cases}. \tag{C.8}$$

That is large coefficients, those exceeding $2L$ in magnitude, are left unmodified. Those coefficients with magnitude between L and $2L$ are shrunk, while those less than L are replaced with zero.

APPENDIX D

PUBLICATIONS

D.1 Best Paper Award

Aboaba O.A., and Chung K.S., "Pathlet: A new wavelet for resolving the constituent components in a multipath channel," In Proc. of the 12th Asia-Pacific Conference on Communications (APCC), Busan, South Korea, August 2006.

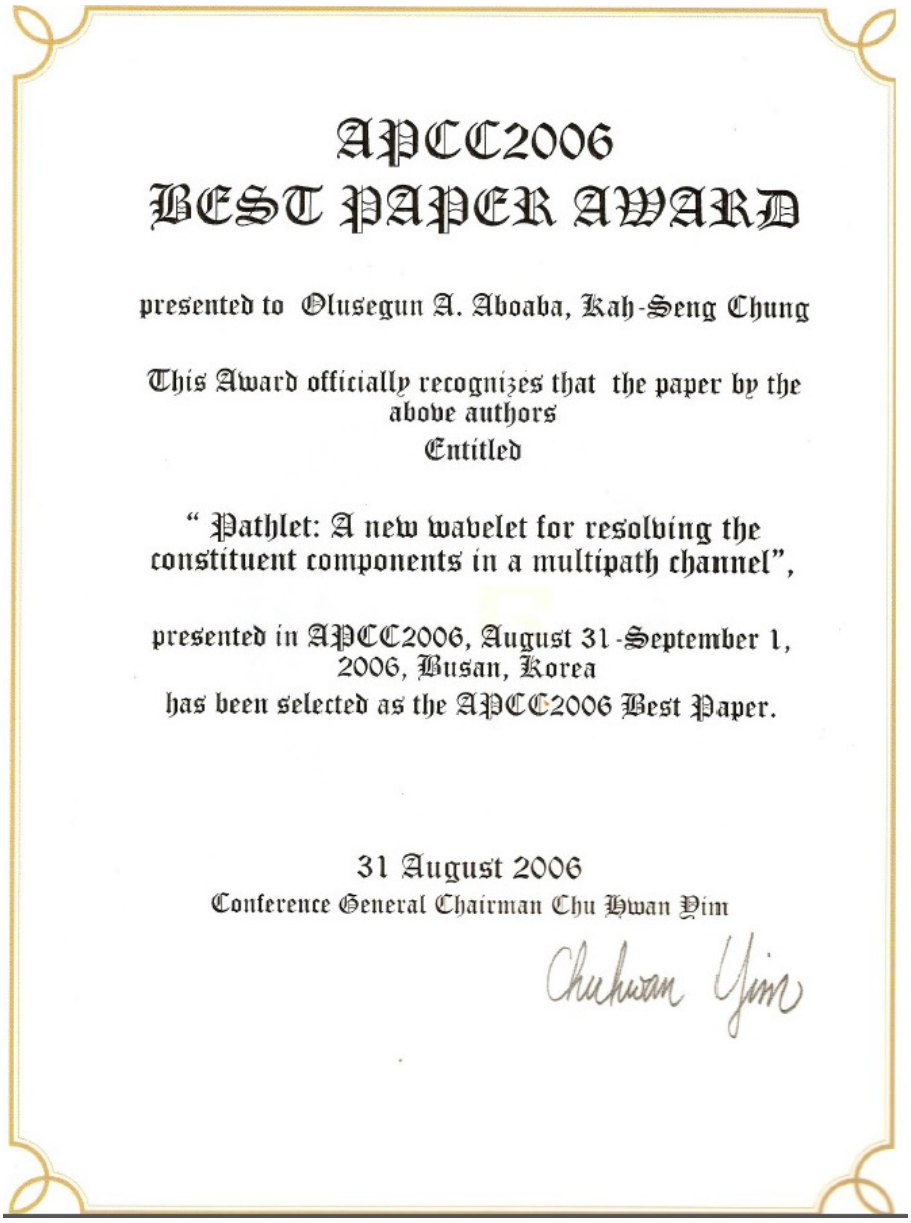

APCC2006
BEST PAPER AWARD

presented to Olusegun A. Aboaba, Kah-Seng Chung

This Award officially recognizes that the paper by the above authors
Entitled

" Pathlet: A new wavelet for resolving the constituent components in a multipath channel",

presented in APCC2006, August 31-September 1, 2006, Busan, Korea
has been selected as the APCC2006 Best Paper.

31 August 2006
Conference General Chairman Chu Hwan Yim

D.2 Other Papers

The following papers have also been published on topics related to this research study:

Aboaba O.A., "Noise Analysis in Mobile Radio Environments Using Pathlets and Symlet 2 Wavelets," In Proc. of the TENCON 2010 conference, Fukuoka, Japan, pp. 1318-1323, November 2010.

Aboaba O.A., and Chung K.S., "Multipath Channel Parameter Estimation in Mobile Radio Environments Using Stationary Wavelet Transform," In Proc. of the 11th Asia-Pacific Conference on Communications, Perth, Western Australia, pp. 203-207, October 2005.

Aboaba O.A., "Noise Reduction by Singularity Detection and Processing with Wavelets," In Proc. of the 6th Inter-University Postgraduate Electrical Engineering and Computing Symposium, Perth, Western Australia, pp. 7-11, September 2005.

Aboaba O.A., "A Wavelet-based Method for Hyper-Resolution Multipath Channel Parameter Estimation," In Proc. of the 5th Inter-University Postgraduate Electrical Engineering and Computing Symposium, Perth, Western Australia, pp. 1-6, September 2004.

Aboaba O.A., and Chung K.S., "Estimation of Multipath Channel Parameters in Mobile Radio Environments Using Wavelet Packet Analysis," In Proc. of the 4th Inter-University Postgraduate Electrical Engineering and Computing Symposium, Perth, Western Australia, pp. 7-12, October 2003.

Aboaba O.A., and Chung K.S., "Resolution of constituent components in multipath field using Discrete Wavelet Transform," In Proc. of the 8th Asia-Pacific Conference on Communications, Bandung, Indonesia, pp. 208-211, September 2002.

Aboaba O.A., "Multiresolution wavelet analysis of nonstationary signals," In Proc. of the 3rd Inter-University Postgraduate Electrical Engineering and Computing Symposium, Perth, Western Australia, October 2002.